BioMed Research International

Bone Tissue Engineering for Dentistry and Orthopaedics

Guest Editors: Yin Xiao, Michael Gelinsky, Mei Wei, and Jiang Chang

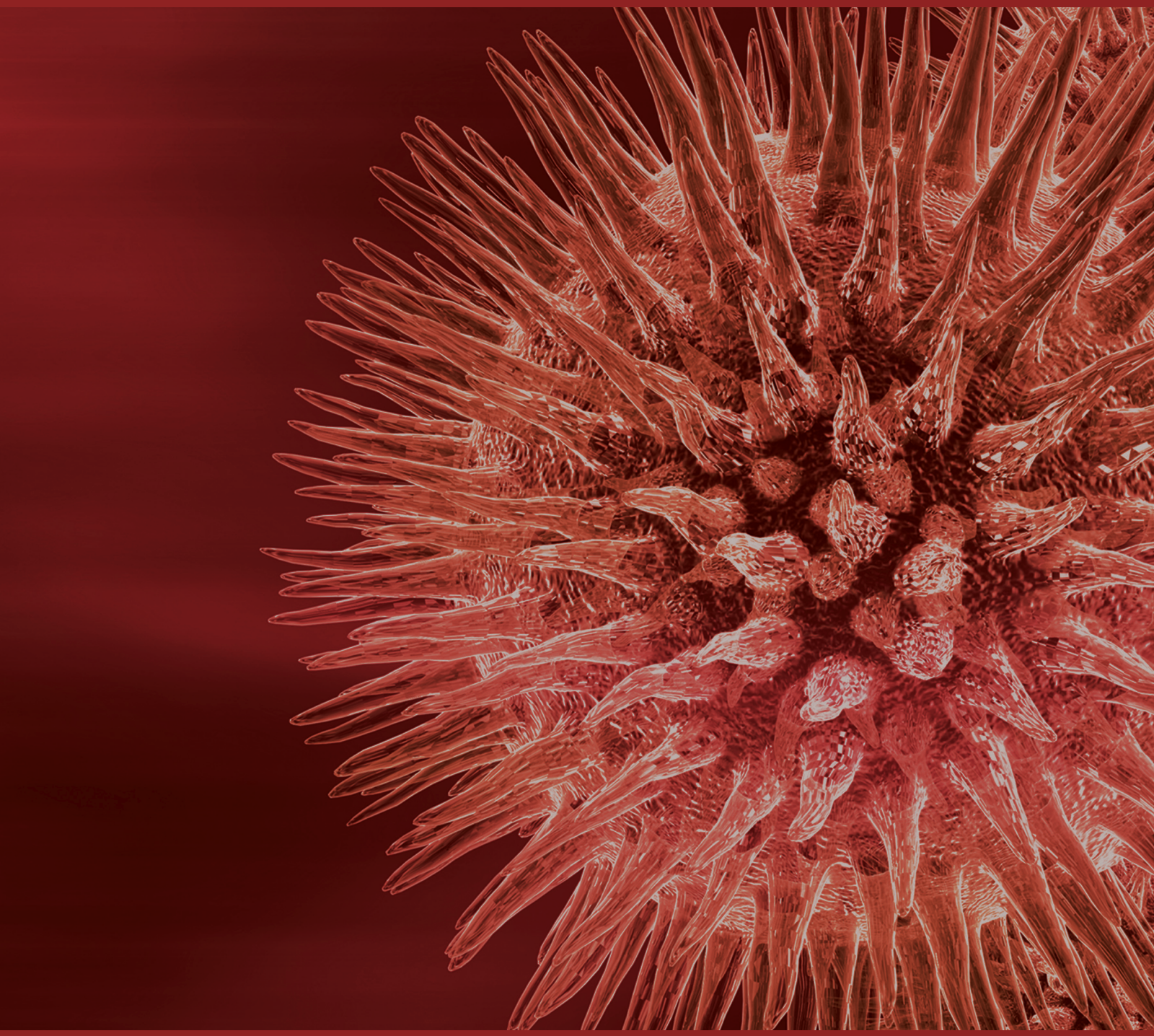

Bone Tissue Engineering for Dentistry and Orthopaedics

BioMed Research International

Bone Tissue Engineering for Dentistry and Orthopaedics

Guest Editors: Yin Xiao, Michael Gelinsky, Mei Wei, and Jiang Chang

Contents

Hindawi Publishing Corporation
BioMed Research International
Volume 2014, Article ID 241067, 2 pages
http://dx.doi.org/10.1155/2014/241067

Editorial

Bone Tissue Engineering for Dentistry and Orthopaedics

Yin Xiao[1,2]

[1] *Institute of Health and Biomedical Innovation, Queensland University of Technology, 60 Musk Avenue, Kelvin Grove, Brisbane, QLD 4059, Australia*
[2] *Australia-China Centre for Tissue Engineering and Regenerative Medicine (ACCTERM), Brisbane, QLD 4059, Australia*

Correspondence should be addressed to Yin Xiao; yin.xiao@qut.edu.au

Received 5 November 2014; Accepted 5 November 2014; Published 26 November 2014

Bone has a strong capacity for self-repair; however, conditions such as complex trauma, tumor, infection, and congenital disorders, which can cause large bone defects and resorption, often result in devastating deficits of dental and skeletal tissues. Clinically, this can lead to nonunion of bone and the loss of functional support to surrounding tissues, with the consequence of significant impact on the quality of life of patients. This is a challenging situation that typically requires bone grafting and complicated and expensive treatment strategies.

Currently the gold standard material for bone defect repair is autografts; however, donor site morbidity and limited supply prevent the wide application of this method. Allografts and xenografts can address the supply issue but face issues such as immune rejection and potential transmission of infectious diseases. In view of the limitations inherent with conventional bone graft strategies, tissue engineering represents a promising approach for bone repair and regeneration. Advances in tissue engineering have led to innovative scaffold designs, complemented by progress in the understanding of cell-based therapies and bioactive growth factor delivery.

Bone tissue engineering strategies have demonstrated that there is great potential to address the ever-pressing clinical need and have attracted attention from scientists, engineers, and clinicians worldwide over the past 25 years. This is reflected by the increasing interest shown by our readership and authors in this promising field and we are, therefore, pleased to present this special issue. In this issue, we have compiled fourteen exciting papers, including research articles and reviews that reflect the diversity of this fascinating subject and provide a better understanding of recent advances in the field of bone tissue engineering.

The fundamental concept of bone tissue engineering is to combine progenitor cells or osteogenically differentiated/mature cells (for osteogenesis) seeded onto biocompatible scaffolds and ideally in three-dimensional structures (for osteoconduction and vascular ingrowth), with appropriate growth factors (for osteoinduction) to generate functional bone structures. Effective cell-based therapies for bone tissue engineering typically employ the coordinated manipulation of cells and biologically active signaling molecules. Y. Wu et al. have demonstrated the potential use of temporomandibular joint derived synovial stem cells (TMJ-SDSCs) in TMJ disc repair and regeneration. Y. Zhou et al. report that a hypoxic microenvironment can maintain cell proliferation capacity, enhance pluripotency, and promote differentiation, indicating that effective cell isolation and expansion under hypoxic conditions may be a viable technique for autologous cell-based therapies. S. Tuan et al. present a review on the functional regulation of osteoblast lineage cells in health and osteoporosis, with an emphasis on the application of strontium and its role in regulating bone remodeling via its involvement in a number of pathways. B. Chen et al. have focused on the role of nuclear factor-κB ligand (RANKL) in periodontal bone resorption and explored the factors involved in the regulation of the RANKL expression. Q. Zhang et al. provide an overview of the role of interleukin-10 (IL-10) in bone loss diseases and discuss the possibility of IL-10 adoption in the treatment of bone-related diseases, whereas K. Luo et al. show evidence that suggests that changes

of the expression of cytokines and bone turnover markers in periodontium of ovariectomized rats can contribute to the damage of periodontal tissues.

Optimizing and refining the use of scaffolds is another important aspect for bone tissue engineering. Taking their cues from the extracellular matrix, C. Rentsch et al. have developed embroidered polycaprolactone-co-lactide (PCL) scaffolds that are coated with collagen/chondroitin sulphate and which can enhance *de novo* bone formation and be used as skull bone implants for large *in vivo* defects. M. Shi et al. have constructed multifunctional nanosized mesoporous bioactive glass/poly(lactic-co-glycolic acid) composite-coated $CaSiO_3$ scaffolds that have improved mechanical strength, apatite-mineralization activity, cytocompatibility, and drug-delivery properties and which have promising applications in bone tissue engineering. G. Wu et al. have shown that the drug loading efficiency and release profile of bioactive scaffolds can be adjusted by changing the internal phase of the microparticles. This provides better understanding when fabricating multipurpose *in situ* drug releasing scaffolds for future clinical applications. X. Yu et al. report that the cellular responses to biomimetic calcium phosphate coatings are inferior to an alkaline-treated titanium surface, highlighting that substrate surface properties directly influence cell adhesion on different biomaterials.

With a firm focus on maintaining biomechanical properties, Z. Zhou et al. report that injection of hydrogel into the intervertebral discs can greatly restore the shock absorption of this tissue, suggesting that hydrogel injections may be a promising clinical approach to manage intervertebral disc degeneration. B. Lohberger et al. have evaluated the effects of cyclic tensile strain on the cell differentiation towards an osteogenic lineage, thereby contributing to a better understanding of strain-induced bone remodeling. E. Chung et al. further demonstrate that the combination of tensile and thermal stress conditioning over a short period has the potential to modify cellular performance and thus synergistically promotes bone regeneration. In order to provide scientific and empirical evidence for the clinical application of the polyaxial self-locking anatomical plate, W. Liang et al. have gathered geometrical data on the distal tibias and manufactured a variable locking screw trajectory to improve screw-plate stability through the design of a polyaxial self-locking anatomical plate.

Bone tissue engineering has become increasingly dependent on the emergence of innovations from all of these fields, even as they have continued to evolve independently. By gathering these papers in this issue, we seek to incorporate the diverse areas of research in order to reflect current trends. It is our hope that this will enrich our readers and the wide range of researchers in the field of bone tissue engineering for the application in orthopaedics and dentistry.

Yin Xiao

Hindawi Publishing Corporation
BioMed Research International
Volume 2014, Article ID 461724, 7 pages
http://dx.doi.org/10.1155/2014/461724

Research Article

Shock Absorbing Function Study on Denucleated Intervertebral Disc with or without Hydrogel Injection through Static and Dynamic Biomechanical Tests In Vitro

Zhiyu Zhou,[1,2] Manman Gao,[2] Fuxin Wei,[2] Jiabi Liang,[3] Wenbin Deng,[4] Xuejun Dai,[2] Guangqian Zhou,[1] and Xuenong Zou[2]

[1] *The Medical School of Shenzhen University, Shenzhen 518061, China*
[2] *Department of Spinal Surgery/Orthopaedic Research Institute, The First Affiliated Hospital of Sun Yat-sen University, Guangzhou 510080, China*
[3] *Pharmacy Department, The Fifth Affiliated Hospital of Sun Yat-sen University, Zhuhai 519000, China*
[4] *Department of Orthopaedics, The Second Affiliated Hospital of Nanchang University, Nanchang 330031, China*

Correspondence should be addressed to Guangqian Zhou; gqzhou@szu.edu.cn and Xuenong Zou; zxnong@hotmail.com

Received 16 December 2013; Revised 13 April 2014; Accepted 2 June 2014; Published 22 June 2014

Academic Editor: Michael Gelinsky

Hydrogel injection has been recently proposed as a novel therapy for disc degenerative diseases, with the potential to restore the spine motion and the intervertebral disc height. However, it remains unknown whether the new technique could also maintain the shock absorbing property of the treated intervertebral disc. In this study, 18 porcine lumbar bone-disc-bone specimens were collected and randomly divided into three groups: the normal with intact intervertebral discs, the mimic for the injection of disulfide cross-linked hyaluronan hydrogels following discectomy, and the control disc with discectomy only. In the static compression test, specimens in the mimic group exhibited displacements similar to those in the normal discs, whereas the control group showed a significantly larger displacement range in the first two steps ($P < 0.05$). With the frequency increasing, all specimens generally displayed an increasing storage modulus, decreasing loss modulus, and tanδ. At any frequency point, the control group exhibited the largest value in all the three parameters among three groups while the normal group was the lowest, with the mimic group being mostly close to the normal group. Therefore, the hydrogel injection into the intervertebral discs greatly restored their shock absorbing function, suggesting that the technique could serve as an effective approach to maintaining biomechanical properties of the degenerative intervertebral disc.

1. Introduction

Intervertebral discs, located between two vertebral bodies, are mainly composed of endplate, nucleus pulposus, and annulus fibrosus, which play a central role in permitting motion, allowing spinal flexibility, and dissipating energy during activities of daily living [1]. Compared with the annulus fibrosus composed of layers of collagen fiber lamellae, organized into centric rings around the nucleus pulposus [2, 3], the nucleus pulposus is normally hydrated and principally composed of water in a matrix of proteoglycan and other matrix proteins, appearing as observed translucent and gel-like [4, 5]. The nucleus pulposus and the annulus fibrosus are integrated together to maintain the normal biomechanical functions of the disc.

Disc degeneration is a common process that can result in degenerative disc diseases with low back pain and affect millions of people [2, 6, 7]. Disc degeneration is generally initiated from morphological and compositional changes of the nucleus pulposus [8]. Nucleus discectomy is therefore a common surgery for patients having herniated nucleus pulposus [4]. Through this surgery, most patients have their pain relieved [9]. However, increasing investigations have pointed out that nucleus discectomy greatly affects spinal structure and biomechanical functions, probably leading to

further degeneration of the adjacent discs and facet joint [9, 10].

So as to overcome limitations of the current surgical treatment, it is necessary to develop products and techniques for nucleus replacement to restore the normal function of the degenerative disc. Hydrogel injection has been developed in recent years [11–14]. The hydrogel made of hyaluronic acid and/or collagen-hyaluronan has been used for injection and proven to be effective to restore the range of spine motion and the height of intervertebral space [13–15]. As one of the most important functions of the intervertebral disc, cushion and distribution of compression load (shock absorbing function), however, has been overlooked in most current studies. Appropriate shock absorption is critical for protecting the nervous system, such as brain and spinal cord.

In this study, we prepared a type of hydrogel by combining hyaluronic acid and other extracellular matrix materials. This composite hydrogel can cross-link in situ and is therefore an ideal material for injection as a nucleus replacement. In an attempt to understand the function reconstruction (especially the function of shock absorbing) of degenerative disc by hydrogel injection, we investigated the static and dynamic biomechanical characteristics of lumbar intervertebral disc with or without hydrogel injection after nucleus discectomy.

2. Materials and Methods

2.1. Materials. All materials and reagents used in this study were purchased from Sigma-Aldrich except that the hyaluronic acid (HA, Mw = 0.26 MDa, kinetic viscosity = 5 mm^2/s, and intrinsic viscosity = 6.1 dL/g) was purchased from Bloomage Freda Biopharm Co., Ltd.

2.2. Hydrogel Preparation. The hydrogel was disulfide cross-linked from thiol-modified HA. Synthesis of the thiol-modified HA derivative followed exactly the same methods from a previous study [16]. There was 50–60% of carboxyl groups of HA that were transformed to thiol groups. The thiol groups could be oxidized in air to form disulfide linkages and further treated with diluted H_2O_2 to form additional disulfide linkages. The diluted H_2O_2 was added to thiol-modified HA immediately before injection into the intervertebral disc. Other extracellular matrix materials, including collagen II and chondroitin sulfate, could be premixed with the hydrogel.

2.3. Specimen Preparation. Three fresh frozen spines (L1-S1) from pigs were used in this study. All methods and procedures were peer reviewed and approved by the Institutional Review Board and Ethic Committee of the First Affiliated Hospital of Sun Yat-sen University (number 2008-55). MRI examining was used to validate intact of the spines (Figure 1). All ligaments of lumbar spines were stripped off except anterior and posterior ligaments around each of lumbar intervertebral discs. Each specimen was initially made out by cutting off horizontally in the medium of the adjacent vertebra. All the bone-disc-bone specimens were randomized into normal group, mimic group, and control group. Six specimens in normal group possessed relatively intact lumbar vertebral discs without any other operation. By contrast, specimens in the other two groups were subjected to subsequent operations. At the first step, the bone-disc-bone specimens in the mimic and control groups were drilled a hole at the center of the superior surface of specimen with a diameter of 1.5 mm. Then a hooked needle was inserted through the hole and the nucleus pulposus was mashed up softly avoiding the damage of annulus fibrosus. All fragments of nucleus pulposus were washed out completely with validation of MRI examining. 1.0 mL hydrogel material was injected in each disc of mimic group (Figure 1).

2.4. Biomechanical Tests. The biomechanical properties of each specimen were studied via static compression test and dynamic compression test, utilizing the instrument Bose ElectroForce which had been validated on the accuracy as well as precision [16]. The subsequence of static and dynamic tests was arranged according to random number. A procedure of static compression test was set up primarily including 4 steps as follows: step 1: the compression load was increased from 0 to 180 N in 2 seconds; step 2: the compression load was kept at 180 N for 5 minutes; step 3: the compression load decreased to 10 N in 2 seconds; and step 4: the compression load was kept at 10 N for 5 minutes (Figure 2(a)). The loading and displacement at each step were recorded by Bose ElectroForce and the histogram was shown in Figure 2(b). Similarly, a procedure of dynamic compression test was set up as well (i.e., at each frequency from 0.5 to 5.5 Hz, the cyclic compression load was set with median of 150 N and amplitude of 50 N and the test was sustained for 8 minutes). During the dynamic test, constant displacement of each specimen was recorded and series of mechanical parameters were exported by Bose ElectroForce including storage modulus, loss modulus, and tanδ.

The maximum compressive load of 180–200 N was selected to represent the human body weight scaled for differences in cross-sectional area of the human and porcine intervertebral discs [17, 18]. The minimum compressive load was 10 N because the disc of human body was still compressed even in a horizontal position [18]. The maximum frequency of 5.5 Hz was set to represent the frequency of how often the intervertebral disc was compressed by body weight when a human runs very fast (400–600 meters/minute). During the experiments, a saline humidifier was used to keep the specimens moist. And the room temperature was kept at 20–22°C. The specimens were definitely preserved in PBS 4°C for 72 h after every test to make sure that it had been recovered for the next test.

2.5. Statistical Analyses. All data were expressed as mean ± SEM. Data from the three groups in the static compression test were analyzed statistically using a one-way ANOVA. Univariate analysis of variance was used to statistically analyze data of each group in the dynamic compression test at different frequencies. All statistical tests were performed with SPSS 13.0 and $P < 0.05$ was considered to be significant.

3. Results

In step 1 of the static compression test, when the compression load was increased from 0 N to 180 N in 2 seconds, specimens

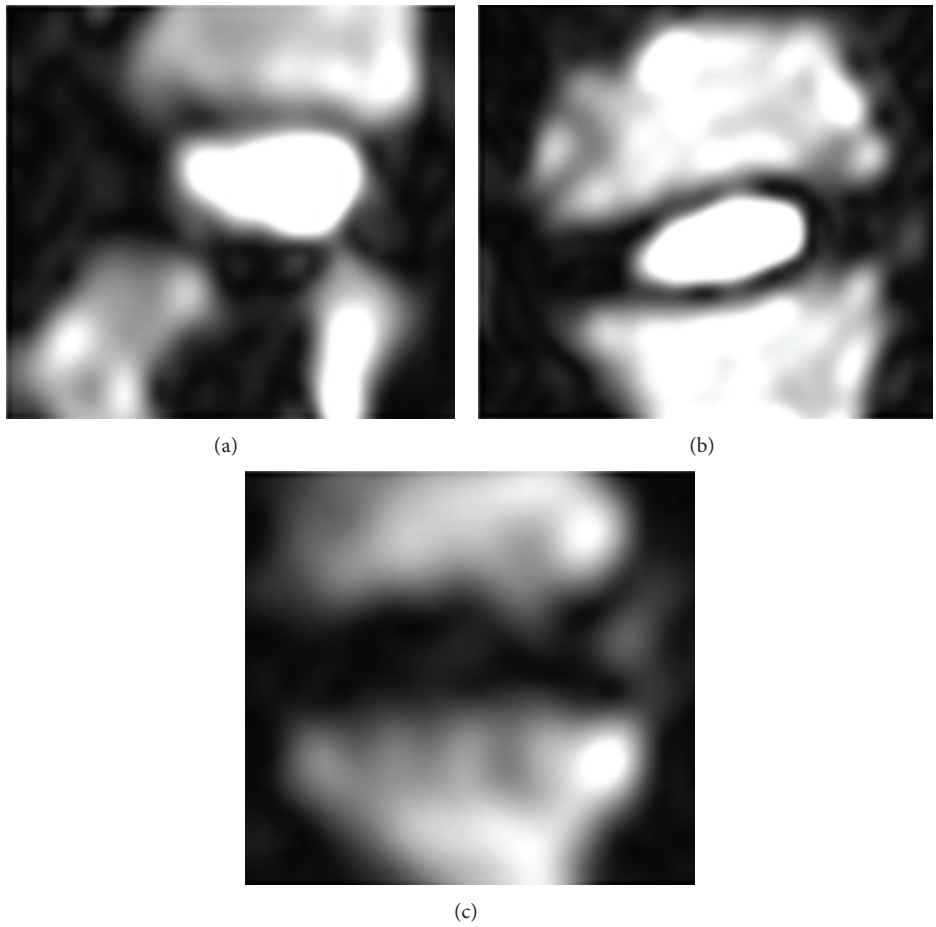

Figure 1: MRI examining of bone-disc-bone specimens. (a) The discectomied discs injected with hydrogel (mimic group). (b) The normal discs (normal groups). (c) The discectomied discs (control group).

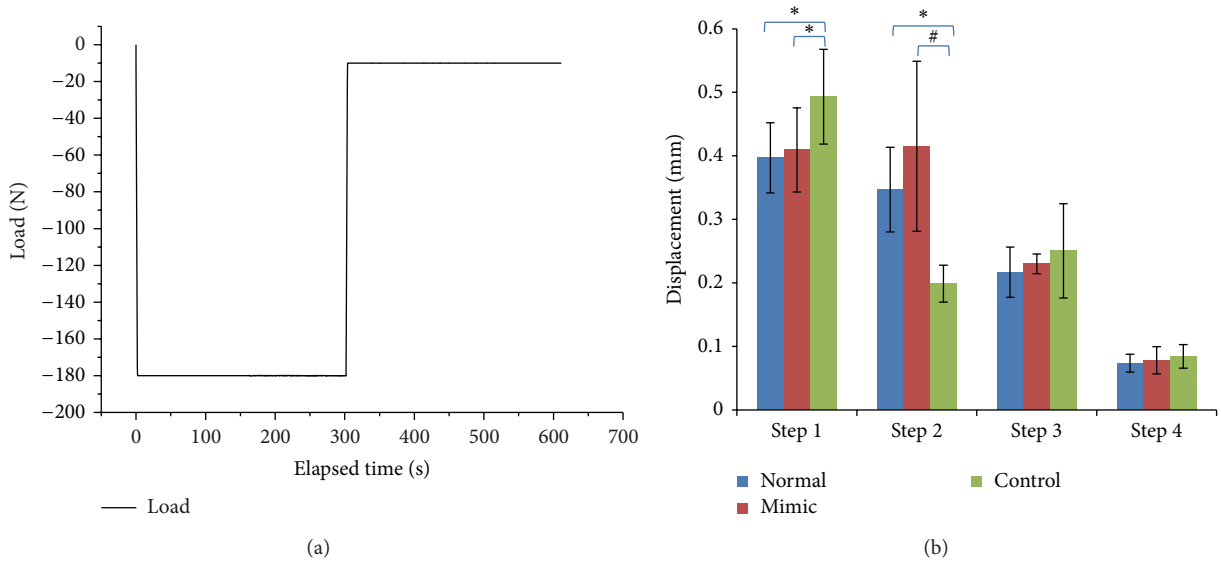

Figure 2: (a) Procedures of the static compression test. (b) Displacement in each step of different groups in the static compression test ($^{*}P < 0.05$, $^{\#}P < 0.01$).

in the control group exhibited significantly more displacement compared with the other two groups ($P < 0.05$), while there was no significant difference between the normal group and the mimic group ($P > 0.05$). In step 2, all specimens were continuously kept 180 N compressed for 5 minutes and values of displacement in the normal group and in the mimic group were significantly higher than those in the control group ($P < 0.01$ and $P < 0.05$, resp.), while there was not any significant difference between the normal group and the mimic group ($P > 0.05$). However, either in step 3 when the load decreased from 180 N to 10 N in 2 seconds or in step 4 when 10 N was kept to the end of test, no significant difference was found between any two groups ($P > 0.05$).

In the dynamic compression test, series of mechanical parameters were received and we chose storage modulus, loss modulus, and tanδ (δ represents phase angle) to analyze the viscoelasticity of specimens [19]. The storage modulus, loss modulus, and tanδ were mainly determined by both the materials per se and the frequency. Values of each parameter at 11 selected frequencies ranging from 0.5 HZ to 5.5 HZ were exhibited as curve graphs (Figure 3). As shown, values of the loss modulus were much lower than those of storage modulus in all groups. With frequency increasing, the storage modulus increased significantly ($P < 0.01$), and both the loss modulus and the tanδ decreased significantly ($P < 0.01$). The storage modulus, as well as the loss modulus and tanδ in the control group, was significantly higher than the other two groups ($P < 0.01$). The mimic group exhibited similar storage modulus and tanδ with the normal group ($P > 0.05$), while the loss modulus in the mimic group was significantly higher than the normal group ($P < 0.05$).

4. Discussion

The nucleus pulposus of the intervertebral disc could cushion and distribute the compression load to the surrounding annulus fibrosus under circumferential tension [4, 20]. Discectomy, the current surgical procedure to cut the nucleus pulposus off, often leads to disc dysfunctions. The development of the nucleus replacement could provide a promising way to break through the present clinical limitations. We compared the biomechanical properties among the normal discs (normal groups), the denucleated discs (control group), and the denucleated discs with hydrogel injection (mimic group). We found that the hydrogel injection in the mimic group could almost restore shock absorbing function of the discs.

How to restore the disc biomechanical properties of the degenerative disc has been always the focus in the study of the degenerative lumbar spine. Eyholzer et al. synthesized one kind of photoreactive nanomaterials, which could mimic the swelling and mechanical behavior of the native human nucleus pulposus [21]. Vernengo et al. verified that poly(N-isopropylacrylamide) could improve elasticity and meet the minimum stiffness of 50 kPa for the restoration of intervertebral disc stiffness in the presence of a small amount of poly(ethylene)glycol dimethacrylate [22]. However, these studies only tested the mechanical properties of nucleus and biomaterials, while these materials were not injected into the intervertebral space for mechanical test to evaluate how the disc biomechanical properties improved.

Using porcine spinal motion segments, Balkovec et al. showed that the injectable hydrogel is able to restore the height of the intervertebral space, angular stiffness to cyclically fatigued spinal motion segments [12]. Through thirteen human cadaver lumbar anterior column units, Cannella et al. [23] found that intervertebral disc instability, evidenced by increased neutral zone and ranges of motion, associated with degeneration, can be restored by volume filling of the nucleus pulposus using a synthetic hydrogel. However, no study investigated whether the hydrogel could rebuild the shock absorbing function of the disc. In the present study, we verified that the hydrogel could restore shock absorbing function of denucleated intervertebral discs through static and dynamic biomechanical tests.

Viscoelastic behavior is the most important biomechanical characteristic of the nucleus pulposus, especially for its shock absorbing function [24–26]. As it is acknowledged, the storage modulus, loss modulus, and tanδ are important parameters in evaluating viscoelasticity of tissues and biomaterials. The storage modulus reflects the elasticity, the loss modulus reflects the viscosity, and tanδ, the ratio of the storage and loss modulus, presents the mathematical description of the dynamic experiment under strains within a sample's range of viscoelasticity [19, 27]. When the compression loads on the disc, the viscoelasticity enables the disc to absorb the energy and dissipate to surrounding tissue via shape changes. After the loading disappears, the viscoelasticity enables the disc to release energy and dissipate to surrounding tissue via recovery of shape. Therefore, the disc plays an important role in shock absorbing. In this study, the three parameters were obtained via dynamic compression test and analyzed comprehensively to evaluate the alterations in viscoelasticity of the disc with or without hydrogel injection after nucleus discectomy.

The storage modulus of specimens in the control group was statistically greater than those in the normal group ($P < 0.01$) and mimic group ($P < 0.01$), revealing that discs got stiffer after discectomy while hydrogels injection was conductive to restore the disc normal elasticity. Similarly, the loss modulus was significantly greater in the control group than in the other two groups ($P < 0.01$), suggesting that discectomy caused the disc to be more viscous and hydrogel injection could largely alter the viscosity though it was still statistically greater than the normal group ($P < 0.05$). It is acknowledged that the storage modulus and loss modulus are closely related with material properties, procession conditions, and even molecular structure. Annulus fibrosus contains more collagen fiber while nucleus pulposus is richer in proteoglycan [4, 5]. What is more, it has been proved that their viscoelastic properties showed obvious difference. Results in this study were in line with Freeman et al.' study [28]. It was found that annulus and fibrous had similar storage modulus and loss modulus, which were greater than the nucleus. Interestingly, it was demonstrated that the whole disc dynamic shear moduli was increased with aging and degeneration and the observed increase was

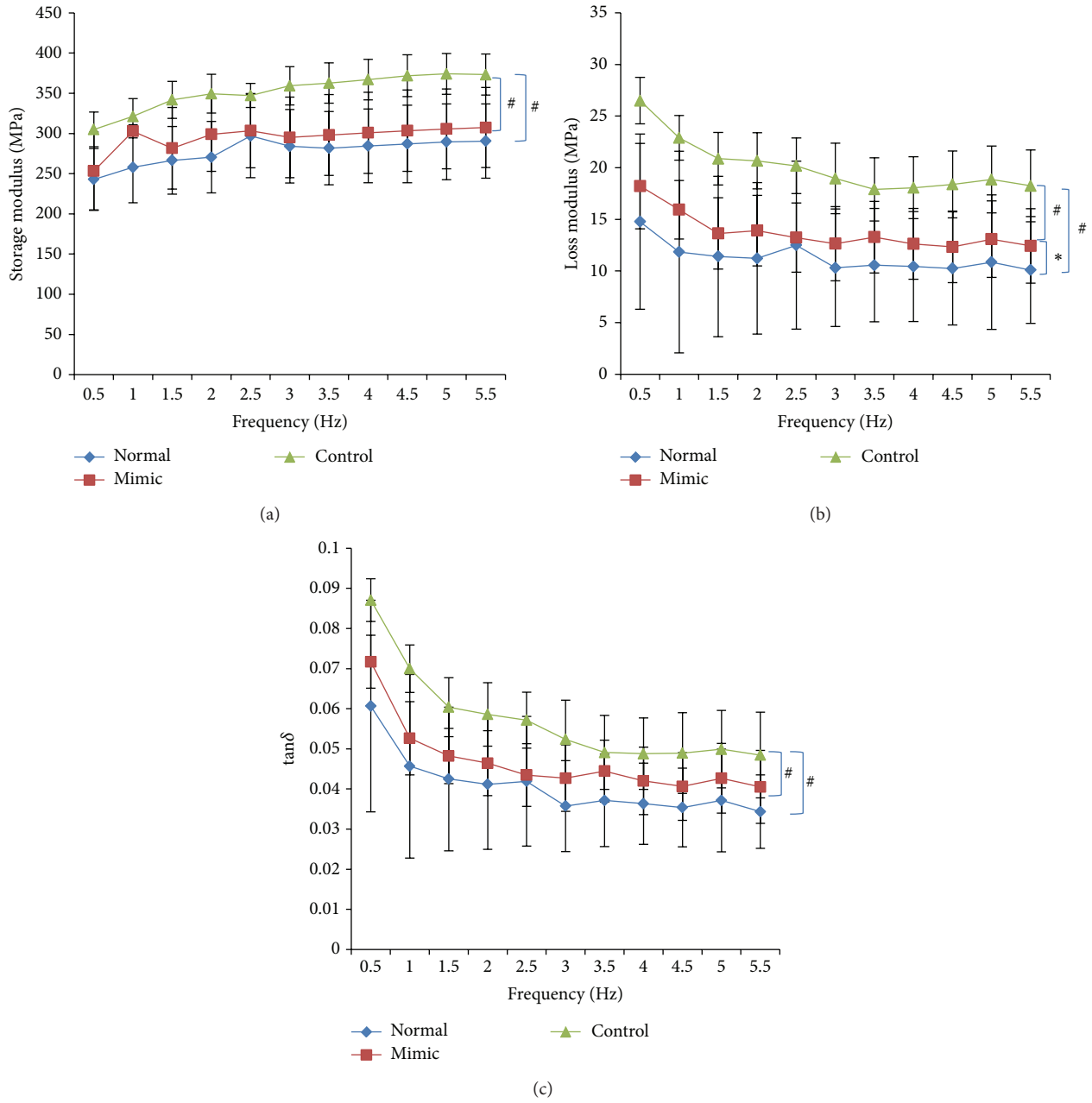

FIGURE 3: Results of the dynamic compression test. With the frequency increasing, the storage modulus increased significantly ($P < 0.01$) and both the loss modulus and tanδ decreased significantly ($P < 0.01$). (a) Storage modulus of control group was significantly higher than the other two groups ($P < 0.01$). (b) Loss modulus of control group was significantly higher than the other two groups ($P < 0.01$). (c) tanδ of control group was significantly higher than the other two groups ($P < 0.01$).

coincident with increased fibrotic tissue [8]. Nevertheless, the annulus fibrosus changes the mode of motion after discectomy, which would also alter the disc storage and loss modulus [29, 30]. Above all, we firstly illustrate how the dynamic compressive moduli of the whole disc changed after discectomy and whether hydrogel injection could restore the normal properties.

Figure 3(c) showed that tanδ was statistically greater in the control group compared with the other two groups ($P < 0.01$), while it was similar between the mimic group and normal group ($P > 0.05$), suggesting that hydrogel injection contributed in improving the viscoelasticity. tanδ equals the ratio between the storage modulus and the loss modulus. Specimens in the control group possessed greater tanδ, suggesting that they were more elastic and less viscous [28]. Furthermore, tanδ, the lag between the displacement and the load, could be interpreted as the ratio between the energy dissipated and the energy stored, which is mainly involved in the shocks absorbing function of the disc.

It is evident in MRI images (Figure 1) that the intervertebral space in the control group was filled with air after dicectomy. Therefore, in the first step of the static compression test,

displacement in the control group was larger than those in the other two groups because air in specimens of the control group was easily compressed. This result demonstrated that hydrogel injection was helpful to recover the response to rapid compression. In step 2, 180 N was continuously loaded for 5 minutes and specimens in the control group showed less displacement than those in the other two groups, which demonstrated that they were harder to be compressed. Hydrogel injection reversed the situation. Normal nucleus pulposus is viscoelastic, transmitting compression load to surrounding annulus fibrosus and maintaining the normal biomechanical properties [5, 20]. After discectomy, there was only annulus fibrosus left to support compression load, so that inner boundaries moved inwards while outer boundaries moved outwards after nucleus discectomy [29, 30]. Though there have been no investigations comparing the viscoelastic properties of the annulus fibrosus and the normal disc, it has been reported that the annulus fibrosus possessed larger modulus than the nucleus pulposus [19, 31, 32], which made the annulus fibrosus harder to compress. It is suggested that the alterations of both disc response to load and the viscoelasticity resulted in specimens that were harder compressed after discectomy. The results were coincident with those of the dynamic compression test.

The integrity of intervertebral disc is necessary for the effective disc functions [33]. These functions are highly dependent upon the integrity of the annulus fibrosus and endplates. Therefore, even though it is much easier to measure the biomechanical function of nucleus pulposus alone [19], we have established this study using bone-disc-bone specimens [4, 34, 35]. The results showed not only the effective role of the artificial nucleus pulposus, but also the possible adverse events associated with the discectomy.

One of limitations in this study was the loading on the samples lower than other studies (about 300–500 N). It is because the vertebras in this study came from the minipig (weighted about 25 kg), which weighted much lower than normal adult. Therefore, we chose 150~180 N in this study to avoid broking of the vertebras and annulus fibrosus. Another limitation in this study was that the samples came from minipigs, whose discs are a little different from human discs. However, the bone-disc-bone specimens, which possess the integrity of the endplates, annulus fibrosus, and nucleus pulposus, could satisfy the requirement of a biomechanical study [12].

5. Conclusion

In conclusion, discectomy greatly alters the biomechanical function of the disc, especially shock absorbing. On the other hand, hydrogel injection could largely restore the biomechanical function including shock absorbing, which is a promising clinical treatment in the future.

Conflict of Interests

The authors declare that there is no conflict of interests regarding the publication of this paper.

Authors' Contribution

Zhiyu Zhou, Manman Gao, and Fuxin Wei contributed equally to this work.

Acknowledgments

This study was supported by National Basic Research Program of China (973 Program, nos. 2012CB619105), China Postdoctoral Science Foundation (2013M531876), National Natural Science Foundation of China (nos. u0732001, 81071512, and u1032001), Research Fund for the Doctoral Program of Higher Education of China (no. 20100171110054), Science and Technology Planning Project of Guangdong Province (2010B010800019), Science and Technology Planning Project of Dongguan (20101051503501), and Shenzhen High-Tech Development Project (CXZZ20130516103012168).

References

[1] S. Sen, N. T. Jacobs, J. I. Boxberger, and D. M. Elliott, "Human annulus fibrosus dynamic tensile modulus increases with degeneration," *Mechanics of Materials*, vol. 44, pp. 93–98, 2012.

[2] J. C. Salvatierra, T. Y. Yuan, H. Fernando et al., "Difference in energy metabolism of annulus fibrosus and nucleus pulposus cells of the intervertebral disc," *Cellular and Molecular Bioengineering*, vol. 4, no. 2, pp. 302–310, 2011.

[3] F. Marchand and A. M. Ahmed, "Investigation of the laminate structure of lumbar disc anulus fibrosus," *Spine*, vol. 15, no. 5, pp. 402–410, 1990.

[4] N. R. Malhotra, W. M. Han, J. Beckstein, J. Cloyd, W. Chen, and D. M. Elliott, "An injectable nucleus pulposus implant restores compressive range of motion in the ovine disc," *Spine*, vol. 37, no. 18, pp. E1099–E1105, 2012.

[5] J. C. Iatridis, M. Weidenbaum, L. A. Setton, and C. V. Mow, "Is the nucleus pulposus a solid or a fluid? Mechanical behaviors of the nucleus pulposus of the human intervertebral disc," *Spine*, vol. 21, no. 10, pp. 1174–1184, 1996.

[6] J. E. Schroeder, J. R. Dettori, E. D. Brodt, and L. Kaplan, "Disc degeneration after disc herniation: are we accelerating the process?" *Evidence-Based Spine-Care Journal*, vol. 3, no. 4, pp. 33–40, 2012.

[7] M. Krismer and M. van Tulder, "Low back pain (non-specific)," *Best Practice and Research: Clinical Rheumatology*, vol. 21, no. 1, pp. 77–91, 2007.

[8] J. C. Iatridis, L. A. Setton, M. Weidenbaum, and V. C. Mow, "Alterations in the mechanical behavior of the human lumbar nucleus pulposus with degeneration and aging," *Journal of Orthopaedic Research*, vol. 15, no. 2, pp. 318–322, 1997.

[9] Q.-B. Bao, G. M. McCullen, P. A. Higham, J. H. Dumbleton, and H. A. Yuan, "The artificial disc: theory, design and materials," *Biomaterials*, vol. 17, no. 12, pp. 1157–1167, 1996.

[10] L. M. Boyd and A. J. Carter, "Injectable biomaterials and vertebral endplate treatment for repair and regeneration of the intervertebral disc," *European Spine Journal*, vol. 15, supplement 3, pp. S414–S421, 2006.

[11] P. M. Klara and C. D. Ray, "Artificial nucleus replacement: clinical experience," *Spine*, vol. 27, no. 12, pp. 1374–1377, 2002.

[12] C. Balkovec, J. Vernengo, and S. M. McGill, "The use of a novel injectable hydrogel nucleus pulposus replacement in restoring

the mechanical properties of cyclically fatigued porcine intervertebral discs," *Journal of Biomechanical Engineering*, vol. 135, no. 6, Article ID 061004-1, 2013.

[13] A. E. Leckie, M. K. Akens, K. A. Woodhouse, A. J. M. Yee, and C. M. Whyne, "Evaluation of thiol-modified hyaluronan and elastin-like polypeptide composite augmentation in early-stage disc degeneration: comparing 2 minimally invasive techniques," *Spine*, vol. 37, no. 20, pp. E1296–E1303, 2012.

[14] A. Gloria, A. Borzacchiello, F. Causa, and L. Ambrosio, "Rheological characterization of hyaluronic acid derivatives as injectable materials toward nucleus pulposus regeneration," *Journal of Biomaterials Applications*, vol. 26, no. 6, pp. 745–759, 2012.

[15] L. Calderon, E. Collin, D. Velasco-Bayon, M. Murphy, D. O'Halloran, and A. Pandit, "Type II collagen-hyaluronan hydrogel—a step towards a scaffold for intervertebral disc tissue engineering," *European Cells and Materials*, vol. 20, pp. 134–148, 2010.

[16] X. Z. Shu, Y. Liu, Y. Luo, M. C. Roberts, and G. D. Prestwich, "Disulfide cross-linked hyaluronan hydrogels," *Biomacromolecules*, vol. 3, no. 6, pp. 1304–1311, 2002.

[17] G. M. Jensen, "Biomechanics of the lumbar intervertebral disk: a review," *Physical Therapy*, vol. 60, no. 6, pp. 765–773, 1980.

[18] G. D. O'Connell, E. J. Vresilovic, and D. M. Elliott, "Comparison of animals used in disc research to human lumbar disc geometry," *Spine*, vol. 32, no. 3, pp. 328–333, 2007.

[19] J. C. Leahy and D. W. L. Hukins, "Viscoelastic properties of the nucleus pulposus of the intervertebral disk in compression," *Journal of Materials Science: Materials in Medicine*, vol. 12, no. 8, pp. 689–692, 2001.

[20] S. R. S. Bibby, D. A. Jones, R. B. Lee, J. Yu, and J. P. G. Urban, "The pathophysiology of the intervertebral disc," *Joint Bone Spine*, vol. 68, no. 6, pp. 537–542, 2001.

[21] C. Eyholzer, A. B. de Couraça, F. Duc et al., "Biocomposite hydrogels with carboxymethylated, nanofibrillated cellulose powder for replacement of the nucleus pulposus," *Biomacromolecules*, vol. 12, no. 5, pp. 1419–1427, 2011.

[22] J. Vernengo, G. W. Fussell, N. G. Smith, and A. M. Lowman, "Evaluation of novel injectable hydrogels for nucleus pulposus replacement," *Journal of Biomedical Materials Research B: Applied Biomaterials*, vol. 84, no. 1, pp. 64–69, 2008.

[23] M. Cannella, J. Isaacs, S. Allen, A. Orana, E. Vresilovic, and M. Marcolongo, "Nucleus implantation: the biomechanics of augmentation versus replacement with varying degrees of nucleotomy," *Journal of Biomechanical Engineering*, 2014.

[24] L.-C. Lin, T. P. Hedman, S.-J. Wang, M. Huoh, and S.-Y. Chuang, "The analysis of axisymmetric viscoelasticity, time-dependent recovery, and hydration in rat tail intervertebral discs by radial compression test," *Journal of Applied Biomechanics*, vol. 25, no. 2, pp. 133–139, 2009.

[25] J. Wendlová, "Chondrosis of the disc—risk factor for osteoporotic vertebral fractures (biomechanical analysis)," *Wiener Medizinische Wochenschrift*, vol. 160, no. 17-18, pp. 464–469, 2010.

[26] K. Masuoka, A. J. Michalek, J. J. MacLean, I. A. F. Stokes, and J. C. Iatridis, "Different effects of static versus cyclic compressive loading on rat intervertebral disc height and water loss in vitro," *Spine*, vol. 32, no. 18, pp. 1974–1979, 2007.

[27] A. B. Bashaiwoldu, F. Podczeck, and J. M. Newton, "Application of dynamic mechanical analysis (DMA) to determine the mechanical properties of pellets," *International Journal of Pharmaceutics*, vol. 269, no. 2, pp. 329–342, 2004.

[28] A. L. Freeman, G. R. Buttermann, B. P. Beaubien, and W. E. Rochefort, "Compressive properties of fibrous repair tissue compared to nucleus and annulus," *Journal of Biomechanics*, vol. 46, no. 10, pp. 1714–1721, 2013.

[29] J. R. Meakin and D. W. L. Hukins, "Effect of removing the nucleus pulposus on the deformation of the annulus fibrosus during compression of the intervertebral disc," *Journal of Biomechanics*, vol. 33, no. 5, pp. 575–580, 2000.

[30] J. R. Meakin, T. W. Redpath, and D. W. L. Hukins, "The effect of partial removal of the nucleus pulposus from the intervertebral disc on the response of the human annulus fibrosus to compression," *Clinical Biomechanics*, vol. 16, no. 2, pp. 121–128, 2001.

[31] D. Périé, D. Korda, and J. C. Iatridis, "Confined compression experiments on bovine nucleus pulposus and annulus fibrosus: sensitivity of the experiment in the determination of compressive modulus and hydraulic permeability," *Journal of Biomechanics*, vol. 38, no. 11, pp. 2164–2171, 2005.

[32] J. J. Roberts, A. Earnshaw, V. L. Ferguson, and S. J. Bryant, "Comparative study of the viscoelastic mechanical behavior of agarose and poly(ethylene glycol) hydrogels," *Journal of Biomedical Materials Research B: Applied Biomaterials*, vol. 99, no. 1, pp. 158–169, 2011.

[33] J. C. Iatridis, S. B. Nicoll, A. J. Michalek, B. A. Walter, and M. S. Gupta, "Role of biomechanics in intervertebral disc degeneration and regenerative therapies: what needs repairing in the disc and what are promising biomaterials for its repair?" *Spine Journal*, vol. 13, no. 3, pp. 243–262, 2013.

[34] W. Johannessen, J. M. Cloyd, G. D. O'Connell, E. J. Vresilovic, and D. M. Elliott, "Trans-endplate nucleotomy increases deformation and creep response in axial loading," *Annals of Biomedical Engineering*, vol. 34, no. 4, pp. 687–696, 2006.

[35] W. Johannessen, E. J. Vresilovic, A. C. Wright, and D. M. Elliott, "Intervertebral disc mechanics are restored following cyclic loading and unloaded recovery," *Annals of Biomedical Engineering*, vol. 32, no. 1, pp. 70–76, 2004.

Hindawi Publishing Corporation
BioMed Research International
Volume 2014, Article ID 436325, 7 pages
http://dx.doi.org/10.1155/2014/436325

Research Article

Construction and Biomechanical Properties of PolyAxial Self-Locking Anatomical Plate Based on the Geometry of Distal Tibia

Weiguo Liang,[1] Weixiong Ye,[1] Dongping Ye,[1,2] Ziqiang Zhou,[1] Zhiguang Chen,[1] Aiguo Li,[1] Zong-Han Xie,[3] Lihai Zhang,[4] and Jiake Xu[1,2]

[1] *Guangzhou Institute of Traumatic Surgery, Guangzhou Red Cross Hospital, Medical College, Jinan University, Guangzhou 510220, China*
[2] *School of Pathology and Laboratory Medicine, The University of Western Australia, Crawley, WA 6009, Australia*
[3] *School of Mechanical Engineering, University of Adelaide, SA 5005, Australia*
[4] *Department of Infrastructure Engineering, The University of Melbourne, VIC 3010, Australia*

Correspondence should be addressed to Weiguo Liang; liangweiguo1011@126.com and Jiake Xu; jiake.xu@uwa.edu.au

Received 4 February 2014; Accepted 24 May 2014; Published 16 June 2014

Academic Editor: Jiang Chang

In order to provide scientific and empirical evidence for the clinical application of the polyaxial self-locking anatomical plate, 80 human tibias from healthy adults were scanned by spiral CT and their three-dimensional images were reconstructed using the surface shaded display (SSD) method. Firstly, based on the geometric data of distal tibia, a polyaxial self-locking anatomical plate for distal tibia was designed and constructed. Biomechanical tests were then performed by applying axial loading, 4-point bending, and axial torsion loading on the fracture fixation models of fresh cadaver tibias. Our results showed that variation in twisting angles of lateral tibia surface was found in various segments of the distal tibia. The polyaxial self-locking anatomical plate was constructed based on the geometry of the distal tibia. Compared to the conventional anatomical locking plate, the polyaxial self-locking anatomical plate of the distal tibia provides a better fit to the geometry of the distal tibia of the domestic population, and the insertion angle of locking screws can be regulated up to 30°. Collectively, this study assesses the geometry of the distal tibia and provides variable locking screw trajectory to improve screw-plate stability through the design of a polyaxial self-locking anatomical plate.

1. Introduction

The anatomical plate is an ideal internal fixation treatment for distal tibia fractures [1]. Since the distal tibia has a forward twisting transition anatomy, it is important to match the anatomical plate with the proper geometric structure of the distal tibia [2]. In order to provide anatomical information for the design of the anatomical plate of distal tibias for the domestic population in Southern China, it is of crucial importance to study morphologic characteristics of the distal tibia [3]. The distal tibia is close to the ankle joint with special anatomical morphology and a poor soft tissue envelope. Effective treatment of fractures in this special region remains a challenge to orthopaedic surgeons [4]. In recent years, the use of an anatomical locking plate for the treatment of distal tibia fractures has been widely reported with satisfactory results [5]. However, in the first generation of locking plates currently available, screw insertion angles are predetermined by manufacturers and are not able to be adjusted during instrumentation [6]. In order to make the plate better suited to the tibia geometry of Chinese people and to provide variable locking screw trajectory to improve screw-plate stability, we have designed a polyaxial self-locking anatomical plate for the distal tibia and performed biomechanical tests on cadaver fracture models.

2. Methods

2.1. Morphological Study of the Distal Tibia with Spiral CT. 80 human tibia bones from healthy adults (38 male, aged

Table 1: GE Hispeed ZX/i scanner configuration used in this study.

Parameter	Value
Position	Full-length of tibia
Method	Through horizontal surface
Layer distance	2 mm
Show vision	204
Tube voltage	120 kV
Elective current	240 mA

from 20 to 70 years; 42 female, aged from 23 to 68 years) were scanned using spiral CT, and three-dimensional images were reconstructed using the surface shaded display (SSD) method. GE Hispeed ZX/i scanning was performed using the configuration shown in Table 1.

Three-dimensional reconstruction of tibia geometry was performed using a GE ADW4.0 Image workstation. Three anatomical indices (i.e., the length of twisting segment on the lateral surface of the tibia, twisting angles on different twisting segments, and the anteversion angle of the lateral surface of the tibia) were measured in the three-dimensional images by the GE ADW4.0 Image workstation. Because there was a different torsion angle on the outer surface of the tibia, in order to understand the torsion angle changes, we divided the twist section into four equal parts, that is, first twisting section, second twisting section, third twisting section, and fourth twisting section. The measured indices were then statistically analyzed using SPSS 12.0 statistical analysis software with T-test, ANOVA test and correlation analysis test. There was no history of trauma, surgery, or skeletal disorders in any of the individuals involved in this study.

2.2. Design of Polyaxial Self-Locking Anatomical Plate. The polyaxial self-locking anatomical plate for distal tibia was designed according to the morphologic characteristics of distal tibiae of the Chinese people. This design was granted a practical Patent by the Patent Bureau of China (number 201020525718.X). The plates are made from titanium alloy and were manufactured by Trauson Medical Instrument Company (Jiangsu, China).

2.3. Biomechanical Testing of the Polyaxial Self-Locking Anatomical Plate. Paired fresh cadaver tibiae were used to make fracture fixation models. Each pair of tibiae was examined radiographically to rule out any relevant pathological changes. Both ends of the tibia were potted in polymethylmethacrylate (PMMA) after explantation of soft tissues, during which normal saline was sprayed to keep the specimens moist. Each bone specimen was wrapped in a double layer plastic bag and stored at −20°C. Before instrumentation and biomechanical testing, each frozen bone was thawed at room temperature.

All paired cadaver tibiae from left and right tibiae were randomly distributed into two groups with six pairs in each group, and the conventional anatomical locking plates and polyaxial self-locking anatomical plates with 9 holes were applied in each group, respectively. For polyaxial self-locking anatomical plates, three locking screws were inserted into the three separated most proximal polyaxial holes on the plate to fix the proximal fracture segment while another three locking screws were inserted into the three most distal polyaxial holes to fix the distal fracture segment with the screw trajectories being regulated far from the fracture line. For conventional anatomical locking plates, six locking screws were inserted into the corresponding holes on the plate to fix the fracture segments, respectively. Osteotomies were performed to produce a highly unstable type-A fracture with the implant alone transferring all loads. The osteotomy levels were designed at the transition of segments 42 and 43 according to AO classification and 10 mm above it to create a 10 mm sized bone defect.

The biomechanical testing was conducted using the 858 Mini Bionix testing machine. For the axial loading test, a maximum of 500 N was loaded at a rate of 5 N/s on the point 10 mm mediodorsally to the intercondylar eminence. In 4-point bending test, a maximum of 300 N was loaded at a rate of 5 N/s with 4 cm loading distance and 12 cm pivot distance. To assess axial torsion loading, a maximum of 5 Nm was loaded at a rate of 0.1°/s. The constructs were preloaded to 10% of the maximum load before every test to rule out error caused by creep deformation.

2.4. Statistical Analysis of Data. Statistical analyses were performed using SPSS 12.0 statistical analysis software with t-test and ANOVA test.

3. Results

In order to obtain precise geometrical measurement of the distal tibia in individuals in Southern China, 80 healthy adults were examined using three-dimensional spiral CT. Three parameters were collected as illustrated in Figure 1 including twisting length and twisting angles from the first, second, third and fourth quarters. The length of the twisting segment of the lateral tibia surface was determined to be 12.9±0.41 cm in males and 12.34 ± 0.31 cm in females (Figure 1(c)). The twisting angle of the lateral surface of the tibia was determined to be as follows (Figure 1(d)): (1) in the first quarter, the twisting angle of the lateral tibia surface was 13.98 ± 2.72° in males and 13.38±3.11° in females; (2) in the second quarter, it was 32.49±3.66° in males and 31.85±3.86° in females; (3) in the third quarter, it was 55.18±3.53° in males and 50.95±6.24° in females; and (4) in the fourth quarter, it was 82.13±2.89° in males and 72.45 ± 4.81° in females. The anteversion angle of the lateral surface of the distal tibia was 7.34 ± 0.91° in males and 6.20±0.41° in females, respectively (Figure 1(d)). Among all the measurements, the twisting angles of the third and fourth quarters and the anteversion angle were statistically significant between the males and females (P value <0.05) (Figure 1(d)). In addition, it can be seen that there is a strong correlation between the third twisting angle and the age of individuals (P value <0.01) (Figure 2(a)). Further, the twisting length, the 3rd and 4th twisting angles, and the anteversion angle were statistically significantly and correlated to the height of individuals with a P value <0.01; <0.01; <0.01; and <0.05, respectively (Figure 2(b)).

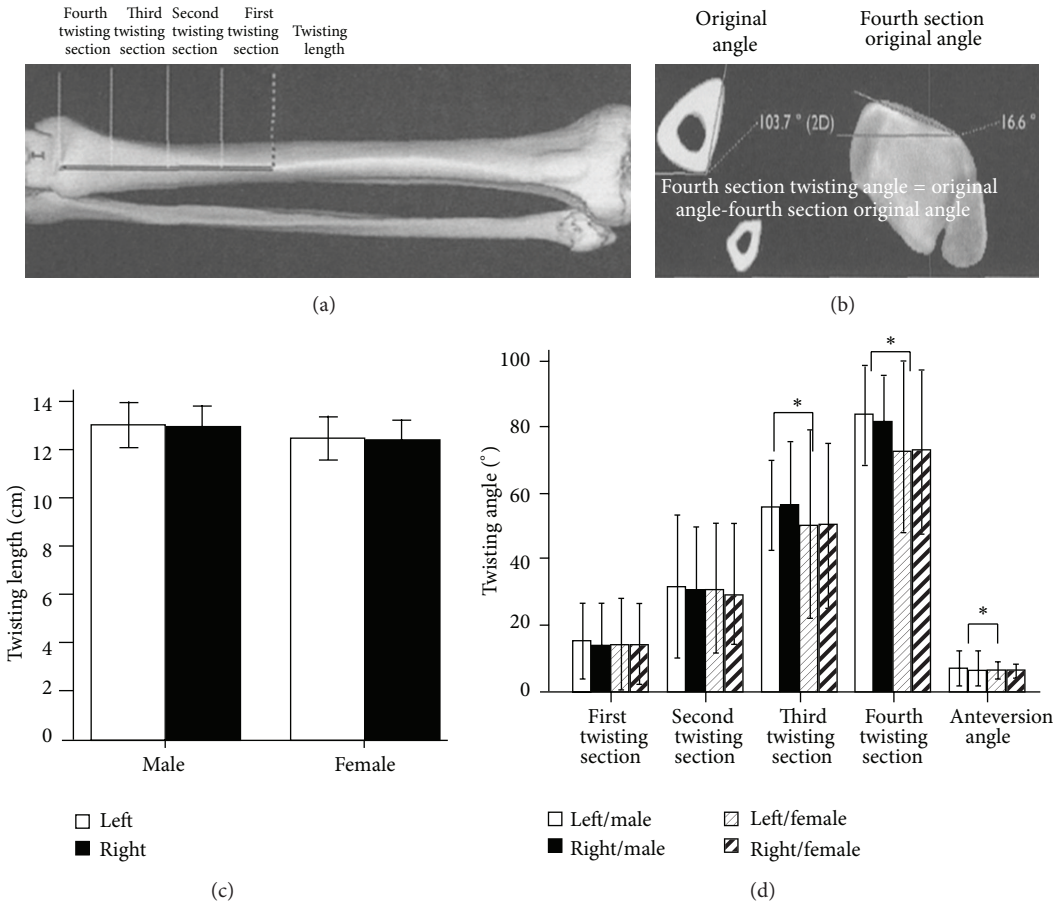

Figure 1: (a) The measurement of tibia anatomic lengths by spiral CT scanning. The torsion section was divided into four equal parts and the outer side torsion angle was measured individually in these four parts. (b) Measurement of the tibia twisting angle by CT scanner. (c) The length of the twisting segment of the lateral tibia surface, the twisting angle of the lateral surface of tibia in the first quarter, the second quarter, the third quarter, and the fourth quarter as well as the anteversion angle of the lateral surface of distal tibia were measured both in male and female individuals.

Based on the data collected, the polyaxial self-locking anatomical plate was designed in a spoon-like shape with a flared distal part and a long-stem proximal segment (Figure 3). The distal segment of the plate twists anterior with the largest twisting angle being 80° and a 12 cm long twisting segment. Three polyaxial locking holes are located at distal part of the plate and are distributed triangularly. In the proximal stem part of the plate, polyaxial locking holes are distributed separately to each other with conventional anatomical locking holes. The top view of the polyaxial hole is a round shape whilst the cross section of the polyaxial hole is concave tympaniform, allowing the polyaxial self-locking bushing to be rotated laterally within it to a maximum of 5°.

The polyaxial self-locking bushing is situated within the polyaxial hole, which is round shaped from the top view with a C-shaped defect (Figure 3(c)). On the obverse surface of the bushing, there are three triangularly distributed small concaves which are separated 90° from the C-shaped defect. A cross sectional view of the polyaxial self-locking bushing shows that it is bucket-shaped with a polished outer surface and threaded inner surface. The inner axis is intersected with the outer axis at 10°. The polyaxial bushing is clasped by the upper and lower outlets of the polyaxial hole and fits precisely with the inner surface of the polyaxial hole. The C-shaped defect of the polyaxial bushing and the three concaves on its obverse surface fit precisely with the four dental processes on the tip of the polyaxial regulating sleeve which drives the rotation of polyaxial bushing in the polyaxial hole to regulate the locking angle of the screw. Once the locking screw is tightened, the polyaxial self-locking bushing is expanded and fits tightly with the concave surface of the polyaxial hole so that strong friction is produced, fixing the locking angle with the screw. The polyaxial bushing can be laterally rotated up to 5°, which together with the 10° eccentric angle of its inner thread axis can increase angular regulation amplitude for the locking screw up to 30°.

The polyaxial self-locking anatomical plate provides a better fit to the geometry of the distal tibia when compared with the conventional anatomical locking plate as it can increase the angular regulation amplitude for the locking screw up to 30°. However, there was no statistical significance in the mechanical properties between the polyaxial self-locking anatomical plate and the conventional anatomical locking plate. For example, compression stiffness of the

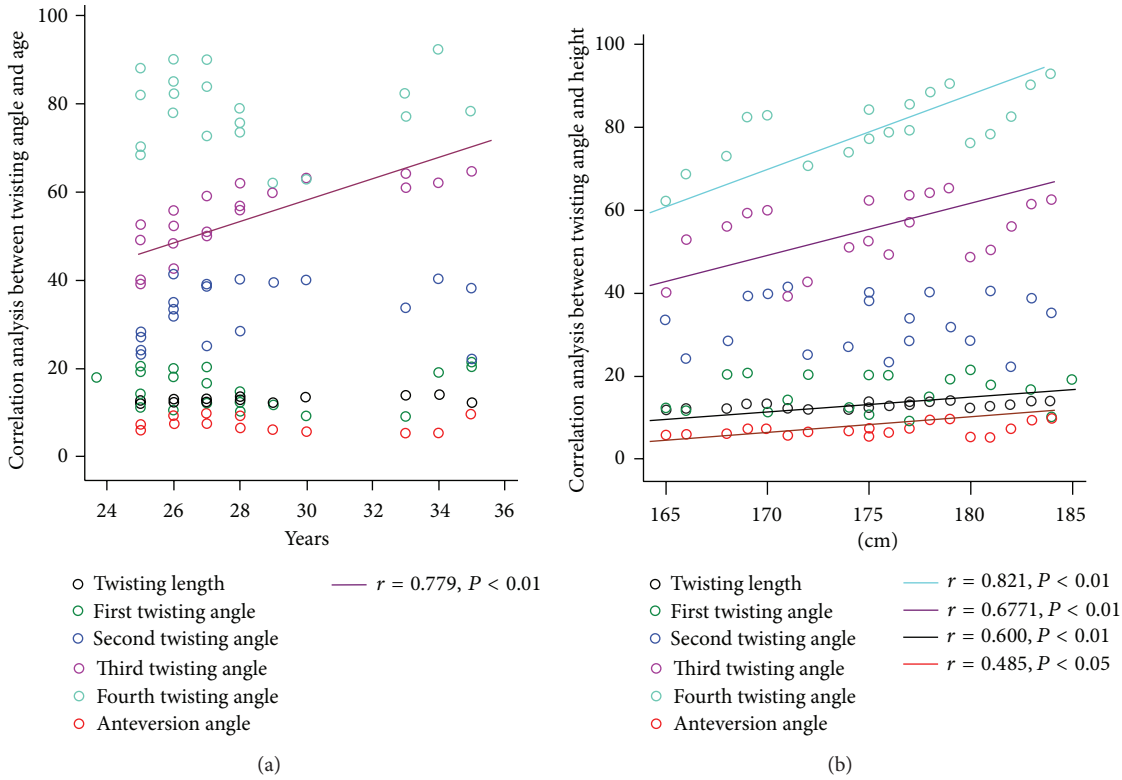

Figure 2: Correlation analyses between twisting angle and the age of individuals (a) and between twisting angle and the height of individuals (b).

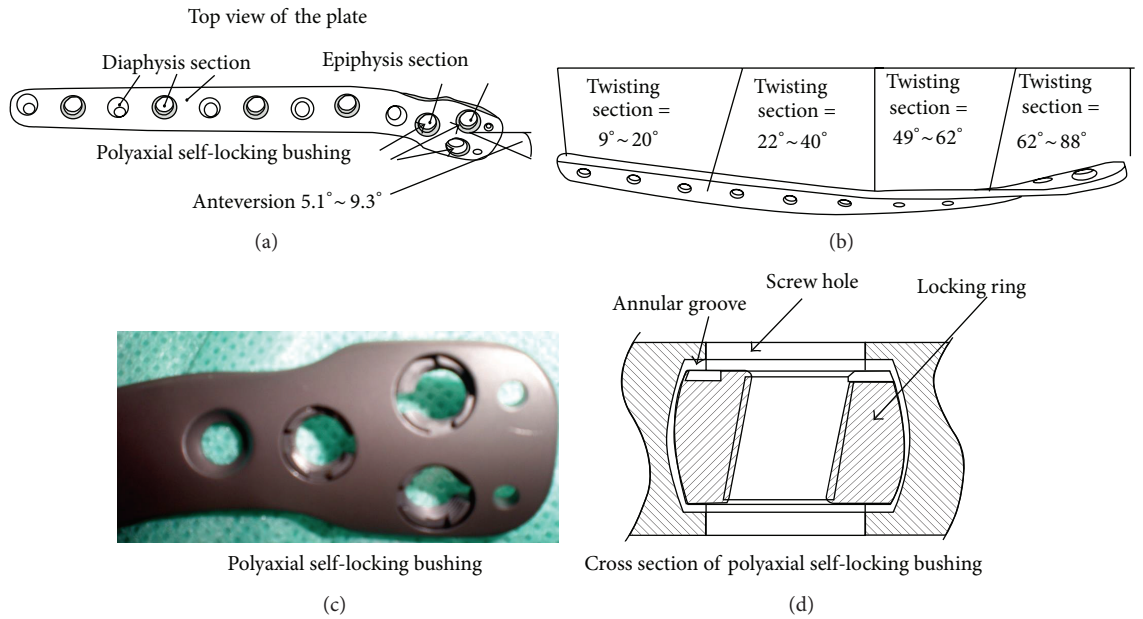

Figure 3: (a)-(b) Design of polyaxial self-locking anatomical plate, anteversion, 5.1° ~9.3°; twisting section, 9°~20°; twisting section, 22°~40°; twisting section, 49°~62°; twisting section, 62°~88°. (c) The polyaxial self-locking bushing is situated within the polyaxial hole, which is round shaped from the top view with a C-shaped defect. On the obverse surface of the bushing, there are three triangularly distributed small concaves. (d) A cross sectional view of the polyaxial self-locking bushing shows that it is bucket-shaped with a polished outer surface and threaded inner surface.

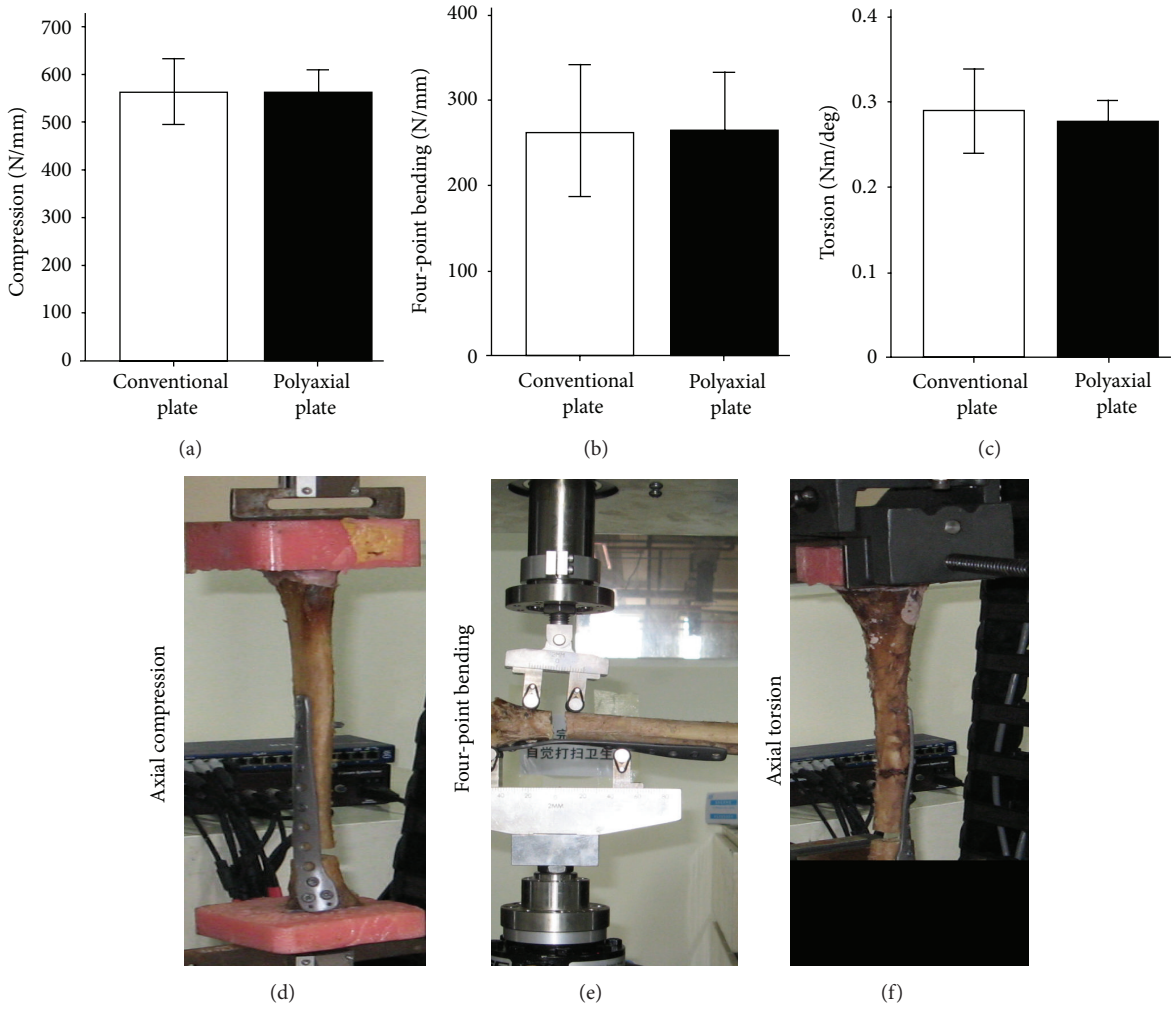

Figure 4: Biomechanical tests of the polyaxial self-locking anatomical plate. (a, d) Compression stiffness of conventional anatomical locking plate versus the polyaxial self-locking anatomical plate. (b, e) 4-point bending stiffness of conventional anatomical locking plate versus the polyaxial self-locking anatomical plate. (c, f) Torsion stiffness of conventional anatomical plate versus the polyaxial self-locking anatomical plate. Note that there is no statistical significance in all three tests.

conventional anatomical locking plate was 557.53 ± 20.72 N/mm, and the polyaxial self-locking anatomical plate was 562.80 ± 28.26 N/mm (Figures 4(a) and 4(d). The 4-point bending stiffness of the conventional anatomical locking plate was 268.02 ± 36.77 N/mm, and the polyaxial self-locking anatomical plate was 265.76 ± 27.21 N/mm (Figures 4(b) and 4(e)). The torsion stiffness of the conventional anatomical locking plate was 0.28 ± 0.01 Nm/deg and that of the polyaxial self-locking anatomical plate was 0.29 ± 0.02 Nm/deg (Figures 4(c) and 4(f)).

4. Discussion

Anatomical locking plates have been successfully used in the treatment of a large number of metaphyseal fractures [7–9]. The anatomical locking plate for the distal tibia was developed to accommodate the need for the biological osteosynthesis of distal tibia fractures, which can effectively preserve the blood supply of the fracture site by MIPPO (minimally invasive percutaneous plate osteosynthesis) technique, therefore reducing the incidence of delay union, nonunion, and soft tissue complications [10]. However, the screw insertion trajectories of the first generation locking plates are predetermined by manufacturers and are not able to be regulated during instrumentation, thus limiting the plates' clinical application. In certain fracture patterns even if the screws were located at the fracture site, the bone defect area, or not the main fracture fragment, the screw insertion trajectory could not be changed, thereby severely affecting the fixation and even leading to failure [11].

In the present study, we measured the geometry of the lateral distal tibiae in 80 healthy adults using a three-dimension spiral CT scanner. According to parameters obtained in the study, the maximal twisting angle for the polyaxial plate was determined to be 80° and the twisting segment was 12 cm. With the regulation of polyaxial bushing in the plate hole by

an angular regulation sleeve, the locking angle of the screw can be regulated as much as 30° which allows the surgeon to insert the locking screw more desirably. It is important to note that in order to design the polyaxial self-locking anatomical plate with optimal twist angle and anteversion, the difference in gender, age, and height of a patient must be considered.

We also compared the biomechanical properties of the polyaxial self-locking anatomical plate with those of a conventional anatomical locking plate and provided scientific evidence for its clinical application. A relatively high transverse defect osteotomy, 10-mm-wide, at the transition of diaphysis and metaphysis was chosen as a fracture model. This model mimicked a highly unstable metaphyseal fracture, with the implant alone transferring all loads between the two fracture fragments. A limitation of this model is that the defined defect, which prevents interlocking of the bony fragments during biomechanical testing, may influence the test results.

The tibia torsion angle was first defined as the connection between the horizontal line of the proximal tibia's articular surface and the coronal line of the distal tibia's articular surface by Tuttle and Manley [12]. In order to design the polyaxial self-locking anatomical plate, the outer side of the distal tibia torsion angle must be considered [13, 14]. In this study, we found that the outer side of the distal tibia torsion angle was different from that found in previous studies [15, 16]. The torsion segment length is from where the outer side of the tibia begins to twist to the front of distal tibia's articular surface [17–19]. To determine the torsion change of the transition section, we divided the torsion section into four equal parts and measured the outer side torsional angle for each part individually [20–22]. It was also observed that when the outer side of the middle and distal tibia twist from the sagittal plane to the coronal plane, its longitudinal axis has a little forward offset, which we define as the outer side tibia anteversion. One limitation of this study has been the relatively small number of experimental samples to determine Chinese people's distal tibial plate parameters, considering that Chinese people might have a large stature gap across different regions. Nevertheless, the results should be a valuable reference for future clinical studies.

Taken together, this study provides geometrical data on the distal tibias of Chinese people and constructs a variable locking screw trajectory to improve screw-plate stability by using the polyaxial self-locking anatomical plate of the distal tibia.

Conflict of Interests

The authors declare that there is no conflict of interests regarding the publication of this paper.

Acknowledgments

This work was supported by the Guangzhou Medical-Pharmaceutical Fund (Key Grant). This design has been granted a practical Patent by the Patent Bureau of China (no. 201020525718.X). This work was supported by the Medical and Health Key Project of Guangzhou City, no. 2009-zdi-04; the Guangdong Provincial Natural Science Foundation of China, nos. 10151022001000005 and S2011010000910; and the Natural Science Foundation of China (NSFC) (no. 81228013). Drs Ye and Xu made mutual international collaborative visits between their institutes in 2013. The authors thank Cai Yong (Engineer of Trauson Medical Instrument Company, Jiangsu China) for supervising production of the implants, Zhao Weidong (Researcher of the Biomechanical Institute of the Southern University, Guangzhou China) for helping with the biomechanical tests, and Dr. Jasreen Kular for critical reading of the paper.

References

[1] P. A. Kloc II, M. P. Kowaleski, A. S. Litsky, N. O. Brown, and K. A. Johnson, "Biomechanical comparison of two alternative tibial plateau leveling osteotomy plates with the original standard in an axially loaded gap model: an in vitro study," *Veterinary Surgery*, vol. 38, no. 1, pp. 40–48, 2009.

[2] M.-P. Hellio Le Graverand, R. J. Buck, B. T. Wyman et al., "Subregional femorotibial cartilage morphology in women—comparison between healthy controls and participants with different grades of radiographic knee osteoarthritis," *Osteoarthritis and Cartilage*, vol. 17, no. 9, pp. 1177–1185, 2009.

[3] L. McCann, E. Ingham, Z. Jin, and J. Fisher, "An investigation of the effect of conformity of knee hemiarthroplasty designs on contact stress, friction and degeneration of articular cartilage: a tribological study," *Journal of Biomechanics*, vol. 42, no. 9, pp. 1326–1331, 2009.

[4] S. Fatone, S. A. Gard, and B. S. Malas, "Effect of ankle-foot orthosis alignment and foot-plate length on the gait of adults with poststroke hemiplegia," *Archives of Physical Medicine and Rehabilitation*, vol. 90, no. 5, pp. 810–818, 2009.

[5] J. H. Lee, J. P. Dyke, D. Ballon, D. M. Ciombor, M. P. Rosenwasser, and R. K. Aaron, "Subchondral fluid dynamics in a model of osteoarthritis: use of dynamic contrast-enhanced magnetic resonance imaging," *Osteoarthritis and Cartilage*, vol. 17, no. 10, pp. 1350–1355, 2009.

[6] A. K. O. Wong, K. A. Beattie, P. D. Emond et al., "Quantitative analysis of subchondral sclerosis of the tibia by bone texture parameters in knee radiographs: site-specific relationships with joint space width," *Osteoarthritis and Cartilage*, vol. 17, no. 11, pp. 1453–1460, 2009.

[7] M. Ronga, C. Shanmugam, U. G. Longo, F. Oliva, and N. Maffulli, "Minimally invasive osteosynthesis of distal tibial fractures using locking plates," *Orthopedic Clinics of North America*, vol. 40, no. 4, pp. 499–504, 2009.

[8] Z. Cheng, F. Zhang, F. He et al., "Osseointegration of titanium implants with a roughened surface containing hydride ion in a rabbit model," *Oral Surgery, Oral Medicine, Oral Pathology, Oral Radiology and Endodontology*, vol. 110, no. 1, pp. e5–e12, 2010.

[9] V. R. Rapuri, H. D. Clarke, M. J. Spangehl, and C. P. Beauchamp, "Five cases of failure of the tibial polyethylene insert locking mechanism in one design of constrained knee arthroplasty," *The Journal of Arthroplasty*, vol. 26, no. 6, pp. 976.e21–976.e24, 2011.

[10] B. G. I. Spiegelberg, M. D. Sewell, W. J. S. Aston et al., "The early results of joint-sparing proximal tibial replacement for primary bone tumours, using extracortical plate fixation," *Journal of Bone and Joint Surgery B*, vol. 91, no. 10, pp. 1373–1377, 2009.

[11] J. T. Bordelon, D. Coker, M. Payton, and M. Rochat, "An in vitro mechanical comparison of tibial plateau levelling osteotomy plates," *Veterinary and Comparative Orthopaedics and Traumatology*, vol. 22, no. 6, pp. 467–472, 2009.

[12] T. A. Tuttle and P. A. Manley, "Risk factors associated with fibular fracture after tibial plateau leveling osteotomy," *Veterinary Surgery*, vol. 38, no. 3, pp. 355–360, 2009.

[13] M. Ronga, U. G. Longo, and N. Maffulli, "Minimally invasive locked plating of distal tibia fractures is safe and effective," *Clinical Orthopaedics and Related Research*, vol. 468, no. 4, pp. 975–982, 2010.

[14] J. S. Hayes, U. Seidenglanz, A. I. Pearce, S. G. Pearce, C. W. Archer, and R. G. Richards, "Surface polishing positively influences ease of plate and screw removal," *European Cells and Materials*, vol. 19, pp. 117–126, 2010.

[15] J. Gessmann, D. Seybold, H. Baecker, G. Muhr, and M. Graf, "Correction of supramalleolar deformities with the Taylor spatial frame," *Zeitschrift für Orthopädie und Unfallchirurgie*, vol. 147, no. 3, pp. 314–320, 2009.

[16] M. Hoenig, F. Gao, J. Kinder, L. Q. Zhang, C. Collinge, and B. R. Merk, "Extra-articular distal tibia fractures: a mechanical evaluation of 4 different treatment methods," *Journal of Orthopaedic Trauma*, vol. 24, no. 1, pp. 30–35, 2010.

[17] J. K. Oh, D. Sahu, J. H. Hwang, J. W. Cho, and C. W. Oh, "Technical pitfall while reducing the mismatch between LCP PLT and upper end tibia in proximal tibia fractures," *Archives of Orthopaedic and Trauma Surgery*, vol. 130, no. 6, pp. 759–763, 2010.

[18] D. Apelt, A. Pozzi, D. J. Marcellin-Little, and M. P. Kowaleski, "Effect of cranial tibial closing wedge angle on tibial subluxation: an ex vivo study," *Veterinary Surgery*, vol. 39, no. 4, pp. 454–459, 2010.

[19] A. L. Conkling, B. Fagin, and R. M. Daye, "Comparison of tibial plateau angle changes after tibial plateau leveling osteotomy fixation with conventional or locking screw technology," *Veterinary Surgery*, vol. 39, no. 4, pp. 475–481, 2010.

[20] R. F. LaPrade, F. B. Oro, C. G. Ziegler, C. A. Wijdicks, and M. P. Walsh, "Patellar height and tibial slope after opening-wedge proximal tibial osteotomy: a prospective study," *The American Journal of Sports Medicine*, vol. 38, no. 1, pp. 160–170, 2010.

[21] N. Fitzpatrick, J. Johnson, K. Hayashi, S. Girling, and R. Yeadon, "Tibial plateau leveling and medial opening crescentic osteotomy for treatment of cranial cruciate ligament rupture in dogs with tibia vara," *Veterinary Surgery*, vol. 39, no. 4, pp. 444–453, 2010.

[22] P. J. DeMeo, E. M. Johnson, P. P. Chiang, A. M. Flamm, and M. C. Miller, "Midterm follow-up of opening-wedge high tibial osteotomy," *The American Journal of Sports Medicine*, vol. 38, no. 10, pp. 2077–2084, 2010.

Hindawi Publishing Corporation
BioMed Research International
Volume 2014, Article ID 354260, 16 pages
http://dx.doi.org/10.1155/2014/354260

Research Article

Influence of Heating and Cyclic Tension on the Induction of Heat Shock Proteins and Bone-Related Proteins by MC3T3-E1 Cells

Eunna Chung,[1] Alana Cherrell Sampson,[1] and Marissa Nichole Rylander[1,2]

[1] *Virginia Tech-Wake Forest University School of Biomedical Engineering and Sciences, Virginia Tech, ICTAS Building, Stanger Street (MC 0298), Blacksburg, VA 24061, USA*
[2] *Department of Mechanical Engineering, Virginia Tech, ICTAS Building, Stanger Street (MC 0298), Blacksburg, VA 24061, USA*

Correspondence should be addressed to Marissa Nichole Rylander; mnr@vt.edu

Received 14 December 2013; Revised 25 March 2014; Accepted 26 March 2014; Published 11 June 2014

Academic Editor: Yin Xiao

Stress conditioning (e.g., thermal, shear, and tensile stress) of bone cells has been shown to enhance healing. However, prior studies have not investigated whether combined stress could synergistically promote bone regeneration. This study explored the impact of combined thermal and tensile stress on the induction of heat shock proteins (HSPs) and bone-related proteins by a murine preosteoblast cell line (MC3T3-E1). Cells were exposed to thermal stress using a water bath (44°C for 4 or 8 minutes) with postheating incubation (37°C for 4 hours) followed by exposure to cyclic strain (equibiaxial 3%, 0.2 Hz, cycle of 10-second tensile stress followed by 10-second rest). Combined thermal stress and tensile stress induced mRNA expression of HSP27 (1.41 relative fold induction (RFI) compared to sham-treated control), HSP70 (5.55 RFI), and osteopontin (1.44 RFI) but suppressed matrix metalloproteinase-9 (0.6 RFI) compared to the control. Combined thermal and tensile stress increased vascular endothelial growth factor (VEGF) secretion into the culture supernatant (1.54-fold increase compared to the control). Therefore, combined thermal and mechanical stress preconditioning can enhance HSP induction and influence protein expression important for bone tissue healing.

1. Introduction

Bone is exposed to complex mechanical cues during motion, such as tension, compression, and fluid shear stress [1]. These mechanical forces modulate cell morphology, proliferation, migration, differentiation, and production of bone-related proteins in cells via complex signaling cascades [2]. As a result, mechanical cues regulate bone growth by maintaining a fine balance between the bone-forming activity of osteoblasts and the bone-resorbing activity of osteoclasts. To build bone, osteoblasts produce extracellular matrix proteins such as osteocalcin (OCN), osteonectin (ON), osteopontin (OPN), and the enzyme alkaline phosphatase (ALP) [3–5]. Conversely, osteoclasts secrete enzymes like matrix metalloproteinase-9 (MMP-9) to digest the bone matrix [6]. Osteoprotegerin (OPG), an antiosteoclastic protein, reduces bone degradation by inhibiting osteoclast function [7]. Overall, bone-related proteins are indicators of osteoblastic/osteoclastic activity and are essential for maintaining proper bone physiology.

Numerous conditioning protocols involving mechanical stress or heating have been applied *in vitro* to osteoblasts or osteogenic stem cells to promote the regenerative potential of bone. These conditioning treatments are envisioned to generate a stress regimen to enhance the protective and regenerative capacity of bone cells without causing cell death [8]. The degree of mechanical strain is dictated by parameters such as magnitude [9, 10], frequency [11], duration [12], cyclic number [13], and mode (e.g., continuous/intermittent [14] and uniaxial/equibiaxial [14, 15]). Cyclic strain imposed by the Flexcell tension system, a commercially available tensile bioreactor, can upregulate bone-related proteins such as types I and III collagen [15], osteopontin (OPN) [16, 17], osteocalcin (OCN) [16, 17], vascular endothelial growth factor (VEGF)

[12, 17], bone morphogenetic protein-2 (BMP-2) [17], transforming growth factor beta 1 (TGF-β1) [18], osteoprotegerin (OPG) [10], and cyclooxygenase-2 (COX-2) [9] in bone cells. Varying tensile stress parameters determine the magnitude of stress that cells experience and can therefore influence cell behavior.

Thermal stress can activate various intracellular mechanisms and cellular responses depending on the type of heating system (e.g., water bath, incubator [19], or laser irradiation [12]), loading temperature [20–22], and heating duration [22]. Numerous research groups agree that heating with temperatures of 46–50°C for less than 10 minutes or temperatures of 43-44°C for longer durations than 15 minutes may cause cytotoxicity or decreased protein production [22–25]. With mild thermal stress endothelial cells exhibit enhanced angiogenic capacity 24 hours following exposure to 41°C for 1 hour [8]. Direct application of thermal stress to bone [19] and indirect thermal stress conditioning by adding supernatant collected from heat-treated osteoblasts [26] can promote cell proliferation and upregulate OCN. Based on our previously published work, water bath heating at 44°C for 8 minutes induced heat shock proteins (HSPs) and bone-specific proteins, such as OPN [27]. Although thermal stress is known to modulate protein production, the mechanism by which stress modulates cell behavior is unknown.

Thermal and mechanical stress can elicit the cytoprotective effects of molecular chaperones known as heat shock proteins (HSPs) [28]. As multifunctional proteins, HSPs are involved in mitosis [29], differentiation [30, 31], cytoskeleton stabilization [32], intracellular processing of matrix proteins (e.g., collagen) [33], immune system control [34], and the wound healing process [35, 36]. HSPs are characterized according to their molecular weight (e.g. HSP27) and each HSP has distinct functions and expression profiles depending on external stresses and cell type. HSP47 is associated with the collagen synthesis process by binding to procollagen [33, 37]. Both HSP27 and HSP70 rescue stressed cells from apoptotic cell death through various mechanisms [30]. Therapeutic approaches using the beneficial aspects of HSPs have been investigated in sepsis, transplantation, skin damage, and ischemic diseases of bone, brain, and heart, as reviewed by Jäättelä [38]. HSP27, HSP47, and HSP70 are highly expressed in bone-forming osteoblasts of rat bone demonstrated by immunohistochemistry [39]. In addition, heating using an incubator and water bath at 42–50°C can upregulate HSP expression [19, 22, 28, 40]. HSP70 expression can increase in trabecular meshwork cells and tendon fibroblasts following cyclic tension [41, 42]. Our previous study demonstrated heating and tension alone induced gene expression for all previously mentioned HSPs [27, 43].

Taken together, there may be a critical correlation between HSP expression and protective/osteogenic responses of bone cells in response to stress. Prior studies utilizing mechanical [10, 12, 15, 16, 44, 45] and thermal [19, 46] stress conditioning have suggested that these stresses can be beneficial stimulators for bone cell activity. However, few studies have explored the potential of combined stress protocols to improve bone regeneration. This study investigated whether the combination of thermal and mechanical stress could facilitate enhancement in cell proliferation, induction of HSPs, and upregulation of angiogenic/osteogenic proteins. Preosteoblasts were exposed to a single dose of water bath heating (44°C, 4 or 8 minutes) and cyclic strain (equibiaxial 3% elongation, 0.2 Hz, cycle of 10-second tension followed by a 10-second resting phase), and subsequently we evaluated cell morphology, cell proliferation, induction of HSPs (HSP27, HSP47, and HSP70), osteogenic matrix proteins (e.g., collagens, OPN, and OCN), and enzyme levels of MMP-9. An angiogenic growth factor, VEGF, and an antiosteoclastic cytokine, OPG, served as additional metrics for evaluating the contribution of stress conditioning to osteogenesis. To the best of our knowledge, this is the first study exploring the effects of combined thermal and mechanical stress on preosteoblasts. The results from our study may provide a better understanding of cellular response to multiple stresses and may also be useful in developing a stress protocol that stimulates cell activity for bone regeneration.

2. Materials and Methods

2.1. Cell Culture and Preparation for Stress Treatment. A murine preosteoblastic cell line, MC3T3-E1 (subclone 4, American Type Culture Collection, Manassas, VA), was cultured with growth media composed of alpha minimal essential medium (αMEM) (Mediatech, Manassas, VA) supplemented with 10% fetal bovine serum (FBS) and 1% penicillin-streptomycin (PS) in a 5% CO_2 incubator at 37°C. Prior to stress conditioning, cells were plated in a 6-well BioFlex plate at 2×10^5 cells per well and cultured overnight (for 16-17 hours) to allow cell adhesion.

2.2. Combined Stress Conditioning with Heating and Cyclic Tension. After cell adhesion, cells underwent the following stress conditioning protocols consisting of four different test groups: (1) sham-treated control, (2) thermal stress only, (3) tensile stress only, and (4) combined thermal and tensile stress. During thermal stress treatments, heating media, which consisted of Eagle's MEM without L-glutamine (Sigma-Aldrich), were added to fill the entire volume of the wells within the Flexcell plate. This specialized media composition was used because, at high temperatures experienced with thermal stress, L-glutamine can degrade quickly and become cytotoxic to cells. To maintain consistency, these media were used during all stress treatments. Thermal stress was applied by submerging the Flexcell well plate in a water bath (ISOTEMP 210, Fisher Scientific) set at 44°C for heating durations of 4 or 8 minutes, similar to prior work by Rylander et al. [22, 47]. For samples exposed to tension only, Flexcell tension plus system (Flexcell International Corporation, Hillsborough, NC) was utilized to apply cyclic tensile stress conditioning protocols of equibiaxial 3% maximum elongation and 0.2 Hz (cycle of 10-second tension followed by a 10-second resting phase) for identical tension durations used during combined stress treatments. A circular loading post (diameter = 25 mm) was used to apply equibiaxial tension. Combinatorial stress treatment was conducted as depicted in Figure 1 using identical methods for

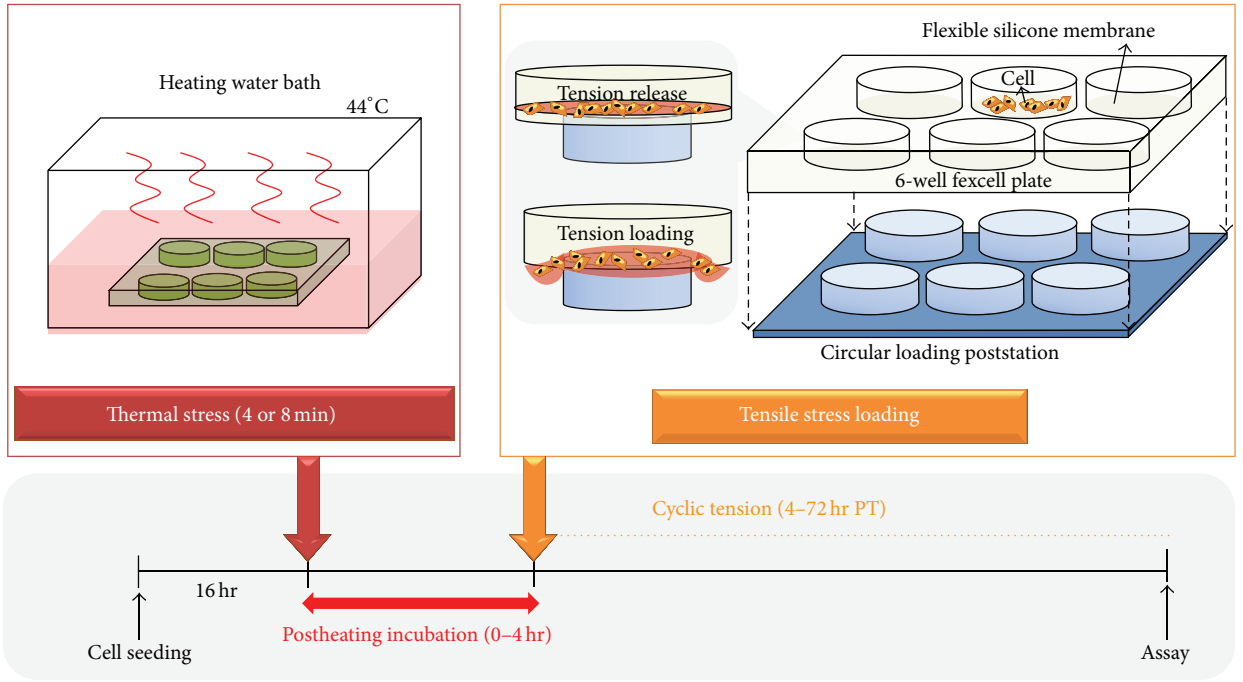

Combinatorial stress preconditioning

Thermal stress		Postheating incubation (hours)	Tensile stress		Analysis
Temp (°C)	Duration (min)		Type	Duration (hours)	
44	4	4	Equibiaxial 3% (0.2 Hz, 10 s tension on/10 s rest)	24	Real Time RT-PCR ELISA MTS/DNA assay
				72	ELISA MTS/DNA assay
	8	4		4	Real Time RT-PCR
				24	F-actin Real Time RT-PCR MTS/DNA assay
				72	ELISA MTS/DNA assay
				1	Western blot

Figure 1: Method of combined thermal and tensile stress conditioning for MC3T3-E1 monolayers. Cells were seeded on 6-well BioFlex plates with flexible culture substrate 16 hours before stress preconditioning. First, thermal stress was applied by heating in a water bath at 44°C for 4 or 8 minutes followed by 4-hour postheating incubation at 37°C and cyclic tensile stress conditioning protocols of equibiaxial 3% maximum elongation and 0.2 Hz (cycle of 10-second tension followed by a 10-second resting phase) using the Flexcell tension system. PT denotes the period of tensile stress treatment before cell analysis. The table summarizes the specific preconditioning protocols and associated assays performed.

thermal and tensile conditioning described previously. For these experiments, a single dose of water bath heating (44°C, 4 or 8 minutes) was applied followed by 4-hour postheating incubation at 37°C. Subsequently, cells were exposed to cyclic tension using the Flexcell tension system for varying durations (1–72 hours period of tensile stress (PT)) depending on test measurements. PT time denotes the duration of tensile stress conditioning and the timepoint for collecting data. Sham-treated control groups were not exposed to any stress treatment but were cultivated with identical media as stress-treated groups and maintained in an incubator. Each type of measurement within a single test group was performed at the same time regardless of whether tension or heating was applied. For poststress recovery, osteogenic media (αMEM supplemented with 50 μg/mL L-ascorbic acid, 10 mM β-glycerol phosphate, 10% FBS, and 1% PS) was added to cells and all samples were returned to a 5% CO_2 incubator at 37◦C. Media formulation was based on a previously described protocol for osteogenic media which was demonstrated to be conducive for differentiation of MC3T3-E1 cells [48].

2.3. Morphology Analysis. Cell morphology following stress treatment was visualized by fixing the cells immediately after stress and staining for F-actin, a cellular skeleton protein,

using rhodamine phalloidin (Invitrogen). Cells were fixed with 3.7% paraformaldehyde in a phosphate buffered solution (PBS) (Fisher Scientific) and permeabilized using 0.1% Triton X-100 (Sigma)/PBS. For blocking, samples were incubated in 1% bovine serum albumin (Amersham) dissolved in PBS for 30 minutes at room temperature followed by 20-minute incubation in rhodamine phalloidin solution in the dark. For nucleus counterstaining, cells were mounted with VECTASHIELD mounting medium with DAPI (DAPI: 4′,6-diamidino-2-phenylindole) (Vector Laboratories). Stained images were acquired using a fluorescent inverted microscope (CTR6500, Leica Microsystems).

2.4. Proliferation Assay. Cell proliferation was measured at 24 and 72 hours following thermal (44°C, 4 and 8 minutes) and tensile stress applied independently or in combination. We implemented two different assays: 3-(4,5-dimethylthiazol-2-yl)-5-(3-carboxymethoxyphenyl)-2-(4-sulfophenyl)-2H-tetrazolium (MTS) assay using CellTiter96 Aqueous one solution cell proliferation assay (Promega Corporation, Madison, WI) and DNA assay using Quant-iT PicoGreen dsDNA reagent kit (Invitrogen) according to the manufacturer's protocols. MTS stock solution was mixed with basal αMEM without FBS and PS (the volume ratio of MTS stock to media was 1 : 5). Diluted MTS working solution was added to cultured cells. After 4-hour incubation at 37°C, the solution was transferred to a 96-well plate and optical density was measured at 490 nm by a microplate reader (SpectraMax M2^e, Molecular Devices, Sunnyvale, CA). DNA was isolated at identical timepoints as the MTS assay. In brief, cells were lysed using Tris-EDTA buffer (10 mM Tris, 1 mM EDTA, pH 8.0, Fisher Scientific) including 0.1% Triton X-100 (Sigma) and 0.1 mg/mL proteinase K (Fisher Scientific). Cell lysate was incubated at 56°C overnight and transferred into a 96-well plate with standard solutions. Quant-iT PicoGreen dsDNA was added to each sample at a volume ratio of 1 : 1 and incubated at room temperature in the dark for 3 minutes. Fluorescence of each sample was measured by a microplate reader (SpectraMax M2^e, Molecular Devices, Sunnyvale, CA) set at the 480/520 nm (excitation/emission).

2.5. Quantitative Real Time RT-PCR. Gene expression of HSPs and bone-related proteins was measured following individual or combined treatment with thermal and tensile stress. RNA was isolated by spin protocol using an RNeasy Mini kit (Qiagen) and a QIAshredder (Qiagen), according to the manufacturer's protocol. RNA isolation was performed immediately after 4–72-hour cyclic tension or directly following heating at 44°C and 4-hour postheating incubation at 37°C. Isolated RNA was converted to cDNA using reverse transcription system (Promega). RNA from each sample was reacted at 25°C for 10 minutes and 42°C for 45 minutes followed by heating at 99°C for 5 minutes. After reverse transcription, cDNA samples were mixed with Taqman PCR Master Mix (Applied Biosystems) and each specific primer and polymerized in a 7300 Real Time PCR System (Applied Biosystems). The PCR reaction was performed at 50°C for 2 minutes followed by 95°C for 10 minutes. For each polymerization (total PCR reaction = 45 cycles), temperature was set at 95°C for 15 seconds and 60°C for 1 minute. Taqman gene expression assay (Applied Biosystems) for specific gene detection was used as a primer and probe as follows: GAPDH (Mm99999915_g1), HSP27 (Mm00517908_m1), HSP47 (Mm00438056_m1), HSP70 (Mm03038954_s1), OPN (Mm01611440_mH), OPG (Mm01205928_m1), MMP-9 (Mm00600164_g1), ALP (liver/bone/kidney) (Mm01187113_g1), OCN (Mm00649782_gH), type I collagen (alpha 1) (Mm00801666_g1), and VEGF (Mm00437308_m1). Relative fold induction (RFI) of each mRNA was calculated according to the $2^{-\Delta\Delta C_T}$ method used in Lee et al.'s study [49]. Threshold cycle (C_T), derived using SDS v1.2× system software of 7300 Real Time PCR System, denotes the fractional cycle number at threshold polymerized gene and $\Delta\Delta C_T$ was derived from the following equation: (C_T of target gene − C_T of GAPDH)$_{\text{treated group}}$ − (C_T of target gene − C_T of GAPDH)$_{\text{control group}}$ [49]. Treated groups denote thermal stress alone, tension alone, or combined thermal and tensile stress treatments. Control groups indicate sham-treated cells without heating and tension.

2.6. Enzyme-Linked Immunosorbent Assay Analysis (ELISA). Protein secretion by MC3T3-E1 cells following thermal and tensile stress independently or in combination was analyzed by enzyme-linked immunosorbent assay (ELISA), according to the manufacturer's protocol. In brief, immediately after 24-hour (for VEGF) and 72-hour (for OPN, OPG, and MMP-9) cyclic tension loading, the conditioned osteogenic culture supernatant was collected. For untreated and heated samples, supernatant was isolated at identical timepoints although no tension was applied. The concentrations of OPG, VEGF, OPN, and MMP-9 in the conditioned cell culture medium were determined using Quantikine ELISA (R&D Systems). The culture supernatant was added to a 96-well microplate coated with antibodies for the desired proteins and incubated for 2 hours at room temperature. After washing, samples were incubated in the conjugate for 2 hours. Subsequently, peroxidase substrate solution was added to initiate an enzymatic reaction that generates a colored product in proportion to protein concentrations in each sample. After 30 minutes, the optical absorbance was measured at 450 nm by a microplate reader (SpectraMax M2^e, Molecular Devices, Sunnyvale, CA) and converted into the concentration level using a standard absorbance curve.

2.7. Statistical Analysis. All data and graphs are presented as mean ± standard deviation. Experimental groups with a minimum of three replicates were tested and analyzed independently. Using JMP 8.0 statistical software, a one-way ANOVA and a Tukey multiple comparison test were performed to compare the means between each group. The significance of each treatment in the study was defined by a P value lower than 0.05.

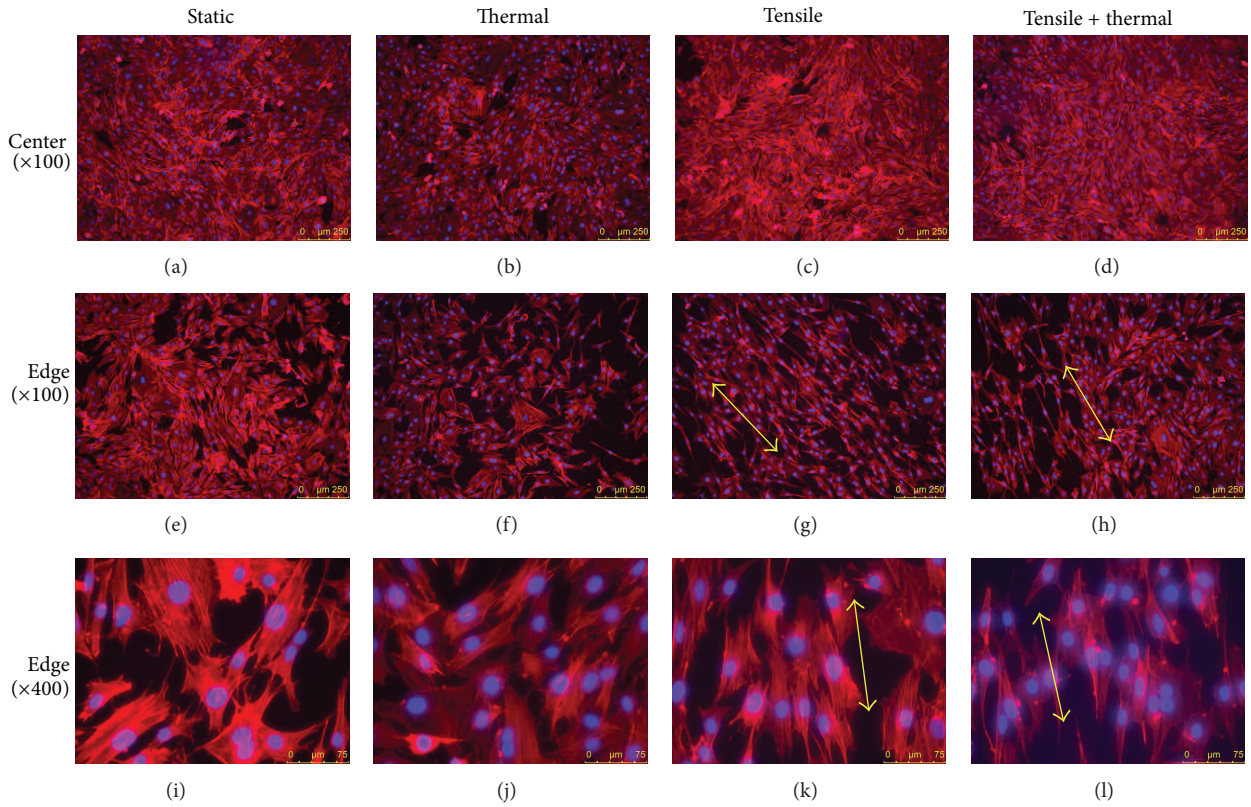

FIGURE 2: Cell morphology as visualized by F-actin staining following stress conditioning. Cell morphology is shown in response to thermal stress ((b), (f), and (j)), tensile stress ((c), (g), and (k)), and combined thermal and tensile stress ((d, (h), and (l)). Static-cultured cells ((a), (e), and (i)) were used as a control. Varying positions within the well were imaged, including the center ((a)–(d)) and the edge under 100x ((e)–(h)) and 400x magnification ((i)–(l)). Yellow arrows denote the direction of tensile stress generated due to the loading post. Heating at 44°C for 8 minutes (postheating incubation = 4 hours); cyclic tension (equibiaxial 3%, 0.2 Hz, 10-second tension on/10-second rest, 24 hours).

3. Results and Discussion

This study investigated the effect of combined tensile and thermal stress on preosteoblasts by evaluating their *in vitro* osteogenic response. Due to the varied response of cells to diverse stress conditions, the parameters used in our stress protocols were selected based on studies in the literature. Our heating protocols were chosen based upon our previous published work in which heating at 44°C for periods less than 10 minutes induced HSPs rapidly without any cytotoxicity [27]. Our heating protocols are also comparable to those used by other groups at temperatures of 40–43°C (for heating durations of 30 minutes to 1 hour) [26, 28, 50]. Although the water bath was set to ca. 44°C, the cell culture vessels required time to equilibrate to the surrounding water bath temperature (data not shown here) causing the cells to experience temperatures in the range of 40–43°C for short periods. The tensile stress protocol used in our study was selected based on prior literature, which employed tensile stress conditioning typically lower than 18% strain and documented positive osteogenic effects inducing upregulation of collagen, VEGF, and COX-2 [9, 15, 51, 52]. Furthermore, 0.1–1 Hz frequency and 6 cycle numbers per minute also have been investigated commonly in bone-related studies [10, 15, 51, 53]. In Winter et al.'s study, intermittent stretching induced higher levels of DNA and calcium in osteoblasts compared to continuous tensile stress [14], suggesting the importance of rest periods to enhance cellular response to tension. Also, equibiaxial strain has been demonstrated to increase collagen expression, cell proliferation, and VEGF in bone-related cells [9, 15, 52]. Based on these studies, our tensile stress protocols employed 3% cyclic equibiaxial stretching with 0.2 Hz frequency and 6 cycle numbers per minute in an intermittent manner (10-second tension followed by 10-second rest period) for MC3T3-E1 preosteoblasts. To improve the beneficial effects seen with individual thermal and tensile stress, this study investigated the ability of combined stress protocols to enhance bone development.

3.1. Effect of Combined Heating and Cyclic Tension on Cell Morphology. Cell morphology was visualized by F-actin fluorescence staining to determine the effect of heating and mechanical tensile stress alone or in combination (Figure 2). Similar to sham-treated controls, cells had a broad, flat morphology and there was no apparent alteration in response to heating. However, tension and combined stress caused cell alignment and elongation around the perimeter of the culture plate. Mechanical stress can influence cell morphology by

disrupting cellular focal adhesions that connect the cytoskeleton to the substrate. The subsequent rearrangement of the actin cytoskeleton can cause cells to align in the direction of stretching (yellow arrows in Figure 2).

3.2. Effect of Combined Heating and Cyclic Tension on Cell Proliferation. We investigated MC3T3-E1 proliferation by measuring metabolic activity and DNA concentrations using an MTS assay and Quant-iT PicoGreen dsDNA assay, respectively (Figure 3). Cells did not show any associated cytotoxicity following heating for individual and combinatorial conditioning of 4 (Figures 3(a) and 3(b)) or 8 minutes (Figures 3(c) and 3(d)) of heating and tension (24 and 72 hours). In addition, cells did not experience apoptotic damage following stress as evidenced by minimal changes in metabolic activity and DNA concentrations for longer cultivation (72-hour PT) in all groups. There were not significant differences in cell metabolic activities depending on stress types.

Previous studies investigating cell proliferation or cytotoxicity in response to stress have shown outcomes comparable to our results when similar stress conditions were used. For thermal stress, Riederer et al. showed that low-level heat treatment at 42°C for 1 hour using an incubator did not significantly influence the proliferation rate of human myoblasts [50]. Another study described that water bath heating at 39–41°C for 1 hour induced a slight, but nonsignificant, increase in cell proliferation [19]. The effect of tensile stress on proliferation has also been evaluated in prior studies using similar stress conditions as our work. For example, Huang et al. demonstrated tension (3%, 0.1 Hz) slightly increased metabolic activity of MSCs on day 1 but exhibited similar levels as static-cultured cells on days 3 and 5 [53]. The results from these studies are comparable to our MTS and DNA data, which shows no significant increases in cell proliferation following stress treatment on MC3T3-E1 cells. Furthermore, our study did not demonstrate any statistically significant reduction in cell proliferation, suggesting that our stress conditioning protocols do not induce apoptosis or negatively affect metabolic activity of the cells.

3.3. Effect of Combined Heating and Cyclic Tension on HSP Expression. To evaluate the influence of stress conditioning on cytoprotective proteins and the cellular stress response, we measured gene expression and protein secretion of HSPs following individual and combined heating (44°C, 4 or 8 minutes) and cyclic mechanical strain (24 hours, 4 hours, or 1 hour) conditioning. Messenger RNA (mRNA) expression for HSPs (HSP27, HSP47, and HSP70) and the protein level of HSP70 after stress treatments are shown in Figure 4. Long durations of cyclic tension (24 hours) alone or in combination with 4- or 8-minute heating showed no significant induction of mRNA for any of the HSPs measured (data not shown). For shorter durations of tensile conditioning (4 hours) and 8-minute heating, individual heating and cyclic tension did not produce a substantial effect, but combined stress treatments significantly altered HSP expression. Combined stress conditioning of 8-minute heating followed by 4 hours of cyclic tension caused significant induction of HSP70 (5.55 RFI) and HSP27 (1.41 RFI) mRNA compared to tensile or thermal stress alone (Figures 4(a) and 4(c)). In addition, HSP47 mRNA was suppressed by tension alone (0.76 RFI), but combined stress caused a reduction in HSP47 mRNA expression (0.72 RFI) (Figure 4(b)). Furthermore, protein induction of HSP70 following combined heating (at 44°C for 4 minutes) and 1-hour tension (Figure 4(d)) was significantly promoted.

Our data suggests that combined stress conditioning has a greater influence on HSP expression than individual stress. In addition, the degree of HSP induction in response to the type of stress varies among different HSPs. For example, we observed that HSP70 gene (5.55 RFI) and protein expression were more sensitive to combined stress treatments compared to HSP27 (1.41 RFI) and HSP47 (0.72 RFI). Also, we observed that tensile stress alone significantly altered HSP47 mRNA but had little influence on HSP27. These results are similar to findings in prior studies which have shown differential HSP induction depending on the type and degree of stress [27, 43]. Although cellular induction of HSPs varies depending on the stimuli, the ability of our combined tensile and thermal stress protocol to induce significant changes in gene expression for all HSPs measured compared to the control suggests that combined stress can provide the appropriate level of stimulation to broadly influence cellular protein production.

In our study, the upregulation of HSP70 and HSP27 following combined stress has important implications since previous studies have shown the cytoprotective effects of HSPs in a variety of tissues. For example, elevated levels of HSP70 in the heart following stress preconditioning resulted in increased tolerance of myocardiocytes to subsequent ischemia [54]. Zheng et al. demonstrated that overexpression of the HSP70 gene in mice prevented cell death after brain injury [55]. Prior studies have also revealed that the level of HSP induction is directly related to the amount of protection [56]. Based on this, our data suggests that combined stress conditioning has a greater ability to invoke cytoprotection by upregulating HSPs, compared to individual stress. Despite exposing cells to a higher degree of stress, the minimal changes in cellular metabolism and cell proliferation we observed demonstrate that our combined stress protocol can modify cellular response without causing cytotoxic effects. Although the mechanism is not known, combined stress can have a significant impact by exposing cells to multiple stresses that can act individually or synergistically to enhance cellular response.

Our data showing induction of HSP70 expression in response to heating is consistent with prior studies showing elevated HSP70 in chondrocytes [57] and endothelial cells [22] in response to heating. Shui and Scutt demonstrated that thermal stress (ca. 41–45°C for 1 hour or 39°C for 96 hours) conditioning of bone cells induced beneficial osteogenic effects by significantly enhancing calcium production, ALP activity, and HSP70 following heating at 39°C for 96 hours [19]. Our prior work [27] showed significant induction of mRNA of all HSPs at 8-hour postheating following 8-minute heating, but HSP upregulation by heating in this study was lower or did not exhibit induction. This may be due to differences in cell density and culture plates used (general plastic

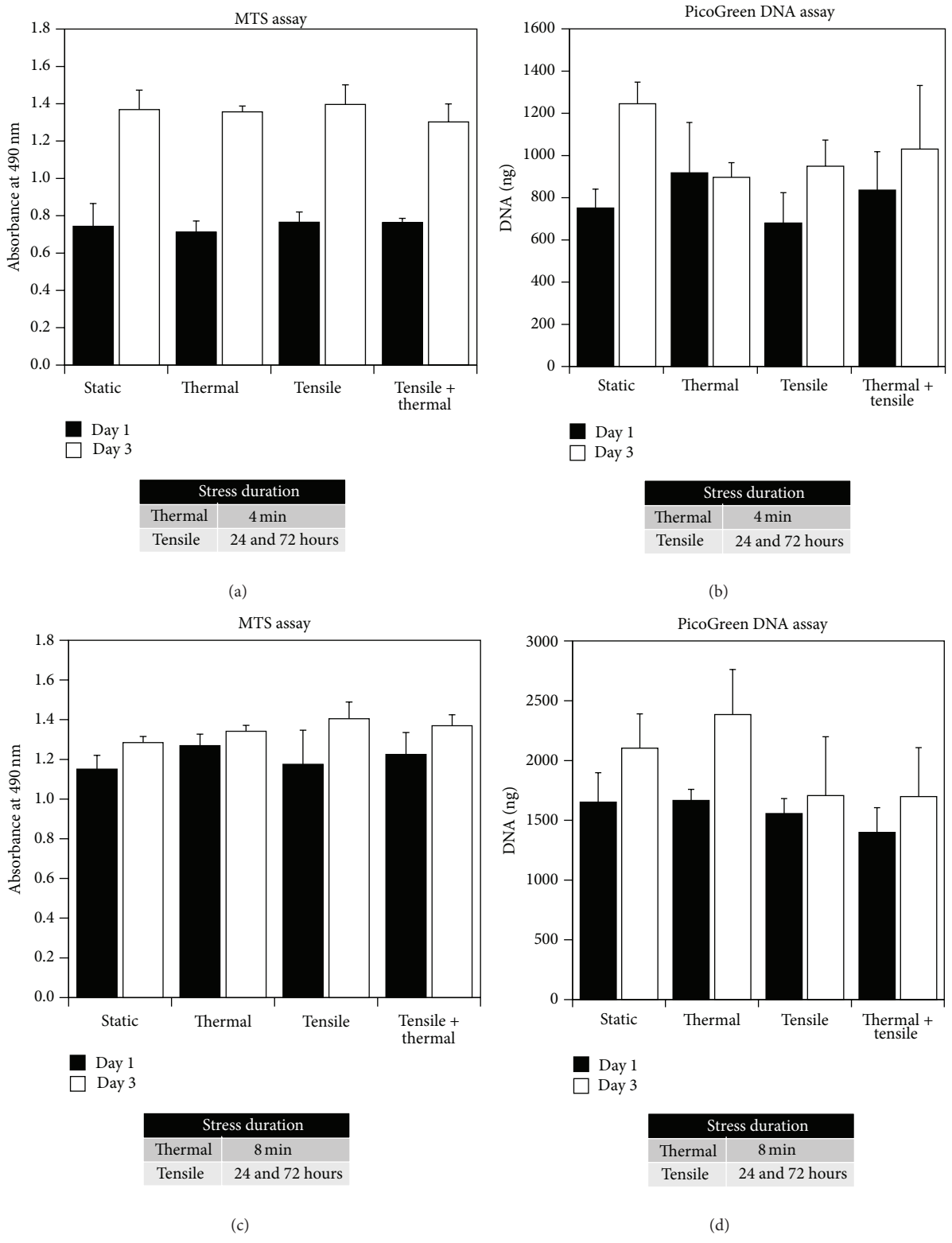

Figure 3: MC3T3-E1 proliferation was measured 24 and 72 hours following a single dose of thermal stress (44°C, 4 or 8 minutes, postheating incubation = 4 hours) and cyclic tension (equibiaxial 3%, 0.2 Hz, 10-second tension on/10-second rest, 24 and 72 hours) individually or in combination. Cell proliferation was measured using MTS and PicoGreen DNA assay with varying heating durations of 4 minutes ((a) and (b)) and 8 minutes ((c) and (d)) ($n = 3$).

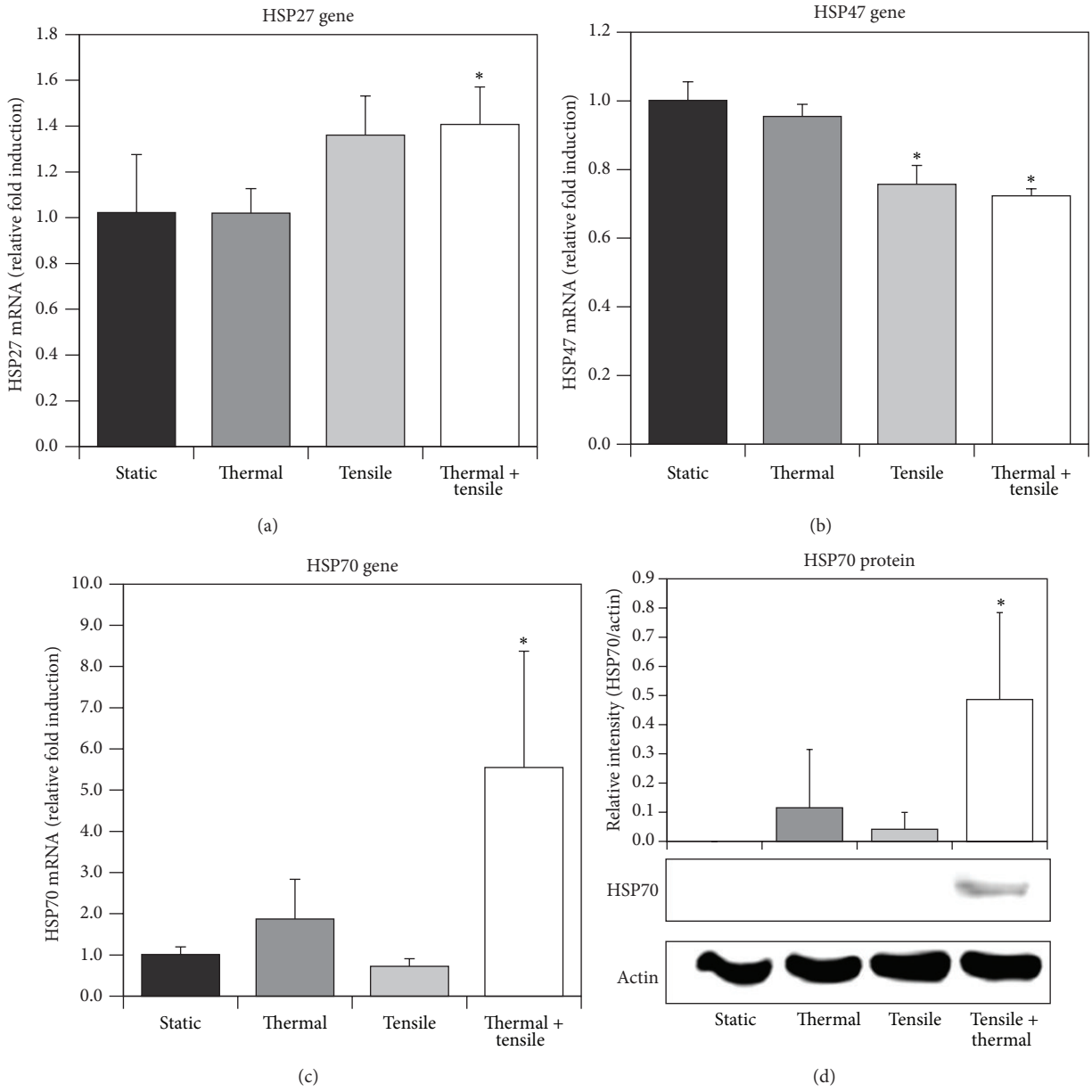

Figure 4: HSP (HSP27, HSP47, and HSP70) expression following a single dose of thermal stress (44°C, 4 or 8 minutes) and cyclic tension (equibiaxial 3%, 0.2 Hz, 10-second tension on/10-second rest) individually or in combination. Gene expression of HSP27 (a), HSP47 (b), and HSP70 (c) following heating for 8 minutes and 4-hour cyclic strain ($n = 4$ for (a)–(c)). Protein expression of HSP70 following heating for 4 minutes and 1-hour cyclic tension (d). $*$ denotes statistical significance between stress-treated and sham-treated control groups ($P < 0.05$) ($n = 3$).

T-flask for previous study and Flexcell BioFlex plate coated with type I collagen for the current study). Furthermore, in terms of tensile stress, our previous studies showed 1% tension transiently induced HSP27 (1.82 RFI) and HSP70 (1.53 RFI) mRNA at day 3, but this induction level was relatively lower than induction by heating [27, 43]. To our knowledge this is the first study measuring HSP70 induction in preosteoblasts in response to combined heating and tension.

3.4. Effect of Combined Heating and Cyclic Tension on Bone-Related Proteins. Relative changes in gene expression and protein secretion of bone-related proteins in response to heat (44°C, 4 and 8 minutes) and/or tensile stress (24 hours) are shown in Figure 5. OPN mRNA was slightly increased by the combination of heating for 4 and 8 minutes and 24 hours of tension compared to either stress individually (Figures 5(a) and 5(c)). OPG mRNA increased following 24-hour tension alone and in combination with 4-minute heating (Figure 5(b)). Although tension alone exhibited the greatest upregulation of OPG, combined stress stimulated comparable mRNA levels. OCN mRNA was not affected by any of the stress protocols (data not shown). Secreted OPN

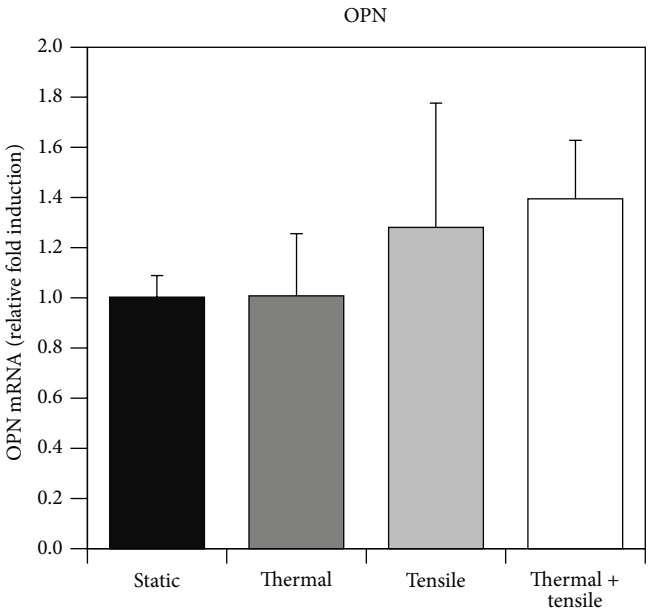

Stress duration	
Thermal	4 min
Tensile	24 hours

(a)

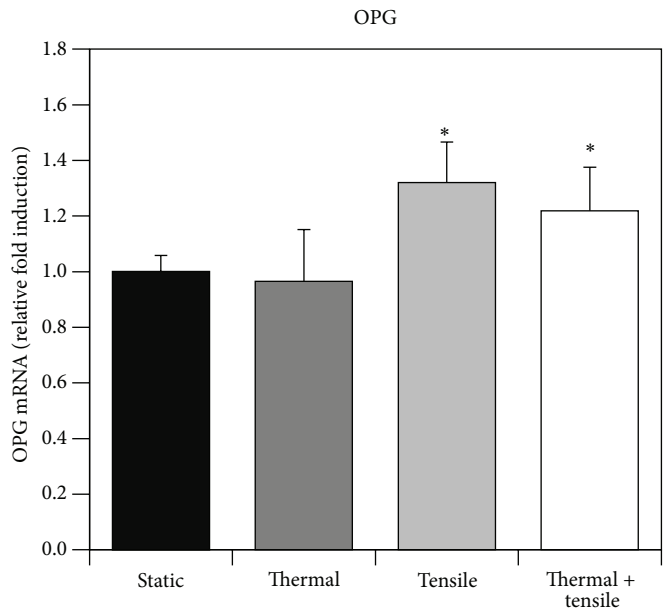

Stress duration	
Thermal	4 min
Tensile	24 hours

(b)

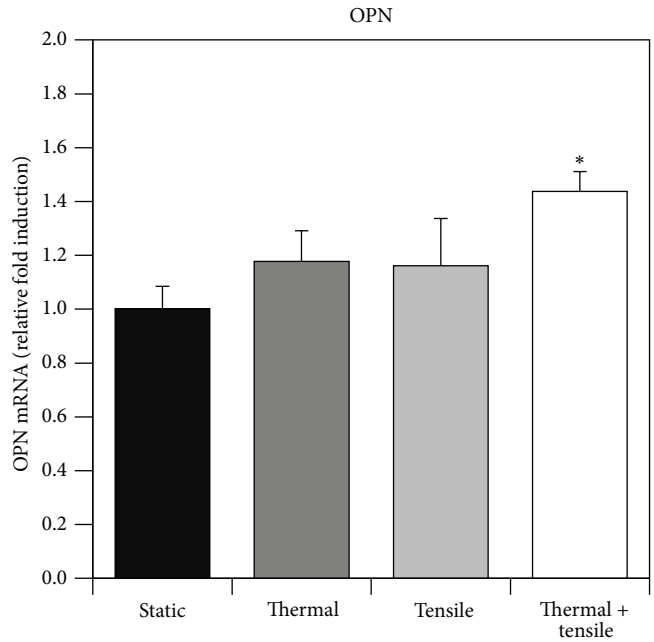

Stress duration	
Thermal	8 min
Tensile	24 hours

(c)

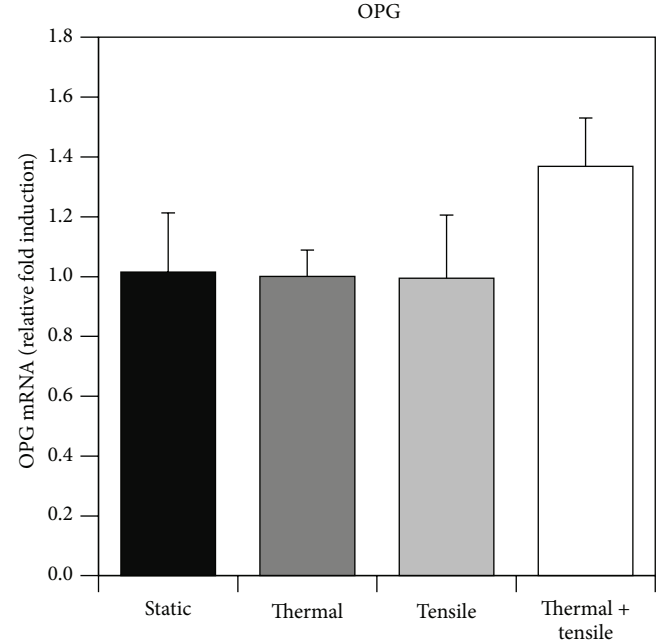

Stress duration	
Thermal	8 min
Tensile	24 hours

(d)

Figure 5: Continued.

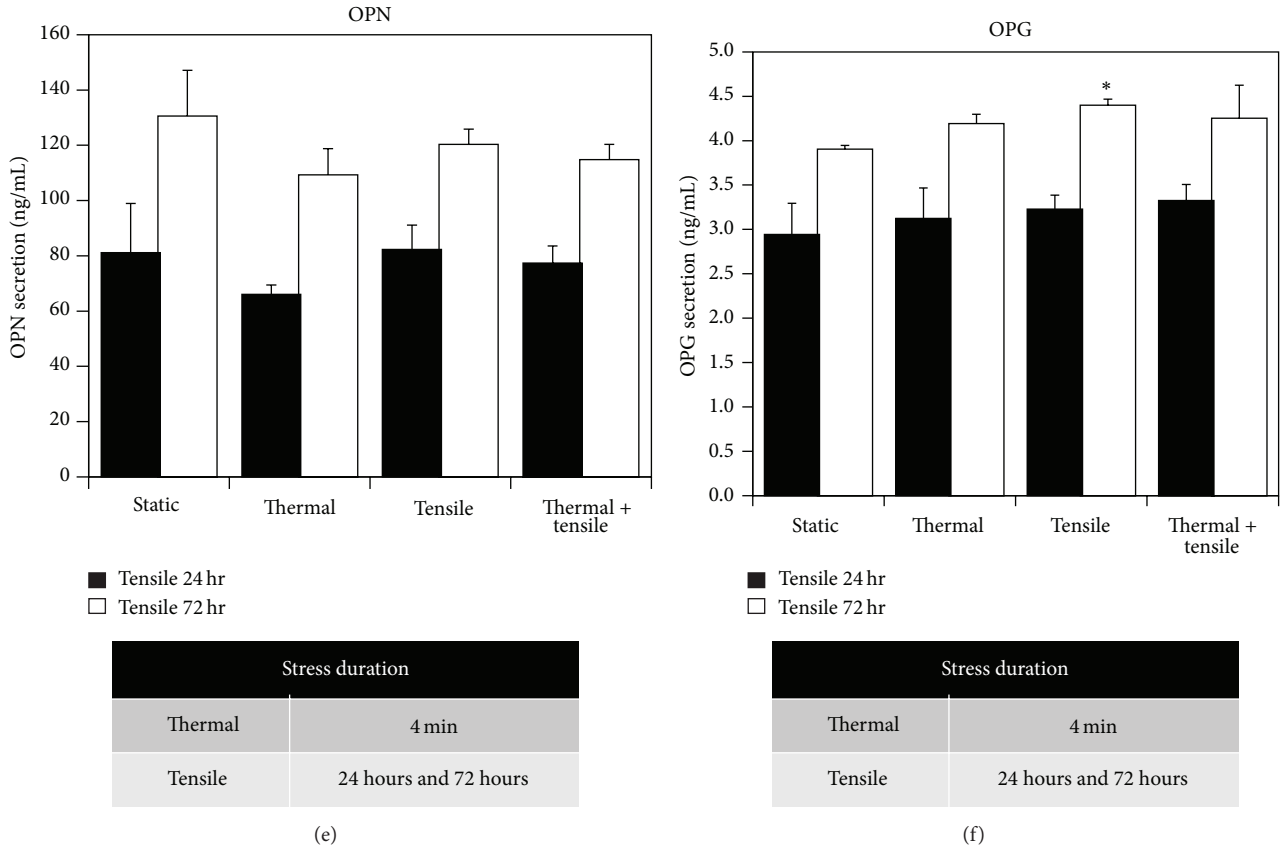

Stress duration	
Thermal	4 min
Tensile	24 hours and 72 hours

(e)

Stress duration	
Thermal	4 min
Tensile	24 hours and 72 hours

(f)

Figure 5: Gene expression and protein secretion of OPN and OPG by MC3T3-E1 cells following a single dose of thermal stress (44°C, 4 or 8 minutes) and cyclic tension (equibiaxial 3%, 0.2 Hz, 10-second tension on/10-second rest, 24 hours or 72 hours) individually or in combination. OPN and OPG gene expression is shown in response to varying heating durations of 4 minutes ((a) and (b)) and 8 minutes ((c) and (d)) alone or in combination with cyclic tension for 24 hours. OPN (e) and OPG (f) concentration secreted in the culture supernatant (measured by ELISA) is shown following heating for 4 minutes and cyclic tension for 24 or 72 hours. $*$ denotes statistical significance between stress-treated and sham-treated groups ($P < 0.05$) ($n = 4$).

and OPG in the culture media were analyzed by ELISA kits following 4-minute heating and 24- or 72-hour tension (Figures 5(e) and 5(f)). There was a statistical difference between OPG induction (13% increase) following tension for 72 hours compared to the control. However, OPN secretion did not show any significant difference between test groups at 24- and 72-hour PT.

The upregulation of OPG, a protein that inhibits osteoclast differentiation, and OPN, a protein that mediates cell-bone ECM interactions, can be beneficial for bone growth by limiting osteoclast activity, decreasing bone resorption, and regulating ECM maturation. In this study, combined stress was influential in increasing gene expression of OPG and OPN. Previous studies have shown comparable results to our data. For example, in Tang et al.'s study, OPG mRNA in MC3T3-E1 cells was increased in a magnitude-dependent manner following 6–18% (6 cycles per minute) for 24 hours but the relative fold induction of 6% stretching to sham-treated cells was lower than 2 RFI [10]. Similar to our previous study [43], OCN and OPN genes appear not to be influenced by 24-hour tension alone. However, heating (for 8 minutes) alone induced mRNA expression of OCN (3.8 RFI), OPN (1.8 RFI), and OPG (2.1 RFI) genes at 8-hour postheating in our previous study [27]. Furthermore, in our prior work [43], we observed significant OPG secretion in response to 5% tensile stress preconditioning, comparable to the current study employing 3% tension, suggesting that OPG can be upregulated by tension, but not significantly by thermal stress. The discrepancy may be caused by culturing cells on a type I collagen-coated flexible substrate and the use of a different FBS concentration in the osteogenic culture media between these two studies. In addition, our study analyzed type I collagen, which showed no apparent changes in gene expression regardless of which stress conditioning protocol was applied (data not shown). These results are comparable to previous studies [27], where type I collagen mRNA was not influenced by either heating (for 4 or 8 minutes) and tension (for 24 hours) or mechanical strain of 10–12% magnitude (0.1 Hz, cycle number 6 per minute for 24 hours) [51]. Based on these findings, type I collagen gene expression may not be responsive to short-term stress conditioning. However, even without drastic changes in gene expression, collagen deposition can still be influenced by stress and further investigation is necessary.

3.5. Effect of Combined Heating and Cyclic Tension on MMP-9 Expression. MMP-9 mRNA expression and protein secretion were suppressed in response to thermal (4 or 8 minutes) and tensile stress (24 or 72 hours) alone or in combination (Figure 6). Combined heating and tensile stress caused MMP-9 mRNA expression and protein secretion to decrease at 24-hour PT and 72-hour PT, respectively (Figures 6(a)–6(d)). Although MMP-9 secretion at 72-hour PT increased with 8-minute heating alone (Figure 6(d)), the greatest change in secretion was observed with combined stress and individual tensile stress. Combined 8 minute heating and tension was able to significantly decrease gene expression of MMP-9 compared to the control.

Similar to our previous study, MMP-9 secretion was inhibited by heating [27] and 3% mechanical strain [43]. Therefore, MMP-9 mRNA in MC3T3-E1 cells appears to be suppressed by cyclic tensile stress following short periods of tension. Our results compare well with a prior study using a Flexcell bioreactor applying 10% tension (0.5 Hz) which caused diminished MMP-9 gene expression of RAW264.7 osteoclastic cells [58]. Based on these studies, our results imply that tension is the main factor stimulating MMP-9 suppression. Since combined stress yields similar or more pronounced levels of MMP-9 inhibition, we can deduce that tension contributes significantly to the results observed with combined stress. Although the mechanism is unknown, combined stress could promote enhanced effects over individual stress by exposing cells to multiple stimuli that can act individually or synergistically to promote an enhanced cellular response.

MC3T3-E1 cells express several types of MMPs including MMP-2, MMP-9, and MMP-13 [59], but MMP-9 was chosen because it is a well-known enzyme involved in bone remodeling/development. Although primarily associated with osteoclasts, this enzyme is also produced by osteoblasts to influence osteoclast activity [58, 60, 61]. MMP-9 overexpression in the bone microenvironment could be an osteoclastic activator for bone resorption. Recently, reducing MMP-9 expression has become a promising therapeutic strategy for bone diseases with high osteoclast activity such as osteoporosis. Therefore, MMP-9 suppression by stress conditioning could provide a beneficial impact for bone regeneration. Despite the suggested MMP-9 suppression by tension alone or in combination with heating, this phenomenon should be investigated further to determine whether suppressed MMP-9 can alter bone development.

3.6. Effect of Combined Heating and Cyclic Tension on VEGF Expression. VEGF mRNA and protein secretion were measured following individual and combined thermal (44°C, 4 and 8 minutes) and tensile stress (Figure 7). Stress conditioning did not influence VEGF mRNA expression (Figures 7(a) and 7(b)), except for 8-minute heating alone (Figure 7(b)). VEGF secretion significantly increased with tension alone, but slightly higher concentrations were observed after combined heating and tensile stress compared to tension only, as demonstrated by ELISA data (Figures 7(c) and 7(d)): 4-minute heating and tension (Figure 7(c)) (static 41.5 pg/mL; thermal 64.2; tensile 72.5; combined 94.9); 8 minute heating and tension tension (Figure 7(d)) (102.0; 95.5; 138.9; 156.6).

Prior studies have suggested that thermal or mechanical stress can stimulate VEGF induction [52, 62, 63]. For example, heating at 42°C for 15 minutes using a heating blanket has been shown to induce VEGF in rat cardiac tissue at 4–72-hour postheating [62]. Kim et al. showed an increase in VEGF expression after 90-minute heat stress at 43°C using a heating pad and infrared radiation at 42°C [63]. Tensile stress has been shown to rapidly promote VEGF gene expression in osteoblasts in response to 3-hour equibiaxial tension (10% magnitude) [52] and prior studies by our group have shown that tension can increase VEGF secretion [44]. These trends are comparable to results from our study, although VEGF gene expression and protein secretion were regulated differently depending on the type of stress. For example, our results show individual thermal stress upregulated VEGF gene expression but had no effect on protein secretion. For individual tensile stress, negligible effects in VEGF gene expression were observed, but these treatments were able to stimulate cells to secrete increased concentrations of VEGF. In addition, our results for combined stress followed a similar trend as individual tensile stress but exhibited slightly increased VEGF secretion levels, suggesting that tensile stress may be the dominant stimulus in our combined stress protocol. Although only a slight difference was observed, the increased VEGF secretion invoked by combined stress compared to tension alone/thermal alone suggests that exposing cells to multiple stresses may have an enhanced effect over individual stress. However, additional research is necessary to determine whether combined stress can induce more pronounced differences in VEGF secretion.

In our previous studies [27] VEGF gene expression was induced at 8-hour postheating by thermal stress (44°C, 8 minutes) and more significantly with growth factors (GFs) (i.e., BMP-2 and TGFβ-1). In our prior study [43], tension alone did not cause VEGF gene induction, but the combination of tension and growth factors increased VEGF gene and protein upregulation compared to growth factor addition or tension alone. Although GFs have been documented as powerful angiogenic inducers, combined heating and tensile stress conditioning may be a promising stress protocol that influences angiogenesis without exogenous delivery of GFs. Our study supports this concept by demonstrating that combined thermal and mechanical stress can increase VEGF secretion. Therefore, given that angiogenesis and VEGF are critical in the bone healing process [64], our stress conditioning protocols utilizing heating and cyclic tension may enhance VEGF-mediated communication between osteoblasts and endothelial cells. These protocols could potentially be used to stimulate blood vessel formation in a bone microenvironment or within bone scaffolds.

In conclusion, our study revealed that combined stress conditioning for short periods has the potential to modify cellular activity. Combined stress induced HSPs, upregulated OPN and OPG mRNA expression, increased VEGF secretion, and suppressed MMP-9 mRNA and secretion. Compared to heating or tension alone—which only affected some proteins—the combined stress treatments were able to

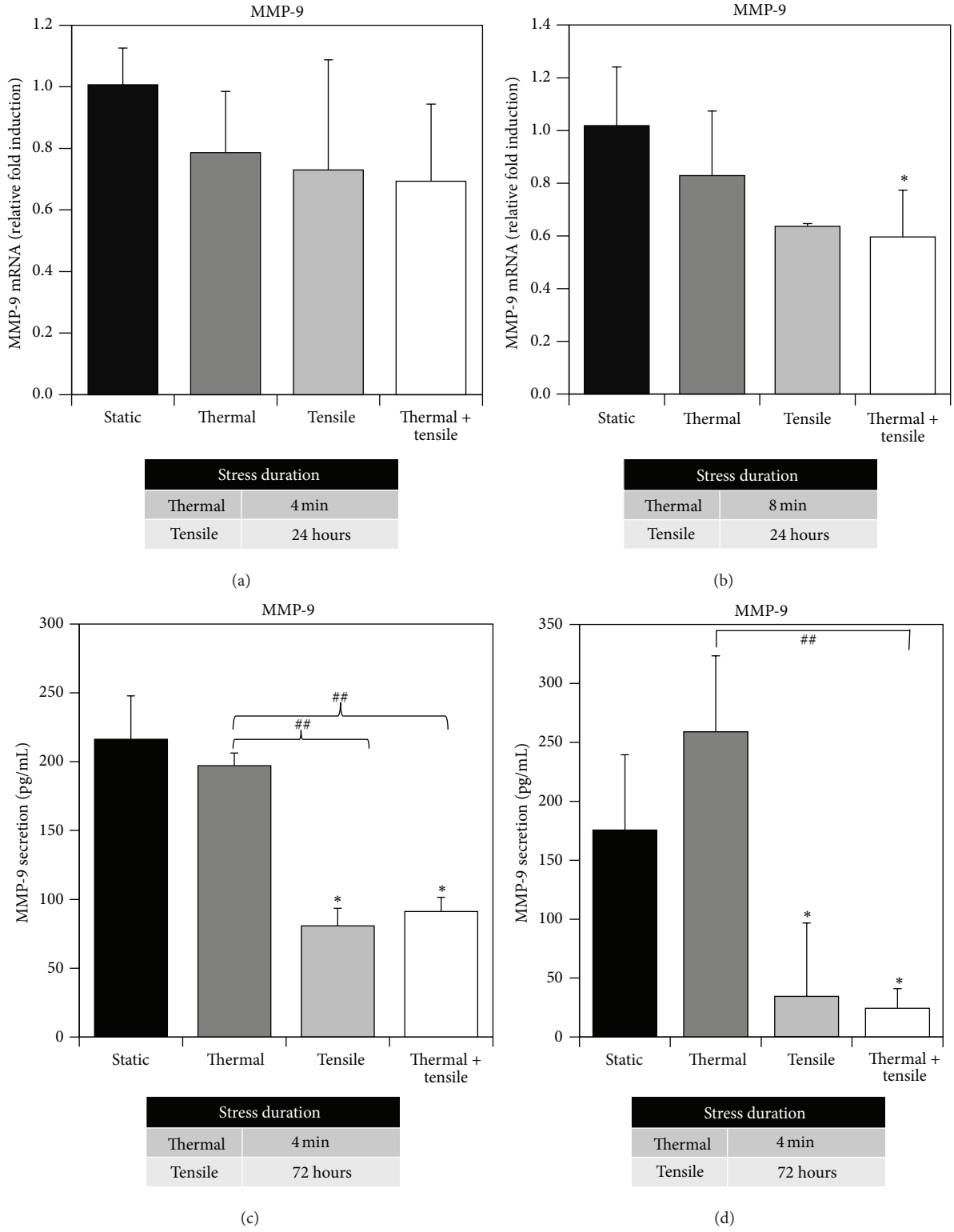

Figure 6: MMP-9 gene expression and protein secretion by MC3T3-E1 cells following a single dose of thermal stress (44°C, 4 or 8 minutes) and cyclic tension (equibiaxial 3%, 0.2 Hz, 10-second tension on/10-second rest) alone or in combination. MMP-9 mRNA expression was measured with RT-PCR following heating for 4 minutes (a) or 8 minutes (b) alone or in combination with cyclic tension for 24 hours. MMP-9 protein secretion was measured with ELISA in response to heating for 4 minutes (c) or 8 minutes (d) alone or in combination with cyclic tension for 72 hours. ∗ denotes statistical significance between stress-treated and sham-treated control groups ($P < 0.05$). ## denotes statistical significance between individual thermal stress and combined thermal and tensile stress ($n = 8$ for (a); $n = 4$ for (b)–(d)).

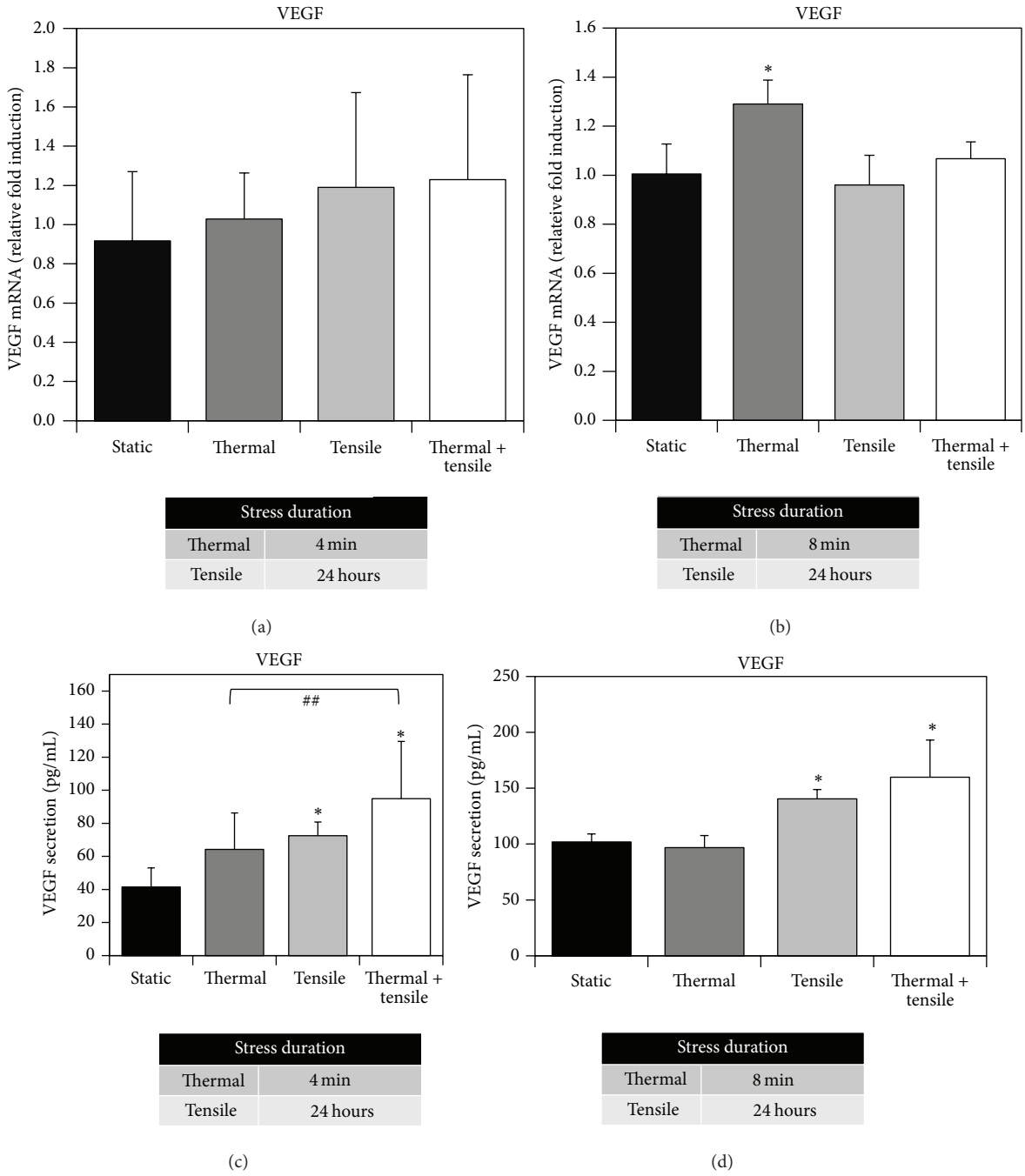

Figure 7: VEGF gene and protein expression by MC3T3-E1 cells following a single dose of thermal stress (44°C, 4 or 8 minutes) and cyclic tension for 24 hours (equibiaxial 3%, 0.2 Hz, 10-second tension on/10-second rest) alone or in combination. VEGF mRNA expression was measured with RT-PCR following heating for 4 minutes (a) or 8 minutes (b) alone or in combination with cyclic tension. VEGF protein secretion was measured with ELISA in response to heating for 4 minutes (c) or 8 minutes (d) alone or in combination with cyclic tension. ∗ denotes statistical significance between stress-treated and sham-treated control groups ($P < 0.05$). ## denotes statistical significance between individual thermal stress and combined thermal and tensile stress ($n = 8$ for (a) and (c); $n = 4$ for (b) and (d)).

produce changes across all proteins and enzymes investigated in this study. Therefore, our conditioning protocol of combined tensile stress (i.e., equibiaxial 3%, 0.2 Hz, intermittent mode of 10-second tension and 10-second rest) and thermal stress at 44°C for shorter duration than 10 minutes has the potential to impact bone healing and regeneration by upregulating cytoprotective proteins, modifying expression of bone-related proteins, and inducing synthesis of proteins essential for angiogenesis. Future research should focus on 3D *in vitro* studies that apply our combined thermal and mechanical stress protocol to cell-seeded constructs in order to develop bone tissue replacements suitable for healing

bone defects. These experiments should investigate long-term conditioning using single or repeated stress treatments to investigate whether this could more effectively enhance bone ECM maturation. Overall, the ability of combined stress to broadly influence cellular protein production, without inducing apoptosis, is a beneficial strategy for bone tissue engineering.

Conflict of Interests

The authors declare that there is no conflict of interests regarding the publication of this paper.

Acknowledgments

This research was supported by the following funding sources: National Science Foundation Grant CBET 0966546 and Institute for Critical Technologies and Applied Sciences (ICTAS) at Virginia Tech.

References

[1] A. C. Allori, A. M. Sailon, J. H. Pan, and S. M. Warren, "Biological basis of bone formation, remodeling, and repair—part III: biomechanical forces," *Tissue Engineering B: Reviews*, vol. 14, no. 3, pp. 285–293, 2008.

[2] J. Rubin, C. Rubin, and C. R. Jacobs, "Molecular pathways mediating mechanical signaling in bone," *Gene*, vol. 367, no. 1-2, pp. 1–16, 2006.

[3] J. Klein-Nulend, J. Roelofsen, C. M. Semeins, A. L. Bronckers, and E. H. Burger, "Mechanical stimulation of osteopontin mRNA expression and synthesis in bone cell cultures," *Journal of Cellular Physiology*, vol. 170, no. 2, pp. 174–181, 1997.

[4] E. A. B. E. Kaufmann, P. Ducheyne, and I. M. Shapiro, "Evaluation of osteoblast response to porous bioactive glass (45S5) substrates by RT-PCR analysis," *Tissue Engineering*, vol. 6, no. 1, pp. 19–28, 2000.

[5] M. Mizuno and Y. Kuboki, "Osteoblast-related gene expression of bone marrow cells during the osteoblastic differentiation induced by type I collagen," *Journal of Biochemistry*, vol. 129, no. 1, pp. 133–138, 2001.

[6] Y. Kaneshita, S. Goda, and T. Kawamoto, "The effect of matrix metalloproteinase-9 on the differentiation into osteoclast cells on RAW264 cells," *Orthodontic Waves*, vol. 66, no. 4, pp. 122–128, 2007.

[7] J. E. Aubin and E. Bonnelye, "Osteoprotegerin and its ligand: a new paradigm for regulation of osteoclastogenesis and bone resorption," *Osteoporosis International*, vol. 11, no. 11, pp. 905–913, 2000.

[8] S. I. S. Rattan, H. Sejersen, R. A. Fernandes, and W. Luo, "Stress-mediated hormetic modulation of aging, wound healing, and angiogenesis in human cells," *Annals of the New York Academy of Sciences*, vol. 1119, no. 1, pp. 112–121, 2007.

[9] M. Narutomi, T. Nishiura, T. Sakai, K. Abe, and H. Ishikawa, "Cyclic mechanical strain induces interleukin-6 expression via prostaglandin E2 production by cyclooxygenase-2 in MC3T3-E1 osteoblast-like cells," *Journal of Oral Biosciences*, vol. 49, no. 1, pp. 65–73, 2007.

[10] L. Tang, Z. Lin, and Y.-M. Li, "Effects of different magnitudes of mechanical strain on osteoblasts *in vitro*," *Biochemical and Biophysical Research Communications*, vol. 344, no. 1, pp. 122–128, 2006.

[11] S. P. Singh, E. I. Chang, A. K. Gossain et al., "Cyclic mechanical strain increases production of regulators of bone healing in cultured murine osteoblasts," *Journal of the American College of Surgeons*, vol. 204, no. 3, pp. 426–434, 2007.

[12] M. Motokawa, M. Kaku, Y. Tohma et al., "Effects of cyclic tensile forces on the expression of vascular endothelial growth factor (VEGF) and macrophage-colony-stimulating factor (M-CSF) in murine osteoblastic MC3T3-E1 cells," *Journal of Dental Research*, vol. 84, no. 5, pp. 422–427, 2005.

[13] C. M. Stanford, J. A. Morcuende, and R. A. Brand, "Proliferative and phenotypic responses of bone-like cells to mechanical deformation," *Journal of Orthopaedic Research*, vol. 13, no. 5, pp. 664–670, 1995.

[14] L. C. Winter, X. F. Walboomers, J. D. Bumgardner, and J. A. Jansen, "Intermittent versus continuous stretching effects on osteoblast-like cells *in vitro*," *Journal of Biomedical Materials Research A*, vol. 67, no. 4, pp. 1269–1275, 2003.

[15] X. Liu, X. Zhang, and Z.-P. Luo, "Strain-related collagen gene expression in human osteoblast-like cells," *Cell and Tissue Research*, vol. 322, no. 2, pp. 331–334, 2005.

[16] L. V. Harter, K. A. Hruska, and R. L. Duncan, "Human osteoblast-like cells respond to mechanical strain with increased bone matrix protein production independent of hormonal regulation," *Endocrinology*, vol. 136, no. 2, pp. 528–535, 1995.

[17] K. A. Bhatt, E. I. Chang, S. M. Warren et al., "Uniaxial mechanical strain: an *in vitro* correlate to distraction osteogenesis," *Journal of Surgical Research*, vol. 143, no. 2, pp. 329–336, 2007.

[18] J. E. Cillo Jr., R. Gassner, R. R. Koepsel, and M. J. Buckley, "Growth factor and cytokine gene expression in mechanically strained human osteoblast-like cells: implications for distraction osteogenesis," *Oral Surgery, Oral Medicine, Oral Pathology, Oral Radiology, and Endodontics*, vol. 90, no. 2, pp. 147–154, 2000.

[19] C. Shui and A. Scutt, "Mild heat shock induces proliferation, alkaline phosphatase activity, and mineralization in human bone marrow stromal cells and Mg-63 cells *in vitro*," *Journal of Bone and Mineral Research*, vol. 16, no. 4, pp. 731–741, 2001.

[20] H. G. Park, S. I. Han, S. Y. Oh, and H. S. Kang, "Cellular responses to mild heat stress," *Cellular and Molecular Life Sciences*, vol. 62, no. 1, pp. 10–23, 2005.

[21] K. R. Diller, "Stress protein expression kinetics," *Annual Review of Biomedical Engineering*, vol. 8, pp. 403–424, 2006.

[22] M. N. Rylander, K. R. Diller, S. Wang, and S. J. Aggarwal, "Correlation of HSP70 expression and cell viability following thermal stimulation of bovine aortic endothelial cells," *Journal of Biomechanical Engineering*, vol. 127, no. 5, pp. 751–757, 2005.

[23] S. Li, S. Chien, and P.-I. Brånemark, "Heat shock-induced necrosis and apoptosis in osteoblasts," *Journal of Orthopaedic Research*, vol. 17, no. 6, pp. 891–899, 1999.

[24] J. Ye, H. Haro, M. Takahashi, H. Kuroda, and K. Shinomiya, "Induction of apoptosis of articular chondrocytes and suppression of articular cartilage proteoglycan synthesis by heat shock," *Journal of Orthopaedic Science*, vol. 8, no. 3, pp. 387–395, 2003.

[25] T. Hojo, M. Fujioka, G. Otsuka, S. Inoue, U. Kim, and T. Kubo, "Effect of heat stimulation on viability and proteoglycan metabolism of cultured chondrocytes: preliminary report," *Journal of Orthopaedic Science*, vol. 8, no. 3, pp. 396–399, 2003.

[26] P. Y. Chao, C. H. Boon, H. Liu, S. T. Wei, and T. Cao, "Culture media conditioned by heat-shocked osteoblasts enhances the osteogenesis of bone marrow-derived mesenchymal stromal cells," *Cell Biochemistry and Function*, vol. 25, no. 3, pp. 267–276, 2007.

[27] E. Chung and M. N. Rylander, "Response of preosteoblasts to thermal stress conditioning and osteoinductive growth factors," *Cell Stress & Chaperones*, vol. 17, no. 2, pp. 203–214, 2012.

[28] M.-W. Lee, T. Muramatsu, T. Uekusa, J.-H. Lee, and M. Shimono, "Heat stress induces alkaline phosphatase activity and heat shock protein 25 expression in cultured pulp cells," *International Endodontic Journal*, vol. 41, no. 2, pp. 158–162, 2008.

[29] P. M. Pechan, "Heat shock proteins and cell proliferation," *The FEBS Letters*, vol. 280, no. 1, pp. 1–4, 1991.

[30] D. Lanneau, A. de Thonel, S. Maurel, C. Didelot, and C. Garrido, "Apoptosis versus cell differentiation: role of heat shock proteins HSP90, HSP70 and HSP27," *Prion*, vol. 1, no. 1, pp. 53–60, 2007.

[31] A. R. Shakoori, A. M. Oberdorf, T. A. Owen et al., "Expression of heat shock genes during differentiation of mammalian osteoblasts and promyeloctic leukemia cells," *Journal of Cellular Biochemistry*, vol. 48, no. 3, pp. 277–287, 1992.

[32] W. T. Gerthoffer and S. J. Gunst, "Invited review: focal adhesion and small heat shock proteins in the regulation of actin remodeling and contractility in smooth muscle," *Journal of Applied Physiology*, vol. 91, no. 2, pp. 963–972, 2001.

[33] K. Nagata, "Expression and function of heat shock protein 47: a collagen-specific molecular chaperone in the endoplasmic reticulum," *Matrix Biology*, vol. 16, no. 7, pp. 379–386, 1998.

[34] P. Srivastava, "Roles of heat-shock proteins in innate and adaptive immunity," *Nature Reviews Immunology*, vol. 2, no. 3, pp. 185–194, 2002.

[35] M. Atalay, N. Oksala, J. Lappalainen, D. E. Laaksonen, C. K. Sen, and S. Roy, "Heat shock proteins in diabetes and wound healing," *Current Protein and Peptide Science*, vol. 10, no. 1, pp. 85–95, 2009.

[36] A. F. Laplante, V. Moulin, F. A. Auger et al., "Expression of heat shock proteins in mouse skin during wound healing," *Journal of Histochemistry and Cytochemistry*, vol. 46, no. 11, pp. 1291–1301, 1998.

[37] T. R. Dafforn, M. Della, and A. D. Miller, "The molecular interactions of heat shock protein 47 (Hsp47) and their implications for collagen biosynthesis," *Journal of Biological Chemistry*, vol. 276, no. 52, pp. 49310–49319, 2001.

[38] M. Jäättelä, "Heat shock proteins as cellular lifeguards," *Annals of Medicine*, vol. 31, no. 4, pp. 261–271, 1999.

[39] J. C. Tiffee, J. P. Griffin, and L. F. Cooper, "Immunolocalization of stress proteins and extracellular matrix proteins in the rat tibia," *Tissue and Cell*, vol. 32, no. 2, pp. 141–147, 2000.

[40] Y. Harder, C. Contaldo, J. Klenk, A. Banic, S. M. Jakob, and D. Erni, "Improved skin flap survival after local heat preconditioning in pigs," *Journal of Surgical Research*, vol. 119, no. 1, pp. 100–105, 2004.

[41] C. Luna, G. Li, P. B. Liton, D. L. Epstein, and P. Gonzalez, "Alterations in gene expression induced by cyclic mechanical stress in trabecular meshwork cells," *Molecular Vision*, vol. 15, pp. 534–544, 2009.

[42] M. Jagodzinski, S. Hankemeier, M. van Griensven, U. Bosch, C. Krettek, and J. Zeichen, "Influence of cyclic mechanical strain and heat of human tendon fibroblasts on HSP-72," *European Journal of Applied Physiology*, vol. 96, no. 3, pp. 249–256, 2006.

[43] E. Chung and M. N. Rylander, "Response of a preosteoblastic cell line to cyclic tensile stress conditioning and growth factors for bone tissue engineering," *Tissue Engineering A*, vol. 18, no. 3-4, pp. 397–410, 2012.

[44] M.-C. Qi, S.-J. Zou, L.-C. Han, H.-X. Zhou, and J. Hu, "Expression of bone-related genes in bone marrow MSCs after cyclic mechanical strain: implications for distraction osteogenesis," *International Journal of Oral Science*, vol. 1, no. 3, pp. 143–150, 2009.

[45] A. Kadow-Romacker, J. E. Hoffmann, G. Duda, B. Wildemann, and G. Schmidmaier, "Effect of mechanical stimulation on osteoblast- and osteoclast-like cells *in vitro*," *Cells Tissues Organs*, vol. 190, no. 2, pp. 61–68, 2009.

[46] S. E. Theocharis, H. Kanelli, A. P. Margeli, C. A. Spiliopoulou, and A. S. Koutselinis, "Metallothionein and heat shock protein expression during acute liver injury and regeneration in rats," *Clinical Chemistry and Laboratory Medicine*, vol. 38, no. 11, pp. 1137–1140, 2000.

[47] M. N. Rylander, Y. Feng, K. Zimmermann, and K. R. Diller, "Measurement and mathematical modeling of thermally induced injury and heat shock protein expression kinetics in normal and cancerous prostate cells," *International Journal of Hyperthermia*, vol. 26, no. 8, pp. 748–764, 2010.

[48] Y.-F. Chou, J. C. Y. Dunn, and B. M. Wu, "*in vitro* response of MC3T3-E1 preosteoblasts within three-dimensional apatite-coated PLGA scaffolds," *Journal of Biomedical Materials Research B Applied Biomaterials*, vol. 75, no. 1, pp. 81–90, 2005.

[49] Y. W. Lee, S. Y. Eum, K. C. Chen, B. Hennig, and M. Toborek, "Gene expression profile in interleukin-4-stimulated human vascular endothelial cells," *Molecular Medicine*, vol. 10, no. 1–6, pp. 19–27, 2004.

[50] I. Riederer, E. Negroni, A. Bigot et al., "Heat shock treatment increases engraftment of transplanted human myoblasts into immunodeficient mice," *Transplantation Proceedings*, vol. 40, no. 2, pp. 624–630, 2008.

[51] B. I. Knoll, T. L. McCarthy, M. Centrella, and J. Shin, "Strain-dependent control of transforming growth factor-β function in osteoblasts in an *in vitro* model: biochemical events associated with distraction osteogenesis," *Plastic and Reconstructive Surgery*, vol. 116, no. 1, pp. 224–233, 2005.

[52] K. D. Fong, R. P. Nacamuli, E. G. Loboa et al., "Equibiaxial tensile strain affects calvarial osteoblast biology," *The Journal of Craniofacial Surgery*, vol. 14, no. 3, pp. 348–355, 2003.

[53] C.-H. Huang, M.-H. Chen, T.-H. Young, J.-H. Jeng, and Y.-J. Chen, "Interactive effects of mechanical stretching and extracellular matrix proteins on initiating osteogenic differentiation of human mesenchymal stem cells," *Journal of Cellular Biochemistry*, vol. 108, no. 6, pp. 1263–1273, 2009.

[54] D. S. Latchman, "Heat shock proteins and cardiac protection," *Cardiovascular Research*, vol. 51, no. 4, pp. 637–646, 2001.

[55] Z. Zheng, J. Y. Kim, H. Ma, J. E. Lee, and M. A. Yenari, "Anti-inflammatory effects of the 70 kDa heat shock protein in experimental stroke," *Journal of Cerebral Blood Flow and Metabolism*, vol. 28, no. 1, pp. 53–63, 2008.

[56] M. M. Hutter, R. E. Sievers, V. Barbosa, and C. L. Wolfe, "Heat-shock protein induction in rat hearts: a direct correlation between the amount of heat-shock protein induced and the degree of myocardial protection," *Circulation*, vol. 89, no. 1, pp. 355–360, 1994.

[57] D. A. Sawatzky, R. Foster, M. P. Seed, and D. A. Willoughby, "Heat-shock proteins and their role in chondrocyte protection,

an application for autologous transplantation," *Inflammopharmacology*, vol. 12, no. 5-6, pp. 569–589, 2005.

[58] N. Suzuki, Y. Yoshimura, Y. Deyama, K. Suzuki, and Y. Kitagawa, "Mechanical stress directly suppresses osteoclast differentiation in RAW264.7 cells," *International Journal of Molecular Medicine*, vol. 21, no. 3, pp. 291–296, 2008.

[59] A. Fornoni, F. Cornacchia, G. A. Howard, B. A. Roos, G. E. Striker, and L. J. Striker, "Cyclosporin A affects extracellular matrix synthesis and degradation by mouse MC3T3-E1 osteoblasts *in vitro*," *Nephrology Dialysis Transplantation*, vol. 16, no. 3, pp. 500–505, 2001.

[60] G.-Z. Zeng, N.-H. Tan, X.-J. Hao, Q.-Z. Mu, and R.-T. Li, "Natural inhibitors targeting osteoclast-mediated bone resorption," *Bioorganic and Medicinal Chemistry Letters*, vol. 16, no. 24, pp. 6178–6180, 2006.

[61] C. Colnot, Z. Thompson, T. Miclau, Z. Werb, and J. A. Helms, "Altered fracture repair in the abscence of MMP9," *Development*, vol. 130, no. 17, pp. 4123–4133, 2003.

[62] B. Gong, G. K. Asimakis, Z. Chen et al., "Whole-body hyperthermia induces up-regulation of vascular endothelial growth factor accompanied by neovascularization in cardiac tissue," *Life Sciences*, vol. 79, no. 19, pp. 1781–1788, 2006.

[63] M.-S. Kim, Y. K. Kim, K. H. Cho, and J. H. Chung, "Infrared exposure induces an angiogenic switch in human skin that is partially mediated by heat," *British Journal of Dermatology*, vol. 155, no. 6, pp. 1131–1138, 2006.

[64] R. A. D. Carano and E. H. Filvaroff, "Angiogenesis and bone repair," *Drug Discovery Today*, vol. 8, no. 21, pp. 980–989, 2003.

Hindawi Publishing Corporation
BioMed Research International
Volume 2014, Article ID 217078, 15 pages
http://dx.doi.org/10.1155/2014/217078

Research Article

ECM Inspired Coating of Embroidered 3D Scaffolds Enhances Calvaria Bone Regeneration

C. Rentsch,[1,2] B. Rentsch,[3] S. Heinemann,[4] R. Bernhardt,[4] B. Bischoff,[1] Y. Förster,[1,2] D. Scharnweber,[4,5] and S. Rammelt[1,5]

[1] *Department of Trauma and Reconstructive Surgery, University Hospital Carl Gustav Carus, Technische Universität Dresden, Fetscherstraße 74, 01307 Dresden, Germany*
[2] *Centre for Translational Bone, Joint and Soft Tissue Research, University Hospital and Medical Faculty, Technische Universität Dresden, Fetscherstraße 74, 01307 Dresden, Germany*
[3] *Catgut GmbH, Gewerbepark 18, 08258 Markneukirchen, Germany*
[4] *Max Bergmann Center of Biomaterials, Budapester Straße 27, 01069 Dresden, Germany*
[5] *DFG-Center for Regenerative Therapies Dresden (CRTD), Fetscherstraße 105, 01307 Dresden, Germany*

Correspondence should be addressed to C. Rentsch; claudia.rentsch@uniklinikum-dresden.de

Received 6 November 2013; Revised 27 March 2014; Accepted 11 April 2014; Published 11 June 2014

Academic Editor: Yin Xiao

Resorbable polymeric implants and surface coatings are an emerging technology to treat bone defects and increase bone formation. This approach is of special interest in anatomical regions like the calvaria since adults lose the capacity to heal large calvarial defects. The present study assesses the potential of extracellular matrix inspired, embroidered polycaprolactone-co-lactide (PCL) scaffolds for the treatment of 13 mm full thickness calvarial bone defects in rabbits. Moreover the influence of a collagen/chondroitin sulfate (coll I/cs) coating of PCL scaffolds was evaluated. Defect areas filled with autologous bone and empty defects served as reference. The healing process was monitored over 6 months by combining a novel ultrasonographic method, radiographic imaging, biomechanical testing, and histology. The PCL coll I/cs treated group reached 68% new bone volume compared to the autologous group (100%) and the biomechanical stability of the defect area was similar to that of the gold standard. Histological investigations revealed a significantly more homogenous bone distribution over the whole defect area in the PCL coll I/cs group compared to the noncoated group. The bioactive, coll I/cs coated, highly porous, 3-dimensional PCL scaffold acted as a guide rail for new skull bone formation along and into the implant.

1. Introduction

The majority of cranial bone defects are caused by trauma, congenital deformity, or tumor resection. The skull bone has to be reconstructed to improve the functional and cosmetic outcome, correlating with the subsequent quality of life [1–3]. Since successful spontaneous healing only occurs in infants younger than two years, a variety of materials have been proposed to repair such defects, including autologous or allogeneic bone grafts, alloplastic materials, and tissue engineered bone scaffolds optionally seeded with cells or growth factors [2, 4]. Autologous bone grafts are the gold standard, but their clinical use is limited by donor site morbidity, availability, additional surgery, bone resorption at the recipient site, and difficulties with three-dimensional contouring [3, 4]. The most commonly used alloplastic materials are metals (e.g., stainless steel, titanium, gold, and aluminum), polymers (e.g., polymethyl methacrylate), and ceramics based on hydroxyapatite (HA). All metals, most ceramics, and many polymers are not considered to be biodegradable and therefore cannot be fully replaced by host bone tissue [5]. Foreign body reactions, stress shielding, and long term problems like infections, bone resorption, wound dehiscence, sunken bone flap, hematoma, and intraoperative hemodynamic instability are further issues [3]. The large amount of methods reflects that each technique has its own advantages and disadvantages as well as the need for new and improved treatment options [2].

Synthetic biodegradable scaffolds have been developed as an alternative for bone reconstruction. Implant materials based on calcium phosphate, biodegradable polymers, and composites, partly in combination with growth factors, bone marrow, or mesenchymal stem cells, are currently being studied as alternatives, but until now none of the synthetic bone graft materials has been generally accepted [6–11].

Natural or synthetic polymers can provide customized three-dimensional porous matrices that can temporarily support cells and guide their development [10–13].

The polyester of D,L-lactid, glycolid, or ε-caprolactone and their copolymers are approved by health authorities in various countries and commonly studied materials for biomedical applications in bone and cartilage repair [11, 14–19].

The polycaprolactone-co-lactide (PCL) used for this study was synthesized by ring-opening copolymerization of L-lactide and ε-caprolactone, with a molecular ratio of 75/25 (Gunze Ltd., Kyoto, Japan). Melt spinning of the material resulted in a resorbable, monofilament fiber, which is commercially available and approved as a medical device (PCL, surgical suture, Catgut GmbH, Markneukirchen, Germany) [14, 16, 20].

Embroidering, a traditional manufacturing technique, was used to produce PCL scaffolds allowing the control of their shape and size, the arrangement, and the orientation of the fibers. In addition, this technique is an effective tool to produce highly porous scaffolds that are required to allow cell ingrowth and an efficient transport of nutrients, oxygen, growth factors, and waste products through a rich vascularization. Despite these advantages, only few reports on this method are available [11, 18, 20–23].

Tissue engineering strategies include the transplantation of different kinds of cells alone or seeded on a variety of scaffolds and/or the use of biomolecules (growth factors, proteins, peptides, or polysaccharides), which affect the cells of the target tissue [24, 25].

In bone the organic extracellular matrix (ECM) consists of a highly ordered, site-specific network that is mainly composed of collagen type I (coll I) and smaller amounts of glycoproteins like fibronectin, proteoglycans like decorin and biglycan, and the glycosaminoglycans (GAGs) like chondroitin sulfate (cs), hyaluronan, dermatan, and heparan sulfate [26].

A promising approach to guide morphogenesis and tissue repair is mimicking the extracellular matrix to actively influence the cellular reaction and interaction with growth factors and cytokines [10, 27, 28]. A first step in the formation of an artificial ECM (aECM) is the immobilization of coll I to the surface of scaffolds or implants [20, 29–31].

The properties of bone implants can be further improved by the addition of GAGs like cs [11, 28, 32–35]. CS plays a key role in bone development, remodeling, and healing by interacting with other molecules of the ECM, mediating cell adhesion, and providing the binding of different growth factors or cytokines on the ECM [11, 20, 28, 33, 36, 37]. Several *in vitro* and *in vivo* studies on long bones have demonstrated that embroidered PCL scaffolds biologically modified with coll I/cs provide an appropriate network of interconnecting pores to act as a temporary matrix for cell adhesion, migration, proliferation, and differentiation [11, 18, 20, 21, 23].

In the light of these results, the present study was designed to assess the healing capacity of the bioactive, coll I/cs coated, highly porous, 3-dimensional PCL scaffolds as skull bone implants.

During skeletal formation the calvarial bone involves a process known as intramembranous ossification (cartilage is not present) which is different from endochondral ossification processes in long bones. Compared to long bones, calvarial bone is more biological inert due to its reduced blood supply. It has to be considered that calvarial bone lacks muscle enclosures so the blood supply is less than in long bones. According to that it is even more important to reach a good scaffold vascularization in animal experimental investigations.

The aim of this study was to verify the design of the implant as skull bone implant. Additionally, the bone healing quality in a mechanically unloaded bone defect, the performance of the implant material, the status of inflammation, and vascularization were evaluated.

To achieve this goal four groups ($n = 8$) of randomly divided New Zealand white rabbits were treated with either noncoated or coll I/cs coated PCL scaffolds. Untreated defects and defects treated with autologous bone grafting, as the current clinical gold standard, served as controls. New bone formation was determined using ultrasound as life imaging method as well as by radiological, computer tomographical, biomechanical, and histological investigations.

2. Materials and Methods

2.1. Production and Coating of the PCL Scaffolds. The polycaprolactone-co-lactide was synthesized of L-lactide and ε-caprolactone, with a molecular ratio of 75/25 (Gunze Ltd., Kyoto, Japan), melt spun, and resulted in a resorbable, monofilament fiber (PCL, surgical suture, Catgut GmbH, Markneukirchen, Germany). The textile scaffolds were made on a computer aided embroidery machine and had a triaxial structure with a stitch length of 1.4 mm and a mesh spacing of 1.2 mm. The polyvinyl alcohol (ground fabrics) was removed from the embroidered scaffolds by washing them with water and the protecting glaze was washed from the scaffolds with n-heptane. Afterwards the scaffolds were treated with 1 M NaOH in 50% methanol for hydrophilization of the scaffold surface, washed with water, dried, and finally sterilized with ethylene oxide [20].

The PCL scaffolds were coated with the coll I/cs matrix using a dip coating process. Porcine skin coll I (MBP GmbH, Neustadt-Glewe, Germany) was suspended in 0.01 M acetic acid, diluted to 2.5 mg/mL in phosphate buffer (10 mM KH_2PO_4, 50 mM Na_2HPO_4, pH 7.4) with 1.25 mg/mL porcine cs A (cs of porcine trachea, Kraeber & Co GmbH, Ellerbek, Germany). Coll I fibrils were adsorbed on the scaffold surface, whereas cs was immobilized within the collagen matrix after an incubation of 2 h at 37°C. The scaffolds were washed twice with water, dried, and finally sterilized with ethylene

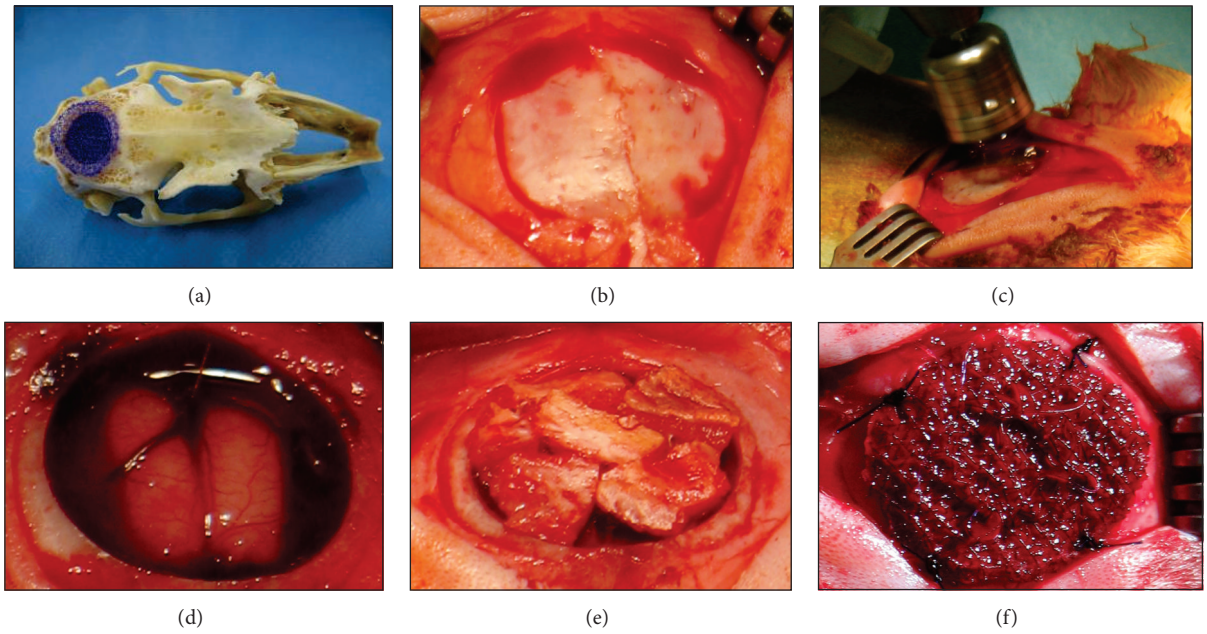

Figure 1: Surgical procedure. (a) Representing photograph showing the scaffold and the implantation site (defect) in a macerated rabbit skull. (b) Intraoperative situs of the cranium after removal of the periost in a diameter of 15 mm. (c) Creation of the defect by trephine drilling. (d) Untreated defect. (e) Autologous bone pieces were fixed with fibrin glue. (f) Defect filling with a PCL scaffold.

oxide. The characterization of the scaffold coating and the cell response was previously described by Rentsch et al., [20].

2.2. Scaffold Design. Scaffolds for the skull defect had a size of 13 mm in diameter and a total thickness of 3 mm according to that of the calvarial bone. An overlapping lid of 19 mm in diameter and 1 mm thickness was added to prevent subsidence. Both embroidered scaffold parts (main scaffold and lid scaffold) were made and sewn together on electronically guided machines (Möckel embroidery and engineering company, Auerbach, Germany). The 13 × 3 mm part of the scaffold was placed within the calvarial defect area. The 19 mm in diameter lid fixed the implant in place due to the contact of the surrounding skull bone.

2.3. Microcomputer Tomography (μCT) of the Scaffolds. For a nondestructive μCT analysis a Scanco vivaCT 75 system (Scanco Medical, Brüttisellen, Switzerland) was used. The samples were measured by radiological energy of 55 keV and 1500 projections. The voxel resolution of the reconstructed volume was 20 μm. The porosity and the pore size distribution were measured with the Scanco evaluation software.

2.4. Scanning Electron Microscopy (SEM). Samples were mounted on stubs, coated with a 50 nm gold layer (Leica EM SCD 005, Leica Microsystems GmbH, Vienna, Austria), and scaffolds were observed in a XL30 FEG ESEM (Philips, Eindhoven, Netherland) in a HiVak mode with acceleration voltages of 2–10 kV.

2.5. Animal Experiments. The study has been licensed by the regional veterinary board (24-9168.11-1/2009-5). All animals were cared for according to the European guidelines for the care and use of laboratory animals (Directive 24.11.1986, 86/609/CEE). A total number of 32 New Zealand white rabbits (female, on average 3 kg, Charles River Laboratories, Sulzfeld, Germany) were divided randomly into the following 4 groups of 8 animals: empty control group; autologous bone group (representing the clinical gold standard); PCL noncoated group; and PCL coll I/cs coated group.

The rabbits were anaesthetized with a combination of ketamine (35 mg/kg body weight, Kemint, Alvetra GmbH, Neumünster, Germany) and xylazine (5 mg/kg body weight, Rompun, Bayer, Germany). The surgical sites were depilated using depilatory cream (Veet GmbH, Mannheim, Germany) and disinfected (Cutasept G, Bode Chemie GmbH, Hamburg, Germany). A sagittal incision was made at the skull along the midline from the frontal to the occipital bone. The periosteum was resected in a diameter of 15 mm and a 13 mm full thickness defect bone was created carefully in the central parietal skull with a dental trephine (L10 mm, D13 mm, Meisinger, Neuss, Germany) with continuous irrigation of sterile saline (NaCl 0.9%, Fresenius GmbH, Bad Homburg, Germany). The cranial cap was removed and care was taken to prevent damage to the dura (Figures 1(b)–1(d)).

The defect in the autologous bone group was filled with preserved fragmented autologous skull bone. Therefore, the removed cranial cap was split into 8–10 bone fragments using surgical tongs. The bone pieces were placed upside down directly onto the dura covering the defect area as good as possible, followed by a fixation with fibrin glue (Tissucol Dus S, Baxter GmbH, Unterschleißheim, Germany) to prevent migration of the bone pieces. PCL groups received either noncoated or coll I/cs coated implants (Figures 1(e) and 1(f)). Finally, the soft tissue was folded

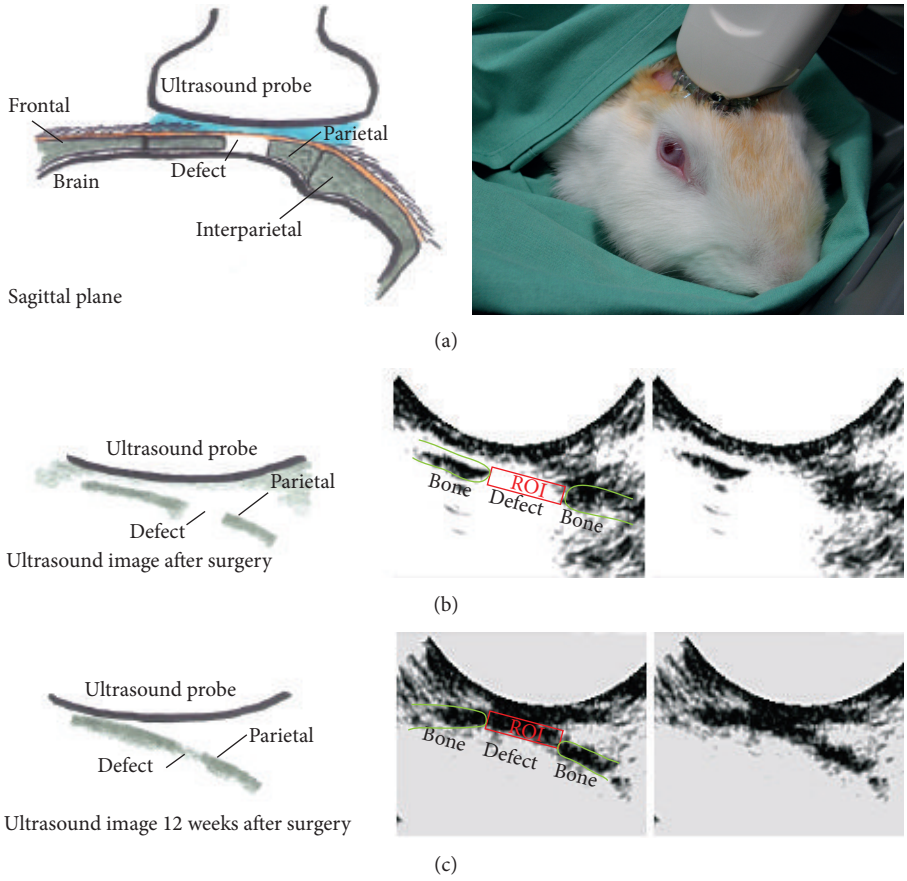

FIGURE 2: Schematic presentation of ultrasonographic examination of the rabbit skull and image analysis. (a) Defect location and ultrasound probe positioning during examination. (b) Schematic drawing (left) and corresponding ultrasound image (right) of an empty defect 24 h after surgery. (c) Schematic drawing (left) and ultrasound image (right) of a PCL coll I/cs coated scaffold at 12 weeks after surgery with evident new tissue formation. A defined ROI (red square) was used to quantify the tissue formation within the defect area and both parietal bone ends are marked in green.

back and closed with a nonresorbable suture (Mariderm, Catgut GmbH, Markneukirchen). A single-shot antibiotic prophylaxis (15 mg/kg body weight, Duphamox, Pfizer GmbH, Berlin, Germany) was administered and Carprofen (1.4 mg/kg body weight, Rimadyl, Pfizer GmbH, Berlin, Germany) was given immediately and 24 hours after surgery for pain prevention. The healing process was monitored using ultrasonography. After 6 months all animals were anesthetized (ketamine/xylazine mixture) and euthanized with a combination compound of 200 mg Embutramide, 50 mg Mebezonium, and 5 mg Tetracaine per 1 mL (0.3 mL/kg body weight i.v., T61, Intervent GmbH Unterschleißheim, Germany). The entire cranial vault was carefully removed from each animal with an oscillating saw and all samples were fixed in 4% formalin (SAV LP GmbH, Flintsbach, Germany) until further analysis.

2.6. Tracking of New Bone Formation via Ultrasound. A PC-sonographic system (taberna pro medicum GmbH, Lüneburg, Germany) containing a TELEMED eco blaster 128 (TELEMED, Vilnius, Lithuania) and a C3.5/20/128 sensor was used for imaging the defect at 24 hours and 6 and 12 weeks following surgery (Figure 2). The following measurement parameters were defined: a frequency of 3 MHz, 53 frames per second, depth of 90 mm, averaging 8 images, and a dynamic of 72 dB. Rabbits were placed in a small animal care box and covered with a blanket; thereby no anesthesia was necessary during the examination. Approximately 5 mL of ultrasound gel (Dahlhausen & Co. GmbH, Köln, Germany) was applied onto the skull. Three images were obtained for each animal per group and time point. Images were quantified by ImageJ (http://rsb.info.nih.gov/ij/) using a defined region of interest (ROI) (Figures 2(a), 2(b), and 2(c)). The gray scale picture was transferred to an 8 bit image presenting a color range between 0 (white) and 255 (black). After applying a threshold frame of 188–255, all black pixels per area of ROI were quantified.

2.7. Radiographic Imaging. Plain radiographs were taken of all explants with a mobile X-ray unit (AMX 4, GE Healthcare, Buckinghamshire, UK) using 52 kV and 2.5 mAs.

2.8. Microcomputed Tomography (μCT) Analysis of the Explants. All explants of each group were assessed with a nondestructive μCT analysis using the Scanco vivaCT

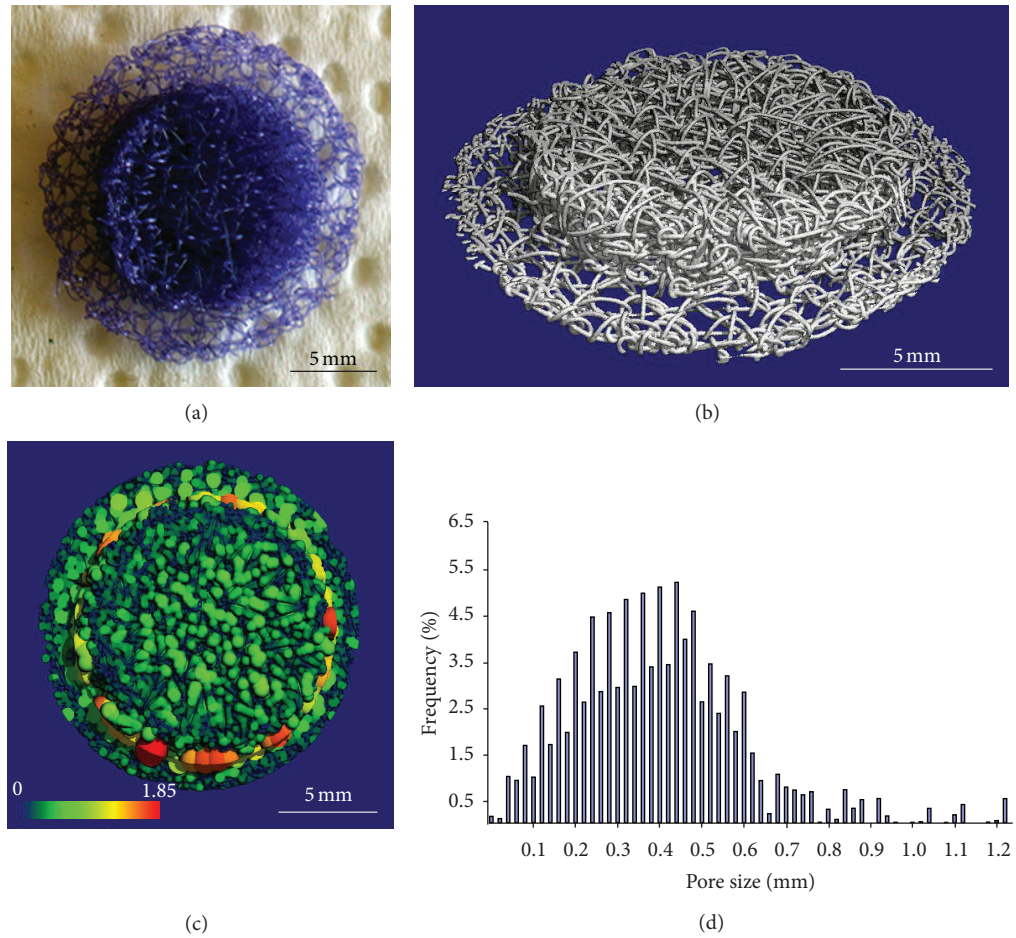

FIGURE 3: Characteristics of the embroidered scaffold designed for calvarium reconstruction. (a) Photograph and (b) three-dimensional μCT reconstruction of the embroidered scaffold showing an open porosity of 87%. ((c) and (d)) The analysis of the pore size distribution (Scanco vivaCT 75 system) showed homogeneously interconnected pores ranging between 0.06 and 0.7 mm distributed over the whole stack.

75 systems (Scanco Medical, Brüttisellen, Switzerland). The explanted and fixed samples were measured with X-ray energy of 70 keV and 500 projections. The voxel resolution of the reconstructed images was 70 μm. The quantification of the new bone volume within the defect area was done using 55 sagittal μCT images (8 animals/group) with an image distance of 0.236 mm each. A region of interest (ROI) was defined and the pixel/area was quantified using ImageJ (Figure 6(c)). The bone volume within the ROI of each group was then expressed as a percentage of the total defect volume of nonoperated calvarial bone (not shown). The latter was set to 100%.

2.9. Biomechanical Testing. Push-out tests of the tissue-engineered calvaria and control samples were performed to evaluate the mechanical integrity of the defect area. An Instron 5566 uniaxial testing system (Instron, Pfungstadt, Germany) equipped with a 10 kN load cell and a flat 10 mm diameter indenter fitting centered in the defect area was used. An initial load of 1 N was applied, followed by constant displacement at a strain rate of 0.9 mm/min until implant failure. Force and displacement were recorded simultaneously. Relative stiffness of the implant site was calculated as a quotient of ultimate force and corresponding displacement. Four samples were tested for each group.

2.10. Histology. A 2 × 2 cm sample centered around the defect was cut out of the rabbit calvarium. The samples were washed, decalcified for 1 week in ethylenediaminetetraacetic acid (OSTEOSOFT, Merck KGaA, Darmstadt, Germany; to adjust pH to 7.4–7.6 use NaOH) using an automated microwave based tissue Processor RHS-1 (Diapath S.p.A, Martinengo, Italy), and dehydrated overnight in a Thermo Scientific STP 420ES Tissue Processor (Microm International GmbH, Walldorf, Germany). Each sample was divided into two equal parts and one was embedded in a horizontal and one in a vertical orientation in methyl methacrylate (Technovit 9100 N, Heraeus Kulzer GmbH, Werheim, Germany). Sections of 3 μm of were prepared with a rotation microtome RM2055 (Leica Microsystems, Wetzlar, Germany) and the methyl methacrylate was removed using twice xylene for 20 min, twice 2-methoxy ethyl acetate for 20 min, twice acetone for 5 min, and 80% ethanol. Samples were stained for light

Table 1: Characteristics of the embroidered scaffolds designed for calvarial defects in rabbits.

Scaffold disk thickness (mm)	Diameter (mm)	Weight (mg)	Porosity (%)	Mean pore size (μm)	Range pore size > 1% (μm)
Total 4					
Overlapping lid 1	Overlapping lid 19	107.2 ± 7.2	87	425	60–700
Basis scaffold 3	Basis scaffold 13				

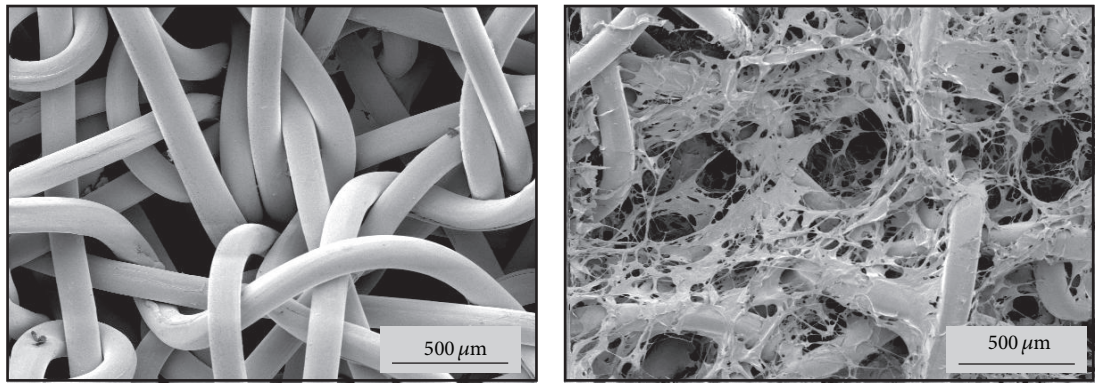

(a) (b)

Figure 4: SEM micrographs of the embroidered PCL scaffolds. (a) Noncoated PCL scaffold. The triaxial structure had a stitch length of 1.4 mm and a mesh spacing of 1.2 mm. (b) PCL coll I/cs coated scaffold. The coating covers the polymer fibers and partly fills the pores.

microscopy (Leica DMRBE Research Microscope, Camera Leica DC300, Leica Microsystems, Wetzlar, Germany) with Haematoxylin & Eosin (HE), (VWR, International GmbH, Darmstadt, Germany) and Masson-Goldner trichrome staining (Masson-Goldner trichrome staining kit, Merck KGaA, Darmstadt, Germany). Finally, sections were mounted in Canada balsam solution (Sigma-Aldrich Chemie GmbH, Munich, Germany). Four samples were tested for each group. Three histological sections of each animal (both section planes) were evaluated individually.

2.11. Data Analysis. All statistical analyses were done using the Student's t-test.

3. Results

3.1. μCT and SEM of PCL Scaffolds. Scaffolds for the skull defect had a size of 13 mm in diameter and a total thickness of 3 mm according to that of the calvarial bone, including an overlapping lid of 19 mm to prevent subsidence (Figures 3(a) and 3(b)). Scaffold analysis, using μCT, revealed an open porous network of 87% with a pore size of 0.06–0.7 mm (Figures 3(c) and 3(d); Table 1).

Figure 4 presents an SEM image of the PCL fibers within the 3-dimensional scaffold (Figure 4(a)). After surface coating with coll I/cs an additional network of extracellular components was presented to the new ingrowing tissue (Figure 4(b)).

3.2. Surgical Procedure. All 32 animals survived the surgery and the following 6 months without any complications.

3.3. Tracking of Tissue Formation within the Defect Area with Ultrasonography. The 13 mm skull defect could be detected reliably via ultrasound after surgery and new bone formation could be followed up to 12 weeks (Figure 5). The empty defect showed the lowest tissue formation compared to all other groups over all time points of measurement. Within the 12 weeks a significant increase of tissue formation could be measured (3.6%, 22.2%, and 54.5%). The group containing autologous bone showed a permanent tissue volume of around 80% over all time points. According to that fact, possible healing processes within bone fragments could not be detected via sonification. The PCL noncoated and PCL coll I/cs coated group showed a higher ultrasound reflecting matrix (17.8% and 14.3% after surgery) in the defect area compared to the empty control group (3.60% after surgery). After 6 weeks, the PCL noncoated and PCL coll I/cs coated groups presented four times as much (70%) matrix within the defect area compared to the postsurgery measurements, indicating a matrix forming process. Finally, the PCL coll I/cs coated group showed significantly more (90.6%) detectable tissue than the PCL noncoated group (80.6%).

3.4. Radiographic and μCT Analysis of the Explants. Six months after surgery new bone formation could be visualized in all animals of each group in plain radiographs (Figure 6(a)) and μCT (Figure 6(b)). The empty defect group showed new bone formation predominantly at the margin of the defect. All reimplanted bone fragments of the autologous bone group were reconnected to the skull bone or among themselves, but no new homologous bone formation occurred. Single fragments could still be detected. Both implant groups showed a higher new bone formation compared to the empty

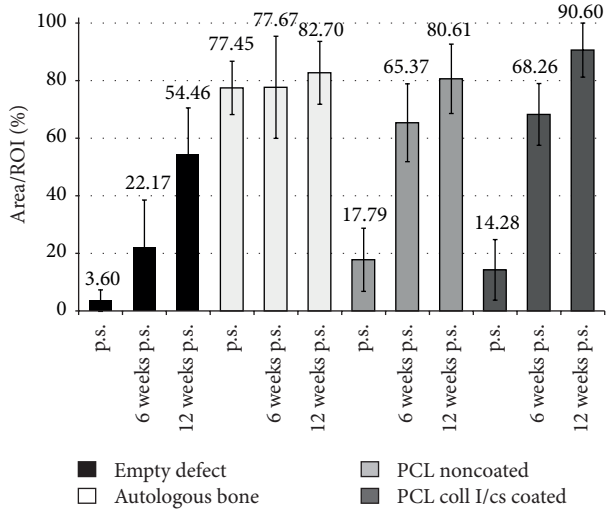

Significances	After surgery (p.s.)	6 weeks p.s.	12 weeks p.s.
Empty defect/autologous bone	***	***	***
Empty defect/PCL noncoated	***	***	***
Empty defect/coll I/cs coated	***	***	***
Autologous bone/PCL noncoated	***	*	0.67
Autologous bone/PCL coll I/cs coated	***	0.053	*
PCL noncoated/PCL coll I/cs coated	0.45	0.57	*

FIGURE 5: Tracking of new tissue formation with ultrasonography. Significances as indicated: $^{*}P < 0.05$, $^{**}P < 0.01$, $^{***}P < 0.001$ (Student's t-test).

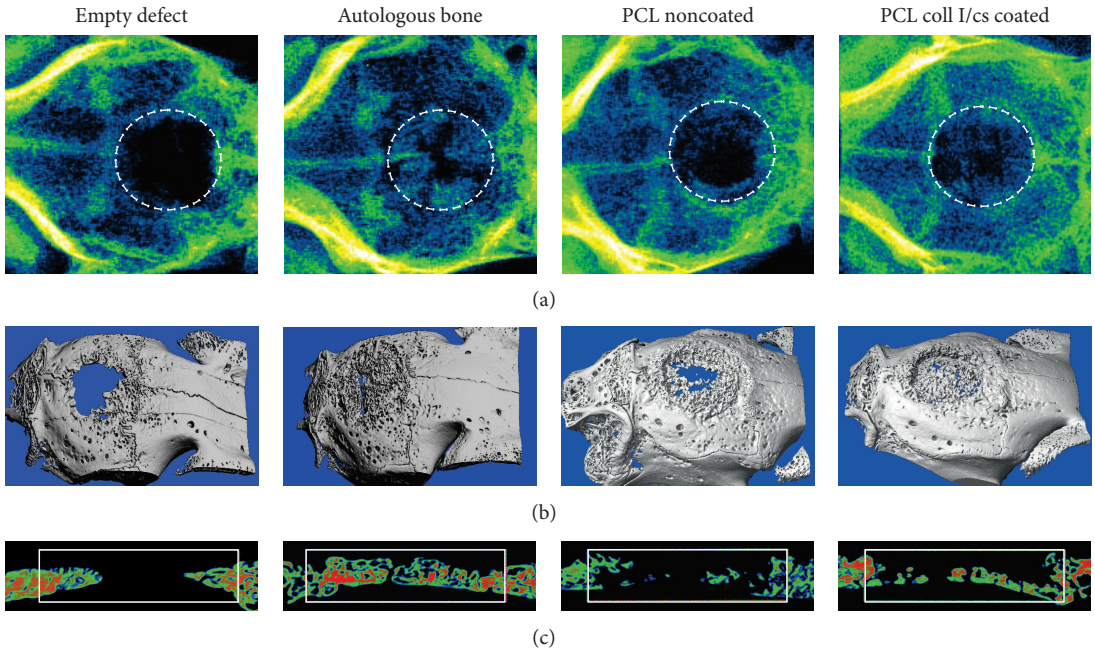

FIGURE 6: Radiography, 3-dimensional μCT reconstruction, and μCT bone quantification. (a) Radiographs taken after skull preparation (false coloring). The defect area is marked with a white circle. (b) Image of a 3-dimensional μCT reconstruction. (c) Sagittal section plane of the defect area. The white frame presents the ROI for bone quantification. One representative image of one animal from each group is shown.

group. The PCL coll I/cs coated scaffolds showed a more homologous new bone formation across the whole defect area compared to the PCL noncoated implants. Cross sections for bone quantification confirmed these findings (Figure 6(c)).

3.5. Quantification of New Bone Formation (μCT Analysis). Based on the μCT quantification of newly produced bone in the defect area, the PCL coll I/cs coated group (47.1%) showed the largest amount of new bone formation compared to PCL

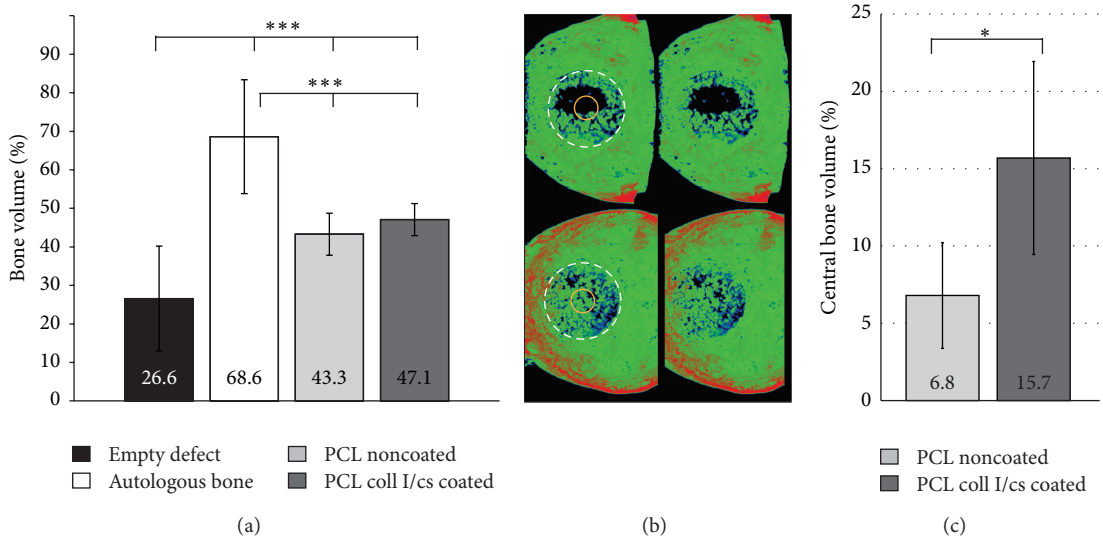

Figure 7: Quantification of bone volume within the defect area. (a) Quantification of bone volume related to the entire bone defect area of 13 mm. (b) Representative images of PCL noncoated (top) and PCL coll I/cs coated (bottom) 3-dimensional μCT reconstructions. The left images are marked for visualization and right picture presents the original. The white circles in the left images represent the whole defect area and the yellow circles the 4 mm central part. (c) Quantification of bone formation in the central defect area. Significant differences as indicated: $^{*}P < 0.05$, $^{***}P < 0.001$ (Student's t-test).

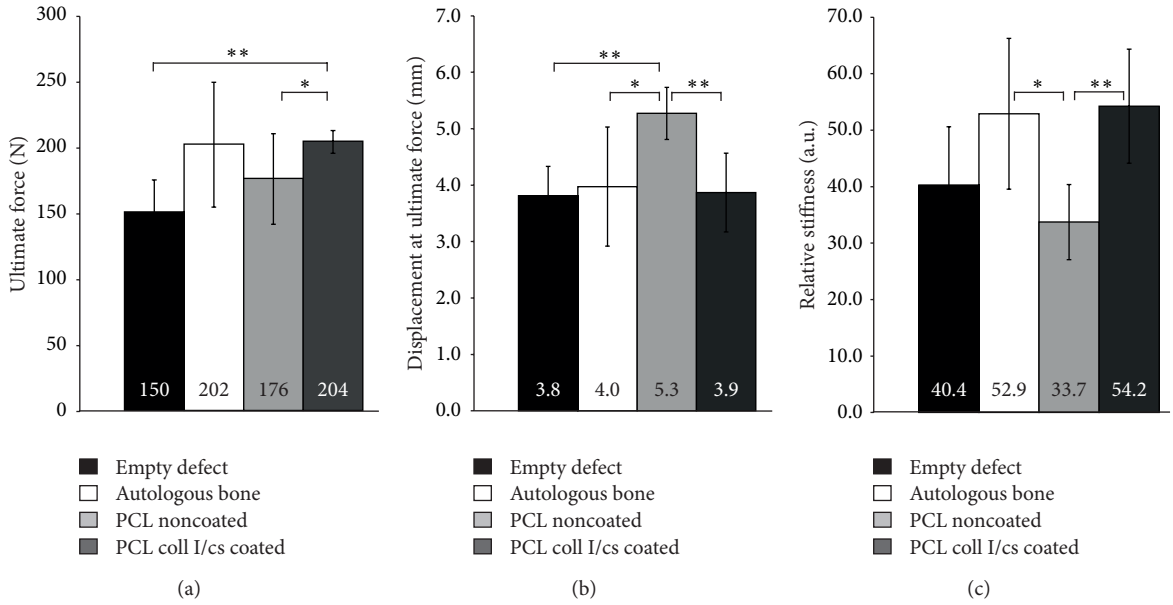

Figure 8: Biomechanical evaluation. (a) Ultimate force in newton (N). (b) Displacement of ultimate force in millimeter (mm). (c) Relative stiffness. Significant differences as indicated: $^{*}P < 0.05$, $^{**}P < 0.01$, $^{***}P < 0.001$ (Student's t-test).

noncoated (43.3%) and the empty defect (26.6%) group. Bone volume averaged 68.6% in the autologous group (Figure 7(a)).

Detailed analysis of the whole defect area revealed a more homogenous bone distribution within the PCL coll I/cs coated scaffold group compared to the PCL noncoated group (Figure 7(b)). The central area of PCL coll I/cs coated scaffolds showed more than twice as much bone (15.7%) as the PCL noncoated scaffolds (6.8%) (Figure 7(c)). This difference was statistically significant.

3.6. Biomechanical Testing. The push-out test was performed in order to evaluate the mechanical integrity of the scaffold reconstructed calvaria region. The empty defects and autologous bone treated defects served as a reference. In all tests the push-out of the reconstructed area was observed to be the dominant type of failure whereas the host calvaria maintained its integrity. Statistical analysis of characteristic values obtained from the force/displacement curves is shown in Figures 8(a) and 8(b). The ultimate force recorded during complete push-out was the lowest for the empty defects (150

N) and the highest for the PCL coll I/cs coated treated defects (204 N) whereby they reached autologous bone level (202 N).

Regarding the relative stiffness of the reconstructed area, the results also demonstrate the significant influence of the biomaterial and its coating to achieve a bone like stability. Whereas PCL noncoated showed no effect, the relative stiffness was nearly 60% higher for PCL coll I/cs coated and therefore similar to the gold standard (Figure 8(c)).

3.7. Histology. Masson-Goldner trichrome staining presented bone in turquoise/red color, whereas fibrous tissue is presented in light turquoise color. All groups showed new bone formation within the 13 mm defect (Figure 9). The empty group presented new bone formation at the margins without bridging the defect. The central part of the defects was filled with fibrous tissue (Figure 9(b)). All implanted autologous bone fragments of the autologous group were vital and reconnected to the skull bone or among themselves, but no homogeneous new bone formation occurred. Single bone fragments could still be detected and empty spots were still measurable after 6 months of implantation (Figure 9(c)).

Both PCL groups showed newly formed lamellar bone inside the scaffolds presenting osteons, including Haversian canals (see orange circle in Figures 9(d) and 9(e) III). Bone formation occurred mostly at the lamina interna (located next to the dura mater) Figures 9(d) I and 9(e) I). The scaffolds were completely vascularized (see blood vessel (bv) in Figures 9(d) and 9(e) III) and no area appeared completely free of tissue. The PCL scaffolds still existed 6 months after implantation. No signs of a chronic inflammatory reaction like accumulation of granulation tissue, lymphocytes, macrophages, or foreign body giant cells were visible around the implant material. The PCL coll I/cs coated group showed a higher amount of new bone formation within the central defect as compared to the PCL noncoated group (Figure 9(e) II).

4. Discussion

The aim of this *in vivo* study was to characterize the polycaprolactone-co-lactid (PCL) scaffold as a skull bone implant and to evaluate the effect of surface coating with colI I/cs on these scaffolds in relation to untreated defects and defects filled with autologous bone. Parameters for evaluation were based on ultrasonographic and radiological investigations, biomechanical testing, and histology.

The PCL material used in this study describes a copolymer made of polycaprolactone-co-lactid (see Section 2). The commercially available copolymer suture is sold under this (PCL) trade name from the Catgut GmbH and therefore the abbreviation PCL is used in this publication. To avoid confusion with polycaprolactone, also described as PCL, which is not copolymer, the following discussion will refer to polycaprolactone.

4.1. Animal Model and Defect Size. Various types and sizes of calvarial bone defects are described in rabbits [38–45]. In the present study, the defects could be created safely between the frontal and interparietal skull bone without touching the coronal or lambdoid suture in order to avoid as much fibrous suture tissue within the defect as possible. To create a defect with the same thickness of bone on either side of the sagittal suture at the parietal bone anatomical conditions were not given. Resulting, a circular skull defect of 13 mm diameter was chosen and placed centrally within the parietal bone.

To fulfil the definition of a critical size defect (CSD), less than 10% of bone formation within the CSD should be observed during the lifetime of the animal [46]. Since the empty defect showed 26.6% new bone formation after 6 months, but no bridging, the defect size does not fulfil this definition of a CSD.

According to data available from the literature (Table 2), new bone formation within a 15 mm defect ranges from 17.5 to 24.4% after 12 weeks [38, 42, 44]. In contrast, Schantz et al. discovered only 1.2% new bone formation after 12 months and Kroese-Deutman et al. mentioned that all 15 mm defects in their study were open after 12 weeks but did not provide bone volume data for this group [39, 45]. While the available data do not allow a precise definition of a CSD in the rabbit calvaria, the amount of newly formed bone within the 13 mm defect at 6 months in our study is comparable to most of the previous studies [38, 42, 44]. The sparse amount of new bone formation from the margins makes the untreated defects reliable as a control group.

4.2. Bone Quantification within the Defects. In the present study, the PCL scaffolds were successfully integrated into large bone defects. PCL noncoated and PCL coll I/cs coated scaffolds showed significantly more (43.3 and 47.1%) new bone formation within the defect area compared to the empty defects (26.6%) after 6 months. The distribution of new bone formation within the defect area was more uniform with significantly more new bone in the central portion of the coll I/cs coated scaffold compared to the noncoated PCL scaffold (Figure 7(c)).

An extensive review of the literature revealed 26 studies on the repair of rabbit skull defects. Eight studies presented the final amount of new bone formation within the defect in percentage and therefore seemed to be appropriate for comparison (Table 2). However, these comparisons are limited because of strong variations in defect size, time points, implant materials, and the number of investigated animals.

It becomes obvious that skull implants made of different polymers like polycaprolactone, poly(lactic-co-glycolic acid) (PLGA), tyrosine-derived polycarbonate (TyrPC), or tricalcium phosphate (TCP) derivative resulted in considerably less new bone formation within the defects than the PCL used in the present study (Table 2). The amount of new bone formation ranged from 1.2% for medical grade polycaprolactone [45] to 16.0% for TyrPC [43], 25.1% for PGLA [40], and 32.0–34.9% for composites made of PLGA/TCP or polycaprolactone-TCP [40, 41]. Biologization of medical grade polycaprolactone scaffolds with bone marrow or osteoblasts increased the bone volume up to 12.5% or 14.1% [45] but never reached the amount of new bone formation in the present study (43.3% for PCL noncoated and 47.1% for PCL coll I/cs coated).

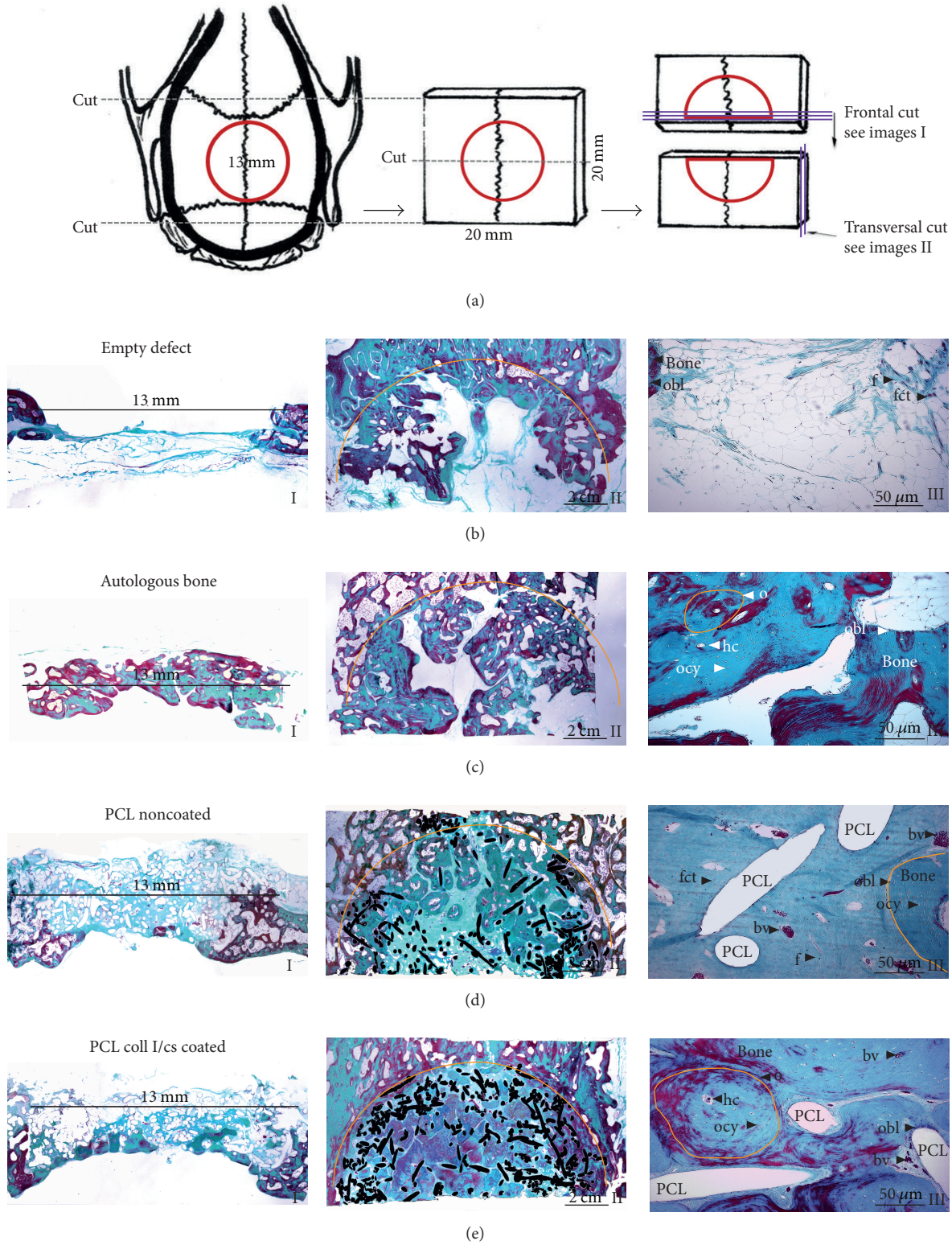

Figure 9: Representative histological images of one animal from each group (Masson-Goldner trichrome staining). (a) Schematic drawing of the histological sample preparation. (b) Empty defect. (c) Autologous bone. (d) PCL noncoated. (e) PCL coll I/cs coated. I: frontal plane with the defect area marked by the 13 mm line (1x). II: transversal plane with the defect area is marked by the orange semicircle (1x). PCL scaffold is marked in black. III: enlarged section of the defect zone (20x). obl: osteoblast, ocy: osteocyte, o: osteon (orange), hc: Haversian canal, f: fibroblast, bv: blood vessel with erythrocyte, and fct: firm connective tissue.

Table 2: Literature analysis.

Publication	Animal/number/group	Defect size/time of study	Implant	Bone volume in %
[38]	Rabbit/$n = 10$	15 mm/12 weeks	Empty	24.4
			Autologous bone	82
			Empty + Lactosorb	23.9
			DBM + Lactosorb	84
			CPC	13.1
			CPC + BMP	45.8
[39]	Rabbit/$n = 10$	6 mm	Ca-P	17
		6 mm	Empty	n.a.
		9 mm	Ca-P	18
		9 mm	Empty	n.a.
		15 mm	Ca-P	17
		15 mm/12 weeks	Empty	n.a.
[40]	Rabbit/$n = 9$ (4 defects/rabbit)	6 mm/4 weeks	PLGA	25.1
			PLGA/TCP	34.9
			BioOss	30.8
			empty	28.4
[41]	Rabbit/$n = 33$	6 mm/12 weeks	Polycaprolactone-TCP	32
		24 weeks	Polycaprolactone-TCP	25
[42]	Rabbit/$n = 16$	6 mm	6 mm empty	53.6
		8 mm	8 mm empty	41.8
		11 mm	11 mm empty	35.1
		15 mm/12 weeks	15 mm empty	20.1
[43]	Rabbit/$n = 4/5$	15 mm/6 weeks	TyrPC	16
			TyrPC + rhBMP-2	34
			TyrPC + CP	4
			BGS	4
[44]	Rabbit/$n = 10$	15 mm/12 weeks	CPC	14
			BC	21
			Empty	17.5
		6 weeks	BC + rh rhBMP-2	27
[45]	Rabbit/$n = 4$ for mPCL and empty, $n = 6$ for mPCL + BMPC and OB	15 mm/3 months	m-polycaprolactone	n.a.
			m-polycaprolactone + BMPC	4.7
			m-polycaprolactone + cOB	4.7
			empty	n.a.
		12 months	m-polycaprolactone	1.2
			m-polycaprolactone + BMPC	12.5
			m-polycaprolactone + cOB	12.5
			empty	1.2

DBM + Lactosorb (demineralized bone matrix), CPC (calcium phosphate cement), CPC + BMP (calcium phosphate cement + bone morphogenetic protein); Ca-P (calcium phosphate); PLGA (poly(lactide-coglycolide)), PLGA/TCP (PLGA/tricalcium phosphate), BioOss (bovine derived mineral); polycaprolactone-TCP (polycaprolactone-tricalcium phosphate); TyrPC (tyrosine-derived polycarbonate), TyrPC + rhBMP-2 (TyrPC + recombinant human bone morphogenetic protein-2), TyrPC + CP (TyrPC + calcium phosphate), BGS (bovine type-I collagen + tricalcium phosphate); CPC (calcium phosphate cement), BC (biocomposite = lysine derived polyurethane and allograft), BC + rhBMP-2 (BC + recombinant human bone morphogenetic protein-2); m-polycaprolactone (medical grade polycaprolactone), m-polycaprolactone + BMPC (m-polycaprolactone + bone marrow derived mesenchymal progenitor cells), m-polycaprolactone + cOB (m-polycaprolactone + calvarial osteoblasts).

The application of bone morphogenetic protein (BMP-2) resulted in a considerable increase of the amount of new bone formation within TyrPC (34.0%), biocomposite (BC: 27.0%), and calcium phosphate cement (CPC: 45.8%) scaffolds [38, 43, 44]. These BMP-2 induced bone quantities come into the range of the new bone formation using PCL noncoated or PCL coll I/cs coated scaffolds without any growth factor application, indicating that the PCL scaffold by itself acts beyond osteoconductive properties. Although growth factor applications are used for animal tissue engineering studies, the clinical use of BMP is limited by the cost, rapid degradation *in situ,* and inconsistent biological activity [47, 48].

The superior biological performance of the PCL scaffolds used in our study could be explained by the copolymer composition which comes along with a compatible degradation rate and degradation products [14, 17]. The used PCL fiber shows a degradation rate of around 25 weeks via hydrolysis at *in vitro* as well as *in vivo* investigations [14]. The PCL material used in this study was still visible after 6 months of implantation. This is not unexpected, given that the extent and the mechanism of the polymer hydrolysis are depending on the amount and the location of water molecules [49].

The PCL scaffold provides an appropriate network of material and interconnecting pores to act as a temporary matrix for new bone formation similar to autologous bone. The structure allows cell penetration and proper vascularization which is needed for bone formation. Compared to long bones, calvarial bone is more biological inert due to its reduced blood supply. It has to be considered that large areas of human skull bone are lacking muscle insertions so the blood supply to the human calvaria is even less than in other mammals [50]. According to that it is even more important to reach a good scaffold vascularization in animal experimental investigations. The importance of blood vessel formation for intramembranous ossification in cranial bones and bone repair is also described by Kanczler and Oreffo [51]. The vasculature transports oxygen, nutrients, and different cell types within the implant and supports tissue formation [51]. In this study the bone formation within the PCL scaffold occurred mostly at the lamina interna indicating a better nutrition and blood supply from the side of the dura mater compared to the scalp side.

The surface coating with components of the ECM (coll I/cs) further increased the amount of new bone formation within the scaffolds. This leads to the conclusion that the coll I/cs coating tents to an increased surface area for cell binding and growth factor adsorption and as a result of a more homogenous bone distribution within the PCL coll I/cs coated scaffold. This is in accordance with earlier *in vivo* and *in vitro* studies that have shown similar effects in several cell culture experiments and in long bone defects in small and large animal models [11, 18, 20, 21, 23].

The effect of collagen coatings may be based on the interaction with osteoblastic cells via integrin receptors. Glycosaminoglycans (GAGs) like chondroitin sulfate or dermatan sulfate are important components of the bone ECM and play a key role in bone development, remodeling, and regeneration by interacting with other ECM molecules, growth factors, cytokines, and cells [11, 18, 20, 21, 23, 28, 32, 33, 36, 37, 52, 53]. GAGs are known to specifically bind growth factors and modulate their activity. This is due primarily to an interaction of the GAGs negatively charged sulfate groups with positively charged amino acid sequences of the growth factors and has been reported among others, for fibroblast growth factor (FGF) and transforming growth factor beta, (TGF-β) [54].

4.3. Tracking of Tissue Formation within the Defect Area with Ultrasonography. *In vivo* tracking of new tissue formation within large defects can be done by life computed tomography (CT) imaging [55] because standard radiographic methods are not applicable due to the three-dimensional structure of the rabbit skull. However, life CT is expensive and often not available in animal care units, especially for animals larger than rats. Additionally, the animals have to be anesthetized for each investigation and so the risk of death is increasing during anesthesia stress.

The skull defect was easily accessible with an ultrasound probe and the defect was clearly detectable after surgery and over the further course. The obtained data roughly match those from the postmortal μCT. The authors conclude that ultrasonography can be used as a method to track tissue formation within large calvarial bone defects. Because ultrasound is not associated with radiation it is of potential clinical use. However, the method has several limitations. The given setup could not distinguish between new bone and new firm connective tissue formation because the ultrasonic waves were reflected in a similar manner by both tissues. Furthermore, for skull defects, this method can only be used for implants with a very low ultrasound reflecting matrix like PCL.

Wefer et al. established an ultrasound method on sheep long bones to predict the healing of a defect filled with a bone graft substitute or cancellous bone graft. They also come to an agreement that a follow-up study for bone healing using sonography is possible, but the bony integration inside of the implant cannot be given definitely [56].

4.4. Clinical Outlook. The PCL scaffold seems to be a promising bone implant for mechanically unloaded defect filling like skull defects. It can be provided in any size and shape due to the embroidery technique. The scaffold design allows the fixation of the implant by suturing the scaffold lid to the surrounding periost tissue so no implant movement occurs. Even the scaffold does not provide initial mechanical stability like autologous bone; the 3-dimensional structure protects the underlying brain tissue in first place. The PCL material degrades in a biologically relevant timeframe of 6 to 12 months; meanwhile new bone formation can occur. The applied PCL scaffold could be additionally fixed by metal nets to provide a stronger mechanical stabilization in case of larger defects in human.

5. Conclusion

This work has demonstrated that embroidered PCL scaffolds can act as skull bone implants for large defects in rabbits.

The implant design and the material allowed good surgical handling and a high amount of new bone formation within the scaffold after six months. The combination of scaffold and bioactive surface coating (coll I/cs) enhanced new bone formation and led to a more homogeneous distribution of newly formed bone within the scaffolds. The use of these scaffolds finally resulted in a homogeneous bridging of the defect with high-quality bone that was histologically and biomechanically similar to autologous bone.

Conflict of Interests

The authors declare that there is no conflict of interests regarding the publication of this paper.

Acknowledgments

The authors would like to acknowledge the Sächsische AufbauBank for financing the current study, the Catgut GmbH (Markneukirchen, Germany), and the company Möckel embroidery and engineering (Auerbach, Germany) for producing the PCL scaffolds as well as Suzanne Manthey and Annett Wenke (University Hospital "Carl Gustav Carus" Dresden, Dresden Germany) for histological work-up of the specimens.

References

[1] C. Zong, D. Xue, W. Yuan et al., "Reconstruction of rat calvarial defects with human mesenchymal stem cells and osteoblast-like cells in poly-lactic-co-glycolic acid scaffolds," *European Cells & Materials*, vol. 20, pp. 109–120, 2010.

[2] N. J. Mokal and M. F. Desai, "Calvarial reconstruction using high-density porous polyethylene cranial hemispheres," *Indian Journal of Plastic Surgery*, vol. 44, no. 3, pp. 422–431, 2011.

[3] W.-M. Kung, F.-H. Lin, S.-H. Hsiao et al., "New reconstructive technologies after decompressive craniectomy in traumatic brain injury: the role of three-dimensional titanium mesh," *Journal of Neurotrauma*, vol. 29, no. 11, pp. 2030–2037, 2012.

[4] P. Dinarvand, E. Seyedjafari, A. Shafiee et al., "New approach to bone tissue engineering: simultaneous application of hydroxyapatite and bioactive glass coated on a poly(L-lactic acid) scaffold," *ACS Applied Materials and Interfaces*, vol. 3, no. 11, pp. 4518–4524, 2011.

[5] D. Rohner, D. W. Hutmacher, T. K. Cheng, M. Oberholzer, and B. Hammer, "In vivo efficacy of bone-marrow-coated polycaprolactone scaffolds for the reconstruction of orbital defects in the pig," *Journal of Biomedical Materials Research B: Applied Biomaterials*, vol. 66, no. 2, pp. 574–580, 2003.

[6] H. Chim and J.-T. Schantz, "New frontiers in calvarial reconstruction: integrating computer-assisted design and tissue engineering in cranioplasty," *Plastic and Reconstructive Surgery*, vol. 116, no. 6, pp. 1726–1741, 2005.

[7] T. J. Blokhuis and T. Lindner, "Allograft and bone morphogenetic proteins: an overview," *Injury*, vol. 39, no. 2, pp. S33–S36, 2008.

[8] M. Kruyt, J. de Bruijn, J. Rouwkema et al., "Analysis of the dynamics of bone formation, effect of cell seeding density, and potential of allogeneic cells in cell-based bone tissue engineering in goats," *Tissue Engineering A*, vol. 14, no. 6, pp. 1081–1088, 2008.

[9] O. B. Betz, V. M. Betz, A. Abdulazim et al., "The repair of critical-sized bone defects using expedited, autologous BMP-2 gene-activated fat implants," *Tissue Engineering A*, vol. 16, no. 3, pp. 1093–1101, 2010.

[10] J. Yuan, Y. Cao, and W. Liu, "Biomimetic scaffolds: implications for craniofacial regeneration," *Journal of Craniofacial Surgery*, vol. 23, no. 1, pp. 294–297, 2012.

[11] B. Rentsch, R. Bernhardt, D. Scharnweber, W. Schneiders, S. Rammelt, and C. Rentsch, "Embroidered and surface coated polycaprolactone-co-lactide scaffolds: a potential graft for bone tissue engineering," *Biomatter*, vol. 2, no. 3, pp. 158–165, 2012.

[12] H. J. Chung and T. G. Park, "Surface engineered and drug releasing pre-fabricated scaffolds for tissue engineering," *Advanced Drug Delivery Reviews*, vol. 59, no. 4-5, pp. 249–262, 2007.

[13] A. Gloria, R. de Santis, and L. Ambrosio, "Polymer-based composite scaffolds for tissue engineering," *Journal of Applied Biomaterials & Biomechanics*, vol. 8, no. 2, pp. 57–67, 2010.

[14] K. Tomihata, M. Suzuki, T. Oka, and Y. Ikada, "A new resorbable monofilament suture," *Polymer Degradation and Stability*, vol. 59, no. 1–3, pp. 13–18, 1998.

[15] J. M. Williams, A. Adewunmi, R. M. Schek et al., "Bone tissue engineering using polycaprolactone scaffolds fabricated via selective laser sintering," *Biomaterials*, vol. 26, no. 23, pp. 4817–4827, 2005.

[16] K. Tomihata, M. Suzuki, and N. Tomita, "Handling characteristics of poly(L-lactide-co-ε-caprolactone) monofilament suture," *Bio-Medical Materials and Engineering*, vol. 15, no. 5, pp. 381–391, 2005.

[17] H. Bramfeldt, P. Sarazin, and P. Vermette, "Characterization, degradation, and mechanical strength of poly(D,L-lactide-co-ε-caprolactone)-poly(ethylene glycol)-poly(D,L-lactide- co-ε-caprolactone)," *Journal of Biomedical Materials Research A*, vol. 83, no. 2, pp. 503–511, 2007.

[18] C. Rentsch, B. Rentsch, A. Breier et al., "Long-bone critical-size defects treated with tissue-engineered polycaprolactone-co-lactide scaffolds: a pilot study on rats," *Journal of Biomedical Materials Research A*, vol. 95, no. 3, pp. 964–972, 2010.

[19] P.-P. A. Vergroesen, R.-J. Kroeze, M. N. Helder, and T. H. Smit, "The use of poly(L-lactide-co-caprolactone) as a scaffold for adipose stem cells in bone tissue engineering: application in a spinal fusion model," *Macromolecular Bioscience*, vol. 11, no. 6, pp. 722–730, 2011.

[20] B. Rentsch, A. Hofmann, A. Breier, C. Rentsch, and D. Scharnweber, "Embroidered and surface modified polycaprolactone-co-lactide scaffolds as bone substitute: in vitro characterization," *Annals of Biomedical Engineering*, vol. 37, no. 10, pp. 2118–2128, 2009.

[21] C. Rentsch, W. Schneiders, R. Hess et al., "Healing properties of surface-coated polycaprolactone-co-lactide scaffolds: a pilot study in sheep," *Journal of Biomaterials Applications*, vol. 28, no. 5, pp. 654–666, 2013.

[22] R. Hess, T. Douglas, K. A. Myers et al., "Hydrostatic pressure stimulation of human mesenchymal stem cells seeded on collagen-based artificial extracellular matrices," *Journal of Biomechanical Engineering*, vol. 132, no. 2, Article ID 021001, 2010.

[23] C. Rentsch, R. Hess, B. Rentsch et al., "Ovine bone marrow mesenchymal stem cells: isolation and characterization of the cells and their osteogenic differentiation potential on embroidered

and surface-modified polycaprolactone-co-lactide scaffolds," *In Vitro Cellular & Developmental Biology—Animal*, vol. 46, no. 7, pp. 624–634, 2010.

[24] D. W. Hutmacher and S. Cool, "Concepts of scaffold-based tissue engineering—the rationale to use solid free-form fabrication techniques," *Journal of Cellular and Molecular Medicine*, vol. 11, no. 4, pp. 654–669, 2007.

[25] B. P. Chan and K. W. Leong, "Scaffolding in tissue engineering: general approaches and tissue-specific considerations," *European Spine Journal*, vol. 17, no. 4, pp. S467–S479, 2008.

[26] X.-D. Chen, "Extracellular matrix provides an optimal niche for the maintenance and propagation of mesenchymal stem cells," *Birth Defects Research C*, vol. 90, no. 1, pp. 45–54, 2010.

[27] J. A. Hubbell, "Materials as morphogenetic guides in tissue engineering," *Current Opinion in Biotechnology*, vol. 14, no. 5, pp. 551–558, 2003.

[28] S. Rammelt, T. Illert, S. Bierbaum, D. Scharnweber, H. Zwipp, and W. Schneiders, "Coating of titanium implants with collagen, RGD peptide and chondroitin sulfate," *Biomaterials*, vol. 27, no. 32, pp. 5561–5571, 2006.

[29] M. Morra, C. Cassinelli, G. Cascardo et al., "Surface engineering of titanium by collagen immobilization. Surface characterization and in vitro and in vivo studies," *Biomaterials*, vol. 24, no. 25, pp. 4639–4654, 2003.

[30] S. Rammelt, E. Schulze, M. Witt et al., "Collagen type I increases bone remodelling around hydroxyapatite implants in the rat tibia," *Cells Tissues Organs*, vol. 178, no. 3, pp. 146–157, 2004.

[31] S. Bierbaum, T. Douglas, T. Hanke et al., "Collageneous matrix coatings on titanium implants modified with decorin and chondroitin sulfate: characterization and influence on osteoblastic cells," *Journal of Biomedical Materials Research A*, vol. 77, no. 3, pp. 551–562, 2006.

[32] W. Schneiders, A. Reinstorf, A. Biewener et al., "In vivo effects of modification of hydroxyapatite/collagen composites with and without chondroitin sulphate on bone remodeling in the sheep tibia," *Journal of Orthopaedic Research*, vol. 27, no. 1, pp. 15–21, 2009.

[33] W. Schneiders, A. Reinstorf, M. Ruhnow et al., "Effect of chondroitin sulphate on material properties and bone remodelling around hydroxyapatite/collagen composites," *Journal of Biomedical Materials Research A*, vol. 85, no. 3, pp. 638–645, 2008.

[34] B. Stadlinger, S. Bierbaum, S. Grimmer et al., "Increased bone formation around coated implants," *Journal of Clinical Periodontology*, vol. 36, no. 8, pp. 698–704, 2009.

[35] J. M. Holzwarth and P. X. Ma, "Biomimetic nanofibrous scaffolds for bone tissue engineering," *Biomaterials*, vol. 32, no. 36, pp. 9622–9629, 2011.

[36] K. J. Manton, D. F. M. Leong, S. M. Cool, and V. Nurcombe, "Disruption of heparan and chondroitin sulfate signaling enhances mesenchymal stem cell-derived osteogenic differentiation via bone morphogenetic protein signaling pathways," *Stem Cells*, vol. 25, no. 11, pp. 2845–2854, 2007.

[37] N. Volpi, "Quality of different chondroitin sulfate preparations in relation to their therapeutic activity," *Journal of Pharmacy and Pharmacology*, vol. 61, no. 10, pp. 1271–1280, 2009.

[38] A. J. Haddad, S. A. F. Peel, C. M. L. Clokie, and G. K. B. Sándor, "Closure of rabbit calvarial critical-sized defects using protective composite allogeneic and alloplastic bone substitutes," *Journal of Craniofacial Surgery*, vol. 17, no. 5, pp. 926–934, 2006.

[39] H. C. Kroese-Deutman, J. G. C. Wolke, P. H. M. Spauwen, and J. A. Jansen, "Closing capacity of cranial bone defects using porous calcium phosphate cement implants in a rabbit animal model," *Journal of Biomedical Materials Research A*, vol. 79, no. 3, pp. 503–511, 2006.

[40] O. D. Schneider, F. Weber, T. J. Brunner et al., "In vivo and in vitro evaluation of flexible, cottonwool-like nanocomposites as bone substitute material for complex defects," *Acta Biomaterialia*, vol. 5, no. 5, pp. 1775–1784, 2009.

[41] A. Yeo, W. J. Wong, and S.-H. Teoh, "Surface modification of PCL-TCP scaffolds in rabbit calvaria defects: evaluation of scaffold degradation profile, biomechanical properties and bone healing patterns," *Journal of Biomedical Materials Research A*, vol. 93, no. 4, pp. 1358–1367, 2010.

[42] J.-Y. Sohn, J.-C. Park, Y.-J. Um et al., "Spontaneous healing capacity of rabbit cranial defects of various sizes," *Journal of Periodontal & Implant Science*, vol. 40, no. 4, pp. 180–187, 2010.

[43] J. Kim, M. H. R. Magno, H. Waters et al., "Bone regeneration in a rabbit critical-sized calvarial model using tyrosine-derived polycarbonate scaffolds," *Tissue Engineering A*, vol. 18, no. 11-12, pp. 1132–1139, 2012.

[44] J. E. Dumas, P. B. Brownbaer, E. M. Prieto et al., "Injectable reactive biocomposites for bone healing in critical-size rabbit calvarial defects," *Biomedical Materials*, vol. 7, no. 2, Article ID 024112, 2012.

[45] J.-T. Schantz, M. A. Woodruff, C. X. F. Lam et al., "Differentiation potential of mesenchymal progenitor cells following transplantation into calvarial defects," *Journal of the Mechanical Behavior of Biomedical Materials*, vol. 11, pp. 132–142, 2012.

[46] J. O. Hollinger and J. C. Kleinschmidt, "The critical size defect as an experimental model to test bone repair materials," *The Journal of Craniofacial Surgery*, vol. 1, no. 1, pp. 60–68, 1990.

[47] K. A. Hing, "Bone repair in the twenty-first century: biology, chemistry or engineering?" *Philosophical Transactions of the Royal Society A: Mathematical, Physical & Engineering Sciences*, vol. 362, no. 1825, pp. 2821–2850, 2004.

[48] J. M. Rueger, J. Hägele, W. Lehmann, A. Rücker, and C. Schlickewei, "Knochenaufbau—Knochenersatzmaterialien," in *Orthopadie Unfallchirurgie*, vol. 5, pp. 295–314, Georg Thieme Verlag KG, New York, NY, USA, 2010.

[49] C. X. F. Lam, M. M. Savalani, S.-H. Teoh, and D. W. Hutmacher, "Dynamics of in vitro polymer degradation of polycaprolactone-based scaffolds: accelerated versus simulated physiological conditions," *Biomedical Materials*, vol. 3, no. 3, Article ID 034108, 2008.

[50] I. Hussain, K. Moharamzadeh, I. M. Brook, P. José de Oliveira Neto, and L. A. Salata, "Evaluation of osteoconductive and osteogenic potential of a dentin-based bone substitute using a calvarial defect model," *International Journal of Dentistry*, vol. 2012, Article ID 396316, 7 pages, 2012.

[51] J. M. Kanczler and R. O. C. Oreffo, "Osteogenesis and angiogenesis: the potential for engineering bone," *European Cells & Materials*, vol. 15, pp. 100–114, 2008.

[52] T. Douglas, S. Heinemann, C. Mietrach et al., "Interactions of collagen types I and II with chondroitin sulfates A-C and their effect on osteoblast adhesion," *Biomacromolecules*, vol. 8, no. 4, pp. 1085–1092, 2007.

[53] S. Bierbaum, V. Hintze, and D. Scharnweber, "Functionalization of biomaterial surfaces using artificial extracellular matrices," *Biomatter*, vol. 2, no. 3, pp. 132–141, 2012.

[54] B. Stadlinger, V. Hintze, S. Bierbaum et al., "Biological functionalization of dental implants with collagen and

glycosaminoglycans—a comparative study," *Journal of Biomedical Materials Research B: Applied Biomaterials*, vol. 100, no. 2, pp. 331–341, 2012.

[55] B. C. Frazier, M. P. Mooney, H. W. Losken et al., "Comparison of craniofacial phenotype in craniosynostotic rabbits treated with anti-Tgf-β2 at suturectomy site," *Cleft Palate-Craniofacial Journal*, vol. 45, no. 6, pp. 571–582, 2008.

[56] J. Wefer, A. Wefer, H. E. Schratt, H. Thermann, and B. W. Wippermann, "Healing of autologous cancellous bone grafts and hydroxylapatite ceramics in tibial segment defects," *Unfallchirurg*, vol. 103, no. 6, pp. 452–461, 2000.

Hindawi Publishing Corporation
BioMed Research International
Volume 2014, Article ID 454021, 10 pages
http://dx.doi.org/10.1155/2014/454021

Research Article

The Pilot Study of Fibrin with Temporomandibular Joint Derived Synovial Stem Cells in Repairing TMJ Disc Perforation

Yang Wu,[1] Zhongcheng Gong,[2] Jian Li,[1] Qinggong Meng,[1] Wei Fang,[1] and Xing Long[1]

[1] *Department of Oral and Maxillofacial Surgery, The State Key Laboratory Breeding Base of Basic Science of Stomatology & Key Laboratory of Oral Biomedicine Ministry of Education, School & Hospital of Stomatology, Wuhan University, No. 237 Luo Yu Road, Wuhan, Hubei 430079, China*

[2] *Oncology Department of Oral & Maxillofacial Surgery, The First Teaching Hospital of Xinjiang Medical University, Stomatology College of Xinjiang Medical University, Stomatology Research Institute of Xinjiang Province, Urumqi, Xinjiang 830054, China*

Correspondence should be addressed to Xing Long; longxing_china@hotmail.com

Received 27 October 2013; Revised 8 March 2014; Accepted 11 March 2014; Published 15 April 2014

Academic Editor: Yin Xiao

TMJ disc related diseases are difficult to be cured due to the poor repair ability of the disc. TMJ-SDSCs were ideal cell sources for cartilage tissue engineering which have been widely used in hyaline cartilage regeneration. Fibrin gel has been demonstrated as a potential scaffold for neocartilage formation. The aim of this study was to repair the TMJ disc perforation using fibrin/chitosan hybrid scaffold combined with TMJ-SDSCs. Rat TMJ-SDSCs were cultured on hybrid scaffold or pure chitosan scaffolds. The cell seeding efficiency, distribution, proliferation, and chondrogenic differentiation capacity were investigated. To evaluate the *in vivo* repair ability of cell/scaffold construct, rat TMJ disc explants were punched with a defect to mimic TMJ disc perforation. Cell seeded scaffolds were inserted into the defect of TMJ disc explants and then were implanted subcutaneously in nude mice for 4 weeks. Results demonstrated that fibrin may improve cell seeding, proliferation, and chondrogenic induction *in vitro*. The *in vivo* experiments showed more cartilage ECM deposition in fibrin/chitosan scaffold, which suggested an enhanced reparative ability. This pilot study demonstrated that the regenerative ability of TMJ-SDSCs seeded in fibrin/chitosan scaffold could be applied for repairing TMJ disc perforation.

1. Introduction

Temporomandibular joint disorder (TMDs) is frequently associated with degenerative changes in severe cases [1]. The degenerative changes including TMJ disc perforation and osteoarthritis usually need surgical repair of the disc or total joint reconstruction due to its poor intrinsic healing ability [2].

The TMJ disc is characterized as fibrocartilage tissue distinct from both hyaline and meniscal cartilage in cell type and extracellular matrix (ECM) composition [3]. Previous studies on the TMJ disc engineering usually used TMJ disc cells [4–6]. However, it was found that this kind of fibrochondrocyte was prone to dedifferentiate during *in vitro* culture, leading to a decrease of ECM synthesis [7, 8].

Synovium derived mesenchymal stem cells (SDSCs) are an attractive cell source for cartilage tissue engineering. SDSCs are able to synthesis cartilage oligomeric matrix protein, link protein, and glycosaminoglycans (sGAG), which demonstrates the same properties as chondrocytes [9]. The ability of multipotential differentiation of TMJ-SDSCs has been confirmed in our previous researches [10, 11]. Although SDSCs have been used in hyaline cartilage tissue engineering, there was no research using TMJ-SDSCs to regenerate TMJ disc tissue, which was regarded as fibrocartilage. In this study, we hypothesized that TMJ-SDSCs can be used in TMJ disc tissue engineering.

Another important aspect of cartilage tissue engineering is the design of three-dimensional scaffold which may maintain the initial shape of cell/scaffold construct and promote tissue regeneration. In our previous research, macroporous sponge-like chitosan was used as scaffold in hyaline cartilage repair [12]. Fibrin gel is a Federal Drug Agency (FDA)

approved biological adhesive which possesses several essential features as a scaffold for cartilage engineering, for it promotes chondrocytes proliferation and cartilaginous ECM production [13]. However, the intrinsic properties of fibrin gel such as poor mechanical strength and fast degradation make it unsuitable to be used independently.

We hypothesize that incorporating fibrin gel with sponge-like chitosan scaffold could improve the biocompatibility of scaffold. In this study, we compared the *in vitro* results of fibrocartilage tissue engineered using TMJ-SDSCs seeded in sponge-like chitosan scaffold with or without fibrin gel incorporation. In the second phase of study, we designed an *in vivo* organ culture model to mimic the perforation of TMJ disc and tested whether fibrin gel could promote TMJ disc repair in a subcutaneous nude mice model.

2. Materials and Methods

2.1. Reagents and Chemicals. Cell culture regents including high glucose Dulbecco's modified Eagle's medium (DMEM), fetal bovine serum (FBS), and phosphate-buffered saline (PBS) were purchased from HyClone (USA); recombinant human TGF-β3 was obtained from Propertech (USA); $ITS^{+premix}$ (insulin, transferring, and selenium) was purchased from Gibco (USA); chitosan with a deacetylation degree of minimum 95% was purchased from Shangon (Shanghai, China); fibrin gel was from Guangzhou BioSeal Company (China).

Other reagents were obtained from Sigma (St. Louis, MO), unless otherwise specified.

2.2. Preparing of Fibrin/Chitosan Scaffolds. Macroporous chitosan scaffold was prepared in the manner of freeze-drying method. In brief, chitosan was dissolved in 0.1 mol/L acetic acid solution to prepare a 1% (w/v) solution. After centrifugation at 4°C for 1000 rpm × 10 min, chitosan solution was poured into a polystyrene 48-well culture plate (0.2 mL per well) and frozen at −70°C for 24 hours and then lyophilized in a freeze dryer (Christ, Germany) for 48 hours. Scaffolds were sterilized with ethylene oxide and soaked in DMEM before use.

The major components of fibrin gel were fibrinogen (50~75 mg/mL) and thrombin (400 IU). Other components included blood coagulation-factor XIII (10~70 U), potassium dihydrogen phosphate (0.68 mg/mL), and calcium chloride (40 mmol). The fibrin gel was formed by mixing fibrinogen and thrombin solution at equal volume in 15 min at 37°C according to the manufacture's protocol.

To achieve homogeneous incorporation of fibrin gel with chitosan scaffold, fibrinogen solution (with or without cells) was dropped equally onto both sides of the half-dry chitosan scaffold. After fibrinogen solution was absorbed, thrombin solution was added to form fibrin gel. In this study, the hybrid chitosan/fibrin scaffolds were used in experiment group and pure chitosan scaffolds were used as controls.

To evaluate the morphological features of two scaffolds, cell-free scaffolds were fixed, dehydrated, critical-point dried, and coated with gold for scanning electron microscopy (SEM; Quanta 200, FEI, The Netherlands) analysis.

2.3. TMJ-SDSCs Isolation and Expansion. TMJ-SDSCs were isolated from the TMJ synovial membrane of 4-week-old Sprague-Dawley rats. All procedures were performed with approval by the Animal Care and Use Committee, school of Stomatology, Wuhan University. After anesthesia of animals, the TMJ capsule of rat was exposed and synovial tissue lining on the posterior band of TMJ disc was harvested aseptically under stereo microscope. Synovial tissue was cut into 1 mm^3 piece and cultured in primary cell culture medium (DMEM with 15% FBS, 100 μg/mL streptomycin, and 100 U/mL penicillin) on 25 cm^2 flasks in a humidified incubator at 5% carbon dioxide and 37°C. When the primary cells attached to the flasks, the synovial tissue was removed. After 12 days of expansion, TMJ-SDSCs of passage 3 were harvested with 0.25% trypsin and counted for future use.

2.4. Preparation of Cell/Scaffold Constructs and Three-Dimensional Culture. In fibrin/chitosan group, TMJ-SDSCs were pelleted by centrifugation and resuspended with 50 μL of fibrinogen solution. Cell/fibrinogen suspension was gently dropped onto the top surface of half-dried chitosan scaffold of both sides and then equal volume of thrombin solution was added onto scaffold in the same way. The cell/fibrin/chitosan construct was incubated at 37°C for 15 min to polymerize the fibrinogen, and then gently the construct was washed with PBS and cultured with culture medium in 24-well plate.

In control group, pure chitosan was used as scaffold. The same amount of cells was resuspended with 100 μL of culture medium. Half of the suspension was gently dropped onto the top surface of half dried scaffold. After an interval of 2.5 hours, the rest of cell suspension was dropped onto the other side of scaffold. The cell/chitosan scaffold was washed and transferred into 24-well plate with culture medium after 3 hours of cell seeding.

2.5. In Vitro Studies on Cell Seeding, Distribution, Expansion, and Chondrogenic Induction. TMJ-SDSCs seeded scaffolds (2×10^6 cells per scaffold) with (experiment group) or without fibrin incorporation (control group) were cultured in 24-well plate with 2 mL culture medium per well at 37°C in a humidified 5% CO_2/95% air incubator.

After 8 hours of cell seeding, cell/scaffold constructs (n = 8 of each group) were transferred to a blank well of plate, and the rest of the cells which were attached to the former well were trypsinized and counted. Cell seeding efficiency was calculated as follows: (total number of cells − rest cells)/total number of cells × 100%.

Cell vitality and distribution after 5 days of cell seeding were assessed using fluorescein diacetate/propidium iodide (FDI/PI) staining. Constructs (n = 4 of each group) were rinsed with PBS and incubated with 5 μg/mL FDA solution for 15 min at 37°C in the dark. Then, the constructs were rinsed again and incubated within 0.1 mg/mL PI solution for 2 min at room temperature. After an additional washing step, the cell vitality and distribution of the constructs

Table 1: The primer sequences of ECM related genes.

Genes	Primer sequence (F, R, $5' \rightarrow 3'$)	Product length (bp)	GenBank accession number
Col 1A1	CCTACAGCACGCTTGTGGATG AGATTGGGATGGAGGGAGTTTAC	195	NM_053304.1
Col 2A1	GACTTTCCTCCGTCTACTGTCC GTGTACGTGAACCTGCTGTTG	171	NM_012929.1
GAPDH	GGCACAGTCAAGGCTGAGAATG ATGGTGGTGAAGACGCCAGTA	143	NM_017008.4

were analyzed with a Confocal Laser Scanning Microscopy (CLSM, Leica TCS SP2, Germany).

Cell proliferation ability among the two groups was measured with the Cell Counting Kit-8 (CCK-8, Dojindo Laboratories, Japan). Cell/scaffold constructs ($n = 6$ of each group) were cultured in 24-well plate with culture medium. The medium was renewed at 3-day interval. At days 1, 7, 14, 21, and 28, the culture medium was changed into incubating medium containing 100 μL of CCK-8 solution and 900 μL of fresh culture medium. After 4 hours of incubation at 37°C, the incubating medium was measured using a microplate absorbance reader (Varioskan Flash, Thermo Electron Corporation, USA) at a wavelength of 450 nm. Blank well with fresh culture medium was used for the zero setting.

To evaluate the influence on chondrogenic induction after fibrin incorporation, experiment and control groups of cell/scaffold constructs were cultured in 24-well plate with serum free chondrogenic medium, including high glucose DMEM, 100 μg/mL ascorbic acid 2-phosphate, 100 μg/mL sodium pyruvate, 100 μg/mL streptomycin, 100 U/mL penicillin, 40 μg/mL proline, 100 μM dexamethasone, $1\times\text{ITS}^{+\text{Premix}}$, and 10 ng/mL TGF-$\beta$3. The chondrogenic medium was renewed every other day. At days 0, 14, and 28, constructs were biochemically analyzed.

Biochemical Analysis. sGAG and collagen are the main components of cartilaginous ECM. sGAG to DNA ratio represents the synthetic ability of cells. It was performed by incubating the constructs ($n = 5$ of each group) in 1 mL of papain buffer solution (5 mg/mL in 0.2 M NaCl, 0.05 M Na_2-EDTA, 0.1 M NaAc, and 0.01 m L-cysteine-HCl, pH 6.0) at 60°C for 24 h. The sGAG content of each construct was evaluated using 1,9-dimethylmethylene blue (DMMB) method. Forty microliters of papain digestive solution of each construct was added to 250 μL of DMMB dye (pH 3.0) in a 96-well microtiter plate. After mixing, the absorbance of the solutions was measured at 595 nm and was compared with the linear standard curve obtained from the known concentration of 6-chondroitin sulfate. To determine the cell amount of each construct, DNA content was measured. 100 μL of digestive solution was mixed with 1 mL of Hoechst 33258 dye/buffer, and 200 μL of mixture was evaluated for the excitation at 365 nm and emission at 458 nm by the microplate absorbance reader. A standard curve was established from the known concentration of calf thymus DNA.

To detect the difference in chondrogenic gene expression between the two constructs, the ECM-related gene expression was evaluated with real-time PCR. Snap frozen constructs ($n = 5$ of each group) were pulverized in liquid nitrogen and total RNA was extracted using RNAiso Plus (TAKARA, D9108A). After elimination of genomic DNA contamination, 450 ng of total RNA was reverse transcribed into cDNA using Oligo $(dT)_{15}$ as a reverse primer (TAKARA, DRR037A). Equivalent amounts of cDNA were used for real-time PCR in a 20 μL reaction mixture with 10 μL of 2x SYBR Green PCR Mastermix and 1 μL of specific primer pair. Reaction was run in triplicate with 40 cycles of amplification on an ABI Prism 7500 real-time PCR (Applied Biosystems, USA). The sequences of primers were shown in Table 1. The expression levels of target genes were normalized by the expression of GAPDH gene measured in parallel samples. Relative transcript levels were calculated as $\chi = 2^{-\Delta\Delta Ct}$, in which $\Delta\Delta Ct = \Delta E - \Delta C$, $\Delta E = Ct_{exp} - Ct_{GAPDH}$, and $\Delta C = Ct_{ct1} - Ct_{GAPDH}$.

2.6. In Vivo Animal Model to Evaluate the Repairing Ability. To evaluate the repairing ability of cell/scaffold constructs in defect of fibrocartilage, an animal model of TMJ disc perforation was designed (Figure 1).

Thirty rat TMJ discs were dissected and separated from mandibular condyle aseptically (Figure 2(a)). After washing in PBS, surrounding synovial tissue of the TMJ disc was removed under stereo microscope. A unified perforation of the TMJ discs was made by punching the disc body with a 2 mm diameter puncher (Figure 2(b)).

Chondrogenic induced constructs and cell-free constructs were punched into same size as disc perforation and were implanted into the site of TMJ disc perforation. Before subcutaneous transplantation, all the disc explants were coated with 2 mm thick fibrin gel to prevent exogenous host cells migration into the constructs (Figure 2(c)). Five groups of TMJ disc explants were set in Table 2.

The fibrin-coated TMJ discs explants were implanted subcutaneously in 2-week-old nude mice (Hubei Medical Laboratory Animal Center). After 4 weeks, mice were euthanize and explants were fixed for histological analysis ($n = 5$ of each group).

For histological analysis, samples were fixed overnight at 4°C in 4% paraformaldehyde in PBS. Samples were embedded in paraffin and sectioned to 5 μm thickness. Consecutive sections were stained with HE and Safranin O/Fast Green for glycosaminoglycans. For immunohistological evaluations, collagen type I and type II were detected. In brief, sections were incubated with primary antibody against collagen type

Table 2

Group A	TMJ disc within chondrogenic induced cell/fibrin/chitosan scaffold
Group B	TMJ disc within chondrogenic induced cell/chitosan scaffold
Group C	TMJ disc within cell-free fibrin/chitosan scaffolds
Group D	TMJ disc within cell-free chitosan scaffold
Group E	TMJ disc within cell-free fibrin scaffold

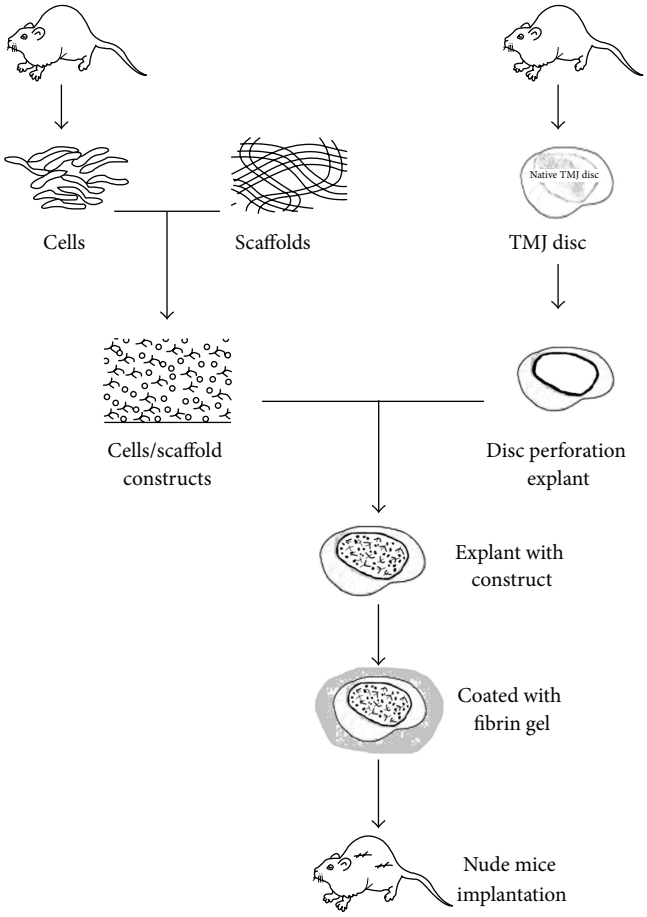

Figure 1: The experiment design and animal models for repairing TMJ disc perforation.

I and type II overnight at 4°C, followed by the secondary antibody of biotinylated goat anti-rabbit IgG, and detected by using ABC reagent with 3,3′-diaminobenzidine as a substrate. Negative control staining against each primary antibody was performed by replacing the primary antibody with distilled water to test the workability of the antibody. All the sections were counterstained with hematoxylin and observed by a light microscope (Leica, Wetzlar, Germany).

2.7. Statistical Analysis. Cell seeding efficiency, proliferation ability, GAG content, GAG/DNA ratio, and mRNA expression levels were compared between the scaffolds with or without fibrin gel incorporation, with a risk factor of less than 0.05 considered statistically significant. All data were expressed as mean ± standard deviation. Statistical differences were evaluated between the two constructs with Student's t-test and two-factor ANOVA using GraphPad Prism 4 statistical software (San Diego, USA).

3. Results

3.1. Morphological Features of Fibrin/Chitosan Scaffold. The pure chitosan scaffold demonstrated a macroporous structure fulfilled with cavity (Figure 3(b-1)). When combining chitosan with fibrin, the cavity of chitosan was extensively filled with fibrin (Figure 3(a-1)).

After 7 days of three-dimensional culture, constructs were stained with FDA/PI to assess cell viability and distribution 100 μm below the surface. More vital cells were homogeneously distributed among fibrin/chitosan scaffolds (Figure 3(a-2)). Although many dead cells (red) were evident in fibrin incorporated scaffold (Figure 3(a-3)), the amount of green vital cells were higher than chitosan scaffold (Figure 3(b-2)).

3.2. Biocompatible and Biochemical Researches of TMJ-SDSCs Seeded into Two Scaffolds. Comparing with the traditional seeding technique, the incorporation of fibrin gel may significantly improve cell seeding efficiency. In fibrin/chitosan constructs, more TMJ-SDSCs (97.28 ± 0.935%) were eventually seeded into the scaffold, while significantly less cells were retained in pure chitosan scaffold (90.46 ± 1.366%) (Figure 4(a)).

In cell proliferation assay, TMJ-SDSCs proliferated in both of the two scaffolds during the first week. From day 7 to day 28, the amount of live cells decreased gradually. Statistic differences were observed at days 14, 21, and 28, indicating a better biocompatibility of the fibrin/chitosan scaffold (Figure 4(b)).

Biochemical quantification of the total DNA amount and sGAG accumulation was performed during the 28 days of chondrogenic induction. In fibrin/chitosan constructs, a significantly higher sGAG/DNA ratio was achieved at 28 days, indicating a stronger sGAG synthetic ability (about 1.4-fold to control) of the cells (Figure 4(c)).

The relative mRNA levels of chondrogenic markers including collagen type I and type II were quantified using real-time RT-PCR. The expression of collagen type I mRNA in fibrin/chitosan scaffold was significantly higher (about 1.97-fold to control) than in pure chitosan scaffold (Figure 4(d)). However, no significant difference of collagen type II mRNA was observed among the two groups (Figure 4(e)).

(a) (b) (c)

Figure 2: (a) Rat TMJ discs were obtained from mandibular condyle (C: condyle and D: TMJ disc); (b) TMJ disc perforation of 2 mm in diameter was surgically made by a puncher; (c) scaffolds with or without cells (arrow) were inserted into the perforation of disc and then coated the explants with pure fibrin before subcutaneous implantation (D: TMJ disc and F: fibrin).

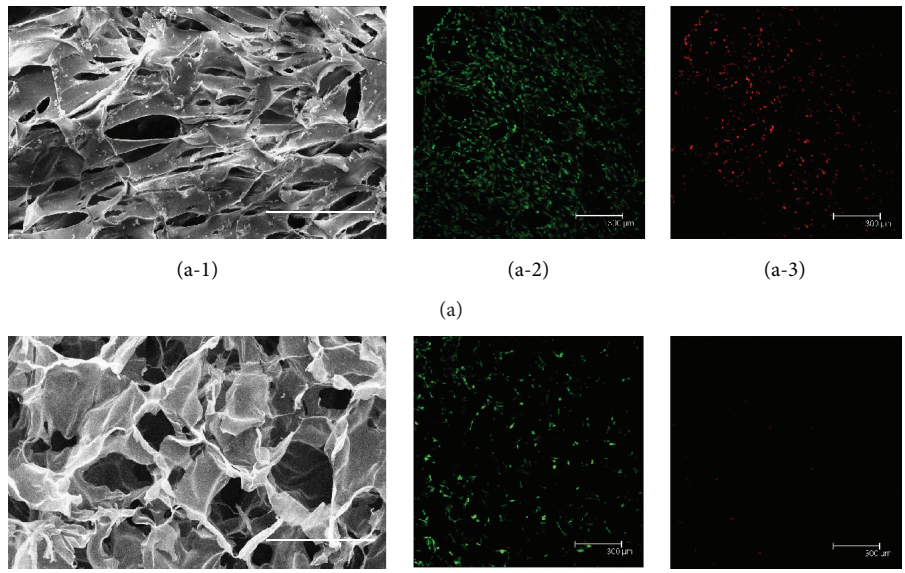

(a-1) (a-2) (a-3)

(a)

(b-1) (b-2) (b-3)

(b)

Figure 3: Morphologic features of two scaffolds. SEM results showed more cavities among pure chitosan scaffold (b-1), while the cavities were filled with fibrin in fibrin/chitosan scaffold (a-1). CLSM results showed that more vital cells (green) existed in fibrin/chitosan scaffold (a-2) than in chitosan scaffold (b-2), although the number of dead cells (red) was relatively higher in hybrid scaffold ((a-3) and (b-3)). Scale bar is equal to 300 μm.

3.3. In Vivo Subcutaneous Implantation of TMJ Disc Explants. After 4 weeks of subcutaneous implantation, all samples were histologically analyzed. Gross view of HE staining demonstrated more matrix depositions with fewer cavities in fibrin/chitosan scaffold (Figure 5(a-1)) than fibrin-free constructs (Figure 5(b-1), Group B). Few host cells were observed in cell-free group with no sign of repair (Figures 5(c-1), 5(d-1), and 5(e-1)).

The conjunction between constructs and native disc tissue (Figures 5(a-2), 5(b-2), 5(c-2), and 5(d-2)) and central part of constructs (Figures 5(a-3), 5(b-3), 5(c-3), and 5(d-3)) was magnified to evaluate the repair capacity. In Group A (Figures 5(a-2) and 5(a-3)), high density of cells and dense staining of ECM accumulation were observed compared to Group B (Figures 5(b-2) and 5(b-3)). No sign of repair was found in cell-free groups (Figures 5(c), 5(d), and 5(e)). In the pure chitosan scaffold (Figure 5(d)), few host oriented cells aggregated to the framework of the chitosan scaffold. In fibrin/chitosan scaffold, host cells were distributed more separately along with the fibrin (Figure 5(c)). In the fibrin group, the perforation was still filled with fibrin without any sign of disc repair (Figure 5(e)).

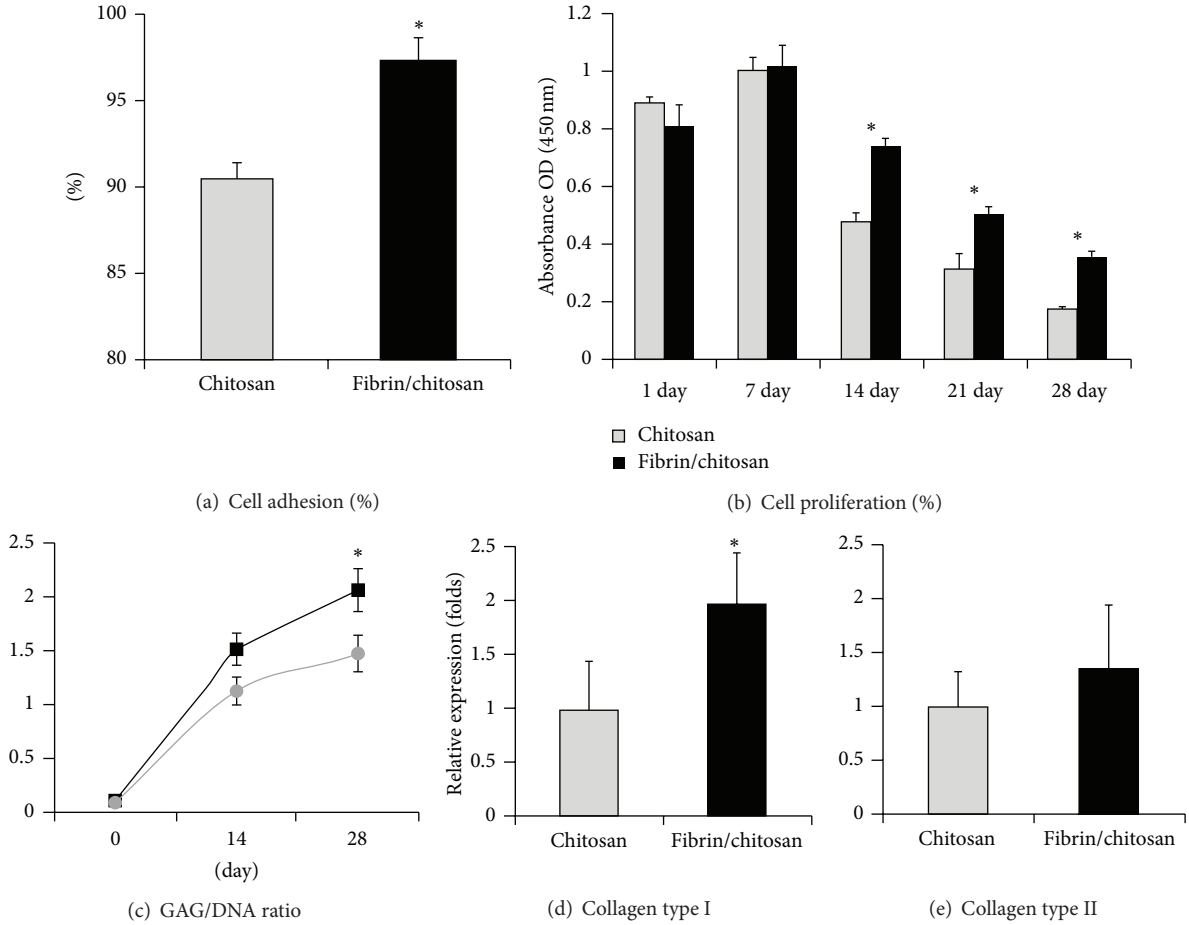

Figure 4: Biocompatible and biochemical results of TMJ-SDSCs seeded in two scaffolds. Columns and error bars represent means and SD. Cell adhesion (a), GAG/DNA ratio (c), and relative expression of Col I (d) were significantly improved in fibrin/chitosan scaffold. Asterisks (∗) indicate significant difference from control ($P < 0.05$), based on the *post hoc* analysis comparing each individual group. Cell proliferation results (b) demonstrated significant difference ($P < 0.05$) in the two-factor ANOVA (fibrin and time duration).

Safranin O/Fast Green staining showed more sGAG accumulation in fibrin-added Group A constructs (Figure 6(a)) than fibrin-free Group B constructs (Figure 6(b)). In cell-free control group, no sGAG deposition was found (Figure 6(c)).

In accordance with mRNA expression results, staining of collagen type I and collagen type II was more intensive in fibrin-added constructs (Figures 7(a-1), 7(a-2)) than in fibrin-free constructs (Figures 7(b-1), 7(b-2)) at 4 weeks. Negative control staining of each primary antibody in Group A specimens was shown in Figures 7(c-1) and 7(d-1), respectively. Figure 7(d) confirmed that strong expression of collagen type I rather than collagen type II was demonstrated in native TMJ disc. However, when compared with native TMJ disc (Figure 7(d-2)), over expression of collagen type II was noted in SDSCs seeded groups (Figures 7(a-2) and 7(b-2)).

4. Discussions

Although many researches focused on cartilage regeneration, only a handful of studies were on TMJ disc engineering. In the field of cartilage engineering, cell source and matrix scaffold were two major factors. This research is the first *in vivo* study using TMJ-SDSCs in TMJ disc engineering and confirms that SDSCs obtained from TMJ synovium may undergo chondrogenic differentiation in a general accepted manner. The addition of fibrin gel enhanced the ability of cartilage ECM production of the TMJ-SDSCs.

In previous study of TMJ disc engineering, the cells were harvested from the disc [3, 5, 6, 14] or from hyaline cartilage [15, 16]. However, the drawbacks of using fibrochondrocyte/chondrocyte including difficult cell harvesting, injury to donor site, and cell dedifferentiation among *in vitro* expansion hindered their utility in cartilage engineering [7, 17, 18].

Bone marrow mesenchymal stem cells (BMSCs) were superior in cell proliferation and chondrogenic differentiation ability. However, researchers found that BMSCs can express collagen type X after chondrogenic induction and tend to undergo endochondral ossification after subcutaneous implantation [19]. MSCs derived from the joint, including adipose-derived stem cells (ADSCs) and SDSCs are promising alternative cell sources that may overcome the

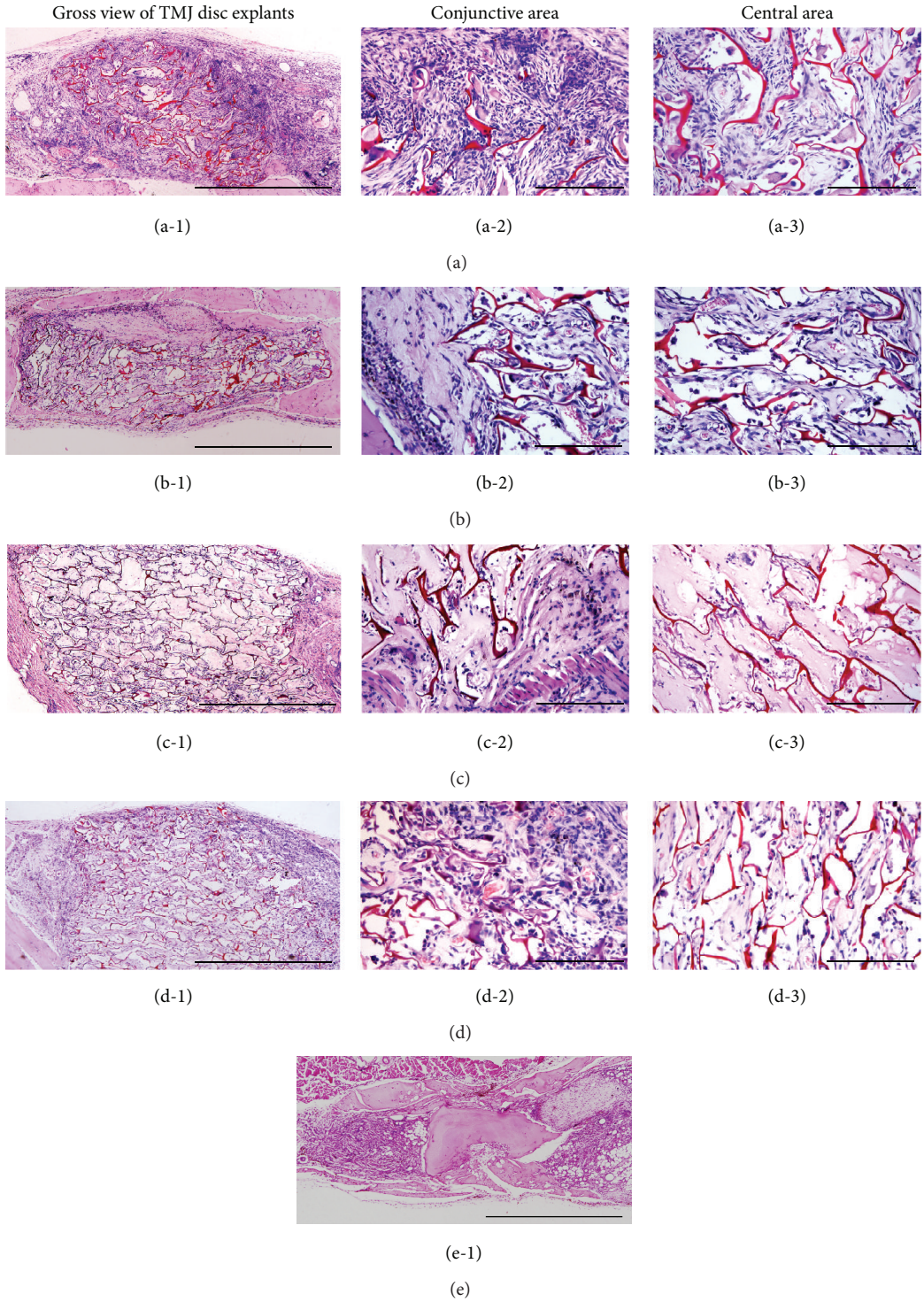

Figure 5: HE staining of TMJ disc explants. (a-1)–(e-1) are gross views of TMJ explants. Scale bar is equal to 1000 μm; (a-2)–(d-2) are magnifications of the conjunction between constructs and native disc tissue; (a-3)–(d-3) are magnifications of the central part of scaffold; scale bar is equal to 100 μm.

intrinsic drawbacks of using chondrocytes [20, 21]. SDSCs have been shown to be prior to ADSCs in cell expansion ability and chondrogenesis potential [20]. In clinical researches, synovial chondromatosis could be found within human TMJ synovial tissues, which illustrates the potential of some subpopulations of TMJ synovial cells to transform into chondrocytes and form cartilage-like tissue [22]. Miyamoto et al. found that SDSCs could be recruited *in vivo* to

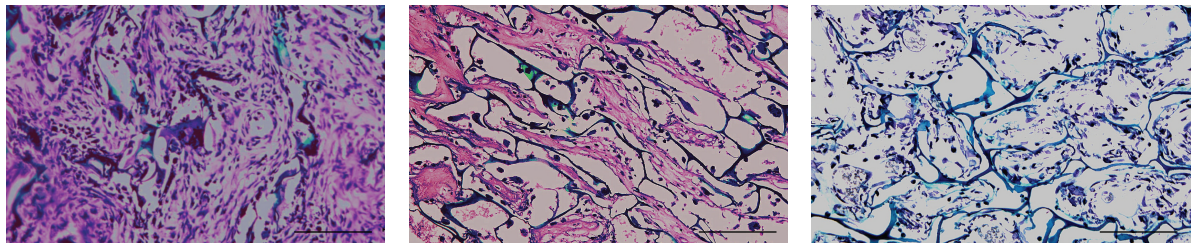

Figure 6: Safranin O/Fast Green staining of each group. Synthesized sGAG were stained red in Groups A and B. Chitosan scaffold was stained green and cell nuclei of cells were stained black. No sign of red staining in Group C indicated that fibrin gel was unable to be stained with safranin O. Scale bar is equal to 100 μm.

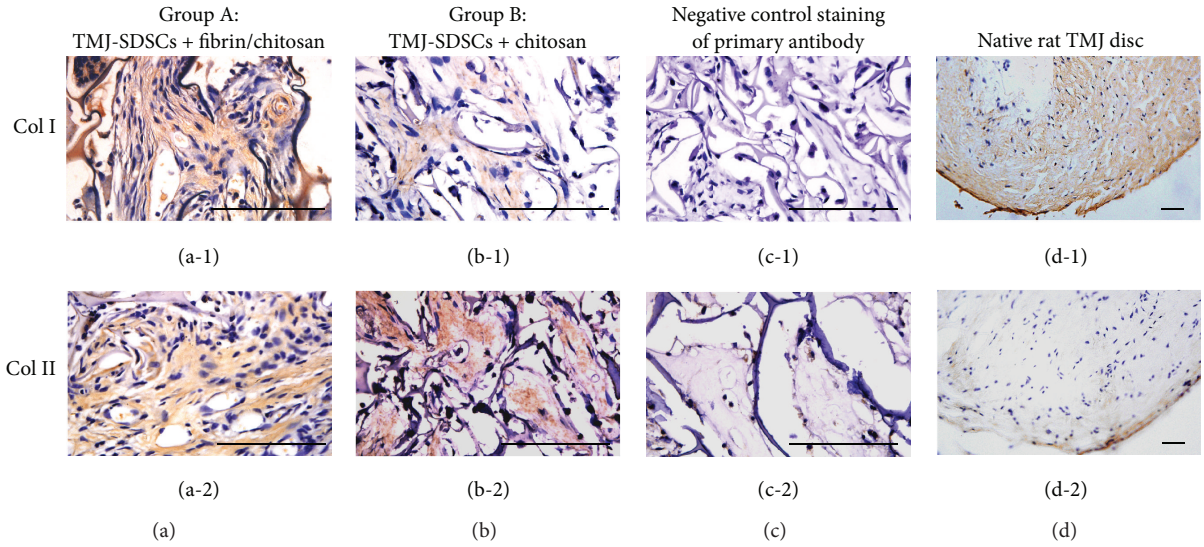

Figure 7: IHC staining of collagen type I ((a-1)–(d-1)) and type II ((a-2)–(d-2)). (a) Group A explants; (b) Group B explants; (c) negative control of primary antibody; (d) native rat TMJ disc. These results confirmed that TMJ-SDSCs may synthesis both collagen types I and II after chondrogenic induction. (d-1) and (d-2) confirmed that collagen type I was the major component of native TMJ disc. Scale bar is equal to 100 μm.

repair adjacent partial-thickness cartilage defects [23]. These evidences imply the possibility of using TMJ-SDSCs in TMJ disc tissue regeneration.

The synovial membrane consists of type-A macrophage-like cells and type-B SDSCs [24]. SDSCs can be generally purified by continuous passage as the poor proliferation ability of type-A cells. However, SDSCs obtained with the conventional method may not be completely pure. Bilgen et al. [25] purified the SDSCs using CD14-negative isolation method and found that purified SDSCs demonstrated higher expression of collagen type II and aggrecan as well as lower expression of collagen type I under the same condition. Their results might be in favour of hyaline cartilage regeneration but might not refer to fibrocartilaginous repair especially in TMJ disc, which is predominately consisted as collagen type I with collagen type II in trace amount [26, 27]. So in this study, TMJ-SDSCs were isolated with the conventional methods and the results show that both collagen type I and cartilage-related ECM including collagen type II and sGAG were synthesized after chondrogenic induction.

Biomaterials used in previous cartilage engineering researches can be divided as hydrogels, fibrous meshed, and sponges with respect to the scaffold structure. Several synthetic materials had been used in TMJ disc engineering, including polylactide (PLA), polyglycolic acid (PGA), and their copolymers (PLGA) [28]. Natural chitosan is polysaccharide material which has been used extensively in the field of cartilage regeneration for its good biocompatibility and similarity to GAG cartilage [29]. Porous chitosan scaffold provides mechanical strength and shape-persistency during both *in vitro* and *in vivo* cultures, which has been confirmed in our researches [12]. However, cell seeding onto this kind of scaffold is unlikely to be homogeneous. Most cells tend to adhere only on the scaffold surface. So improving cell seeding and distribution is essential for the limited amount of joint derived cells.

Hydrogels have great scaffolding potential due to their high biocompatibility, efficient transport of nutrients and waste, ability to uniformly encapsulate cells, and ability to be made into any shape [30]. Besides the clinical application as haemostatic sealant [31], fibrin gel has been widely used in a variety of tissue engineering including cardiovascular [32], liver [33], skin [34], bone [35], and cartilage tissues [36, 37]. It was reported that fibrin gel may benefit chondrocytes for maintaining stable phenotype and synthesizing cartilage ECM in nude mice [38]. Izuta et al. [39] found that fibrin combined with MSCs may promote avascular zone of meniscal healing after 8 weeks of implantation.

The major disadvantages of using fibrin gel as scaffold include the shrinkage of the volume during gel formation, poor mechanical stiffness, and rapid degradation [32]. In this study, fibrin gel was incorporated with porous chitosan scaffold. We hypothesized that this hybrid scaffold may promote cell differentiation and ECM synthesis and may be fixed in the site of disc defect by the adhesive feature of fibrin gel. After cell seeding into this fibrin/chitosan scaffold, a higher seeding efficiency and more homogeneous cell distribution was observed compared with fibrin-free scaffolds. These results were in accordance with Swartz et al.'s study [40]. From day 1 to day 7, TMJ-SDSCs seemed to proliferate quicker in fibrin-added scaffolds than in fibrin-free scaffolds, although no statistic difference was observed. Cell numbers dramatically decreased in both groups from day 7 to day 28. Statistic differences were observed at these time points, indicating a better maintenance of cell viability presented in fibrin-added scaffolds.

In the present research, TGF-β3 was the only growth factor used in chondrogenic induction. Lee et al. [41] compared the use of TGF-β alone with a combination of TGF-β and BMP in chondrogenic induction of calf SDSCs and found that the gene expression of collagen type II, aggrecan, and SOX9 increased along with the addition of BMP-7; however, the expression of collagen type I decreased. In fibrocartilage, collagen type I was predominant, while collagen type II was found in small amount. So in this study, only TGF-β3 was used. After chondrogenic induction, sGAG were synthesized by the TMJ-SDSCs and deposited in scaffolds. The sGAG/DNA ratio indicates the synthetic ability of cells. In fibrin-added groups, sGAG/DNA ratio was higher than fibrin-free groups at day 14 and day 28.

In animal model study, TMJ-SDSCs seeded fibrin/chitosan constructs showed better repair than fibrin-free constructs after 4 weeks of subcutaneous implantation. Most of the cells in Group A were rounded rather than spindle-shaped in fibrin-free group. According to previous researches on the characterization of animal TMJ disc, approximately 2/3 of the cells in the disc are fibroblast-like cells and the rest are chondrocyte-like cells [42]. Histological results including the staining of Col I, Col II, and sGAG were superior in fibrin-added constructs, which was in accordance with the cartilage-related mRNA expression.

In summary, fibrin gel improved the synthesis of fibrocartilage ECM by TMJ-SDSCs. This pilot study demonstrated that the regenerative ability of TMJ-SDSCs seeded fibrin/chitosan constructs could be applied for repairing TMJ disc perforation.

Conflict of Interests

The authors declare that there is no conflict of interests regarding the publication of this paper.

References

[1] M. Jibiki, S. Shimoda, Y. Nakagawa, K. Kawasaki, K. Asada, and K. Ishibashi, "Calcifications of the disc of the temporomandibular joint," *Journal of Oral Pathology and Medicine*, vol. 28, no. 9, pp. 413–419, 1999.

[2] L. G. Mercuri, L. M. Wolford, B. Sanders, R. Dean White, and A. Giobbie-Hurder, "Long-term follow-up of the CAD/CAM patient fitted total temporomandibular joint reconstruction system," *Journal of Oral and Maxillofacial Surgery*, vol. 60, no. 12, pp. 1440–1448, 2002.

[3] K. D. Allen and K. A. Athanasiou, "Scaffold and growth factor selection in temporomandibular joint disc engineering," *Journal of Dental Research*, vol. 87, no. 2, pp. 180–185, 2008.

[4] K. D. Allen and K. A. Athanasiou, "Growth factor effects on passaged TMJ disk cells in monolayer and pellet cultures," *Orthodontics & Craniofacial Research*, vol. 9, no. 3, pp. 143–152, 2006.

[5] M. S. Detamore and K. A. Athanasiou, "Use of a rotating bioreactor toward tissue engineering the temporomandibular joint disc," *Tissue Engineering*, vol. 11, no. 7-8, pp. 1188–1197, 2005.

[6] D. E. Johns and K. A. Athanasiou, "Improving culture conditions for temporomandibular joint disc tissue engineering," *Cells Tissues Organs*, vol. 185, no. 4, pp. 246–257, 2007.

[7] K. D. Allen and K. A. Athanasiou, "Effect of passage and topography on gene expression of temporomandibular joint disc cells," *Tissue Engineering*, vol. 13, no. 1, pp. 101–110, 2007.

[8] I. N. G. Springer, B. Fleiner, S. Jepsen, and Y. Açil, "Culture of cells gained from temporomandibular joint cartilage on non-absorbable scaffolds," *Biomaterials*, vol. 22, no. 18, pp. 2569–2577, 2001.

[9] A. D. Recklies, L. Baillargeon, and C. White, "Regulation of cartilage oligomeric matrix protein synthesis in human synovial cells and articular chondrocytes," *Arthritis and Rheumatism*, vol. 41, no. 6, pp. 997–1006, 1998.

[10] J. Li, X. Long, J. Ke, Q.-G. Meng, and W. Fang, "Identification and characterization of synovial mesenchymal stem cells in temporomandibular joint," *Zhonghua Kou Qiang Yi Xue Za Zhi*, vol. 40, no. 5, pp. 362–364, 2005.

[11] Z. Liu, X. Long, J. Li, L. Wei, Z. Gong, and W. Fang, "Differentiation of temporomandibular joint synovial mesenchymal stem cells into neuronal cells in vitro: an in vitro study," *Cell Biology International*, vol. 35, no. 1, pp. 87–91, 2011.

[12] Z. Gong, H. Xiong, X. Long et al., "Use of synovium-derived stromal cells and chitosan/collagen type I scaffolds for cartilage tissue engineering," *Biomedical Materials*, vol. 5, no. 5, Article ID 55005, 2010.

[13] M. Sha'Ban, S. H. Kim, R. B. H. Idrus, and G. Khang, "Fibrin and poly(lactic-co-glycolic acid) hybrid scaffold promotes early chondrogenesis of articular chondrocytes: an in vitro study," *Journal of Orthopaedic Surgery and Research*, vol. 3, no. 1, article 17, 2008.

[14] A. J. Almarza and K. A. Athanasiou, "Effects of hydrostatic pressure on TMJ disc cells," *Tissue Engineering*, vol. 12, no. 5, pp. 1285–1294, 2006.

[15] D. E. J. Anderson and K. A. Athanasiou, "A comparison of primary and passaged chondrocytes for use in engineering the temporomandibular joint," *Archives of Oral Biology*, vol. 54, no. 2, pp. 138–145, 2009.

[16] D. E. Johns, M. E. Wong, and K. A. Athanasiou, "Clinically relevant cell sources for TMJ disc engineering," *Journal of Dental Research*, vol. 87, no. 6, pp. 548–552, 2008.

[17] T. Tanaka, K. Fujii, and Y. Kumagae, "Comparison of biochemical characteristics of cultured fibrochondrocytes isolated from the inner and outer regions of human meniscus," *Knee Surgery, Sports Traumatology, Arthroscopy*, vol. 7, no. 3, pp. 75–80, 1999.

[18] N. J. Gunja and K. A. Athanasiou, "Passage and reversal effects on gene expression of bovine meniscal fibrochondrocytes," *Arthritis Research and Therapy*, vol. 9, no. 5, article R93, 2007.

[19] E. Farrell, S. K. Both, K. I. Odörfer et al., "In-vivo generation of bone via endochondral ossification by in-vitro chondrogenic priming of adult human and rat mesenchymal stem cells," *BMC Musculoskeletal Disorders*, vol. 12, article 31, 2011.

[20] Y. Sakaguchi, I. Sekiya, K. Yagishita, and T. Muneta, "Comparison of human stem cells derived from various mesenchymal tissues: superiority of synovium as a cell source," *Arthritis and Rheumatism*, vol. 52, no. 8, pp. 2521–2529, 2005.

[21] S. Shirasawa, I. Sekiya, Y. Sakaguchi, K. Yagishita, S. Ichinose, and T. Muneta, "In vitro chondrogenesis of human synovium-derived mesenchymal stem cells: optimal condition and comparison with bone marrow-derived cells," *Journal of Cellular Biochemistry*, vol. 97, no. 1, pp. 84–97, 2006.

[22] L. J.-M. J. Demeulemeester, M. Bossuyt, J. Casselman, C. Deschepper, N. Ectors, and B. Van Damme, "Synovial chondromatosis of the temporomandibular joint," *International Journal of Oral and Maxillofacial Surgery*, vol. 17, no. 3, pp. 181–182, 1988.

[23] A. Miyamoto, M. Deie, T. Yamasaki et al., "The role of the synovium in repairing cartilage defects," *Knee Surgery, Sports Traumatology, Arthroscopy*, vol. 15, no. 9, pp. 1083–1093, 2007.

[24] F. Vandenabeele, C. De Bari, M. Moreels et al., "Morphological and immunocytochemical characterization of cultured firoblast-like cells derived from adult human synovial membrane," *Archives of Histology and Cytology*, vol. 66, no. 2, pp. 145–153, 2003.

[25] B. Bilgen, Y. Ren, M. Pei, R. K. Aaron, and D. M. Ciombor, "CD14-negative isolation enhances chondrogenesis in synovial fibroblasts," *Tissue Engineering A*, vol. 15, no. 11, pp. 3261–3270, 2009.

[26] D. K. Mills, D. J. Fiandaca, and R. P. Scapino, "Morphologic, microscopic, and immunohistochemical investigations into the function of the primate TMJ disc," *Journal of Orofacial Pain*, vol. 8, no. 2, pp. 136–154, 1994.

[27] R. Landesberg, E. Takeuchi, and J. E. Puzas, "Cellular, biochemical and molecular characterization of the bovine temporomandibular joint disc," *Archives of Oral Biology*, vol. 41, no. 8-9, pp. 761–767, 1996.

[28] A. J. Almarza and K. A. Athanasiou, "Seeding techniques and scaffolding choice for tissue engineering of the temporomandibular joint disk," *Tissue Engineering*, vol. 10, no. 11-12, pp. 1787–1795, 2004.

[29] P. J. Vandevord, H. W. T. Matthew, S. P. Desilva, L. Mayton, B. Wu, and P. H. Wooley, "Evaluation of the biocompatibility of a chitosan scaffold in mice," *Journal of Biomedical Materials Research*, vol. 59, no. 3, pp. 585–590, 2002.

[30] S. Ramaswamy, D.-A. Wang, K. W. Fishbein, J. H. Elisseeff, and R. G. Spencer, "An analysis of the integration between articular cartilage and nondegradable hydrogel using magnetic resonance imaging," *Journal of Biomedical Materials Research B: Applied Biomaterials*, vol. 77, no. 1, pp. 144–148, 2006.

[31] M. W. Mosesson, K. R. Siebenlist, and D. A. Meh, "The structure and biological features of fibrinogen and fibrin," *Annals of the New York Academy of Sciences*, vol. 936, pp. 11–30, 2001.

[32] A. Mol, M. I. van Lieshout, C. G. Dam-de Veen et al., "Fibrin as a cell carrier in cardiovascular tissue engineering applications," *Biomaterials*, vol. 26, no. 16, pp. 3113–3121, 2005.

[33] H. Bruns, U. Kneser, S. Holzhüter et al., "Injectable liver: a novel approach using fibrin gel as a matrix for culture and intrahepatic transplantation of hepatocytes," *Tissue Engineering*, vol. 11, no. 11-12, pp. 1718–1726, 2005.

[34] J. L. Balestrini and K. L. Billiar, "Equibiaxial cyclic stretch stimulates fibroblasts to rapidly remodel fibrin," *Journal of Biomechanics*, vol. 39, no. 16, pp. 2983–2990, 2006.

[35] Y.-I. Chung, K.-M. Ahn, S.-H. Jeon, S.-Y. Lee, J.-H. Lee, and G. Tae, "Enhanced bone regeneration with BMP-2 loaded functional nanoparticle-hydrogel complex," *Journal of Controlled Release*, vol. 121, no. 1-2, pp. 91–99, 2007.

[36] D. Eyrich, F. Brandl, B. Appel et al., "Long-term stable fibrin gels for cartilage engineering," *Biomaterials*, vol. 28, no. 1, pp. 55–65, 2007.

[37] D. Passaretti, R. P. Silverman, W. Huang et al., "Cultured chondrocytes produce injectable tissue-engineered cartilage in hydrogel polymer," *Tissue Engineering*, vol. 7, no. 6, pp. 805–815, 2001.

[38] S.-H. Park, S. R. Park, S. I. Chung, K. S. Pai, and B.-H. Min, "Tissue-engineered cartilage using fibrin/hyaluronan composite gel and its in vivo implantation," *Artificial Organs*, vol. 29, no. 10, pp. 838–845, 2005.

[39] Y. Izuta, M. Ochi, N. Adachi, M. Deie, T. Yamasaki, and R. Shinomiya, "Meniscal repair using bone marrow-derived mesenchymal stem cells: experimental study using green fluorescent protein transgenic rats," *Knee*, vol. 12, no. 3, pp. 217–223, 2005.

[40] D. D. Swartz, J. A. Russell, and S. T. Andreadis, "Engineering of fibrin-based functional and implantable small-diameter blood vessels," *American Journal of Physiology—Heart and Circulatory Physiology*, vol. 288, no. 3, pp. H1451–H1460, 2005.

[41] S. Y. Lee, T. Nakagawa, and A. H. Reddi, "Mesenchymal progenitor cells derived from synovium and infrapatellar fat pad as a source for superficial zone cartilage tissue engineering: analysis of superficial zone protein/lubricin expression," *Tissue Engineering A*, vol. 16, no. 1, pp. 317–325, 2010.

[42] M. S. Detamore, J. N. Hegde, R. R. Wagle et al., "Cell type and distribution in the porcine temporomandibular joint disc," *Journal of Oral and Maxillofacial Surgery*, vol. 64, no. 2, pp. 243–248, 2006.

Hindawi Publishing Corporation
BioMed Research International
Volume 2014, Article ID 189516, 10 pages
http://dx.doi.org/10.1155/2014/189516

Research Article

Effect of Cyclic Mechanical Stimulation on the Expression of Osteogenesis Genes in Human Intraoral Mesenchymal Stromal and Progenitor Cells

Birgit Lohberger,[1] Heike Kaltenegger,[1] Nicole Stuendl,[1] Michael Payer,[2] Beate Rinner,[3] and Andreas Leithner[1]

[1] *Department of Orthopaedic Surgery, Medical University of Graz, Auenbruggerplatz 5, 8036 Graz, Austria*
[2] *Department of Oral Surgery and Radiology, School of Dental Medicine, Medical University of Graz, Auenbruggerplatz 5, 8036 Graz, Austria*
[3] *Center for Medical Research, Medical University of Graz, Auenbruggerplatz 5, 8036 Graz, Austria*

Correspondence should be addressed to Birgit Lohberger; birgit.lohberger@medunigraz.at

Received 9 December 2013; Revised 3 March 2014; Accepted 4 March 2014; Published 7 April 2014

Academic Editor: Jiang Chang

We evaluated the effects of mechanical stimulation on the osteogenic differentiation of human intraoral mesenchymal stem and progenitor cells (MSPCs) using the Flexcell FX5K Tension System that mediated cyclic tensile stretch on the cells. MSPCs were isolated from human mandibular retromolar bones and characterized using flow cytometry. The positive expression of CD73, CD90, and CD105 and negativity for CD14, CD19, CD34, CD45, and HLA-DR confirmed the MSPC phenotype. Mean MSPC doubling time was 30.4 ± 2.1 hrs. The percentage of lactate dehydrogenase (LDH) release showed no significant difference between the mechanically stimulated groups and the unstimulated controls. Reverse transcription quantitative real-time PCR revealed that 10% continuous cyclic strain (0.5 Hz) for 7 and 14 days induced a significant increase in the mRNA expression of the osteogenesis-specific markers type-I collagen (Col1A1), osteonectin (SPARC), bone morphogenetic protein 2 (BMP2), osteopontin (SPP1), and osteocalcin (BGLAP) in osteogenic differentiated MSPCs. Furthermore, mechanically stimulated groups produced significantly higher amounts of calcium deposited into the cultures and alkaline phosphatase (ALP). These results will contribute to a better understanding of strain-induced bone remodelling and will form the basis for the correct choice of applied force in oral and maxillofacial surgery.

1. Introduction

Mesenchymal stem and progenitor cells (MSPCs) are promising candidates for cellular therapy in bone repair and regeneration of degenerative diseases due to their accessibility, expandability, and multipotent differentiation potential [1–6]. Bone marrow (BM) is regarded as the main source of MSPCs for experimental and clinical application [6], but due to the limited number of BM-MSPCs available for autogenous use, the implementation of alternative sources of MSPCs is particularly important. In a previous work, we identified intraoral tissues as potential sources of multipotent progenitor cells for tissue engineering approaches [7]. A major goal in implantology is the development of minimally invasive techniques that allow predictable alveolar crest reconstruction as well as reconstruction of critical size defects resulting from resorption, trauma, cancer, or metabolic disorders. Various techniques using mainly autogenous bone grafts alone or in combination with bone substitutes have, with varying degrees of success and with limitations mainly in regard to donor site morbidity, been introduced and established in daily practice [8–10].

It has been well documented that the bone remodelling process is initiated by the sensing of mechanical stimuli by osteocytes which in turn signal osteoblasts to form the bone matrix. By applying what is known about physiological

conditions, it is reasonable to deduce that the same mechanical stimulation may play a role in the differentiation of MSPCs down an osteogenic pathway. Utilizing the principle of mechanically stimulating bone formation, uniaxial tensile strain was successfully used to induce bone regeneration via distraction osteogenesis [11–14]. Undifferentiated human MSPCs are highly sensitive to cyclic tensile strain which transcriptionally controls early osteochondrogenic response *in vitro* [15]. Strain alone can induce a significant increase in bone morphogenetic protein 2 (BMP2) mRNA levels in human BM-MSPCs without any addition of osteogenic supplements [16]. However, *in vivo* bone healing is much more effective when osteogenically differentiated cells are transplanted into the bone defect rather than undifferentiated MSPCs [17].

In this study, we used the FX5K Tension System to assess the effects of mechanical strain on *in vitro* differentiation to osteoblast-like cells, as well as the expression of osteogenesis-related transcription factors. Undifferentiated and osteogenic differentiated human intraoral MSPCs were seeded into BioFlex plates and cultivated statically or dynamically over a 14-day period. Differentiation was assessed using reverse transcription quantitative real-time PCR for the runt-related transcription factor 2 (RUNX2), the early osteogenic markers alkaline phosphatase (ALPL), bone morphogenetic protein 2 (BMP2), type-I collagen (Col1A1), and osteonectin (SPARC), and the osteogenic late stage markers osteocalcin (BGLAP) and osteopontin (SPP1).

The investigation of the effect of mechanical stimulation on human intraoral MSPCs provided insight into the mechanisms of bone regeneration, which play a major role in oral and maxillofacial surgery.

2. Material and Methods

2.1. Intraoral Tissue Harvest and Cell Culture. Explant MSPC cultures were established from intraoral tissue samples of posterior maxilla as well as from mandibular retromolar bone harvested during routine oral surgical interventions (wisdom tooth removal, augmentation procedures, and implantation). The study protocol was approved by the local ethics committee, and informed consent was obtained from each oral surgery patient. A total of ten patients, seven female and three male, aged between 15 and 47 were included in the study. Patients with metabolic bone diseases, local inflammatory processes, and impaired blood coagulation and pregnant women were excluded. The harvesting procedure was performed under sterile conditions with local anaesthesia (Ultracain Dental Forte, Maxilla; Sanofi-Aventis, Vienna, Austria) using a trephine burr 3.8 mm in diameter and 11 mm in length. The harvested bone samples were between 4 and 6 mm in length and showed cortical or cortical and cancellous structure. The obtained bone samples were rinsed extensively with phosphate-buffered saline (PBS; PAA Laboratory, Pasching, Austria) and cleaned with sharp instruments under the 10-fold magnification of a light microscope. After the cleaning procedure, the biopsies were transferred into 75 cm^2 culture flasks (TPP, Trasadingen, Switzerland) with an appropriate volume of culture medium and incubated in a humidified atmosphere with 5% CO_2 at 37°C for cell isolation and expansion.

2.2. Cell Culture and Long-Term Expansion. MSPCs were cultured in α-modified minimum essential medium (α-MEM; Sigma-Aldrich, Vienna, Austria) and supplemented with 10% pooled human platelet lysate (pHPL) [18] after the addition of 2 U/mL stabilisator-free heparin (Biochrom AG, Berlin, Germany), 2% penicillin-streptomycin (GIBCO Invitrogen, Darmstadt, Germany), 0.5% L-glutamine (GIBCO Invitrogen), 0.2% amphotericin B (PAA Laboratory), and 2.5% HEPES buffer (Sigma-Aldrich, Vienna, Austria). Total MSPC cell number and doubling time were evaluated during cell expansion and MSPSs were then cultured with a reduced seeding density technique for three additional passages [19].

2.3. Flow Cytometry. A total of 1×10^5 MSPCs were resuspended in a final volume of 200 μL PBS for flow cytometric analysis. The commercial monoclonal antibodies CD73 PE, CD90 APC, CD105 PE, CD45 APC-Cy7, CD34 APC, CD14 FITC, CD19 APC, and HLA-DR APC (BD Bioscience, San Jose, CA) were applied for characterization. The optimal amount of each antibody had previously been determined by titration and antibodies with nonoverlapping spectra were combined in two-colour staining panels. Background staining for antibodies was performed in negative cell lines and with matched fluorochrome-conjugated isotype controls. Flow cytometry analysis was performed on a FACS LSR II System (BD Bioscience), and data were acquired using FACSDiva software (BD Bioscience) and analysed with FCS Express software (De Novo Software, Los Angeles, CA). The day-to-day consistency of measurements was checked by Rainbow Beads (BD Bioscience). Viable cells were gated on forward scatter (FSC) and side scatter (SSC) in order to exclude debris and cell aggregates. MSPCs were defined by their phenotype and analysed on a logarithmic scale. Data from all donors were collected under identical parameters and analysed by collecting 10,000 events.

2.4. Mechanical Stimulation. The Flexcell FX-5000 Tension System (FX5K; Flexcell International Corp, Hillsborough, NC) was used to apply mechanical cyclic tensile stretch to the MSPCs. The Flexcell FX-5000 is a computer-based system that uses a vacuum to strain cells adhered to flexible silicon membranes (BioFlex plates; Flexcell International Corp) arranged in a format of six wells per plate with a total growth area of 9.62 cm^2/well and a membrane thickness of 0.05 mm. The deformation of the flexible membrane of the plates also causes the attached cells to deform. Programming the magnitude, duration, and frequency of the negative pressure in the Flexcell apparatus creates desired strain profiles. MSPCs were seeded onto the collagen type-I-coated BioFlex plates at a density of 5×10^4 cells/well. When cultures reached approximately 70% to 80% confluence, undifferentiated (EX) and osteogenic differentiated (OG) MSPCs were subjected to continuous mechanical stimulation with a uniaxial sinusoidal waveform with 10% elongation and a frequency of 0.5 Hz for

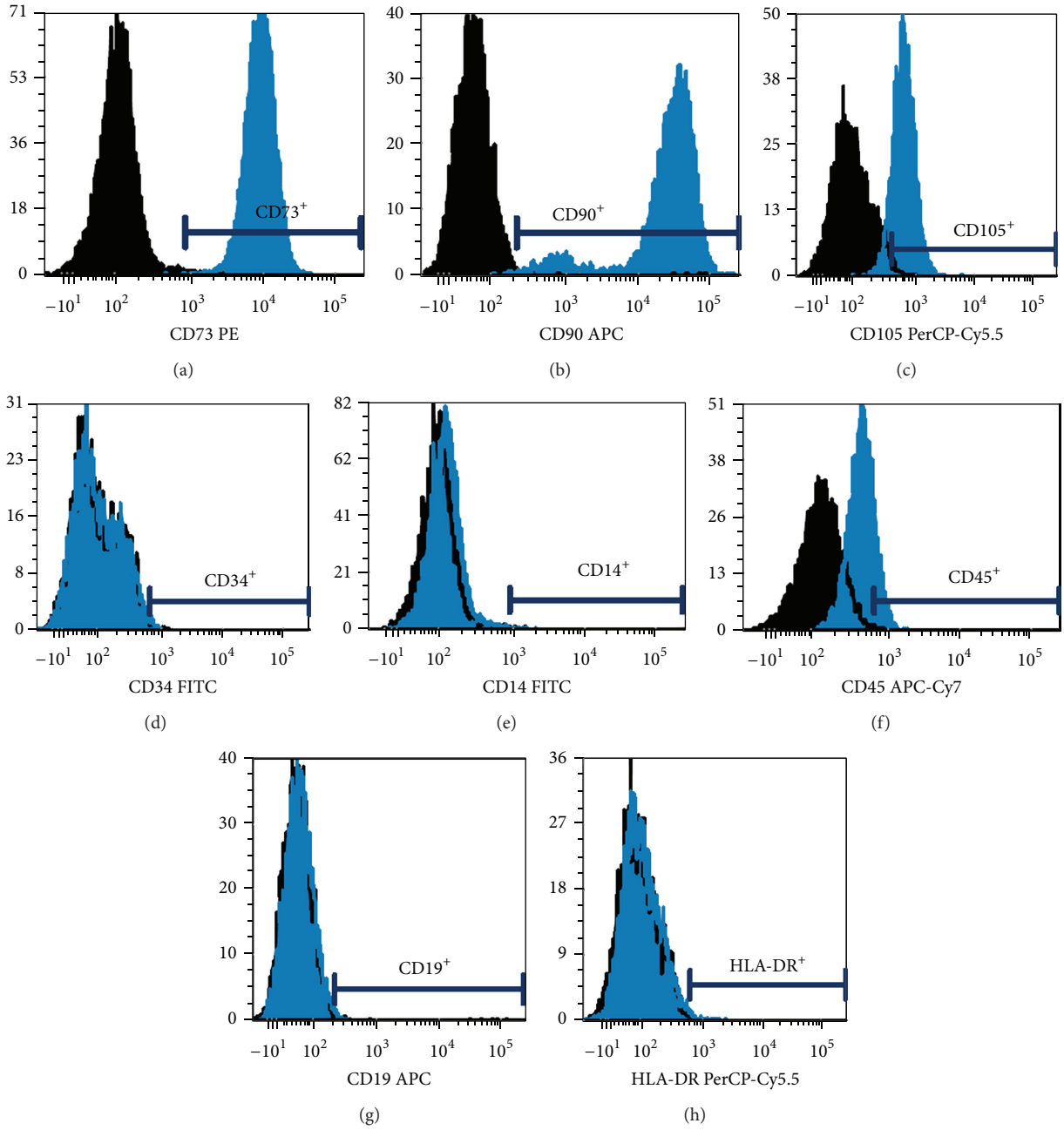

Figure 1: Multicolour flow cytometric immunophenotypic analysis with monoclonal antibodies. Intraoral MSPCs at passages 3–7 were labelled with specific fluorochrome-conjugated monoclonal antibodies against the indicated surface antigens and analysed by flow cytometry. Analysed MSPCs demonstrated the same immunophenotype, with expression of (a) CD73, (b) CD90, and (c) CD105 but no expression of (d) CD14, (e) CD19, (f) CD34, (g) CD45, and (h) HLA-DR. A representative example of ten experiments is shown. PE: phycoerythrin; APC: allophycocyanin; PerCP: peridium-chlorophyll protein complex; FITC: fluorescein isothiocyanate.

7 and 14 days. Each cycle consisted of 10 s strain and 30 s relaxation (Figure 2(a)). Control cultures were grown under the same conditions but without the strain protocol. Control cultures were grown under the same conditions but without the strain protocol.

2.5. Osteogenic Differentiation. Intraoral MSPCs used for osteogenic differentiation were derived from the third to sixth passage. MSPCs were seeded at a density of 10^4 cells/cm^2 in expansion medium containing Dulbecco's Modified Eagle's Medium (DMEM-F12; GIBCO Invitrogen), 10% FBS (Lonza, Braine-l'Alleud, Belgium), 1% penicillin-streptomycin, 1% L-glutamine, and 0.1% amphotericin B. Osteogenic differentiation was induced over two weeks by shifting the cells to an osteoinductive medium (OG) composed of the expansion medium supplemented with

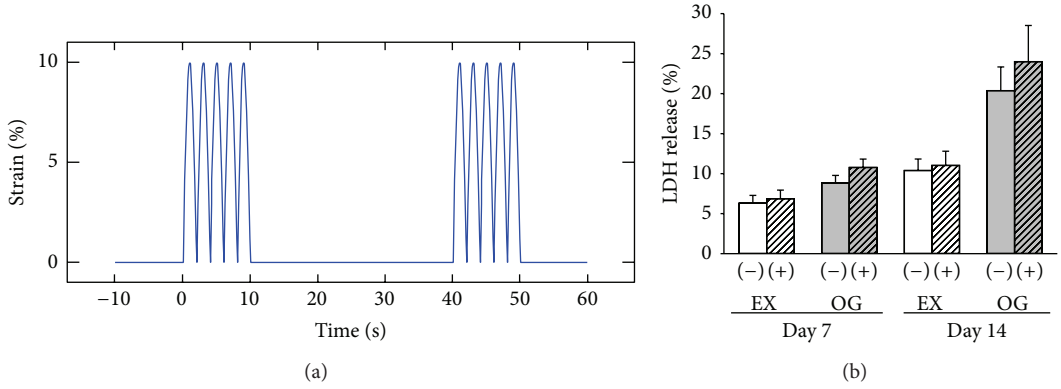

FIGURE 2: Straining profile and effects of mechanical stimulation on the release of lactate dehydrogenase (LDH) from human intraoral MSPCs. (a) Profile of a uniaxial sinusoidal waveform with 10% elongation and a frequency of 0.5 Hz, whereby each cycle consists of 10 s strain and 30 s relaxation. (b) The percentage of LDH released into the culture media was measured after 7 and 14 days of culture. Each bar represents the mean ± SD of independent experiments performed in triplicate ($n = 8$); $^*P < 0.05$.

100 nM dexamethasone, 0.1 mM ascorbic-acid-2-phosphate, and 10 mM β-glycerophosphate (all from Sigma-Aldrich). Alkaline phosphatase (ALP) enzyme activity was photometrically determined at day 14 in triplicate with a p-nitrophenyl phosphate liquid substrate system (Sigma-Aldrich) at 405 nm on a microplate reader (BioRad, Vienna, Austria) [20]. For the visualization and quantification of calcium phosphate deposits, Alizarin Red S (ARS) staining was used at days 7 and 14. Cells were fixed with 10% formaldehyde (Merck, Spittal/Drau, Austria) and incubated with a 1% ARS staining solution. Quantitation of ARS staining was performed by elution of the fixed cells with 10% cetylpyridinium chloride (Sigma-Aldrich) measuring absorbance at 570 nm on a microplate reader [21].

2.6. Lactate Dehydrogenase Assay. Lactate dehydrogenase (LDH) activity was measured using the CytoTox-ONE Homogeneous Membrane Integrity Assay (Promega, Mannheim, Germany). The amount of fluorescence produced is proportional to the number of lysed cells. After 7 and 14 days of mechanical stimulation, cell culture supernatants were collected and analysed to examine the state of cellular damage. In short, 50 μL of supernatant and 50 μL of working solution were mixed in white 96-well microtiter plates and incubated in the dark at room temperature for 30 minutes. The reaction was terminated by the addition of 50 μL stop solution and fluorescence was measured at 560/590 nm (Fluostar; BMC Labtech, Ortenberg, Germany).

2.7. Reverse Transcription Quantitative Real-Time PCR (RT-qPCR). RT-qPCR was performed in order to determine the relative expression of the early osteogenic markers ALPL, BMP2, Col1A1, RUNX2, and SPARC and the osteogenic late stage markers BGLAP and SPP1. Total RNA was isolated from osteogenic differentiated and undifferentiated control cells with RNeasy Mini Kit (Qiagen, Hilden, Germany) according to the manufacturer's recommended protocol. RNA quality was analysed using the Agilent RNA 6000 Nano Kit and the Bioanalyzer 2100 (Agilent Technologies, Santa Clara, CA). All RIN values were between 9.2 and 10.0. DNA was digested with 1 U DNase (Fermentas, St. Leon-Rot, Germany) per μg RNA. One μg RNA was reverse transcribed using RevertAid cDNA Synthesis Kit (Fermentas). RT-qPCR reactions were performed in triplicate using the Platinum SYBR Green Super Mix with ROX (Invitrogen) on AB7900HT (Applied Biosystems, Invitrogen). The reference genes glyceraldehyde 3-phosphate dehydrogenase (GAPDH), β-actin (ACTB), and hypoxanthine phosphoribosyltransferase (hprt-n) were used for normalization and in order to show their stable expression in different tissues [22]. The following primers were used for RT-qPCR: QuantiTect primer assays (Qiagen) for ALPL (ID QT00012957), BMP2 (ID QT00012544), Col1A1 (ID QT00037793), RUNX2 (ID QT00020517), SPARC (ID QT00018620), BGLAP (ID QT00232771), and SPP1 (ID QT01008798). The expression level (C_T) of the target gene was normalized to the reference genes (GAPDH, ACTB, and hprt-n) (ΔC_t) and then the ΔC_t of the test sample was normalized to the ΔC_t of the controls ($\Delta\Delta C_t$). Finally, the expression ratio was calculated with the $2^{-\Delta\Delta C_t}$ method ($^*P < 0.05$) [23].

2.8. Statistical Analysis. All values are expressed as mean ± standard deviation (SD). The exact Wilcoxon test was used to evaluate the differences between groups. The exact Friedman test (more than two time points) and the exact paired Wilcoxon test (2 time points) were applied to test for changes between time points. Two-sided P values below 0.05 were considered statistically significant. P values were not adjusted for multiple comparisons. Graphic data were prepared with SigmaPlot (Systat Software Inc., San Jose, CA).

3. Results

3.1. Expansion of Human Intraoral MSCPs. Bone explants were successfully harvested during routine oral surgery interventions in all patients ($n = 10$). Evaluation of postoperative pain and patient satisfaction revealed no difference compared

Table 1: Expression of intraoral MSPC surface proteins analysed by flow cytometry.

Cluster of differentiation (CD)	Positivity (%)
CD73 PE	99.8 ± 0.1
CD90 APC	99.9 ± 0.1
CD105 PerCP-Cy5.5	69.1 ± 9.8
CD14 FITC	0.2 ± 0.2
CD19 APC	0.6 ± 0.1
CD34 FITC	0.4 ± 0.3
CD45 APC-Cy7	23.9 ± 7.8
HLA-DR PerCP-Cy5.5	0.5 ± 0.3

Expression of intraoral MSPC surface proteins analysed by flow cytometry. Mean values of the percentage of positive cells ± SD to the total number of analysed cells are shown ($n = 10$). PE: phycoerythrin; APC: allophycocyanin; PerCP: peridium-chlorophyll protein complex; FITC: fluorescein isothiocyanate.

to the control group. Cells exhibiting morphologic characteristics of human BM-stromal cells (mononuclear, fibroblast-like, spindle-shaped, and plastic-adherent) were isolated from all samples within 4 to 8 days, independent of donor gender, age, or macroscopic bone explant structure. Confluence was reached after 13 to 15 days. To expand maxillary cells and analyse the cell doubling time, cells were trypsinised and cultivated with a reduced seeding density technique for three additional passages.The doubling time of each culture of passage three was calculated with a two time-point calculation formulas $Td = (t_2 - t_1) * \mathrm{Log}(2)/\log(q_2/q_1)(t_1, t_2 =$ time points; $q_1, q_2 =$ growing quantities. The mean doubling time of the MSPCs was 30.4 ± 2.1 hrs. The mean total number of cells after three passages was $1.2 \pm 0.2 \times 10^7$.

3.2. Characterization of Human Intraoral MSCPs by Flow Cytometry. Viable cells were gated on the forward/side scatter, and aggregates were excluded with the FSC/W and FSC/A. The positive expression of CD73, CD90, and CD105, low level of CD45, and negativity for CD14, CD19, CD34, and HLA-DR confirmed the phenotype of intraoral MSPCs (Figure 1). Intraoral MSPCs from all patients demonstrated the same immunophenotype. Flow cytometry data are shown in Figure 1 and Table 1.

3.3. Intraoral MSPC Morphology and Cellular Activity during Mechanical Stimulation. The strain profile used in the present study was based on the timing and theorized intensity profiles of common repetitive motion strains that are often the result of masticatory movements (Figure 2(a)). No morphological differences were observed between the mechanically stimulated groups and unstimulated groups. However, the uniform alignment of cells was observed for the mechanically stimulated groups. The percentage of LDH release showed no significant differences between the mechanically stimulated groups (EX(+) and OG(+)) and unstimulated groups (EX(−) and OG(−)) (Figure 2(b)).

3.4. Expression of Osteogenesis-Specific Markers Affected by Mechanical Stimulation. To determine the influence of 10% cyclin strain on osteogenesis, undifferentiated (EX) and osteogenic differentiated (OG) human intraoral MSPCs were mechanically stimulated with the Flexcell FX5K Tension System for 14 days. Relative mRNA expression levels of the runt-related transcription factor 2 (RUNX2), the early osteogenic markers type-I collagen (Col1A1), osteonectin (SPARC), bone morphogenetic protein 2 (BMP2), and alkaline phosphatase (ALPL), and the osteogenic late stage markers osteopontin (SPP1) and osteocalcin (BGLAP) were analysed by RT-qPCR after 7 and 14 days of mechanical stimulation. The undifferentiated and mechanically unstimulated group (EX(−)) served as the reference value (ratio = 1). RUNX2 mRNA levels showed a clear, but not statistically significant, increase after 14 days of mechanical stimulation. Following 7 and 14 days of cyclic strain, the expression of Col1A1 increased significantly in the mechanically stimulated OG cells at both time points. The expression of the late stage marker SPP1 increased significantly during osteoinduction in OG(+) cells. However, no significant differences between the four groups were indicated in the mRNA expression of BGLAP. The most significant increase was observed by the BMP2 expression. SPARC expression was increased in the osteogenic differentiated mechanically unstimulated group OG(−) at day 7 and in the OG(+) cells at day 14 when compared to the EX(−) controls. After both time points, a significant increase in ALDL expression was observed in the OG(−) and OG(+) cells. All values are listed in Table 2.

3.5. Mechanical Stimulation Enhanced the Expression of Osteogenesis-Specific Markers. To investigate the influence of the mechanical stimulation on both undifferentiated and osteogenic differentiated intraoral MSPCs, RT-qPCR values were subjected to a further evaluation. Mechanically stimulated cells were compared to the respective unstimulated control cells. Whereas the undifferentiated (EX) intraoral MSPCs showed no change in the osteogenesis-specific marker expression, mechanical stimulation increased the expression of Col1A1, SPP1, BGLAP, BMP2, and SPARC significantly in the osteogenic differentiated (OG) cells. Specifically, whereas no significant differences between cyclic strain and static condition could be observed by RUNX2 (Figure 3(a)), Col1A1 mRNA levels increased to 1.79 ± 0.73 ($P = 0.029$) after 7 days and to 2.09 ± 0.71 ($P = 0.026$) after 14 days of mechanical stimulation (Figure 3(b)). SPP1 increased significantly in the mechanically stimulated OG cells to 2.88 ± 0.34 ($P = 0.0002$) at day 7 and 5.25 ± 1.37 ($P = 0.033$) at day 14 (Figure 3(c)). BGLAP expression considerably to 1.72 ± 0.52 ($P = 0.037$) in OG(+) cells exposed to 14 days of mechanical strain (Figure 3(d)). The most significant increase was observed in the BMP2 expression after 7 days (5.66 ± 3.98; $P = 0.021$) and 14 days (6.60 ± 4.82; $P = 0.048$) of mechanical stimulation (Figure 3(e)). SPARC expression increased significantly to 1.77 ± 0.46 ($P = 0.020$) in OG(+) cells exposed to 14 days of mechanical strain (Figure 3(f))

In addition, ARS staining of calcium deposits and absorbance measurements of ARS-stained intraoral MSPCs

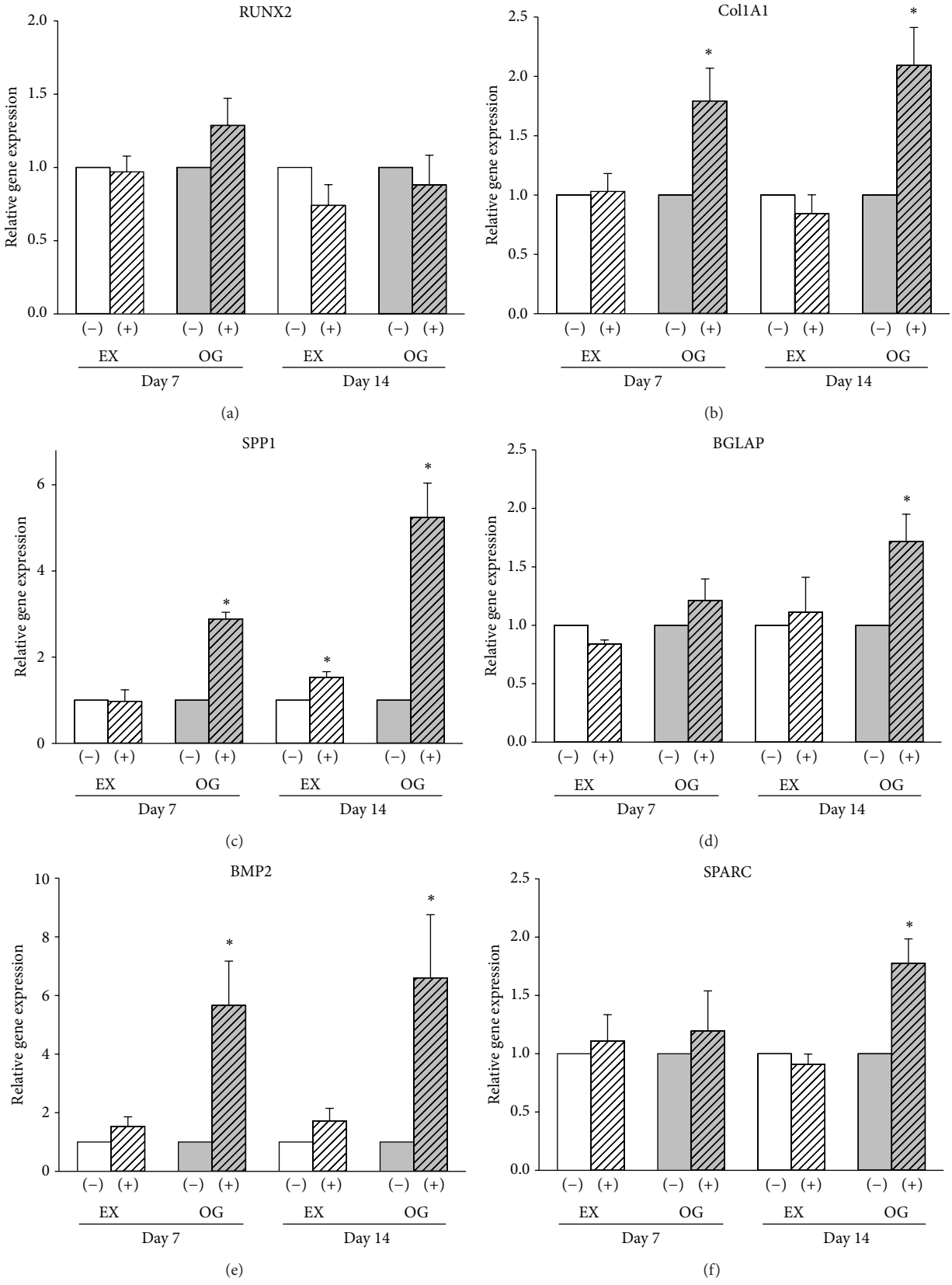

Figure 3: Regulation of osteogenesis-specific markers under the influence of mechanical stimulation. mRNA levels of (a) RUNX2, (b) Col1A1, (c) SPP1, (d) BGLAP, (e) BMP2, and (f) SPARC were normalized to their respective mechanically unstimulated control groups. EX(−) represents the undifferentiated mechanically unstimulated group, EX(+) the undifferentiated mechanically stimulated group, OG(−) the osteogenic differentiated mechanically unstimulated group, and OG(+) the osteogenic differentiated mechanically stimulated group. The values are mean ± SD of independent experiments performed in triplicate ($n = 7$); $^{*}P < 0.05$.

Table 2: Expression of the osteogenesis-specific markers affected by mechanical stimulation for 7 and 14 days.

	Day 7				Day 14			
	EX(−)	EX(+)	OG(−)	OG(+)	EX(−)	EX(+)	OG(−)	OG(+)
RUNX2	1	1.01 ± 0.3	0.98 ± 0.3	1.40 ± 0.5	1	0.75 ± 0.3	2.48 ± 0.6	3.13 ± 1.1
Col1A1	1	1.16 ± 0.3	1.70 ± 0.8	2.92 ± 1.1 *P = 0.0039*	1	0.68 ± 0.4	0.94 ± 0.4	2.02 ± 0.9 *P = 0.049*
SPP1	1	0.95 ± 0.3	1.11 ± 0.4	1.91 ± 0.5 *P = 0.040*	1	1.44 ± 0.7	1.48 ± 0.2	2.92 ± 0.8 *P = 0.038*
BGLAP	1	0.85 ± 0.1	0.78 ± 0.4	0.84 ± 0.5	1	0.67 ± 0.2	0.91 ± 0.5	1.08 ± 0.2
BMP2	1	1.53 ± 0.8	2.17 ± 1.3	5.54 ± 3.2 *P = 0.036*	1	2.06 ± 1.0	3.84 ± 1.8	6.48 ± 3.5 *P = 0.013*
SPARC	1	0.93 ± 0.2	1.47 ± 0.4 *P = 0.035*	1.60 ± 0.9	1	0.88 ± 0.3	0.95 ± 0.4	2.13 ± 0.8 *P = 0.044*
ALPL	1	0.86 ± 0.4	5.35 ± 1.9 *P = 0.042*	4.05 ± 1.8 *P = 0.046*	1	0.78 ± 0.5	3.55 ± 1.6 *P = 0.023*	3.62 ± 1.8 *P = 0.042*

mRNA levels of RUNX2, Col1A1, SPP1, and BGLAP. BMP2 and ALPL were normalized to the undifferentiated mechanically unstimulated control group EX(−) of each day (ratio = 1). EX(+) represents the undifferentiated mechanically stimulated group, OG(−) the osteogenic differentiated mechanically unstimulated group, and OG(+) the osteogenic differentiated mechanically stimulated group. The values are mean ± SD of independent experiments performed in triplicate ($n = 7$); $^{*}P < 0.05$.

Table 3: Quantitation of ARS staining of calcium deposits and ALP enzyme.

	EX(−)	EX(+)	OG(−)	OG(+)
ARS day 7	0.12 ± 0.01	0.11 ± 0.01	0.16 ± 0.02	0.20 ± 0.05
EX versus OG			*P = 2.15E − 05*	*P = 0.002*
(−) versus (+)				*P = 0.037*
ARS day 14	0.24 ± 0.06	0.20 ± 0.02	0.31 ± 0.06	0.92 ± 0.19
EX versus OG			*P = 0.007*	*P = 6.56E − 10*
(−) versus (+)				*P = 2.02E − 9*
ALP day 14	0.09 ± 0.01	0.09 ± 0.01	0.12 ± 0.02	0.18 ± 0.04
EX versus OG				*P = 0.0004*
(−) versus (+)				*P = 0.005*

The ARS staining of calcium deposits and measurements of an OD of 570 nm after cetylpyridinium chloride elution were performed at days 7 and 14. Quantitation of calcium deposits revealed a highly significant increase of an OD of 570 nm values in osteogenic differentiated cells (OG) compared to the corresponding undifferentiated controls (EX). Mechanical stimulation revealed a significant increase in calcium deposits in the OG(−) cells compared to the OG(+) cells. Quantitation of ALP enzyme at day 14 revealed a significant increase in osteogenic differentiated cells (OG) compared to the corresponding undifferentiated controls (EX). The values are mean ± SD of independent experiments performed in triplicate ($n = 12$); $^{*}P < 0.05$.

eluted with cetylpyridinium chloride at an optical density (OD) of 570 nm were performed at days 7 and 14. Representative pictures of unstained (EX(−) and EX(+)) and osteogenic differentiated (OG(−) and OG(+)) MSPCs are shown in Figure 4(a). Values measured at an OD of 570 nm increased significantly over time in osteogenic lineage cells when compared to undifferentiated controls. Corresponding to the RT-qPCR data, mechanical stimulation revealed a significant increase of quantifiable calcium deposits in the OG(−) cells compared to the OG(+) cells (Figures 4(b) and 4(c)). ALP activity was measured over the absorbance of p-nitrophenol phosphate, a chromogenic product with absorbance at 405 nm, in supernatant after 14 days. Again, cyclic strain enhanced the activity of ALP in the OG(+) cells compared to the OG(−) cells ($P = 0.0052$) (Figure 4(d)). All values are listed in Table 3.

4. Discussion

To date, most experimental and clinical tissue engineering trials in craniofacial surgery have used BM-derived stromal cells from the iliac crest [24, 25]. In a previous work we demonstrated that cells isolated from mandibular and maxillary bone, periosteum from the oblique line, and dental pulp exhibit the characteristics of cells described as MSPCs [7]. For the first time, the role of mechanical stimulation in osteogenic differentiated intraoral MSPCs is the subject of investigation. Consequently, explant cultures of human MSPCs have been established from human intraoral tissue samples of posterior maxilla and mandibular retromolar bone and characterized as MSPCs according to the criteria of the International Society for Cellular Therapy [26] using flow cytometry analysis. The low number of CD45-positive cells

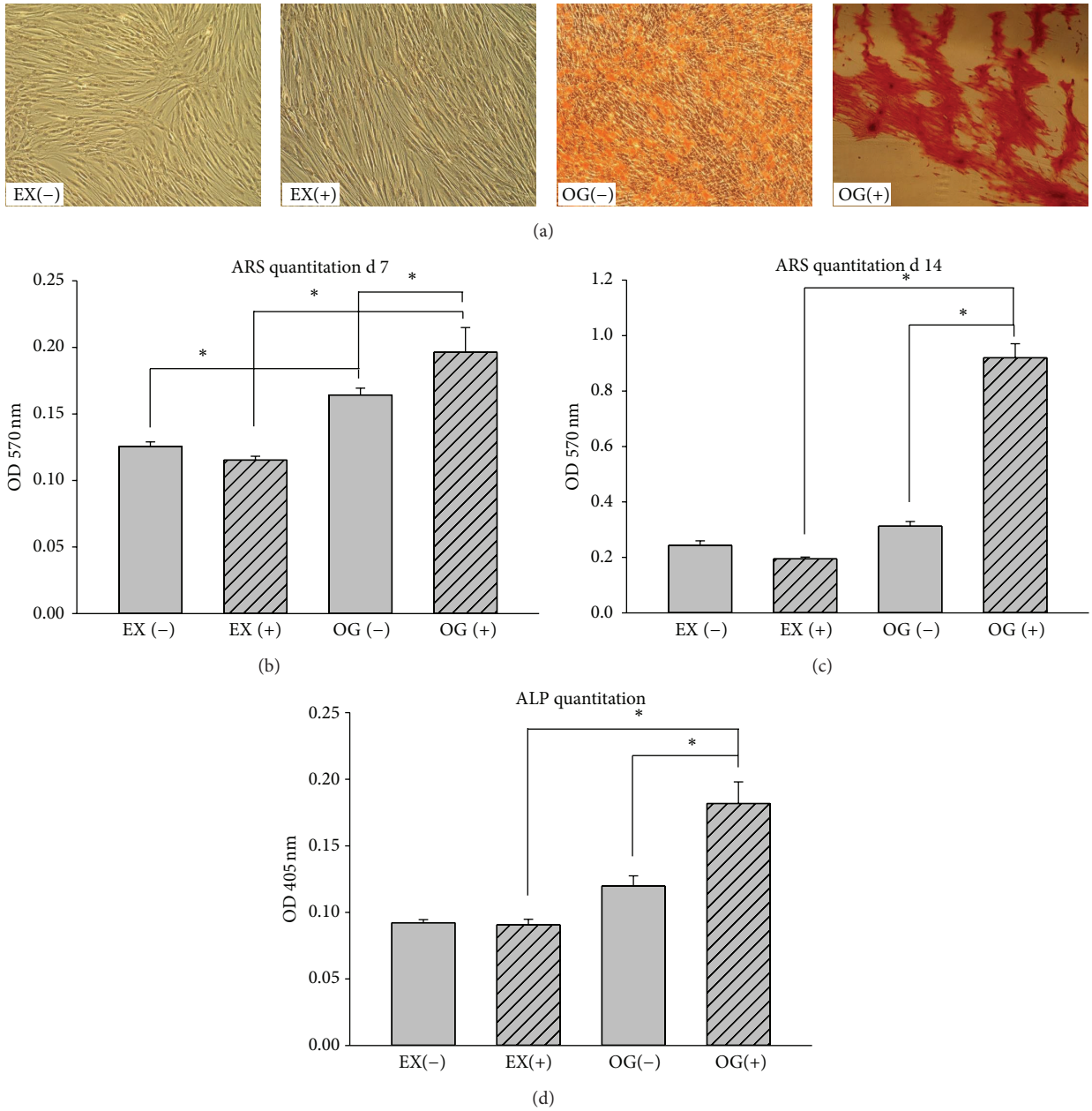

Figure 4: Influence of mechanical stimulation on alkaline phosphatase (ALP) expression and demonstration of mineralized matrix using ARS staining of human intraoral MSPCs. (a) Representative pictures of unstained (EX(−) and EX(+)) and osteogenic differentiated (OG(−) and OG(+)) MSPCs. Quantitation of calcium deposited into the cultures revealed a significant increase in the 570 nm OD in osteogenic differentiated and mechanically stimulated MSPCs after (b) 7 days and (c) 14 days, when compared to undifferentiated controls. (d) Quantitation of ALP enzymes revealed a significant increase compared to corresponding controls. EX(−) represents the undifferentiated mechanically unstimulated group, EX(+) the undifferentiated mechanically stimulated group, OG(−) the osteogenic differentiated mechanically unstimulated group, and OG(+) the osteogenic differentiated mechanically stimulated group. The values are mean ± SD of independent experiments performed in triplicate ($n = 9$); $^{*}P < 0.05$.

indicates that the bone-derived cultures contain immature mesenchymal cells. The small number of CD45-positive cells was reported in the surface profile of adult MSPCs [27]. Yu et al. demonstrated these small CD45-positive subpopulations in adipose tissue-derived MSPCs as well [28].

In vitro, bone cells demonstrate a high responsiveness to mechanical stimuli. Much debate exists regarding the critical components of the load profile and whether different components, such as fluid shear, tension, or compression, influence cells differently. The most widely used mechanical stimuli

in vitro are cyclic stretch and fluid shear flow [29]. We seeded the intraoral MSPCs onto collagen type-I-coated BioFlex plates and stimulated them mechanically using a continuous uniaxial sinusoidal waveform with 10% elongation and a frequency of 0.5 Hz.

LDH release and the expression of osteogenesis-specific markers were analysed after 7 and 14 days. The effect of mechanical loading on the proliferation of osteoblastic cells is controversial. Some studies have shown that an appropriate amount of mechanical force can induce the growth of BM-MSPCs [30], while others have found the opposite [31]. In our experiments, the relative levels of LDH in the 0% and 10% strained groups showed no significant changes. These findings suggest that 10% cyclic strain did not change the survival rate of intraoral MSPCs or induce serious cellular damage.

Similar to the results on rat BM-MSPCs reported by Zhao et al. [32], our RT-qPCR data showed significantly increased mRNA expression levels of type-I collagen (Col1A1), osteonectin (SPARC), bone morphogenetic protein 2 (BMP2), alkaline phosphatase (ALPL), osteopontin (SPP1), and osteocalcin (BGLAP) in the mechanically stimulated groups. The runt-related transcription factor 2 (RUNX2) is considered to be the central control gene within the osteoblast phenotype. Xiao et al. have shown that levels of RUNX2 during *in vitro* differentiation of primary human osteoblasts showed no major changes, whereas levels of downstream genes such as bone sialoprotein and alkaline phosphatase were dramatically increased [32, 33]. Furthermore, real-time PCR and western blot analyses indicated that there was no significant increase in the amount of RUNX2 protein or mRNA during human osteoblast differentiation [34].

However, although the expression level of RUNX2 showed no significant differences in human intraoral MSPCs, our RT-qPCR data showed significantly increased mRNA expression levels of the RUNX2 downstream genes Col1A1, ALPL, SPP1, and BGLAP in the mechanically stimulated groups. The most prominent difference we observed between unstimulated and mechanically stimulated, osteogenic differentiated MSCPs was in the expression of BMP2. This result is similar to the findings of Sumanasinghe et al., who demonstrated that BMP2 mRNA is significantly increased in strained groups [16]. The late stage markers SPP1 and BGLAP play an important role in the differentiation of osteoblast progenitor cells, with significant upregulation observed in both matrix synthesis and mineralisation. Our results are in accordance with other studies, which demonstrated an upregulation of these genes with steady increases as osteoblastic differentiation progresses [34, 35]. Both ALP activity and the production of mineralized matrix were significantly upregulated by mechanical stimulation in our human intraoral MSPCs. The production of mineralised matrix is considered a marker for terminally differentiated MSPCs into osteoblast-like cells [36]. Therefore, mineral formation is an appropriate indicator underpinning the fact that mechanical stimulation accelerates the osteogenic differentiation of MSPCs. The protein levels have also been shown to be upregulated in response to the application of mechanical force [34].

5. Conclusion

Our results revealed that 10% cyclic strain induced a significant increase in the mRNA expression of the osteogenesis-specific markers in osteogenic differentiated intraoral MSPCs. The increasing evidence for mechanical stimulation as a regulator of osteogenic differentiation in MSPCs holds important consequences for the development of craniofacial surgery and orthopaedic tissue engineering solutions. Further, molecular mechanisms underlying cellular responses to mechanical stimulation are not well understood. Thus, further investigation is necessary to better understand the molecular mechanism underlying the effects of mechanical stimulation on the osteogenic differentiation of human intraoral MSPCs.

Conflict of Interests

The authors declare that there is no conflict of interests regarding the publication of this paper.

Acknowledgments

The authors would like to thank Jennifer Ober for excellent technical assistance with flow cytometric analysis and Dr. Katharina Schallmoser, Department of Blood Group Serology and Transfusion Medicine, Medical University of Graz, for providing the pHPL. Financial support by the Medical University of Graz is gratefully acknowledged.

References

[1] R. Quarto, M. Mastrogiacomo, R. Cancedda et al., "Repair of large bone defects with the use of autologous bone marrow stromal cells," *The New England Journal of Medicine*, vol. 344, no. 5, pp. 385–386, 2001.

[2] E. Kon, G. Filardo, A. Roffi et al., "Bone regeneration with mesenchymal stem cells," *Clinical Cases in Mineral and Bone Metabolism*, vol. 9, no. 1, pp. 24–27, 2012.

[3] P. J. Marie, "Cell and gene therapy for bone repair," *Osteoporosis International*, vol. 22, no. 6, pp. 2023–2026, 2011.

[4] C. Clausen, N. U. Hermund, O. Donatsky, and H. Nielsen, "Characterization of human bone cells derived from the maxillary alveolar ridge," *Clinical Oral Implants Research*, vol. 17, no. 5, pp. 533–540, 2006.

[5] E. M. Horwitz, D. J. Prockop, L. A. Fitzpatrick et al., "Transplantability and therapeutic effects of bone marrow-derived mesenchymal cells in children with osteogenesis imperfecta," *Nature Medicine*, vol. 5, no. 3, pp. 309–313, 1999.

[6] E. M. Horwitz, P. L. Gordon, W. K. K. Koo et al., "Isolated allogeneic bone marrow-derived mesenchymal cells engraft and stimulate growth in children with osteogenesis imperfecta: implications for cell therapy of bone," *Proceedings of the National Academy of Sciences of the United States of America*, vol. 99, no. 13, pp. 8932–8937, 2002.

[7] B. Lohberger, M. Payer, B. Rinner et al., "Tri-lineage potential of intraoral tissue-derived mesenchymal stromal cells," *Journal of Cranio-Maxillofacial Surgery*, vol. 41, no. 2, pp. 110–118, 2013.

[8] P. J. Boyne and R. A. James, "Grafting of the maxillary sinus floor with autogenous marrow and bone," *Journal of Oral Surgery*, vol. 38, no. 8, pp. 613–616, 1980.

[9] N. Jakse, F.-J. Seibert, M. Lorenzoni, A. Eskici, and C. Pertl, "A modified technique of harvesting tibial cancellous bone and its use for sinus grafting," *Clinical Oral Implants Research*, vol. 12, no. 5, pp. 488–494, 2001.

[10] C. Y. Lee, "Immediate load protocol for anterior maxilla with cortical bone from mandibular ramus," *Implant Dentistry*, vol. 15, no. 2, pp. 153–159, 2006.

[11] U. Meyer, H. P. Wiesmann, B. Kruse-Lösler, J. Handschel, U. Stratmann, and U. Joos, "Strain-related bone remodeling in distraction osteogenesis of the mandible," *Plastic and Reconstructive Surgery*, vol. 103, no. 3, pp. 800–807, 1999.

[12] E. G. Loboa, T. D. Fang, S. M. Warren et al., "Mechanobiology of mandibular distraction osteogenesis: experimental analyses with a rat model," *Bone*, vol. 34, no. 2, pp. 336–343, 2004.

[13] N. A. Waanders, M. Richards, H. Steen, J. L. Kuhn, S. A. Goldstein, and J. A. Goulet, "Evaluation of the mechanical environment during distraction osteogenesis," *Clinical Orthopaedics and Related Research*, no. 349, pp. 225–234, 1998.

[14] E. A. Smith-Adaline, S. K. Volkman, M. A. Ignelzi Jr., J. Slade, S. Platte, and S. A. Goldstein, "Mechanical environment alters tissue formation patterns during fracture repair," *Journal of Orthopaedic Research*, vol. 22, no. 5, pp. 1079–1085, 2004.

[15] G. Friedl, H. Schmidt, I. Rehak, G. Kostner, K. Schauenstein, and R. Windhager, "Undifferentiated human mesenchymal stem cells (hMSCs) are highly sensitive to mechanical strain: transcriptionally controlled early osteo-chondrogenic response in vitro," *Osteoarthritis and Cartilage*, vol. 15, no. 11, pp. 1293–1300, 2007.

[16] R. D. Sumanasinghe, S. H. Bernacki, and E. G. Loboa, "Osteogenic differentiation of human mesenchymal stem cells in collagen matrices: effect of uniaxial cyclic tensile strain on bone morphogenetic protein (BMP-2) mRNA expression," *Tissue Engineering*, vol. 12, no. 12, pp. 3459–3465, 2006.

[17] A. Peters, D. Toben, J. Lienau et al., "Locally applied osteogenic predifferentiated progenitor cells are more effective than undifferentiated mesenchymal stem cells in the treatment of delayed bone healing," *Tissue Engineering A*, vol. 15, no. 10, pp. 2947–2954, 2009.

[18] K. Schallmoser, C. Bartmann, E. Rohde et al., "Human platelet lysate can replace fetal bovine serum for clinical-scale expansion of functional mesenchymal stromal cells," *Transfusion*, vol. 47, no. 8, pp. 1436–1446, 2007.

[19] C. Bartmann, E. Rohde, K. Schallmoser et al., "Two steps to functional mesenchymal stromal cells for clinical application," *Transfusion*, vol. 47, no. 8, pp. 1426–1435, 2007.

[20] A. Sabokbar, P. J. Millett, B. Myer, and N. Rushton, "A rapid, quantitative assay for measuring alkaline phosphatase activity in osteoblastic cells in vitro," *Bone and Mineral*, vol. 27, no. 1, pp. 57–67, 1994.

[21] C. A. Gregory, W. G. Gunn, A. Peister, and D. J. Prockop, "An Alizarin red-based assay of mineralization by adherent cells in culture: comparison with cetylpyridinium chloride extraction," *Analytical Biochemistry*, vol. 329, no. 1, pp. 77–84, 2004.

[22] S. A. Bustin, V. Benes, J. A. Garson et al., "The MIQE guidelines: minimum information for publication of quantitative real-time PCR experiments," *Clinical Chemistry*, vol. 55, no. 4, pp. 611–622, 2009.

[23] J. Vandesompele, K. de Preter, F. Pattyn et al., "Accurate normalization of real-time quantitative RT-PCR data by geometric averaging of multiple internal control genes," *Genome Biology*, vol. 3, no. 7, 2002.

[24] M. F. Pittenger, A. M. Mackay, S. C. Beck et al., "Multilineage potential of adult human mesenchymal stem cells," *Science*, vol. 284, no. 5411, pp. 143–147, 1999.

[25] E. Kon, A. Muraglia, A. Corsi et al., "Autologous bone marrow stromal cells loaded onto porous hydroxyapatite ceramic accelerate bone repair in critical-size defects of sheep long bones," *Journal of Biomedical Materials Research*, vol. 49, no. 3, pp. 328–337, 2000.

[26] M. Dominici, K. Le Blanc, I. Mueller et al., "Minimal criteria for defining multipotent mesenchymal stromal cells. The International Society for Cellular Therapy position statement," *Cytotherapy*, vol. 8, no. 4, pp. 315–317, 2006.

[27] R. Mafi, S. Hindocha, P. Mafi, M. Griffin, and W. S. Khan, "Sources of adult mesenchymal stem cells applicable for musculoskeletal applications–a systematic review of the literature," *Open Orthopaedics Journal*, vol. 2, pp. 242–248, 2011.

[28] G. Yu, X. Wu, M. A. Dietrich et al., "Yield and characterization of subcutaneous human adipose-derived stem cells by flow cytometric and adipogenic mRNA analyzes," *Cytotherapy*, vol. 12, no. 4, pp. 538–546, 2010.

[29] M. Mullender, A. J. El Haj, Y. Yang, M. A. van Duin, E. H. Burger, and J. Klein-Nulend, "Mechanotransduction of bone cells in vitro: mechanobiology of bone tissue," *Medical and Biological Engineering and Computing*, vol. 42, no. 1, pp. 14–21, 2004.

[30] M. Jagodzinski, A. Breitbart, M. Wehmeier et al., "Influence of perfusion and cyclic compression on proliferation and differentiation of bone marrow stromal cells in 3-dimensional culture," *Journal of Biomechanics*, vol. 41, no. 9, pp. 1885–1891, 2008.

[31] G. Song, Y. Ju, X. Shen, Q. Luo, Y. Shi, and J. Qin, "Mechanical stretch promotes proliferation of rat bone marrow mesenchymal stem cells," *Colloids and Surfaces B: Biointerfaces*, vol. 58, no. 2, pp. 271–277, 2007.

[32] H. Zhao, H. Zhou, X. Wang, J. Dong, Y. Yang, and X. Zhang, "Effect of mechanical strain on differentiation of mesenchymal stem cells into osteoblasts," *Journal of Biomedical Engineering*, vol. 26, no. 3, pp. 518–522, 2009.

[33] G. Xiao, D. Wang, M. D. Benson, G. Karsenty, and R. T. Franceschi, "Role of the α2-integrin in osteoblast-specific gene expression and activation of the Osf2 transcription factor," *The Journal of Biological Chemistry*, vol. 273, no. 49, pp. 32988–32994, 1998.

[34] C. Shui, T. C. Spelsberg, B. L. Riggs, and S. Khosla, "Changes in Runx2/Cbfa1 expression and activity during osteoblastic differentiation of human bone marrow stromal cells," *Journal of Bone and Mineral Research*, vol. 18, no. 2, pp. 213–221, 2003.

[35] M. Jagodzinski, M. Drescher, J. Zeichen et al., "Effects of cyclic longitudinal mechanical strain and dexamethasone on osteogenic differentiation of human bone marrow stromal cells," *European Cells and Materials*, vol. 7, pp. 35–41, 2004.

[36] G. N. Bancroft, V. I. Sikavitsas, J. van den Dolder et al., "Fluid flow increases mineralized matrix deposition in 3D perfusion culture of marrow stromal osteoblasts in a dose-dependent manner," *Proceedings of the National Academy of Sciences of the United States of America*, vol. 99, no. 20, pp. 12600–12605, 2002.

Hindawi Publishing Corporation
BioMed Research International
Volume 2014, Article ID 814057, 12 pages
http://dx.doi.org/10.1155/2014/814057

Review Article

Deregulation of Bone Forming Cells in Bone Diseases and Anabolic Effects of Strontium-Containing Agents and Biomaterials

Shuang Tan,[1] Binbin Zhang,[2] Xiaomei Zhu,[3] Ping Ao,[3] Huajie Guo,[2] Weihong Yi,[4] and Guang-Qian Zhou[1,2]

[1] *Key State Laboratory for Biotherapy, Sichuan University, Chengdu 610065, China*
[2] *Anti-Ageing and Regenerative Medicine Centre, Shenzhen University, 3688 Nanhai Avenue, Shenzhen, Guangdong 518060, China*
[3] *Institute for Systems Biomedicine, Shanghai Jiaotong University, Shanghai 200240, China*
[4] *Department of Spinal Surgery, Nanshan People's Hospital, Shenzhen 518000, China*

Correspondence should be addressed to Weihong Yi; szyiwh@163.com and Guang-Qian Zhou; gqzhou@szu.edu.cn

Received 15 November 2013; Revised 20 February 2014; Accepted 3 March 2014; Published 31 March 2014

Academic Editor: Michael Gelinsky

Age-related bone loss and osteoporosis are associated with bone remodeling changes that are featured with decreased trabecular and periosteal bone formation relative to bone resorption. Current anticatabolic therapies focusing on the inhibition of bone resorption may not be sufficient in the prevention or reversal of age-related bone deterioration and there is a big need in promoting osteoblastogenesis and bone formation. Enhanced understanding of the network formed by key signaling pathways and molecules regulating bone forming cells in health and diseases has therefore become highly significant. The successful development of agonist/antagonist of the PTH and Wnt signaling pathways are profits of the understanding of these key pathways. As the core component of an approved antiosteoporosis agent, strontium takes its effect on osteoblasts at multilevel through multiple pathways, representing a good example in revealing and exploring anabolic mechanisms. The recognition of strontium effects on bone has led to its expected application in a variety of biomaterial scaffolds used in tissue engineering strategies aiming at bone repairing and regeneration. While summarizing the recent progress in these respects, this review also proposes the new approaches such as systems biology in order to reveal new insights in the pathology of osteoporosis as well as possible discovery of new therapies.

1. Introduction

Bone remodeling is a physiological process that maintains the integrity of the skeleton by removing old bone and replacing it with young matrix. An imbalance between bone resorption and bone formation with ageing will result in the increased rate of bone turnover rate and bone loss. The age-related progressive bone loss is exaggerated in patients with osteoporosis, a disease characterized by decreased bone mass, increased bone fragility, and increased risk of fractures [1]. As the elder population in the society rapidly increases, osteoporosis has become one of the most common public health problems.

In the case of the age-related bone loss or osteoporosis, the osteoblast-mediated bone formation is severely impaired [1, 2] due to decreased number and activity of individual osteoblastic cells. Such dysfunctions of osteoblasts may be caused by extrinsic mechanisms, such as changes in levels of systemic hormones and growth factors of bone tissues, and intrinsic mechanisms such as cellular apoptosis and senescence [2–4]. As a consequence, both trabecular and periosteal bone formation decline [5]. Most of the currently available therapies for osteoporosis, including aminobisphosphonates, estrogens and selective estrogen receptor modulators (SERMS), and inhibitors for the receptor activator of nuclear factor κB ligand (RANKL), take effect mainly by reducing bone resorption. However, these therapies frequently exhibit secondary effects due to the coupling phenomenon of bone formation by osteoblasts and bone resorption by osteoclasts [6]. Therefore, anabolic drugs are

hoped to target osteoblastic cells to increase bone formation and bone strength [7], though anticatabolics may be efficient in stabilizing bone mass.

In this paper, accordingly, we focus on the functional regulation of osteoblast lineage cells in health and osteoporosis, the currently proposed anabolic agents such as teriparatide (PTH(1–34)), sclerostin or DKK1 inhibitors, and strontium that target specific signaling mechanisms underlying the osteoblast function and osteoporosis. The wide use of strontium in various orthopaedic scaffolds is also summarized. Through the analysis of current knowledge, some insights into further studies of osteoblast regulation and therapeutic exploration are provided.

2. Osteoprogenitors, Osteoblasts, and Osteocytes

Bone formation is dependent on the recruitment of sufficient number of osteoblasts and activity of individual osteoblasts. Osteoblastic cells are recruited to bone forming surfaces mainly from a group of skeletal stem cells with osteogenic differentiation potential. Bone marrow contains a small population of mesenchymal stem cells (MSCs) that are capable of giving rise to bone, cartilage, fat, or fibrous connective tissue [8]. Cell populations with properties characteristic of bone marrow MSC have been isolated from many other tissues such as adult peripheral blood, dental pulp, adipose tissue, fetal cord blood, and liver. These self-renewing multipotent stem cells can give rise to osteoprogenitor cells in various tissues under the right environmental conditions. Osteoprogenitor cells in turn give rise to and maintain the osteoblasts that synthesize new bone matrix on bone forming surfaces, the osteocytes within bone matrix that support bone structure, and the protective lining cells that cover the surface of quiescent bone. Therefore, osteoblastic lineage cells comprise a diverse population of cells, including immature, differentiating, and mature matrix-producing osteoblasts. Different osteoblasts may express different sets of genes, which may represent the heterogeneity of trabecular microarchitecture at different anatomic sites, the site-specific differences in the response to different signals and disease states, and regional variation in the ability to response to antiosteoporotic agents [9].

Particularly, flattened bone-lining cells are thought to be quiescent osteoblasts that form the endosteum on trabecular and endosteal surfaces and underlie the periosteum on the mineralized surface. More primitive osteoblasts that are found near functioning osteoblasts in the bone remodeling unit can be identified based on their expression of alkaline phosphatase. Active and mature osteoblasts synthesizing bone matrix have large nuclei, enlarged Golgi structures, and extensive endoplasmic reticulum. These osteoblasts secrete type I collagen and other matrix proteins vectorially toward the bone formation surface. Besides, osteoblasts have several other important roles in bone remodeling, including production of osteoclastogenic factors and bone mineralization [10]. Preosteoblasts encompass all cells transitioning from progenitors to mature osteoblasts and therefore are, by definition, hetero geneous. However, they are usually considered to express the transcription factor Runx2, at a more advanced stage of differentiation, both Runx2 and osterix (OSX), which both control the osteodifferentiation [11]. The differentiation stage of osteoblasts influences their functional roles in bone remodeling. Mice deficient in osteoblasts are deficient in osteoclasts [11]. In contrast, conditional depletion of mature osteoblasts *in vivo* only ablates bone formation and osteoclastic bone resorption persists [12]. Therefore, immature osteoblasts also influence osteoclastogenesis whereas mature osteoblasts perform the matrix production and mineralization functions.

During bone formation, a subset of osteoblasts undergoes terminal differentiation and becomes engulfed by unmineralized osteoid [13]. Following mineralization of the bone matrix, these entombed cells are called osteocytes. Osteocytes are cocooned in fluid-filled cavities (lacunae) within the mineralized bone and are highly abundant, accounting for 90–95% of all bone cells [13]. Osteocytes have long dendrite-like processes extending throughout canaliculi (tunnels) within the mineralized matrix. These dendrite-like processes form a network and interact with other osteocytes and with osteoblasts on the bone surface [14]. The primary function of the interaction between the osteocyte-osteoblast/lining cell syncytium is mechanosensation [15]. Osteocytes transduce stress signals from bending or stretching of bone into biologic activity and respond to mechanical load. The network is thought to be integral in the detection of mechanical strain and associated bone microscopic cracks/fractures within the mineralized bone that accumulates as a result of normal skeletal loading and fatigue [16]. Signaling molecules involved in mechanotransduction include prostaglandin E2, cyclooxygenase 2, various kinases, Runx2, and nitrous oxide. Therefore, osteocytes initiate and direct the subsequent remodeling process and support bone structure and metabolism.

Osteocytes express osteocalcin, galectin 3, CD44, and several other bone matrix proteins that support intercellular adhesion and regulate exchange of mineral in the bone fluid within lacunae and the canalicular network. Osteocytes regulate phosphate metabolism and matrix mineralization through the secretion of phosphate-regulating factors such as FGF23, Phex, Dmp1, and expression of sclerostin (encoded by gene SOST) and DKK1 that negatively regulates Wnt and BMPs signaling [17]. Osteocytes are linked metabolically and electrically through gap junctions composed primarily of connexin 43, which are required for osteocyte maturation, function, and survival [18].

3. The Molecular Regulation of Osteoblast Differentiation and Function

Differentiation of mesenchymal stem cells into the osteoblast lineage is under tight regulation orchestrated through multiple signaling pathways. Among the well-characterized are the fibroblast growth factor (FGF), transforming growth factor

β (TGFβ), hedgehog families, Wnt signaling, and notch pathways [19].

3.1. The FGF Signaling. The FGF pathway consists of 23 ligands that transduce their signal through one of the four FGF receptors (FGFRs), functioning in initiating condensation of the mesenchyme and proliferation of progenitor cells. Upon binding to cell surface receptors, FGFs lead to activation of multiple signaling modules, including mitogen-activated protein kinase (MAPK), phosphoinositide 3-kinase (PI3K), STAT1, and PKC. Temporal expression and activity of FGFR are critical for membranous bone formation and regulate the proliferation, differentiation, and apoptosis of osteoblasts [20]. FGFRs contribute to normal skeletal development, as gene mutation or deletions are associated with severe dwarfism [21]. FGF18 plays a critical role in maturation of osteoblast and FGF2 increases RUNX2 phosphorylation and functional activity [22]. Similarly, the activation of FGFR2 signaling results in increased Runx2 expression and enhanced osteoblast differentiation [22]. FGFR1 signaling at an early developmental stage promotes osteoblast differentiation without affecting Runx2 expression. Finally, FGFR3 is involved in regulation of osteoblast number and osteoid mineralization. Therefore, FGF signaling has diverse roles in the regulation of preosteoblast proliferation and osteoblast differentiation through different receptors.

3.2. BMPs. Bone morphogenetic proteins (BMP) are members of the TGFβ superfamily. This group of proteins has a number of diverse functions in multiple developmental processes ranged from embryogenesis, organogenesis, bone formation, cell proliferation, and stem cell differentiation [23–28]. BMPs signal through homomeric or heteromeric type I and type II receptors, which are expressed in all cell types. Specific BMP receptors influence specific lineage direction. BMP2 signaling is required for the stimulation of mesenchymal progenitor cells by inducing expression of both Runx2 and Osterix, leading to osteoblast differentiation [29–31]. Induction of Runx2 and Osterix by BMP2 and subsequent upregulation of osteoblast-specific genes involves Dlx5, Smad transducers, and the MAPK pathway. TGFβ itself plays more complex role during bone remodeling, with the inhibition of Runx2 and osteoblast differentiation *in vitro* but mainly promoting bone formation *in vivo* [29, 32].

3.3. The Wnt Signaling. During skeletal development, the Wnt signaling is implicated in multiple steps and processes, including proximal-distal outgrowth and limb patterning, and in MSC lineage commitment for chondrogenesis, osteogenesis, myogenesis, and adipogenesis [33–36]. Consequently, the Wnt signaling affects all aspects of skeletal development. The importance of Wnt signaling in bone diseases has been recognized since the rare human mutations affecting bone negatively (osteoporosis-pseudoglioma syndrome) or positively (high-bone mass phenotype) were all identified to reside in components of the canonical Wnt signaling machinery a decade ago. Mouse genetic studies have further confirmed the role of the pathway in the regulation of bone homeostasis, with activation of the pathway leading to increased, and inhibition to decreased, bone mass and strength [37] and the Wnt signaling is now known as a key mechanism regulating bone metabolism [38]. Activation of the Wnt signaling results in a generalized increase in bone mass throughout the skeleton. Wnt ligands activate numerous intracellular pathways upon targeting on various membrane receptors, which are either dependent or independent on β-catenin, an intracellular transducer. β-catenin is expressed in mesenchymal precursor cells and its inactivation promotes their differentiation into chondrocytes instead of osteoblast [34]. During the β-catenin-dependent Wnt signaling, β-catenin is stabilized following binding to its receptors Frizzled (FZD) and lipoprotein receptor-related protein 5 (LRP5) or LRP6, which in turn lead to the transcription of target genes such as Runx2. On the basis of extensive studies conducted thus far on Wnt signaling in bone, the pathway has now become the target for therapeutic intervention to restore bone strength in millions of patients at risk for fracture [37].

3.4. Hedgehog. The hedgehog signaling through Indian hedgehog (Ihh), a secreted molecule of the hedgehog family, is required for osteoblast differentiation through endochondral bone formation[39]. Ihh binds to the receptor patched homologue 1 (PTCH1) through the transmembrane protein smoothened (SMO), consequently regulating target gene transcription. Ihh controls osteoblast differentiation firstly by inducing Runx2 in mesenchymal cells. Secondly, Ihh enhances Runx2 action through an interaction between signal transducer Gli2 and Runx2 in osteoblast [40]. Ihh is also needed for osteoblast proliferation and survival and mice deficient Ihh gene lack osteoblast progenitor cells [39].

3.5. The Notch Signaling. The notch signaling mediates broad cell-cell communications. Once their ligands are binding to the neighbouring cell surface, notch receptors are cleaved by the γ-secretase complex. Consequently, the intracellular domain of notch is released from the plasma membrane and translocates to the nucleus, interacting with RBPJκ/CBF1 to activate downstream target transcription factors. By physically associating with Runx2 and interfering with functional activity of Runx2, notch inhibits osteoblast differentiation. Mutations in the notch signaling cause skeletal patterning defects in human and notch deficiency leads to severe osteoporosis in mice [41]. Interestingly, through its expression in osteoblasts, notch exerts dimorphic effect during bone remodeling; notch also inhibits osteoclast differentiation through controlling production of "decoy" receptor OPG by osteoblast [41]. Thus far, the role of the notch signaling in bone diseases remains to be further elucidated.

3.6. Hormones. Besides local growth factors, a number of systemic hormones regulate bone mass by regulating osteoblast differentiation and influencing bone formation. Many of them act on osteoblasts to express M-CSF and RANKL that in turn regulate osteoclast differentiation. We herein only discuss some as examples, particularly those understood well thus far.

Parathyroid hormone (PTH) produced by the chief cells of parathyroid gland plays a primary role in calcium homeostasis through its action on bone and kidney and through enhanced synthesis of another hypercalcemic hormone, 1,25(OH)2 vitamin D3 [42]. The anabolic effects of PTH on bone formation are mediated through PTH receptor-dependent mechanisms. PTH enhances osteoblastic cell proliferation and function, extends mature osteoblast life span through antiapoptotic effects, enhances the Wnt signaling through inhibition of Wnt antagonist sclerostin, and promotes the local production of bone anabolic growth factors such as insulin-like growth factor 1 (IGF1) [43]. In addition, PTH promotes bone formation partially through phosphorylation and activation of Runx2, resulting in expression of osteoblast genes [44]. PTH also inhibits proteasome mediated degradation of Runx2 and increases expression of osterix to enhance osteoprogenitor lineage determination [45]. As the only approved anabolic agent, intermittent PTH therapy has been demonstrated to have beneficial effects on increasing bone mass and diminishing bone fragility associated with osteoporosis resulting from aging, sex hormone deficiency, and glucocorticoids use [46]. The other major hypercalcemic hormone is 1,25(OH)2 vitamin D3, a steroid hormone that favors intestinal absorption of calcium [47]. Deletion or inactivation of the vitamin D receptor (VDR) in mice and in humans leads to rickets, a phenotype completely reversible in both organisms by treatment with calcium. Vitamin D3 positively regulates the expression of osteoblastic phenotype markers. However, continuous exposure to parathyroid hormone (PTH), parathyroid hormone-related protein (PTHrP), and low doses of 1,25-dihydroxyvitamin D3 also stimulates osteoblasts to express M-CSF and RANKL, leading to increased osteoclast production and bone resorption [48, 49].

An important nonsteroidal regulator of bone mass is leptin, a hormone that functions through an inhibitory action of the hypothalamus on bone formation [50, 51]. Leptin is made by fat cells and functions to suppress appetite and inhibit bone formation by binding to receptors in the hypothalamus. Mice and humans deficient in leptin or its hypothalamic receptor are obese and have a higher than normal bone mass. The effector pathway from hypothalamus to bone is the sympathetic nervous system and sympathetic neurons produce noradrenaline, which binds to β2-adrenergic receptors (β2-AR) on osteoblasts [51, 52]. Mutant mice lacking β2-AR have increased bone mass but do not respond to leptin by reduction in bone mass [53], while ovariectomized β2-AR null mice fail to lose bone mass, suggesting that maintenance of the sympathetic nervous system in bone may require estrogen, which is essential in regulating bone remodeling via two related receptors, ERα and ERβ expressed by osteoblasts.

4. Deregulation of Bone Forming Cells in Diseases

The correct balance between bone deposition and resorption is crucial for the proper maintenance of the bone mass and the loss of this coupling is the starting point for osteoporosis [54]. This is a systemic, skeletal disorder characterized by low bone mass with a high susceptibility to fractures. Osteoporosis is characterized by reduced bone mass and deterioration of bone microarchitecture, resulting in bone fragility. Primary osteoporosis is either a postmenopausal or age-related disease of elderly people, essentially occuring because the production of bone by means of osteoblasts cannot compensate for bone resorption by osteoclasts [55]. Sex hormones, including both estrogen and androgen, act on osteoblasts for their survival and, at the same time, induce osteoclast apoptosis through activation of the FASL/FAS pathway [56]. Therefore, withdrawal or decline of sex hormones is the principal determinant of primary osteoporosis. Moreover, estrogens suppress the production of proosteoclastogenic cytokines (such as IL-1, IL-6, TNF-α, and RANKL) and stimulate the secretion of OPG by osteoblasts [57, 58].

4.1. The Activation of the Inflammatory Pathways. Many chronic diseases have a local or a systemic inflammatory basis, which has overall deleterious effects on bone mass [59, 60], leading to the secondary osteoporosis with an onset at any age. The stimulatory action of the NF-κB signal transduction in osteoclast development and functional activity is widely recognized [61]; recently it has also been demonstrated that NF-κB activation is potently inhibitory to osteoblast commitment, differentiation, and mineralization *in vivo* and *in vitro* [62]. Tumor necrosis factor (TNF-α) is a potent NF-κB inducer and activation of p65 (a NF-κB subunit) by TNF-α has been shown to suppress transcription of osteocalcin in osteoblastic cells [63]. Pharmacological suppression of TNF-α is reported to reverse age-related defects in bone formation in a mouse fracture healing model and synergizes TGFβ- and BMP-2-induced Smad signaling in differentiating osteoblasts [64]. In addition, TNF-α upregulates Smurf1, an E3 ligase that promotes proteasomal degradation of bone morphogenetic signaling proteins [65]. NF-κB signaling in osteoblasts has been shown to upregulate Smad7, a general inhibitor of Smad pathway. Finally, a direct inhibitory action of NF-κB on bone formation was demonstrated *in vivo* to show time- and stage-specific inhibition of IB kinase (IKK) in differentiated osteoblasts, increased trabecular bone mass, and ameliorated ovariectomy-induced bone loss [66].

4.2. Other Signaling Alterations and Therapeutics Opportunities. Alterations in the Wnt signaling have profound impact on age-related bone loss in mice [67]. Mechanical loading upregulates the Wnt signaling in MSC [68], suggesting that the combination of reduced β-catenin signaling and decreased mechanical stimulation with age may contribute to the age-related decline in bone formation. Based on these and other studies, the important role of the Wnt signaling in the control of bone formation has been well recognized as this pathway is suggested to be a potential therapeutic target [69]. The Wnt signaling alteration is related to increased marrow adipogenesis. With the aim of increasing osteoblastogenesis and the bone formation, several pharmacological agents have been developed that act on bone marrow MSC to favor

osteoblastogenesis and decrease adipogenesis [70]. Nonpharmacological means to enhance MSC differentiation toward osteoblasts include low-magnitude mechanical signals [71].

Most drugs currently available for the treatment or prevention of osteoporosis are antiresorptive, including estrogens and selective estrogen receptor modulators, bisphosphonates, and denosumab blocking the RANKL/RANK pathway [72]. It is desirable to identify novel agents that can exhibit an anabolic function in order to improve and restore bone mass. Teriparatide (PTH1-34) is currently the only US Food and Drug Administration- (FDA-) approved anabolic agent for the treatment of osteoporosis [37]. Although the effect of PTH can be anabolic or catabolic depending on the dose, intermittent administration increases trabecular bone formation [73, 74]. Systemic administration of antagonists to DKK1 or sclerostin may possibly affect only the skeleton, favoring the endogenous Wnt signaling and increasing bone formation without affecting the Wnt signaling in other organs.

Currently, only strontium ranelate proves to have roles in both the osteoclast inhibition and bone formation promotion. Therefore, further research in the topic may provide insights not only into improving the effects of Sr-containing agents but also into discovering novel and more effective therapies.

5. Anabolic Effects of Strontium-Containing Agents on Osteoblasts

Several strontium-containing agents, such as Sr fructose, 1,6-diphosphate, and strontium citrate [75], have been experimentally demonstrated to have antiosteoporotic effects, among which strontium ranelate is an approved drug [76–78].

At the cellular level, it was shown that bone marrow MSC culture, when exposed to strontium (Sr), displayed a significant increase in the expression of the master gene and Runx2, as well as bone sialoprotein (BSP), and this was associated with a significant increase in the formation of colony-forming unit osteoblasts (CFU-obs). Interestingly, the activation of gene expression by Sr varies with the differentiation stage of MSC: Runx2 and BSP in bone marrow MSC; Runx2 and osteocalcin in preosteoblasts; BSP and osteocalcin in mature osteoblasts. Strontium ranelate-treated ovariectomised (OVX) animals exhibited increased bone formation and decreased bone resorption, leading to prevention of trabecular bone loss and improvement of bone microarchitecture and strength [79–81]. Clinical data also revealed that strontium ranelate treatment increased bone mineral apposition rate and improved trabecular microarchitecture in postmenopausal osteoporotic women [82], which was associated further with reduced fracture risk [76, 78].

In vitro experiments showed that Sr ranelate had positive effects on osteoblastogenesis and activity of primary rat and human osteoblasts [83]. On the one hand, strontium enhanced the replication of preosteoblastic cells [84, 85] and reduced osteoblast apoptosis [86, 87]. On the other hand, strontium was found to activate many osteoblast differentiation markers, such as alkaline phosphatase, type-1 collagen, bone sialoprotein and osteocalcin in murine bone marrow MSC, osteoprogenitor cells, and immature osteoblasts [80, 87, 88]. Furthermore, the agent also promoted the ultimate differentiation of human osteoblasts into osteocytes, as indicated by the increased expression of osteocyte-restrictive markers such as dentin matrix protein 1 [85]. Overall, the available *in vitro* data indicate that strontium promotes the osteogenic differentiation program and reduces osteoblast apoptosis, thereby promoting osteoblastogenesis. The positive effects on preosteoblast eventually result in increased bone nodule formation, a hallmark of *in vitro* osteogenesis [80, 85, 88].

Age-related bone loss is generally associated with osteoblast insufficiency relative to the adipogenesis, which is responsible for the progressive adiposity often observed in osteoporosis. The number of mature osteoblasts and adipocytes in bone marrow is influenced by the differentiation of the common mesenchymal progenitor cell towards one phenotype and away from the other. In contrast to the promoting role in osteoblast, strontium exhibits inhibitory role in adipogenesis of MSC [89]. In murine MSC cultures, strontium increased Runx2 expression and matrix mineralization and decreased peroxisome proliferator-activated receptor gamma 2 (PPARc2) expression and adipogenesis. This effect was associated with enhanced expression of the Wnt noncanonical representative Wnt5a and adipogenic modulator Maf and was abrogated by Wnt- and nuclear factor of activated T-cells (NFATc) antagonists, indicating a critical role for the Wnt and NFATc/Maf signaling in the switch in adipogenesis to osteoblastogenesis induced by strontium [89].

6. Molecular Basis of the Role of Strontium in Bone Forming Cells

6.1. Calcium Sensing Receptor (CaSR). The CaSR belongs to subfamily 3 of G-protein coupled receptor family (GPCR) [90, 91] and can activate Gαi and Gαq/11 G-proteins, consequently resulting in decreased intracellular cyclic adenosine monophosphate (cAMP) level, the stimulation of phospholipase Cβ,inositol1,4,5-triphosphate, and the release of intracellular Ca^{2+} [90]. The CaSR is physiologically expressed at high level in the parathyroid chief cells and senses changes in extracellular Ca^{2+} level, leading to an adjustment in the release of the PTH [90]. Similarly, CaSR can sense other divalent and trivalent cations, including Sr^{2+} because of its similar atomic and ionic properties to Ca^{2+}.

Experimental evidences show that strontium acts on osteoblasts through the CaSR, leading to the activation of MAPK signaling and consequently cell replication. In addition, strontium increases OPG and decreases RANKL expression in osteoblastic cells via the CaSR [92]. However, CaSR does not appear to be the only receptor involved in the effects of strontium on osteoblasts as increased cell replication and decreased apoptosis were still observed in osteoblasts from mice deficient for CaSR when exposed to strontium, indicating that other cation-sensing receptors

are functioning to sense extracellular Sr [93]. Among these receptors are GPRC6A, a GPCR that is closely related to the CaSR and senses extracellular divalent cations [94]. The functional involvement of this and other cation-sensing receptors in the response to strontium remains to be further determined.

6.2. Fibroblast Growth Factor Receptor (FGFR). As mentioned above, strontium also stimulates osteoblast cell growth through the CaSR-independent molecular mechanism. In this regard, a selective inhibitor of FGFR was able to slow down cell growth induced by strontium ranelate in osteoblastic cells, suggesting that the activation of FGFR is a new potential mechanism by which strontium can stimulate osteoblastic cell growth. Activation of FGFR-dependent cell growth is also observed in response to other cations, suggesting that activation of FGFRs may be a new cation-sensing mechanism in osteoblasts [95].

6.3. Ras/MAPK Pathway and Ras/Akt Pathway. Our own recent work demonstrated that rat sarcoma viral oncogene homolog (RAS), an upstream regulator of MAPK and Akt, was activated by strontium treatment and siRNA-mediated Ras knockdown inhibited strontium-stimulated expression of osteogenic markers [96]. Mitogen-activated protein kinase (MAPK) can directly enhance osteogenesis through the phosphorylation and subsequent activation of Runx2 [97]. These studies suggest that strontium can promote osteogenic differentiation of MSCs through activating the Ras/MAPK signaling pathway and the downstream transcription factor Runx2 [96]. Akt kinase plays certain roles in cellular processes, including glucose metabolism and cell proliferation and apoptosis. Studies on mice have demonstrated that strontium increased the proliferation and reduced the apoptosis of osteoblast with activation of the Akt kinase-related pathway [98].

6.4. Prostaglandins (PGE2). It has been confirmed that the effect of strontium on the proliferation and reduced apoptosis of osteoblasts could be neutralized by the selective inhibition of cyclooxygenase-2 (COX-2). The results also indicated that the positive effects of Sr ranelate on osteoblasts depend on the PGE2 production. Strontium induces murine MSCs to express COX-2 that leads to the increased PGE2 production, thus contributing to the increased differentiation of MSC into osteoblasts [99]. This may therefore be a new pathway that is activated by strontium in bone cells.

6.5. The Role of the OPG/RANKL System. The primary mechanism by which strontium reduces osteoclast number is to regulate the production of osteoprotegerin (OPG) by osteoblasts and the receptor activator of nuclear factor κ-B ligand (RANKL) [100], the two molecules that play essential roles in osteoclast differentiation. Osteoblast progenitors and osteoblasts express RANKL, a molecule that binds to the receptor activator of nuclear factor κ-B (RANK) on osteoclast precursors and thereby activates intracellular signaling, resulting in osteoclast differentiation. Osteoblasts can produce OPG, which functions as a decoy receptor for the RANKL and can thereby reduce the production of osteoclasts by inhibiting the differentiation of osteoclast precursors. A positive effect of Sr ranelate was observed on the OPG/RANKL ratio, causing an increased secretion of OPG and a simultaneous reduction of RANKL expression, leading to the suppression of osteoclastogenesis [101]. The increase in the number of OPG-producing cells and the decrease in RANKL expression thus constitute the important mechanism by which strontium exhibits a dissociating effect on the coupling between bone formation and resorption.

6.6. The NFATc Pathway. The involvement of the calcineurin (Cn)/nuclear factor of activated Tc (NFATc) pathway in bone development and bone remodeling was found in patients who were taking Cn inhibitors such as cyclosporine (CsA) and FK506, developed osteopenia, and had a higher incidence of fractures [102]. It is known now that NFATc1 plays an important role in both osteoblasts and osteoclasts [103]. NFAT includes five transcription factors, NFATc1 to NFATc4 and NFAT5, which are all involved in the differentiation of various cell types. Highly phosphorylated NFATc transcription factors are normally localized in the cytoplasm. Increased intracellular calcium levels activate calcineurin (Cn) and dephosphorylate NFATc1, leading to its nuclear translocation to regulate target genes [104]. NFATc1 is expressed in the process of osteoblast differentiation and bone formation [105] and has been shown to be an important signaling pathway involved in the role of strontium. Increasing strontium concentrations in the osteoblast environment activate Cn and subsequently the NFATc/Wnt signaling pathways in osteoblasts, leading to the increased replication and suppressed adipogenesis [89].

6.7. The Role of Wnt Signaling. It is reported that strontium promoted the translocation of β-catenin into the nucleus through the activation of the CaSR and subsequent activation of Akt-signaling in human osteoblasts [98]. In addition, strontium decreased the expression of sclerostin, an inhibitor of the canonical Wnt signaling that acts as a negative regulator of bone formation [98], providing another mechanism by which strontium modulates the Wnt signaling. Further evidences on the involvement of strontium in the Wnt pathway include that the treatment of murine osteoblasts with strontium increased the expression of Wnt3a and Wnt5a and β-catenin transcriptional activity. Inhibitors of the Wnt signaling, DKK1, and sFRP1, a soluble protein with homology to the Wnt-binding site of Frizzled proteins, decreased the Sr-induced expression of osteoblastic genes such as Runx2, ALP, and type 1 collagen [93]. The inhibition of the Wnt5a receptor Ryk and the signaling transducer RhoA were able to partially abrogate Sr-induced cell proliferation and osteoblastic gene expression [93]. Another study showed that Wnt5a was expressed at higher levels in the bone marrow of Sr-treated senescent SAMP6 mice compared to vehicle-treated mice and that it played a role in the differentiation of MSC upon Sr-treatment [89]. Therefore, strontium definitely produces positive effects in bone via the Wnt signaling.

6.8. Insulin-Like Growth Factor. A recent study showed that an increase of the insulin-like growth factor (IGF-1) concentration was observed after six-month administration of Sr ranelate at a daily dose of 2.0 g [106]. This result suggests that IGF deficit plays a definite role in the development of postmenopausal osteoporosis and strontium administration may exert an advantageous influence on BMD increase.

In summary, multiple mechanisms are involved in strontium effects on bone forming cells. Once exposed to strontium, multiple intracellular signaling pathways and key molecules are activated and orchestrated to promote their survival, proliferation, and differentiation of osteoblasts, which in the meantime produce a series of inflammatory and osteoclast-regulatory factors that may eventually favor bone formation via coupling of both bone resorption and bone formation.

7. Strontium-Integrated or Substituted Biomaterials for Bone Regeneration

Tissue engineering is extensively applied in both research and clinical practice of skeletal disease and trauma. For tissue engineering, bioactive materials, with the properties of stimulating osteoblasts and calcimimetics in physiochemical behaviors, are preferential as an implant to facilitate healing or to compensate for bone defects, particularly for osteoporotic fractures where the conventional metallic implant is not applicable because of bone fragility and extremely low bone density. The key of a bioactive material is to form a continuous and highly reactive interface with the surrounding bone tissue to induce abundant bone formation and the ability to be structurally and mechanically compatible with bone tissue and eventually to be replaced by new bones. In some circumstances, it is also demanded that growth factors, drug, and ions are incorporated into such a material, which can in turn be slowly released as the material is biodegraded *in vivo*. As the role in stimulating osteoblast proliferation and differentiation becomes well recognized, strontium is widely applied in many bone regeneration biomaterials in various forms, which are briefly presented as below.

7.1. Strontium Integration into Bone-Supporting or Regenerating Biomaterials. In a study by Zhang et al. [107], strontium-containing mesoporous bioactive glass (Sr-MBG) scaffolds with controlled architecture and enhanced mechanical strength were fabricated using a three-dimensional (3-D) printing technique. The Sr-MBG scaffolds could combine the advantages of Sr-MBG such as good bone forming bioactivity, controlled ion release, and enhanced mechanical strength and thus has potential application in bone regeneration. polycaprolactone (PCL) is a resorbable polymer extensively used in bone tissue engineering owing to good structural properties and processability. Several studies reported that strontium-substituted bioactive glass (SrBG) was incorporated into PCL and fabricated into 3D bioactive composite scaffolds that exhibited better ability to promote osteogenesis than the bioactive glass without strontium [108, 109]. Strontium- (Sr-) substituted hydroxyapatite (HAP) scaffolds in the forms of nanopowders or microspheres were also reported to possess osteoconductive and osteoinductive properties and have the potential to repair bone defects caused by osteoporotic fractures [110].

The most important property of bone cement as inorganic filler in load bearing orthopaedic implants is good integration with host bone with reduced bone resorption and increased bone regeneration at the implant interface. Similar to integration into bioglass, strontium has been introduced into bone cement and the mechanical properties, crystallinic properties, and Sr ion release activities have been well evaluated. Sr-containing bone cement has been shown to promote early bone formation by prolonging the release duration of strontium while remaining the strength [111].

Biomimetic apatites could also be cosubstituted with Sr as well as other elements. In a study by Iafisco et al. [112], hydroxyapatites were cosubstituted with foreign ions such as Mg^{2+}, $CO_3{}^{2-}$, and Sr^{2+} for starting materials for the development of nanostructured biodevices for regeneration of osteoporotic bone. Biological-like amounts of Mg and CO_3 ions were inserted in the apatite structure to mimic the composition of bone apatite by the addition of Sr ions as antiosteoporotic agent. Based on the hypothesis that the combination of Si and Sr may have synergetic effects on osteoporotic bone regeneration, the porous Sr-substituted calcium silicate (SrCS) ceramic scaffolds combining the functions of Sr and Si elements were developed with the goals to promote osteoporotic bone defect repair [113]. Boron is known to play important roles in bone growth and maintenance, immune function, and psychomotor skills. Pan et al. reported that the incorporation of strontium significantly decreased the cytotoxicity that arises with the rapid dissolution of borate glass [114]. In addition, with the degradation of glass, it will not only render boron as a nutritional element, but also deliver strontium for new bone formation.

7.2. Strontium Substitution in Implant Coating Materials. Implants undergoing early instability or even subsidence correlate with an increased risk of aseptic loosening, subsequently requiring revision. A load-bearing orthopaedic implant therefore needs to possess the properties of well integration with host bone tissue and early fixation by osseointegration of the implant is indeed demanded during surgical practices. This is an even greater challenge during revision replacement surgery using the allograft implant because resorption of the allograft may exceed new bone formation and result in the instability of the prosthesis. Implantation of metal-based joint replacements often results in corrosion and particle release, initiating chronic inflammation leading onto osteoporosis of host bone. A compensative solution is the coating of metal implants with hydroxyapatite (HA) or the use of bulk bioglass. For this purpose, strontium could be incorporated into the material surface or applied in doping surface of an implant. Sabareeswaran et al. therefore tested the *in vivo* biocompatibility and bone healing of the strontium- (Sr-) stabilized bulk glass ceramics for short term implantation of up to 12 weeks in rabbit model and observed excellent healing, which is comparable to that seen during the

use of a commercially available implant of HA-based bioglass alone [115]. A strontium-substituted nanohydroxyapatite (Sr-HA) coating, deposited onto porous implant surfaces, has the potential to enhance implant osseointegration [116]. In a cementless, experimental gap model in canine, Vestemark et al. compared a 5% strontium-doped HA bone graft extender with a nondoped HA extender and demonstrated that the extender with strontium doping could protect the allograft from fast resorption and increase gap healing, leading to the improved fixation of the implant, though the results of mechanical test were inconclusive, suggesting that strontium could contribute to reversing the imbalance of fast resorption of allograft and slower formation of new bone because of its anabolic and anticatabolic effects. In addition, it has been reported that a film of strontianite was formed on a bioactive surface of sodium titanate when exposed to a strontium acetate solution. This strontianite film enables the local release of strontium ions from implant surfaces and thus stimulates bone formation *in vivo* [117].

7.3. Strontium in Membrane Materials and Hydrogels. Membrane materials are particularly useful in guided bone regeneration. In this regard, the effects of a strontium hydroxyapatite- (SrHA-) containing membrane have exhibited higher elasticity and strength than the collagen membrane [110]. Meanwhile, slow strontium ion release was also confirmed to stimulate new bone formation.

Strontium has also been introduced into different hydrogels to be used in bone repair. A study reported that a bone tissue engineering approach in which arginine-glycine-aspartic acid- (RGD-)modified alginate hydrogels are crosslinked with bioactive strontium, zinc, and calcium [118]. It was further shown that strontium gels made with a high percentage of guluronic acid residues (high G) were degraded more slowly than those made with alginate rich in mannuronic acid (high M) and supported proliferation of osteoblast-like cells. After an initial burst, strontium release from alginate gels was steady and sustained, and the magnitude of release from high M gels was biologically relevant [118].

An amidated carboxymethylcellulose hydrogel enriched with Sr ions was evaluated for its effects of strontium released in the culture medium on osteodifferentiation. It has been shown that strontium released from the gel promotes the osteodifferentiation as shown by the increase of ALP activity, suggesting that the Sr-containing gel could represent a new strategy in bone tissue engineering.

8. Conclusion and Future Perspectives

Osteoporosis has become a serious and common public health problem. Aging is associated with impaired bone formation as a principal pathogenetic mechanism mediating bone fragility in osteoporosis. At the cellular level, physiology for individual osteoblast survival/growth, apoptosis, migration, and stress response are regulated through elaborated molecular feedback mechanisms. Although further analysis of such mechanisms is still mandatory in order to develop new therapeutics, it is certain that multiple pathways or molecules play important roles from different respects, some of which are emerging as therapeutic targets. Apart from currently proposed or trialed approaches to focusing on agonists/antagonists of certain osteoblastic signaling pathways, such as hPTH1-34 (teriparatide) and antisclerostin or anti-DKK1 antibodies, other strategies aiming at mobilizing skeletal stem cells and activating osteoblastic cell functions are anticipated to be a field worth of much exploring. Strontium, though currently thought as a relatively mild anabolic agent, is considered as a candidate in this respect due to its dual role in regulating osteoblastogenesis/osteoclastogenesis and osteogenesis/adipogenesis via its involvement in multiple pathways. Besides being able to be supplied systemically, the application of strontium is being much extended into various biomaterials and thereby tissue engineering strategies for the local bone lesions and defects.

Further, on the mounting evidences and rapid progress in revealing key molecular factors and signaling pathways regulating bone forming cells and osteoporotic conditions, a systems biology approach to coherently relating these factors with mathematical modeling would be particularly helpful to better understand and evaluate therapeutics. Future progress in this field will hopefully provide opportunities for exploring drug discovery.

Conflict of Interests

The authors declare that there is no conflict of interests regarding the publication of this paper.

Authors' Contribution

Shuang Tan and Binbin Zhang contribute equally to this work.

Acknowledgments

The study was supported by Natural Science Foundation of China (NSFC81130034, 81171746). The content is solely the responsibility of the authors.

References

[1] S. Khosla and B. L. Riggs, "Pathophysiology of age-related bone loss and osteoporosis," *Endocrinology and Metabolism Clinics of North America*, vol. 34, no. 4, pp. 1015–1030, 2005.

[2] S. C. Manolagas and A. M. Parfitt, "What old means to bone," *Trends in Endocrinology and Metabolism*, vol. 21, no. 6, pp. 369–374, 2010.

[3] M. Kassem and P. J. Marie, "Senescence-associated intrinsic mechanisms of osteoblast dysfunctions," *Aging Cell*, vol. 10, no. 2, pp. 191–197, 2011.

[4] P. J. Marie and M. Kassem, "Extrinsic mechanisms involved in age-related defective bone formation," *Journal of Clinical Endocrinology and Metabolism*, vol. 96, no. 3, pp. 600–609, 2011.

[5] E. Seeman, "Pathogenesis of bone fragility in women and men," *The Lancet*, vol. 359, no. 9320, pp. 1841–1850, 2002.

[6] B. L. Riggs and A. M. Parfitt, "Drugs used to treat osteoporosis: the critical need for a uniform nomenclature based on their

action on bone remodeling," *Journal of Bone and Mineral Research*, vol. 20, no. 2, pp. 177–184, 2005.

[7] S. Khosla, J. J. Westendorf, and M. J. Oursler, "Building bone to reverse osteoporosis and repair fractures," *Journal of Clinical Investigation*, vol. 118, no. 2, pp. 421–428, 2008.

[8] M. F. Pittenger, A. M. Mackay, S. C. Beck et al., "Multilineage potential of adult human mesenchymal stem cells," *Science*, vol. 284, no. 5411, pp. 143–147, 1999.

[9] L. J. Raggatt and N. C. Partridge, "Cellular and molecular mechanisms of bone remodeling," *Journal of Biological Chemistry*, vol. 285, no. 33, pp. 25103–25108, 2010.

[10] G. Karsenty, "Transcriptional control of skeletogenesis," *Annual Review of Genomics and Human Genetics*, vol. 9, pp. 183–196, 2008.

[11] T. Komori, H. Yagi, S. Nomura et al., "Targeted disruption of Cbfa1 results in a complete lack of bone formation owing to maturational arrest of osteoblasts," *Cell*, vol. 89, no. 5, pp. 755–764, 1997.

[12] D. A. Corral, M. Amling, M. Priemel et al., "Dissociation between bone resorption and bone formation in osteopenic transgenic mice," *Proceedings of the National Academy of Sciences of the United States of America*, vol. 95, no. 23, pp. 13835–13840, 1998.

[13] L. F. Bonewald, "Osteocytes as dynamic multifunctional cells," *Annals of the New York Academy of Sciences*, vol. 1116, pp. 281–290, 2007.

[14] H. Kamioka, T. Honjo, and T. Takano-Yamamoto, "A three-dimensional distribution of osteocyte processes revealed by the combination of confocal laser scanning microscopy and differential interference contrast microscopy," *Bone*, vol. 28, no. 2, pp. 145–149, 2001.

[15] C. T. Rubin and L. E. Lanyon, "Osteoregulatory nature of mechanical stimuli: function as a determinant for adaptive remodeling in bone," *Journal of Orthopaedic Research*, vol. 5, no. 2, pp. 300–310, 1987.

[16] O. Verborgt, N. A. Tatton, R. J. Majeska, and M. B. Schaffler, "Spatial distribution of Bax and Bcl-2 in osteocytes after bone fatigue: complementary roles in bone remodeling regulation?" *Journal of Bone and Mineral Research*, vol. 17, no. 5, pp. 907–914, 2002.

[17] A. Martin, S. Liu, V. David et al., "Bone proteins PHEX and DMP1 regulate fibroblastic growth factor Fgf23 expression in osteocytes through a common pathway involving FGF receptor (FGFR) signaling," *FASEB Journal*, vol. 25, no. 8, pp. 2551–2562, 2011.

[18] L. I. Plotkin, S. C. Manolagas, and T. Bellido, "Transduction of cell survival signals by connexin-43 hemichannels," *Journal of Biological Chemistry*, vol. 277, no. 10, pp. 8648–8657, 2002.

[19] A. Javed, H. Chen, and F. Y. Ghori, "Genetic and transcriptional control of bone formation," *Oral and Maxillofacial Surgery Clinics of North America*, vol. 22, no. 3, pp. 283–293, 2010.

[20] D. M. Ornitz and P. J. Marie, "FGF signaling pathways in endochondral and intramembranous bone development and human genetic disease," *Genes and Development*, vol. 16, no. 12, pp. 1446–1465, 2002.

[21] Z. Liu, J. Xu, J. S. Colvin, and D. M. Ornitz, "Coordination of chondrogenesis and osteogenesis by fibroblast growth factor 18," *Genes and Development*, vol. 16, no. 7, pp. 859–869, 2002.

[22] H.-J. Kim, J.-H. Kim, S.-C. Bae, J.-Y. Choi, H.-J. Kim, and H.-M. Ryoo, "The protein kinase C pathway plays a central role in the fibroblast growth factor-stimulated expression and transactivation activity of Runx2," *Journal of Biological Chemistry*, vol. 278, no. 1, pp. 319–326, 2003.

[23] X. Chen, M. J. Rubock, and M. Whitman, "A transcriptional partner for MAD proteins in TGF-β signalling," *Nature*, vol. 383, pp. 691–696, 1996.

[24] L. Attisano and J. L. Wrana, "Signal transduction by the TGF-β superfamily," *Science*, vol. 296, no. 5573, pp. 1646–1647, 2002.

[25] B. L. M. Hogan, "Bone morphogenetic proteins: multifunctional regulators of vertebrate development," *Genes and Development*, vol. 10, no. 13, pp. 1580–1594, 1996.

[26] Y. Shi and J. Massagué, "Mechanisms of TGF-β signaling from cell membrane to the nucleus," *Cell*, vol. 113, no. 6, pp. 685–700, 2003.

[27] A. C. Varga and J. L. Wrana, "The disparate role of BMP in stem cell biology," *Oncogene*, vol. 24, no. 37, pp. 5713–5721, 2005.

[28] J. Zhang and L. Li, "BMP signaling and stem cell regulation," *Developmental Biology*, vol. 284, no. 1, pp. 1–11, 2005.

[29] J. B. Lian, A. Javed, S. K. Zaidi et al., "Regulatory controls for osteoblast growth and differentiation: role of Runx/Cbfa/AML factors," *Critical Reviews in Eukaryotic Gene Expression*, vol. 14, no. 1-2, pp. 1–41, 2004.

[30] A. Javed, J.-S. Bae, F. Afza et al., "Structural coupling of Smad and Runx2 for execution of the BMP2 osteogenic signal," *Journal of Biological Chemistry*, vol. 283, no. 13, pp. 8412–8422, 2008.

[31] A. B. Celil and P. G. Campbell, "BMP-2 and insulin-like growth factor-I mediate osterix (Osx) expression in human mesenchymal stem cells via the MAPK and protein kinase D signaling pathways," *Journal of Biological Chemistry*, vol. 280, no. 36, pp. 31353–31359, 2005.

[32] X. Wu, W. Shi, and X. Cao, "Multiplicity of BMP signaling in skeletal development," *Annals of the New York Academy of Sciences*, vol. 1116, pp. 29–49, 2007.

[33] J. A. Kennell and O. A. MacDougald, "Wnt signaling inhibits adipogenesis through β-catenin-dependent and -independent mechanisms," *Journal of Biological Chemistry*, vol. 280, no. 25, pp. 24004–24010, 2005.

[34] T. F. Day, X. Guo, L. Garrett-Beal, and Y. Yang, "Wnt/β-catenin signaling in mesenchymal progenitors controls osteoblast and chondrocyte differentiation during vertebrate skeletogenesis," *Developmental Cell*, vol. 8, no. 5, pp. 739–750, 2005.

[35] T. P. Hill, D. Später, M. M. Taketo, W. Birchmeier, and C. Hartmann, "Canonical Wnt/β-catenin signaling prevents osteoblasts from differentiating into chondrocytes," *Developmental Cell*, vol. 8, no. 5, pp. 727–738, 2005.

[36] H. Hu, M. J. Hilton, X. Tu, K. Yu, D. M. Ornitz, and F. Long, "Sequential roles of Hedgehog and Wnt signaling in osteoblast development," *Development*, vol. 132, no. 1, pp. 49–60, 2005.

[37] R. Baron and M. Kneissel, "WNT signaling in bone homeostasis and disease: from human mutations to treatments," *Nature Medicine*, vol. 19, no. 2, pp. 179–192, 2013.

[38] I. Takada, A. P. Kouzmenko, and S. Kato, "Wnt and PPARgamma signaling in osteoblastogenesis and adipogenesis," *Nature Reviews. Rheumatology*, vol. 5, no. 8, pp. 442–447, 2009.

[39] Y. Maeda, E. Nakamura, M.-T. Nguyen et al., "Indian Hedgehog produced by postnatal chondrocytes is essential for maintaining a growth plate and trabecular bone," *Proceedings of the National Academy of Sciences of the United States of America*, vol. 104, no. 15, pp. 6382–6387, 2007.

[40] A. Shimoyama, M. Wada, F. Ikeda et al., "Ihh/Gli2 signaling promotes osteoblast differentiation by regulating Runx2 expression and function," *Molecular Biology of the Cell*, vol. 18, no. 7, pp. 2411–2418, 2007.

[41] M. J. Hilton, X. Tu, X. Wu et al., "Notch signaling maintains bone marrow mesenchymal progenitors by suppressing osteoblast differentiation," *Nature Medicine*, vol. 14, no. 3, pp. 306–314, 2008.

[42] M. Chorev and M. Rosenblatt, *Parathyroid Hormone: Structure-Function Relations and Analog Design*, Academic Press, San Diego, Calif, USA, 1996.

[43] G. Lombardi, C. di Somma, L. Vuolo, E. Guerra, E. Scarano, and A. Colao, "Role of IGF-I on PTH effects on bone," *Journal of Endocrinological Investigation*, vol. 33, no. 7, pp. 22–26, 2010.

[44] V. Krishnan, T. L. Moore, Y. L. Ma et al., "Parathyroid hormone bone anabolic action requires cbfa1/runx2-dependent signaling," *Molecular Endocrinology*, vol. 17, no. 3, pp. 423–435, 2003.

[45] T. Bellido, A. A. Ali, L. I. Plotkin et al., "Proteasomal degradation of Runx2 shortens parathyroid hormone-induced anti-apoptotic signaling in osteoblasts: a putative explanation for why intermittent administration is needed for bone anabolism," *Journal of Biological Chemistry*, vol. 278, no. 50, pp. 50259–50272, 2003.

[46] P. Esbrit and M. J. Alcaraz, "Current perspectives on Parathyroid Hormone (PTH) and PTH-Related Protein (PTHrP) as bone anabolic therapies," *Biochemical Pharmacology*, vol. 85, no. 10, pp. 1417–1423, 2013.

[47] A. S. Dusso and A. J. Brown, "Mechanism of vitamin D action and its regulation," *American Journal of Kidney Diseases*, vol. 32, no. 2, pp. S13–S24, 1998.

[48] S. L. Teitelbaum, "Bone resorption by osteoclasts," *Science*, vol. 289, no. 5484, pp. 1504–1508, 2000.

[49] R. Erben, "Vitamin D analogs and bone," *Journal of Musculoskeletal and Neuronal Interactions*, vol. 2, no. 1, pp. 59–70, 2001.

[50] P. Ducy, T. Schinke, and G. Karsenty, "The osteoblast: a sophisticated fibroblast under central surveillance," *Science*, vol. 289, no. 5484, pp. 1501–1504, 2000.

[51] S.-I. Harada and G. A. Rodan, "Control of osteoblast function and regulation of bone mass," *Nature*, vol. 423, no. 6937, pp. 349–355, 2003.

[52] C. Chenu, "Role of innervation in the control of bone remodeling," *Journal of Musculoskeletal Neuronal Interactions*, vol. 4, no. 2, pp. 132–134, 2004.

[53] F. Elefteriou, J. D. Ahn, S. Takeda et al., "Leptin regulation of bone resorption by the sympathetic nervous system and CART," *Nature*, vol. 434, no. 7032, pp. 514–520, 2005.

[54] A. del Fattore, A. Teti, and N. Rucci, "Bone cells and the mechanisms of bone remodelling," *Frontiers in Bioscience*, vol. 4, pp. 2302–2321, 2011.

[55] B. L. Riggs, S. Khosla, and L. J. Melton III, "A unitary model for involutional osteoporosis: estrogen deficiency causes both type I and type II osteoporosis in postmenopausal women and contributes to bone loss in aging men," *Journal of Bone and Mineral Research*, vol. 13, no. 5, pp. 763–773, 1998.

[56] L. Xing and B. F. Boyce, "Regulation of apoptosis in osteoclasts and osteoblastic cells," *Biochemical and Biophysical Research Communications*, vol. 328, no. 3, pp. 709–720, 2005.

[57] N. K. Shevde, A. C. Bendixen, K. M. Dienger, and J. W. Pike, "Estrogens suppress RANK ligand-induced osteoclast differentiation via a stromal cell independent mechanism involving c-Jun repression," *Proceedings of the National Academy of Sciences of the United States of America*, vol. 97, no. 14, pp. 7829–7834, 2000.

[58] L. C. Hofbauer, S. Khosla, C. R. Dunstan, D. L. Lacey, T. C. Spelsberg, and B. L. Riggs, "Estrogen stimulates gene expression and protein production of osteoprotegerin in human osteoblastic cells," *Endocrinology*, vol. 140, no. 9, pp. 4367–4370, 1999.

[59] C. Kok and P. N. Sambrook, "Secondary osteoporosis in patients with an osteoporotic fracture," *Best Practice and Research: Clinical Rheumatology*, vol. 23, no. 6, pp. 769–779, 2009.

[60] R. R. McLean, "Proinflammatory cytokines and osteoporosis," *Current Osteoporosis Reports*, vol. 7, no. 4, pp. 134–139, 2009.

[61] M. N. Weitzmann, "The role of inflammatory cytokines, the RANKL/OPG axis, and the immunoskeletal interface in physiological bone turnover and osteoporosis," *Scientifica*, vol. 2013, Article ID 125705, 29 pages, 2013.

[62] M. Yamaguchi and M. N. Weitzmann, "Vitamin K2 stimulates osteoblastogenesis and suppresses osteoclastogenesis by suppressing NF-κB activation," *International Journal of Molecular Medicine*, vol. 27, no. 1, pp. 3–14, 2011.

[63] L. C. Gilbert, J. Rubin, and M. S. Nanes, "The p55 TNF receptor mediates TNF inhibition of osteoblast differentiation independently of apoptosis," *American Journal of Physiology. Endocrinology and Metabolism*, vol. 288, no. 5, pp. E1011–E1018, 2005.

[64] E. C. Wahl, J. Aronson, L. Liu et al., "Restoration of regenerative osteoblastogenesis in aged mice: modulation of TNF," *Journal of Bone and Mineral Research*, vol. 25, no. 1, pp. 114–123, 2010.

[65] R. Guo, M. Yamashita, Q. Zhang et al., "Ubiquitin ligase Smurf1 mediates tumor necrosis factor-induced systemic bone loss by promoting proteasomal degradation of bone morphogenetic signaling proteins," *Journal of Biological Chemistry*, vol. 283, no. 34, pp. 23084–23092, 2008.

[66] J. Chang, Z. Wang, E. Tang et al., "Inhibition of osteoblastic bone formation by nuclear factor-B," *Nature Medicine*, vol. 15, no. 6, pp. 682–689, 2009.

[67] S. C. Manolagas and M. Almeida, "Gone with the Wnts: β-catenin, T-cell factor, forkhead box O, and oxidative stress in age-dependent diseases of bone, lipid, and glucose metabolism," *Molecular Endocrinology*, vol. 21, no. 11, pp. 2605–2614, 2007.

[68] J. A. Robinson, M. Chatterjee-Kishore, P. J. Yaworsky et al., "Wnt/β-catenin signaling is a normal physiological response to mechanical loading in bone," *Journal of Biological Chemistry*, vol. 281, no. 42, pp. 31720–31728, 2006.

[69] P. J. Marie and M. Kassem, "Osteoblasts in osteoporosis: past, emerging, and future anabolic targets," *European Journal of Endocrinology*, vol. 165, no. 1, pp. 1–10, 2011.

[70] J. M. Gimble, S. Zvonic, Z. E. Floyd, M. Kassem, and M. E. Nuttall, "Playing with bone and fat," *Journal of Cellular Biochemistry*, vol. 98, no. 2, pp. 251–266, 2006.

[71] E. Ozcivici, Y. K. Luu, B. Adler et al., "Mechanical signals as anabolic agents in bone," *Nature Reviews Rheumatology*, vol. 6, no. 1, pp. 50–59, 2010.

[72] R. R. Recker and L. Armas, "The effect of antiresorptives on bone quality," *Clinical Orthopaedics and Related Research*, vol. 469, no. 8, pp. 2207–2214, 2011.

[73] D. W. Dempster, F. Cosman, M. Parisien, V. Shen, and R. Lindsay, "Anabolic actions of parathyroid hormone on bone," *Endocrine Reviews*, vol. 14, no. 6, pp. 690–709, 1993.

[74] J. S. Finkelstein, A. Hayes, J. L. Hunzelman, J. J. Wyland, H. Lee, and R. M. Neer, "The effects of parathyroid hormone, alendronate, or both in men with osteoporosis," *New England Journal of Medicine*, vol. 349, no. 13, pp. 1216–1226, 2003.

[75] B. Ma, X. Li, Q. Zhang et al., "Metabonomic profiling in studying anti-osteoporosis effects of strontium fructose 1, 6-diphosphate on estrogen deficiency-induced osteoporosis in rats by GC/TOF-MS," *European Journal of Pharmacology*, vol. 718, no. 1, pp. 524–532, 2013.

[76] P. J. Meunier, C. Roux, E. Seeman et al., "The effects of strontium ranelate on the risk of vertebral fracture in women with postmenopausal osteoporosis," *New England Journal of Medicine*, vol. 350, no. 5, pp. 459–468, 2004.

[77] P. J. Marie, "Strontium as therapy for osteoporosis," *Current Opinion in Pharmacology*, vol. 5, no. 6, pp. 633–636, 2005.

[78] J. Y. Reginster, E. Seeman, M. C. de Vernejoul et al., "Strontium ranelate reduces the risk of nonvertebral fractures in postmenopausal women with osteoporosis: treatment of Peripheral Osteoporosis (TROPOS) study," *Journal of Clinical Endocrinology and Metabolism*, vol. 90, no. 5, pp. 2816–2822, 2005.

[79] S. D. Bain, C. Jerome, V. Shen, I. Dupin-Roger, and P. Ammann, "Strontium ranelate improves bone strength in ovariectomized rat by positively influencing bone resistance determinants," *Osteoporosis International*, vol. 20, no. 8, pp. 1417–1428, 2009.

[80] P. J. Marie, M. Hott, D. Modrowski et al., "An uncoupling agent containing strontium prevents bone loss by depressing bone resorption and maintaining bone formation in estrogen-deficient rats," *Journal of Bone and Mineral Research*, vol. 20, no. 6, pp. 1065–1074, 2005.

[81] S. Peng, X. S. Liu, S. Huang et al., "Intervention timing of strontium treatment on estrogen depletion–induced osteoporosis in rats: bone microstructure and mechanics," *Journal of Orthopaedic Research*, vol. 32, no. 3, pp. 477–484, 2014.

[82] M. E. Arlot, Y. Jiang, H. K. Genant et al., "Histomorphometric and μCT analysis of bone biopsies from postmenopausal osteoporotic women treated with strontium ranelate," *Journal of Bone and Mineral Research*, vol. 23, no. 2, pp. 215–222, 2008.

[83] S. Peng, X. S. Liu, T. Wang et al., "In vivo anabolic effect of strontium on trabecular bone was associated with increased osteoblastogenesis of bone marrow stromal cells," *Journal of Orthopaedic Research*, vol. 28, no. 9, pp. 1208–1214, 2010.

[84] J. Coulombe, H. Faure, B. Robin, Y. Tsouderos, and M. Ruat, "Stimulatory effects of strontium ranelate (S12911) on the rat and mouse cation-sensing receptor," *Journal of Bone and Mineral Research*, vol. 16, p. S428, 2001.

[85] P. Ammann, B. Robin, J. P. Bonjour, I. Tupinon-Mathieu, J. M. Meyer, and R. Rizzoli, "Long-term exposure to strontium ranelate dose-dependently increases bone strength in intact female rats," *Bone*, vol. 28, supplement 5, p. S220, 2001.

[86] P. Marie, M. Hott, D. Modrowski et al., "S-12911, a new agent containing strontium, inhibits bone loss due to immobilization in rats," *Journal of Bone and Mineral Research*, vol. 10, p. S105, 1995.

[87] P. Delannoy, D. Bazot, and P. J. Marie, "Long-term treatment with strontium ranelate increases vertebral bone mass without deleterious effect in mice," *Metabolism: Clinical and Experimental*, vol. 51, no. 7, pp. 906–911, 2002.

[88] J. Buehler, P. Chappuis, J. L. Saffar, Y. Tsouderos, and A. Vignery, "Strontium ranelate inhibits bone resorption while maintaining bone formation in alveolar bone in monkeys *Macaca fascicularis*," *Bone*, vol. 29, no. 2, pp. 176–179, 2001.

[89] Z. Saidak, E. Haÿ, C. Marty, A. Barbara, and P. J. Marie, "Strontium ranelate rebalances bone marrow adipogenesis and osteoblastogenesis in senescent osteopenic mice through NFATc/Maf and Wnt signaling," *Aging Cell*, vol. 11, no. 3, pp. 467–474, 2012.

[90] E. M. Brown and R. J. Macleod, "Extracellular calcium sensing and extracellular calcium signaling," *Physiological Reviews*, vol. 81, no. 1, pp. 239–297, 2001.

[91] A. D. Conigrave and D. T. Ward, "Calcium-sensing receptor (CaSR): pharmacological properties and signaling pathways," *Best Practice & Research Clinical Endocrinology & Metabolism*, 2013.

[92] S. Peng, X. S. Liu, S. Huang et al., "The cross-talk between osteoclasts and osteoblasts in response to strontium treatment: involvement of osteoprotegerin," *Bone*, vol. 49, no. 6, pp. 1290–1298, 2011.

[93] O. Fromigué, E. Haÿ, A. Barbara et al., "Calcium sensing receptor-dependent and receptor-independent activation of osteoblast replication and survival by strontium ranelate," *Journal of Cellular and Molecular Medicine*, vol. 13, no. 8 B, pp. 2189–2199, 2009.

[94] H. Faure, T. Gorojankina, N. Rice et al., "Molecular determinants of non-competitive antagonist binding to the mouse GPRC6A receptor," *Cell Calcium*, vol. 46, no. 5-6, pp. 323–332, 2009.

[95] J. Caverzasio and C. Thouverey, "Activation of FGF receptors is a new mechanism by which strontium ranelate induces osteoblastic cell growth," *Cellular Physiology and Biochemistry*, vol. 27, no. 3-4, pp. 243–250, 2011.

[96] S. Peng, G. Zhou, K. D. K. Luk et al., "Strontium promotes osteogenic differentiation of mesenchymal stem cells through the Ras/MAPK signaling pathway," *Cellular Physiology and Biochemistry*, vol. 23, no. 1–3, pp. 165–174, 2009.

[97] G. Xiao, D. Jiang, P. Thomas et al., "MAPK pathways activate and phosphorylate the osteoblast-specific transcription factor, Cbfa1," *Journal of Biological Chemistry*, vol. 275, no. 6, pp. 4453–4459, 2000.

[98] M. S. Rybchyn, M. Slater, A. D. Conigrave, and R. S. Mason, "An Akt-dependent increase in canonical Wnt signaling and a decrease in sclerostin protein levels are involved in strontium ranelate-induced osteogenic effects in human osteoblasts," *Journal of Biological Chemistry*, vol. 286, no. 27, pp. 23771–23779, 2011.

[99] Z. Xu, S. Choudhary, Y. Okada et al., "Cyclooxygenase-2 gene disruption promotes proliferation of murine calvarial osteoblasts *in vitro*," *Bone*, vol. 41, no. 1, pp. 68–76, 2007.

[100] S. Peng, X. S. Liu, G. Zhou et al., "Osteoprotegerin deficiency attenuates strontium-mediated inhibition of osteoclastogenesis and bone resorption," *Journal of Bone and Mineral Research*, vol. 26, no. 6, pp. 1272–1282, 2011.

[101] G. J. Atkins, K. J. Welldon, P. Halbout, and D. M. Findlay, "Strontium ranelate treatment of human primary osteoblasts promotes an osteocyte-like phenotype while eliciting an osteoprotegerin response," *Osteoporosis International*, vol. 20, no. 4, pp. 653–664, 2009.

[102] S. M. Sprague and M. A. Josephson, "Bone disease after kidney transplantation," *Seminars in Nephrology*, vol. 24, no. 1, pp. 82–90, 2004.

[103] M. M. Winslow, M. Pan, M. Starbuck et al., "Calcineurin/NFAT signaling in osteoblasts regulates bone mass," *Developmental Cell*, vol. 10, no. 6, pp. 771–782, 2006.

[104] T. Koga, Y. Matsui, M. Asagiri et al., "NFAT and Osterix cooperatively regulate bone formation," *Nature Medicine*, vol. 11, no. 8, pp. 880–885, 2005.

[105] M. M. Winslow, E. M. Gallo, J. R. Neilson, and G. R. Crabtree, "The calcineurin phosphatase complex modulates immunogenic B cell responses," *Immunity*, vol. 24, no. 2, pp. 141–152, 2006.

[106] I. Gulhan, S. Bilgili, R. Gunaydin, S. Gulhan, and C. Posaci, "The effect of strontium ranelate on serum insulin like growth factor-1 and leptin levels in osteoporotic post-menopausal women: a prospective study," *Archives of Gynecology and Obstetrics*, vol. 278, no. 5, pp. 437–441, 2008.

[107] J. Zhang, S. Zhao, and Y. Zhu, "Three-dimensional printing of strontium-containing mesoporous bioactive glass scaffolds for bone regeneration," *Acta Biomaterialia*, 2014.

[108] J. Ren, K. A. Blackwood, and A. Doustgani, "Melt-electrospun polycaprolactone strontium-substituted bioactive glass scaffolds for bone regeneration," *Journal of Biomedical Materials Research A*, 2013.

[109] P. S. Poh, D. W. Hutmacher, M. M. Stevens, and M. A. Woodruff, "Fabrication and in vitro characterization of bioactive glass composite scaffolds for bone regeneration," *Biofabrication*, vol. 5, no. 4, Article ID 045005, 2013.

[110] J. Hao, A. Acharya, K. Chen, J. Chou, S. Kasugai, and N. Lang, "Novel bioresorbable strontium hydroxyapatite membrane for guided bone regeneration," *Clinical Oral Implants Research*, 2013.

[111] K. Sekine, M. Sakama, and K. Hamada, "Evaluation of strontium introduced apatite cement as the injectable bone substitute developments," in *Proceedings of the 35th Annual International Conference of the IEEE Engineering in Medicine and Biology Society (EMBC '13)*, pp. 858–861, IEEE, 2013.

[112] M. Iafisco, A. Ruffini, A. Adamiano, S. Sprio, and A. Tampieri, "Biomimetic magnesium-carbonate-apatite nanocrystals endowed with strontium ions as anti-osteoporotic trigger," *Materials Science and Engineering C*, vol. 35, pp. 212–219, 2014.

[113] K. Lin, L. Xia, H. Li et al., "Enhanced osteoporotic bone regeneration by strontium-substituted calcium silicate bioactive ceramics," *Biomaterials*, vol. 34, no. 38, pp. 10028–10042, 2013.

[114] H. B. Pan, X. L. Zhao, X. Zhang et al., "Strontium borate glass: potential biomaterial for bone regeneration," *Journal of the Royal Society Interface*, vol. 7, no. 48, pp. 1025–1031, 2010.

[115] A. Sabareeswaran, B. Basu, S. J. Shenoy, Z. Jaffer, N. Saha, and A. Stamboulis, "Early osseointegration of a strontium containing glass ceramic in a rabbit model," *Biomaterials*, vol. 34, no. 37, pp. 9278–9286, 2013.

[116] G.-l. Yang, L.-N. Song, Q.-H. Jiang et al., "Effect of strontium-substituted nanohydroxyapatite coating of porous implant surfaces on implant osseointegration in a rabbit model," *International Journal of Oral & Maxillofacial Implants*, vol. 27, no. 6, 2012.

[117] J. Forsgren and H. Engqvist, "A novel method for local administration of strontium from implant surfaces," *Journal of Materials Science: Materials in Medicine*, vol. 21, no. 5, pp. 1605–1609, 2010.

[118] E. S. Place, L. Rojo, E. Gentleman, J. P. Sardinha, and M. M. Stevens, "Strontium-and zinc-alginate hydrogels for bone tissue engineering," *Tissue Engineering A*, vol. 17, no. 21-22, pp. 2713–2722, 2011.

Hindawi Publishing Corporation
BioMed Research International
Volume 2014, Article ID 323046, 12 pages
http://dx.doi.org/10.1155/2014/323046

Research Article

Nanosized Mesoporous Bioactive Glass/Poly(lactic-co-glycolic Acid) Composite-Coated $CaSiO_3$ Scaffolds with Multifunctional Properties for Bone Tissue Engineering

Mengchao Shi, Dong Zhai, Lang Zhao, Chengtie Wu, and Jiang Chang

State Key Laboratory of High Performance Ceramics and Superfine Microstructure, Shanghai Institute of Ceramics, Chinese Academy of Sciences, Shanghai 200050, China

Correspondence should be addressed to Chengtie Wu; chengtiewu@mail.sic.ac.cn and Jiang Chang; jchang@mail.sic.ac.cn

Received 10 November 2013; Revised 15 January 2014; Accepted 23 January 2014; Published 2 March 2014

Academic Editor: Michael Gelinsky

It is of great importance to prepare multifunctional scaffolds combining good mechanical strength, bioactivity, and drug delivery ability for bone tissue engineering. In this study, nanosized mesoporous bioglass/poly(lactic-co-glycolic acid) composite-coated calcium silicate scaffolds, named NMBG-PLGA/CS, were successfully prepared. The morphology and structure of the prepared scaffolds were characterized by scanning electron microscopy and X-ray diffraction. The effects of NMBG on the apatite mineralization activity and mechanical strength of the scaffolds and the attachment, proliferation, and alkaline phosphatase activity of MC3T3 cells as well as drug ibuprofen delivery properties were systematically studied. Compared to pure CS scaffolds and PLGA/CS scaffolds, the prepared NMBG-PLGA/CS scaffolds had greatly improved apatite mineralization activity in simulated body fluids, much higher mechanical property, and supported the attachment of MC3T3 cells and enhanced the cell proliferation and ALP activity. Furthermore, the prepared NMBG-PLGA/CS scaffolds could be used for delivering ibuprofen with a sustained release profile. Our study suggests that the prepared NMBG-PLGA/CS scaffolds have improved physicochemical, biological, and drug-delivery property as compared to conventional CS scaffolds, indicating that the multifunctional property of the prepared scaffolds for the potential application of bone tissue engineering.

1. Introduction

As a promising material for bone tissue engineering, $CaSiO_3$ (CS) has been widely studied for years due to its distinct bioactivity and degradability [1–3]. Up to now, CS powders, coatings, and scaffolds have been prepared by various methods and the *in vitro* and *in vivo* biological properties have been studied [2, 4–6]. Among them, CS scaffolds with a porous structure which provides sufficient space for cell migration and ingrowths have gained much attention for bone regeneration application. However, the inherent brittleness and the high local pH environment that resulted from the high ionic dissolution rate of the prepared CS scaffolds limited their further application as bone tissue engineering scaffolds [7]. In order to solve these problems, polymers such as PLA (polylactic acid) and PCL (polycaprolactone) have been used to improve the mechanical property and to decrease degradation rate of CS scaffolds [8–10]. Previous studies demonstrated that with PLGA (poly(lactic-co-glycolic acid)) coating on the surface of pore walls and the CS scaffolds possess better compressive strength and the pH value of biological solution reduced during the degradation of scaffolds [11]. However, as the pore walls of porous CS scaffolds were covered by PLGA coatings, the bioactivity of CS scaffolds was inhibited due to the shielding effect of PLGA on the bioactive inorganic phase.

Ideal scaffolds for bone tissue engineering should have multifunctional properties, such as proper mechanical strength, good bioactivity, proper degradation rate, and even drug-delivery ability [12, 13]. More and more studies have shown that drug and growth factor delivery via porous scaffolds may play an important role to deal with the potential infections and to accelerate the osteogenesis and angiogenesis process during bone regeneration [14–16].

However, how to prepare multifunctional scaffolds with these specific properties still remains a significant challenge.

In the past several years, a new class of biomaterials, mesoporous bioactive glasses (MBG), has attracted much attention for bone regeneration and drug delivery [17]. They have highly ordered mesoporous channel structure, large surface area, and variable pore volume. These features greatly enhanced their apatite-mineralization ability as well as drug-delivery ability [18, 19]. Due to the advantages of MBG, we have previously prepared pure MBG scaffolds which combine hierarchical large pore (300–500 μm) and well-ordered mesopores (5 nm) for bone tissue engineering and drug delivery [20]. However, the shortcoming of the prepared MBG scaffolds is their low mechanical strength since they cannot be sintered at high temperature (no more than 700°C) [21] and the mesopore structure will be damaged if the sintering temperature is higher than 700°C. As we mentioned above, CS scaffolds possess distinct bioactivity and biopolymer-modified CS scaffolds that have excellent mechanical strength [11]. For these reasons, it is assumed that the incorporation of MBG particles into biopolymers for coating CS scaffolds may combine the bioactivity and drug-delivery property of MBG with the improved mechanical strength of biopolymer modification. Therefore, the aim of this study is to prepare CS scaffolds with a coating layer of nanosized MBG (NMBG) particles/PLGA composite and to further investigate the effect of NMBG/PLGA coating on the mechanical property and apatite-mineralization activity of the scaffolds and the proliferation and differentiation of bone-forming cells as well as the drug-delivery property of CS scaffolds.

2. Materials and Methods

2.1. Preparation and Characterization of Nanosized Mesoporous Bioactive Glass Particles. Nanosized mesoporous bioactive glass (NMBG) powders were synthesized using cetyltrimethylammonium bromide (CTAB) as template, in which 6.6 g CTAB was firstly dissolved in 600 mL of distilled water with 12 mL of ammonia water. After stirring for 1 h at 37°C, 30 mL tetraethyl orthosilicate (TEOS) and 31.21 g $Ca(NO_3)_2{\cdot}4H_2O$ were added to the solution and stirred for 6 h. The products were collected by vacuum filtration and washed by distilled water and ethanol for 3 times. Ethanol mixed with 1% HCl solution was used to wash the powders to remove CTAB. After dried at 60°C for 24 h, the powders were calcined at 550°C for 2 h. The NMBG powders were characterized by X-ray diffraction (XRD) (D/Max 2550V, Rigaku Japan), scanning electron microscopy (SEM) (JSM-6700, JEOL, Japan), and transmission electron microscopy (TEM) (2100F, JEOL, Japan). The specific surface area, mesopore size distribution, and pore volume were determined by N_2 adsorption-desorption isotherms (Micromeritics Tristar 3000).

2.2. Preparation and Characterization of Calcium Silicate (CS) Scaffolds, PLGA/CS Scaffolds, and NMBG-PLGA/CS Scaffolds. CS scaffolds were prepared by polyurethane template method according to our previous study [22], CS powders (<40 um) were added to polyvinyl alcohol (PVA) aqueous solution (6% Wt) and stirred to get well-distributed slurry. Polyurethane sponges (PS) with a size of Ø6 × 6 mm and pore size of 300–500 μm were prepared and immersed in a glass beaker containing the slurry and compressed with a glass stick to force the slurry to migrate into the pores of the foams. The struts of the foams were uniformly coated with ceramic slurry, while the pores were kept open. Then the sponges were transferred to a petri dish to dry at 60°C for 24 h. Once the samples were completely dry, they were calcined at 300°C for 2 h to remove the PS and then sintered at 1250°C for 3 h to obtain the CS scaffolds. The shape of scaffolds remained the same after sintering.

To prepared NMBG-PLGA/CS scaffolds, 2 g of PLGA (copolymer ratio of PLA : PGA 75 : 25) was dissolved in 20 mL acetone and stirred at room temperature. Different amounts of NMBG powders (0, 0.2, 0.6 or 1 g) were added to the solution under stirring. Then the CS scaffolds were immersed into the solution for 2 h while continuing to stir. The coated scaffolds were dried at room temperature overnight and then at 60°C for 24 h to remove the residual solvent. As a result, the PLGA/CS scaffolds (without NMBG particles), 10% NMBG-PLGA/CS, 30% NMBG-PLGA/CS, and 50% NMBG-PLGA/CS scaffolds were prepared. The morphology and pore structure of the prepared scaffolds were observed by SEM.

2.3. The Effect of NMBG Particles on the Mechanical Strength of Scaffolds. The compressive strength of scaffolds was tested using a universal mechanical machine at 0.5 mm/min crosshead speed (Shimadza AG-SKN, Japan). Six samples from each group were tested to obtain an average value.

2.4. The Effect of NMBG Particles on Apatite Mineralization of the Scaffolds in SBF. The assessment of *in vitro* bioactivity of the five types of scaffolds was carried out in simulated body fluids (SBF) solution. The SBF solution has a composition and ionic concentration similar to that of human plasma. Each scaffold was soaked in 10 mL of SBF solution in a polyethylene bottle at 37°C for 1, 3, 7, and 14 days. SBF solution was refreshed every other day. Then the scaffolds were collected, washed gently with distilled water, and dried at 60°C. The sizes of all scaffolds were around Ø6 × 6 mm as they were prepared. SEM and electron dispersive spectrometer (EDS) (INCA Energy, Oxford Instruments, UK) were used to examine the mineralized apatite on the surface of the scaffolds. The ion concentration (Ca, P, and Si) of the solution taken after soaking was tested by ICP-AES (Perkin-Elmer Optima 7000DV).

2.5. The Attachment, Proliferation, and Alkaline Phosphatase (ALP) Activity of MC3T3 Cells on Scaffolds. MC3T3 (MC3T3-E1 Subclone 14) cells were purchased from cell bank, Chinese Academy of Sciences. The 4th passage of MC3T3 was used for the evaluation of interaction of cells with the CS, PLGA/CS, and NMBG-PLGA/CS scaffolds

including the attachment, proliferation, and alkaline phosphate (ALP) activity.

For evaluation of cell attachments, five kinds of scaffolds were sterilized in autoclave for 30 min and dried under 60°C. MC3T3 cells were cultured on scaffolds that were placed in 48-well culture plate at an initial density of 1×10^4 cells/cm^2. The cells were then incubated for 24 h in α-MEM culture medium supplemented with 10% FCS in humidified culture conditions. Then scaffolds were removed from the culture wells, rinsed with PBS, and fixed with 1.25% glutaraldehyde. The fixative was removed by washing with buffer containing 4% (w/v) sucrose in PBS and postfixed in 1% osmium tetroxide in PBS followed by sequential dehydration in graded ethanol. The specimens were dried in hexamethyldisilazane (HMDS) for 30 min before coating with gold for SEM analysis according to our previous publication [23].

For investigation of the proliferation of MC3T3 cells on the scaffolds, MTT assay was performed in triplicate according to our previous study protocol [24]. This assay is based on the cleavage of MTT into insoluble formazan crystals by the mitochondrial enzymes of the viable cells. Briefly, MC3T3 cells were seeded on these scaffolds and cultured in growth medium for 1, 3, and 7 days. 40 μL of 0.5 mg/mL of MTT solution was added with 360 μL growth medium at each time point. After incubated for 4 h, the medium was removed and the formazan product was dissolved in 200 μL of dimethyl sulfoxide (DMSO). An aliquot of 100 μL was taken from each well and transferred to a fresh 96-well plate. The absorbance was measured at $\lambda = 590$ nm on a microplate reader. All the results were demonstrated as the optical density values minus the absorbance of blank wells.

The effect of NMBG on the early osteogenic differentiation of MC3T3 cells on the scaffolds was performed to test their ALP activity assay by using PNPP method [25]. Cells were seeded at a concentration of 1×10^4 cells/cm^2 onto each scaffold placed individually in a 48-well plate. The cells were left to grow for 7 and 14 days at 37°C in a humidified atmosphere of 5% CO_2. Aliquots of cell lysates were incubated with reaction solution (containing 2-amino-2-methyl-1-propanol, $MgCl_2$, and p-nitrophenylphosphate) at 37°C for 30 min. The conversion of p-nitrophenylphosphate to p-nitrophenol was stopped by adding NaOH, and the absorbance at 405 nm was measured with a spectrophotometer (UV-Vis 8500, Shanghai). The ALP activity was normalized by total intracellular protein contents.

2.6. Loading and In Vitro Release of Ibuprofen (IBU) for NBMG-PLGA/CS Scaffolds. 2 g of IBU was firstly dissolved in 50 mL hexane. 0.5 g NMBG powders were added to the solution and stirred for 24 h. Then the powders were centrifuged at 300 r/min, washed with distilled water, and dried at 60°C. The loading amount of IBU was determined by thermogravimetry (TG). The IBU-NMBG powders were added to the PLGA solution to prepare the 10%, 30%, and 50% NMBG-PLGA/CS scaffolds as described in Section 2.2. To test the release of IBU from scaffolds, each scaffold was soaked in 10 mL of PBS solution at 37°C on a shaking bed. The release medium was collected at the predetermined time intervals and replaced with fresh PBS solution. Then the released IBU from scaffolds was monitored by UV-Vis analysis.

2.7. Statistical Analysis. All the data were expressed as means ± standard deviation (SD) and were analyzed using one-way ANOVA with a post hoc test. A P value <0.05 was considered statistically significant.

3. Results

3.1. Characterization of NMBG Powders. The XRD pattern (Figure 1(a)) shows that there were no distinctly sharp characteristic peaks except for a wide peak at $2\theta = 20$–30°, suggesting that the prepared NMBG particles are amorphous. The SEM (Figures 1(c) and 1(d)) analysis shows that the size of the prepared NMBG powders is in the range of 50–100 nm. There are obvious nanopores in the inside of NMBG powders (Figures 1(e) and 1(f)). The N_2 adsorption-desorption analysis presented a typical Type IV isotherm pattern (Figure 1(b)), which revealed that the NMBG powders possess mesoporous structure [26]. The mesopore distribution of the NMBG powders was around 3.5 nm. The specific surface area calculated by BET method was around 76.53 m^2/g.

3.2. Characterization of CS Scaffolds, PLGA/CS Scaffolds and NMBG-PLGA/CS Scaffolds. The prepared CS scaffolds present pure pseudowollastonite (α-$CaSiO_3$) phase structure by XRD analysis (Figure 2(a)). Figure 2(b) shows the representative SEM image of the CS scaffolds with interconnected macroporous networks and the pore size is in the range of 300–500 μm.

PLGA-coated CS scaffolds still maintain the nearly same structure (Figures 3(c) and 3(d)) while the surface becomes smoother. Figures 3(e), 3(g), and 3(i) presented the low magnification images of 10%, 30%, and 50% NMBG-PLGA/CS scaffolds, and Figures 3(f), 3(h), and 3(j) presented the high magnification images. As the contents of NMBG particles increased, the particles were mostly embedded in the pore walls of CS scaffolds, but the surface of pore walls became rougher. All these scaffolds remain the interconnected macroporous network (Figure 3).

3.3. The Effect of NMBG Particles on the Mechanical Strength and Apatite Mineralization of Scaffolds. Figure 4 shows the compressive strength of the CS, PLGA/CS, and NMBG-PLGA/CS (10, 30, and 50% NMBG) scaffolds. It can be seen that PLGA coating significantly improves the mechanical property of CS scaffolds. The addition of NMBG powders has no distinct effect on the mechanical strength of scaffolds; however, three NMBG-PLGA/CS scaffolds with different contents of NMBG have significantly improved mechanical strength compared to pure CS scaffolds.

Figure 5 presents the SEM images of five scaffolds after soaked in SBF for 3 days. For CS scaffolds, some apatite microparticles were deposited on the surface of pore walls (Figures 5(a) and 5(b)). For the PLGA/CS scaffolds (Figures 5(c) and 5(d)), the surface remained smooth and there were

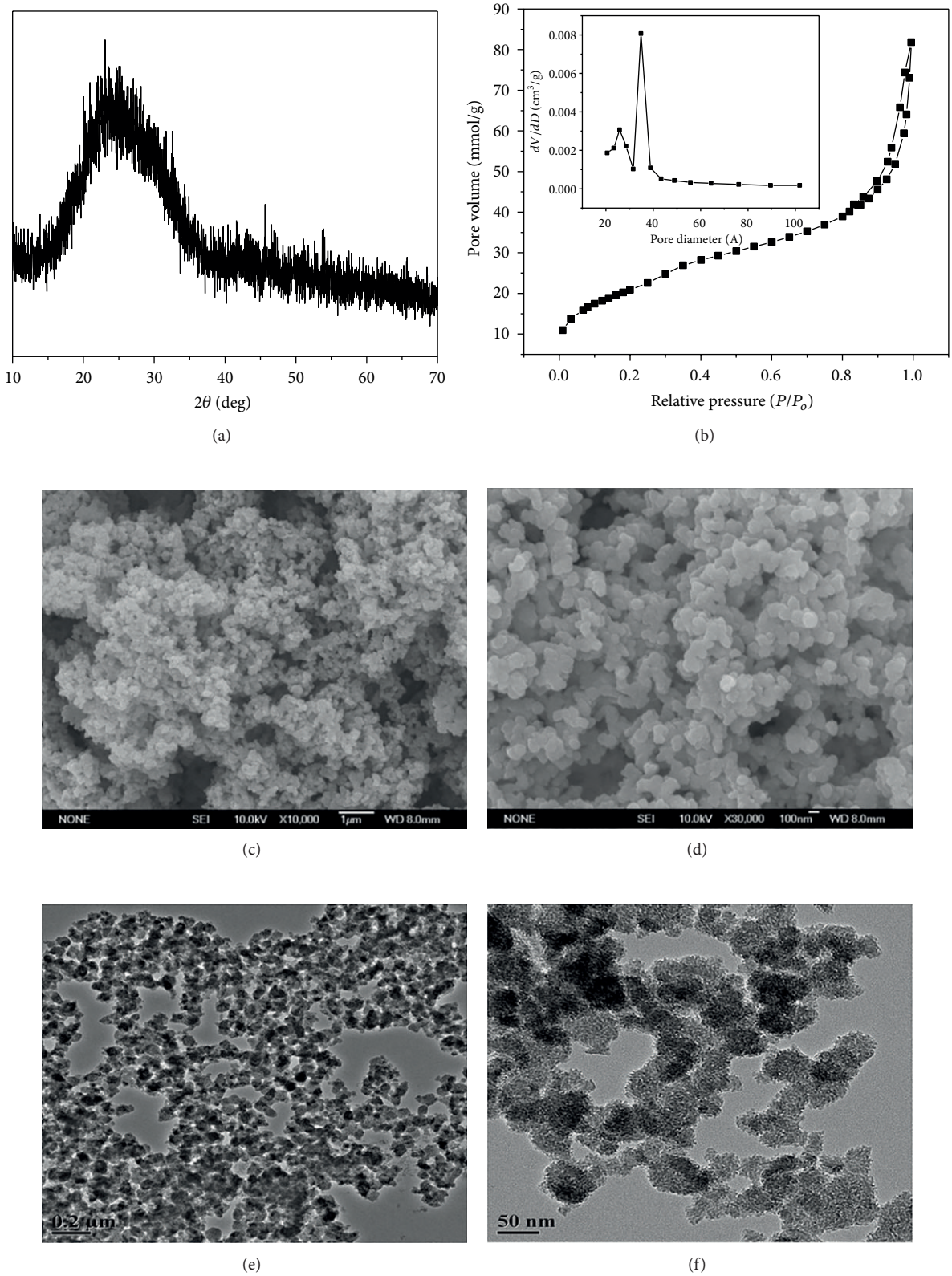

Figure 1: (a) XRD; (b) N_2 adsorption-desorption isotherm; ((c), (d)) low and high magnification SEM images; and ((e), (f)) low and high magnification TEM images for NMBG powders.

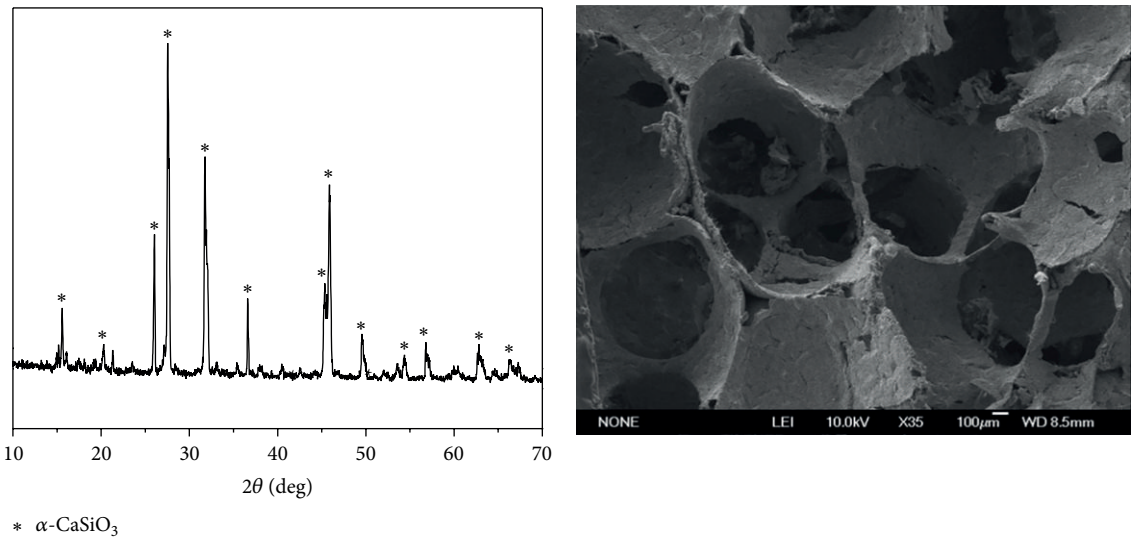

Figure 2: (a) XRD and (b) SEM analysis for CS scaffolds.

no deposited apatite particles. However, there were some apatite particles on the surface of 10% NMBG-PLGA/CS scaffolds (Figures 5(e) and 5(f)). A layer of apatite particles composed of worm-like microcrystals was found on the surface of both 30% NMBG-PLGA/CS and 50% NMBG-PLGA/CS scaffolds (Figures 5(g), 5(h), 5(i), and 5(j)). The EDS analysis exhibits that the ratio of Ca/P for the formed apatite is around 1.67.

Figure 6 shows the change of Si, Ca, and P ions in SBF solution after soaked the scaffolds in SBF. The concentrations of Si and Ca in SBF for NMBG-PLGA/CS scaffolds are obviously higher than CS and PLGA/CS scaffolds (Figures 6(a) and 6(b)), but P concentrations are lower (Figure 6(c)).

3.4. The Attachment, Proliferation, and Alkaline Phosphatase (ALP) Activity of MC3T3 Cells on Scaffolds. Five kinds of scaffolds support the attachment of MC3T3 cells with spreading morphology (Figures 7(a)–7(e)). MTT analysis shows that cell proliferation increased with increased time of culture. There is no obvious difference among the five scaffolds in the first three days. However, after cultured for 7 days, the proliferation on the PLGA/CS and NMBG-PLGA/CS scaffolds was significantly higher than on the pure CS scaffolds (Figure 8(a)). The ALP activity of cells on the PLGA/CS and NMBG-PLGA/CS scaffolds was obviously higher than that on pure CS scaffolds, but there were no obvious differences among the three groups of NMBG-PLGA/CS scaffolds (Figure 8(b)).

3.5. Loading and In Vitro Release of IBU for NMBG-PLGA/CS Scaffolds. The TG analysis suggests that the loading efficiency and amount of IBU in the NMBG powders are about 9.8% and 98 mg IBU/g NMBG (Figure 9(a)). The release amount of IBU increases with the increase of NMBG contents. Within the first 8 h, three NMBG-PLGA/CS scaffolds had a burst release and after 24 h, all scaffolds maintained a sustained release of IBU (Figure 9(b)).

4. Discussion

In this study, multifunctional NMBG-PLGA/CS scaffolds were successfully prepared for bone tissue engineering, which had been proved to possess improved mechanical strength, apatite-mineralization activity, and cytocompatibility as well as drug-delivery property, compared to pure CS and MBG scaffolds. The study indicates that the current method by introducing NMBG particles into the PLGA to coat CS scaffolds is a useful approach to construct multifunctional scaffolds to overcome the shortcomings of most bioceramic scaffolds in mechanical strength, bioactivity, and drug-delivery property. The method can be also applied to coat other kinds of scaffolds, such as β-tricalcium phosphate and hydroxyapatite.

It was found that the addition of NMBG in the PLGA/CS scaffolds had no obvious effect on the morphology of the macropore network, and the macropore size remained at a range between 300 and 500 μm which can benefit cell ingrowth and nutrient transportation [27]. In addition, the compressive strength of NMBG-PLGA/CS scaffolds was significantly improved compared to pure CS scaffolds and similar to PLGA/CS scaffolds, indicating that PLGA modification plays a major role to enhance the mechanical strength of CS scaffolds. The compressive strength of NMBG-PLGA/CS scaffolds was around 2–2.5 MPa, which was higher than that of the PDLLA-modified CS scaffolds (1.45 MPa) [22], and was within the range of human cancellous bones (2–12 MPa) [25].

Previous studies suggest that apatite mineralization of biomaterials plays an important role to maintain the bioactive

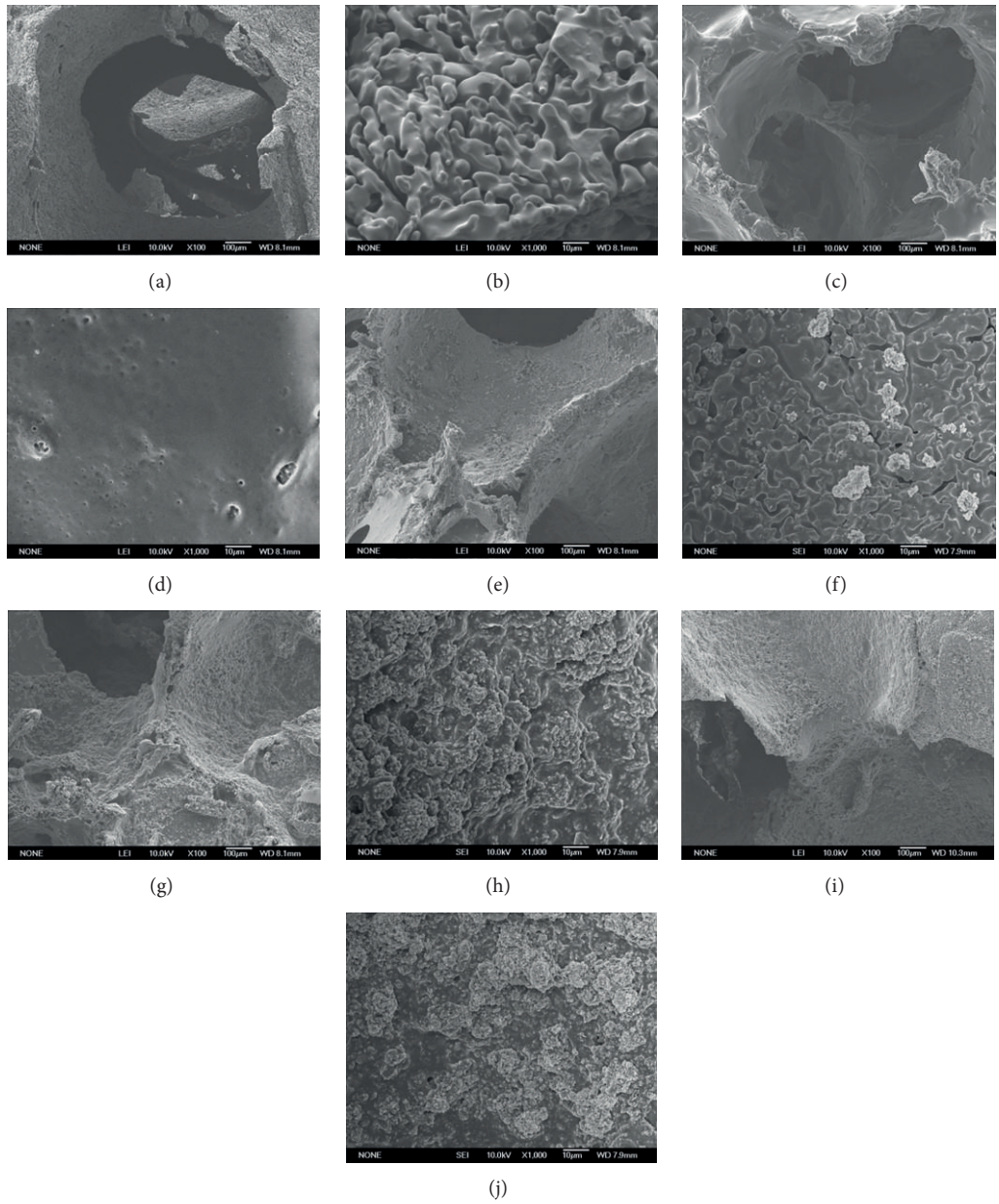

Figure 3: SEM images of CS ((a), (b)), PLGA/CS ((c), (d)), 10% NMBG-PLGA/CS ((e), (f)), 30% NMBG-PLGA/CS ((g), (h)), and 50% NMBG-PLGA/CS scaffolds ((i), (j)). ((a), (c), (e), (g), and (i)) low magnification; ((b), (d), (f), (h), and (j)) high magnification.

interface between materials and host bone tissues and the formed bone-like apatite could stimulate the proliferation and differentiation of osteoblasts [28–30]. In this study, after incorporation of NMBG particles in the scaffolds, the apatite-mineralization ability of the scaffolds was improved remarkably, indicating the stimulatory effect of NMBG particles on the apatite mineralization in SBF. To our knowledge, the typical mechanism of apatite mineralization on biomaterial surfaces mainly involves two important points [7, 31, 32]. Firstly, the release of Na^+ and/or Ca^{2+} from the biomaterials that induces the formation of the negative surface with OH^- groups, providing the nucleation sites for apatite mineralization [33]. In this case, the NMBG had high surface area, which released Ca^{2+} quickly and induced large numbers of OH^- groups to deposit on the surface of scaffolds, further promoting the formation of apatite in SBF. Secondly, the surface microstructure had an impact on the bioactivity of biomaterials [34], while in our experiment, the NMBG particles attached on the pore walls increased the surface roughness of the scaffolds, which might offer more nucleation sites for apatite formation than PLGA/CS and pure CS scaffolds. It was demonstrated in Figure 6 that the P concentration decreased continuously as the formation of apatite consumed large amounts of P ions, while the

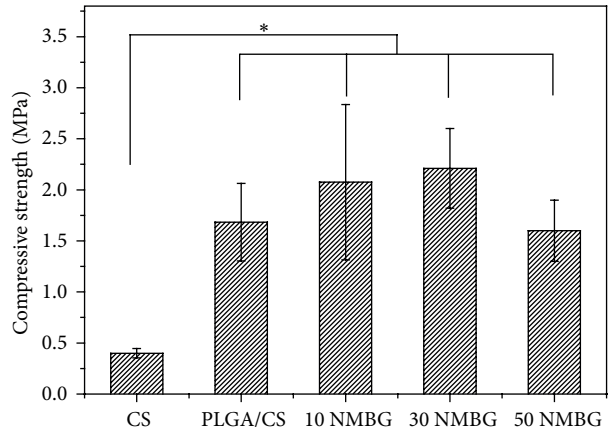

Figure 4: The compressive strength analysis for different scaffolds.

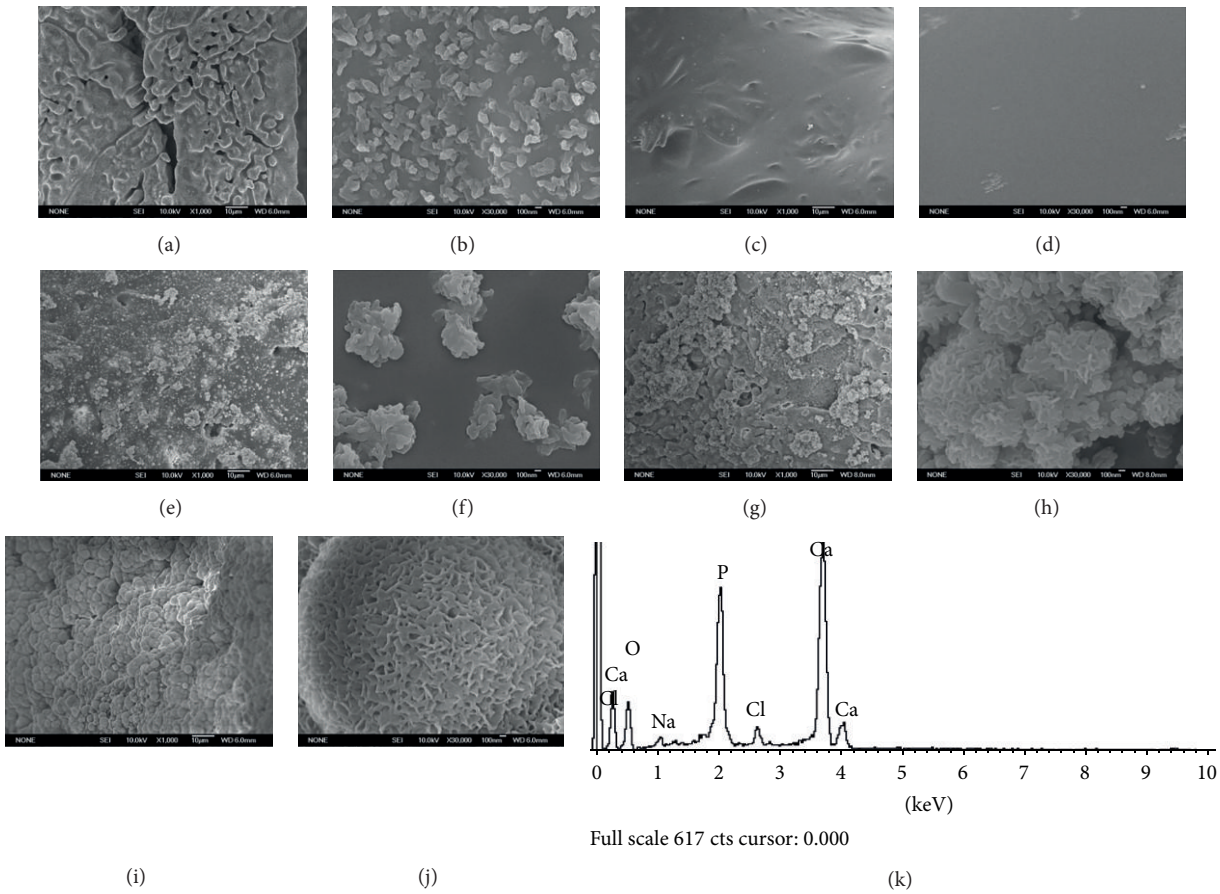

Figure 5: Apatite mineralization on the surface of scaffolds after soaking in SBF for 3 days. ((a), (b)) CS scaffolds, ((c), (d)) PLGA/CS scaffolds, ((e), (f)) 10% NMBG-PLGA/CS scaffolds, ((g), (h)) 30% NMBG-PLGA/CS scaffolds, ((i), (j)) 50% NMBG-PLGA/CS scaffolds, and (k) EDS analysis for 50% NMBG-PLGA/CS scaffolds.

Ca and Si ions concentrations kept increasing because of degradation of scaffolds, which released Si and Ca. Since part of the Ca ions was involved in apatite deposition process, the increase kinetics of Ca ions was slower than Si ions. PLGA/CS scaffolds showed the slowest release of Ca and Si, indicating that the polymer had served as a shield on the scaffold surface, and impeded the apatite formation. However, after NMBG was added in the scaffolds, the shield effect was decreased and Ca and Si ions were easily released.

Further cell experiments were carried out to investigate the effect of NMBG particles on the cell response in the scaffolds. The results indicate that the NMBG-PLGA/CS scaffolds

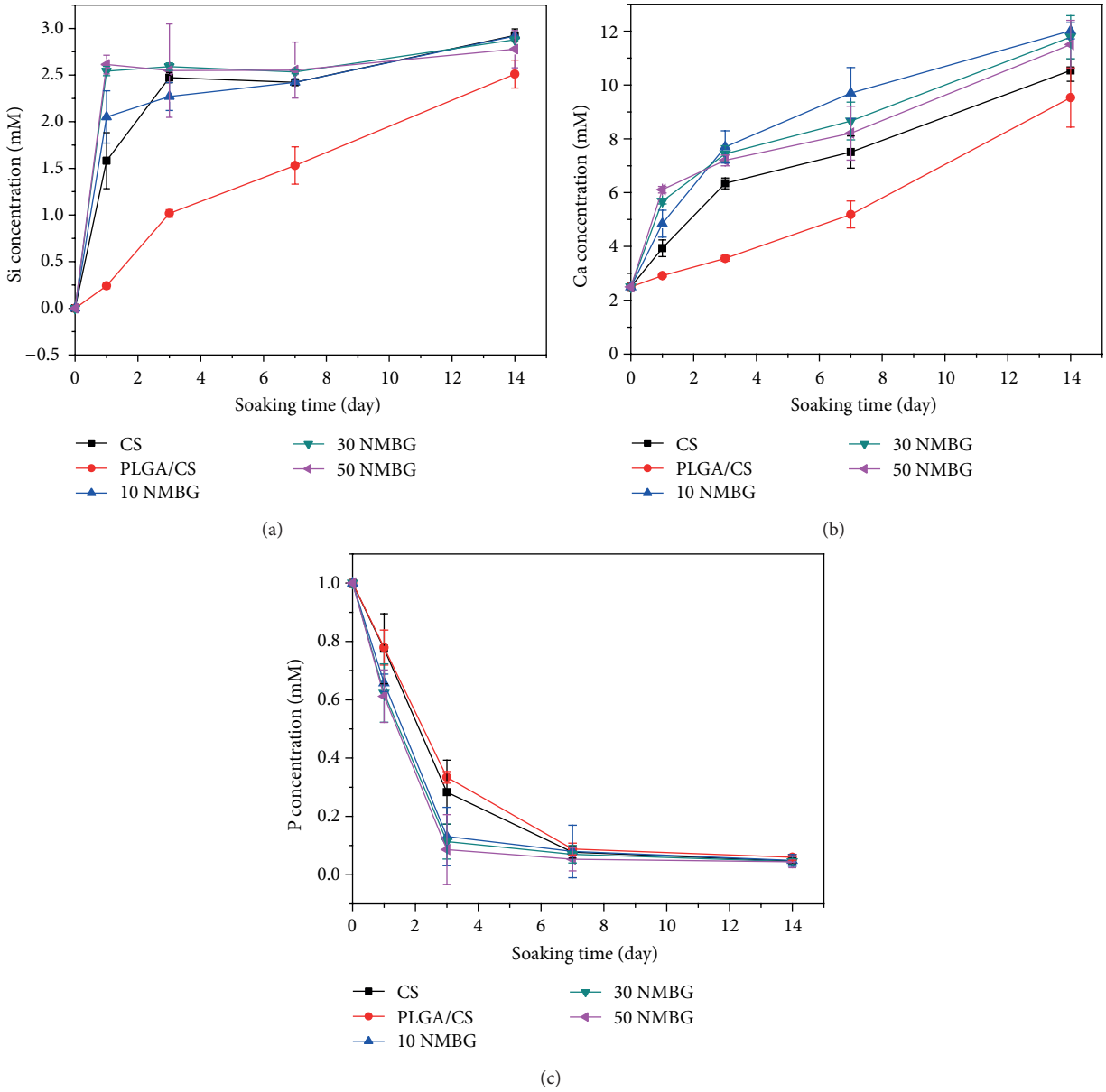

Figure 6: The change of (a) Si, (b) Ca, and (c) P ions in SBF solution after soaking the scaffolds for different times.

have improved cell proliferation and earlier differentiation of MC3T3 than pure CS scaffolds, but similar to PLGA/CS scaffolds. It is known that the surface microstructure and the released ions from biomaterials are two major factors that influence the cell response [32, 35, 36]. Previous studies have shown that, at a certain concentration range, Ca and Si ions can stimulate cell proliferation and differentiation [32, 37]. In this study, although the incorporation of NMBG leads to increased Ca and Si ionic concentrations, it seems that the effect of increased Ca and Si concentrations have no significant effect on cell proliferation and ALP activity of MC3T3 cells. However, the PLGA modification seems to play the key role to enhance the cytocompatibility of scaffolds. We speculated that PLGA coatings on pure CS scaffolds created a more stable surface for cell adhesion, proliferation, and early differentiation [6, 11, 33].

Bacterial infection has been a serious problem in bone related surgery, causing complication and even osteonecrosis in the lesions. Traditional treatments such as wound drainage and implant removal result in much pain of additional surgical intervention to patients [15]. To deal with this problem, an efficient, controllable, and nontoxic local drug release system is needed. In our study, the NMBG particles with mesoporous channel structures can serve as drug carriers. Since pure CS scaffolds lack nanopore structure, they cannot be used as drug-delivery system. However, in this study, the mesopores of NMBG particles had the distinct ability for loading IBU. In addition, with the relatively slow degradation rate of

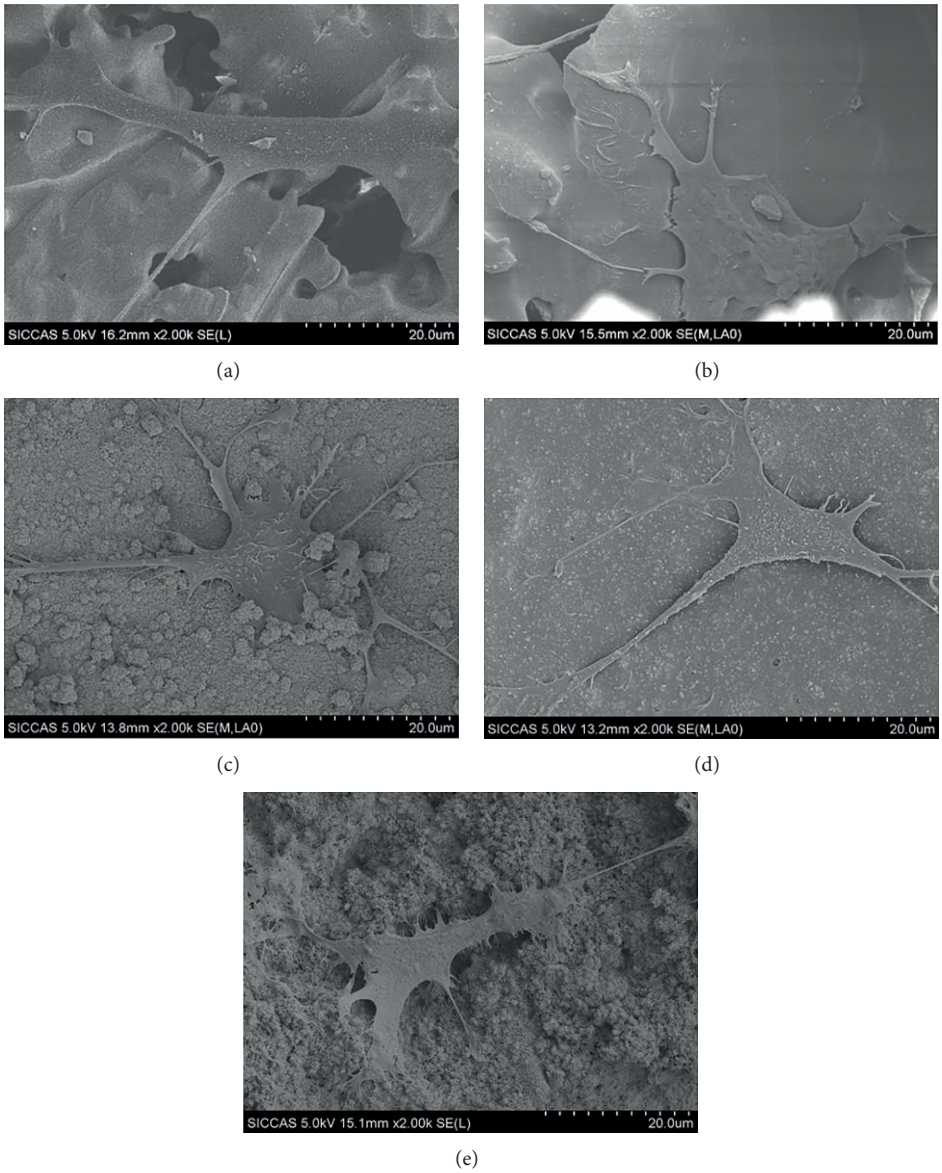

Figure 7: Cell attachments on (a) CS, (b) PLGA/CS, (c) 10% NMBG-PLGA/CS, (d) 30% NMBG-PLGA/CS, and (e) 50% NMBG-PLGA/CS scaffolds.

PLGA coating on the surface, drugs can be released gradually and continuously. It turned out that the NMBG-PLGA/CS scaffolds have sustained drug release property. Therefore, the NMBG-PLGA/CS scaffolds combine the bioactivity and drug-delivery property and might be used for bone tissue engineering.

5. Conclusion

Multifunctional NMBG-PLGA/CS scaffolds were successfully prepared by coating sintered pure CS scaffolds with NMBG incorporated PLGA solution. The NMBG-PLGA/CS scaffolds possess macroporous structures (300–500 μm) and their pore walls contain nanosized mesoporous bioactive glasses (mesopore size: 3.5 nm). Compared with CS scaffolds and pure PLGA-coated CS scaffolds, the mechanical strength and mineralization ability of NMBG-PLGA/CS scaffolds were greatly improved due to the addition of NMBG particles. The prepared NMBG-PLGA/CS scaffolds enhanced the proliferation and early cell differentiation of MC3T3 cells as compared to CS scaffolds. Moreover, the mesopore channels inside the NMBG particles offer NMBG-PLGA/CS scaffolds sustained drug-delivery ability for dealing with potential bacterial infection. All these results indicate that the NMBG-PLGA/CS scaffolds may be used as a multifunctional platform for bone tissue engineering.

Conflict of Interests

The authors declare that there is no conflict of interests regarding the publication of this paper.

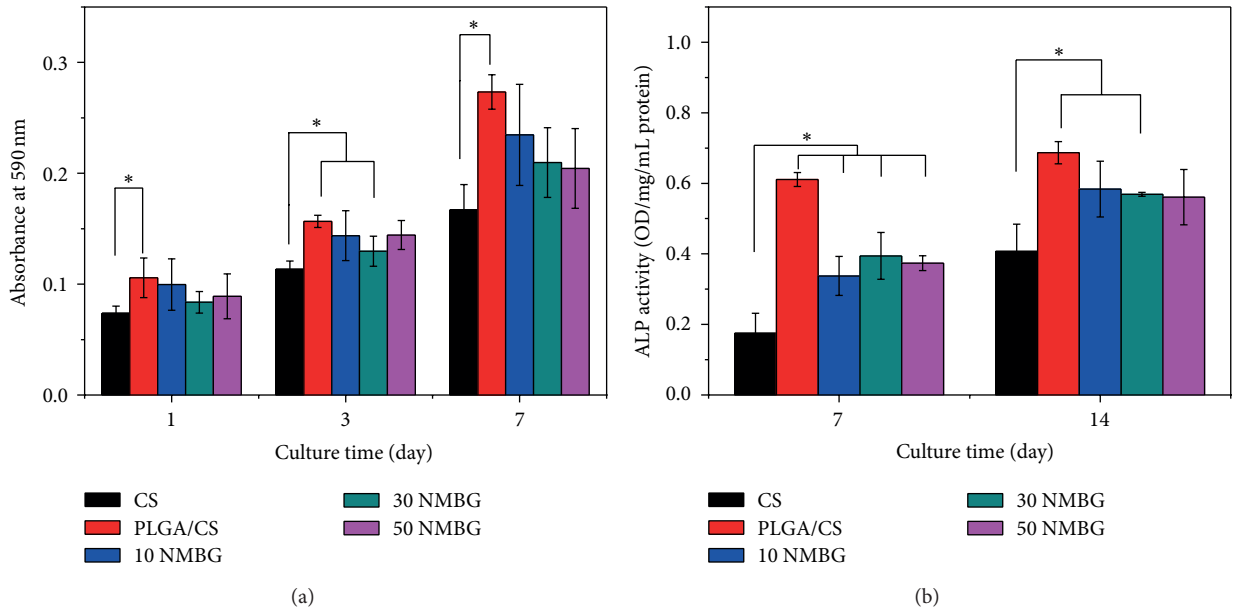

Figure 8: (a) The proliferation and (b) alkaline phosphatase (ALP) activity of MC3T3 cells on the five scaffolds.

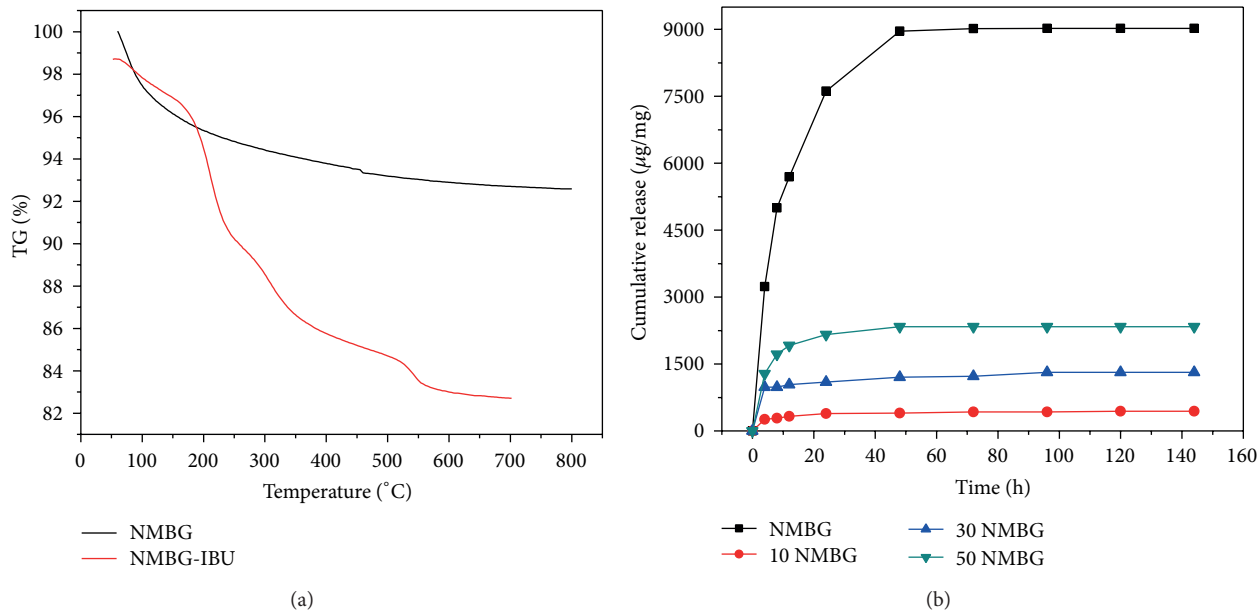

Figure 9: (a) TG analysis of IBU loading and (b) cumulative release of IBU from NMBG-PLGA/CS scaffolds.

Acknowledgments

Funding for this study was provided by the Recruitment Program of Global Young Talent, China (Chengtie Wu), Shanghai Pujiang Talent Program (12PJ1409500), Natural Science Foundation of China (Grants 31370963, 81201202, and 81190132) and Innovative Project of SIC, CAS.

References

[1] P. N. De Aza, F. Guitián, S. De Aza, and F. J. Valle, "Analytical control of wollastonite for biomedical applications by use of atomic absorption spectrometry and inductively coupled plasma atomic emission spectrometry," *Analyst*, vol. 123, no. 4, pp. 681–685, 1998.

[2] S. Ni, J. Chang, and L. Chou, "A novel bioactive porous $CaSiO_3$ scaffold for bone tissue engineering," *Journal of Biomedical Materials Research Part A*, vol. 76, no. 1, pp. 196–205, 2006.

[3] R. G. Carrodeguas, A. H. De Aza, P. N. De Aza et al., "Assessment of natural and synthetic wollastonite as source for bioceramics preparation," *Journal of Biomedical Materials Research Part A*, vol. 83, no. 2, pp. 484–495, 2007.

[4] P. Siriphannon, Y. Kameshima, A. Yasumori, K. Okada, and S. Hayashi, "Influence of preparation conditions on the

microstructure and bioactivity of alpha-$CaSiO_3$ ceramics: formation of hydroxyapatite in simulated body fluid," *Journal of Biomedical Materials Research*, vol. 52, no. 1, pp. 30–39, 2000.

[5] K.-L. Lin, J. Chang, J.-X. Lu, J.-H. Gao, and Y. Zeng, "Fabrication and characterization of β-Ca3(PO4)2/$CaSiO_3$ composite bioceramics," *Journal of Inorganic Materials*, vol. 21, no. 6, pp. 1429–1434, 2006.

[6] J. M. Fernández-Pradas, P. Serra, J. L. Morenza, and P. N. De Aza, "Pulsed laser deposition of pseudowollastonite coatings," *Biomaterials*, vol. 23, no. 9, pp. 2057–2061, 2002.

[7] C. Wu, Y. Ramaswamy, D. Kwik, and H. Zreiqat, "The effect of strontium incorporation into $CaSiO_3$ ceramics on their physical and biological properties," *Biomaterials*, vol. 28, no. 21, pp. 3171–3181, 2007.

[8] S. Dorozhkin and T. Ajaal, "Toughening of porous bioceramic scaffolds by bioresorbable polymeric coatings," *Proceedings of the Institution of Mechanical Engineers, Part H: Journal of Engineering in Medicine*, vol. 223, no. 4, pp. 459–470, 2009.

[9] F. J. Martínez-Vázquez, F. H. Perera, P. Miranda, A. Pajares, and F. Guiberteau, "Improving the compressive strength of bioceramic robocast scaffolds by polymer infiltration," *Acta Biomaterialia*, vol. 6, no. 11, pp. 4361–4368, 2010.

[10] C. Wang, K. Lin, J. Chang, and J. Sun, "Osteogenesis and angiogenesis induced by porous beta-$CaSiO_3$/PDLGA composite scaffold via activation of AMPK/ERK1/2 and PI3K/Akt pathways," *Biomaterials*, vol. 34, no. 1, pp. 64–77, 2013.

[11] L. Zhao, C. Wu, K. Lin, and J. Chang, "The effect of poly(lactic-co-glycolic acid) (PLGA) coating on the mechanical, biodegradable, bioactive properties and drug release of porous calcium silicate scaffolds," *Bio-Medical Materials and Engineering*, vol. 22, no. 5, pp. 289–300, 2012.

[12] C. Wu and J. Chang, "Mesoporous bioactive glasses: structure characteristics, drug/growth factor delivery and bone regeneration application," *Interface Focus*, vol. 2, no. 3, pp. 292–306, 2012.

[13] C. Wu, R. Miron, A. Sculean et al., "Proliferation, differentiation and gene expression of osteoblasts in boron-containing associated with dexamethasone deliver from mesoporous bioactive glass scaffolds," *Biomaterials*, vol. 32, no. 29, pp. 7068–7078, 2011.

[14] Y. Zhu and S. Kaskel, "Comparison of the *in vitro* bioactivity and drug release property of mesoporous bioactive glasses (MBGs) and bioactive glasses (BGs) scaffolds," *Microporous and Mesoporous Materials*, vol. 118, no. 1–3, pp. 176–182, 2009.

[15] L. Zhao, X. Yan, X. Zhou et al., "Mesoporous bioactive glasses for controlled drug release," *Microporous and Mesoporous Materials*, vol. 109, no. 1–3, pp. 210–215, 2008.

[16] C. Wu, Y. Zhou, J. Chang, and Y. Xiao, "Delivery of dimethyloxallyl glycine in mesoporous bioactive glass scaffolds to improve angiogenesis and osteogenesis of human bone marrow stromal cells," *Acta Biomaterialia*, vol. 9, no. 11, pp. 9159–9168, 2013.

[17] C. Wu, W. Fan, and J. Chang, "Functional mesoporous bioactive glass nanospheres: synthesis, high loading efficiency, controllable delivery of doxorubicin and inhibitory effect on bone cancer cells," *Journal of Materials Chemistry B*, vol. 1, no. 21, p. 2710, 2013.

[18] Z. Quan, X. Han, Z. Ye, Y. Chenzhong, and C. Wenjun, "Influence of novel nano-mesoporous bioactive glass on the regulation of IGF-II gene expression in osteoblasts," *Cell Biochemistry and Biophysics*, vol. 62, no. 1, pp. 119–123, 2012.

[19] C. Wu, Y. Zhang, Y. Zhu, T. Friis, and Y. Xiao, "Structure-property relationships of silk-modified mesoporous bioglass scaffolds," *Biomaterials*, vol. 31, no. 13, pp. 3429–3438, 2010.

[20] C. Wu, J. Chang, and Y. Xiao, "Mesoporous bioactive glasses as drug delivery and bone tissue regeneration platforms," *Therapeutic Delivery*, vol. 2, no. 9, pp. 1189–1198, 2011.

[21] C. Wu, Y. Luo, G. Cuniberti, Y. Xiao, and M. Gelinsky, "Three-dimensional printing of hierarchical and tough mesoporous bioactive glass scaffolds with a controllable pore architecture, excellent mechanical strength and mineralization ability," *Acta Biomaterialia*, vol. 7, no. 6, pp. 2644–2650, 2011.

[22] C. Wu, Y. Ramaswamy, P. Boughton, and H. Zreiqat, "Improvement of mechanical and biological properties of porous $CaSiO_3$ scaffolds by poly(d,l-lactic acid) modification," *Acta Biomaterialia*, vol. 4, no. 2, pp. 343–353, 2008.

[23] M. Xu, Y. Zhang, D. Zhai, J. Chang, and C. Wu, "Mussel-inspired bioactive ceramics with improved bioactivity, cell proliferation, differentiation and bone-related gene expression of MC3T3 cells," *Biomaterials Science*, vol. 1, no. 9, pp. 933–941, 2013.

[24] C. Wu, Y. Zhou, W. Fan et al., "Hypoxia-mimicking mesoporous bioactive glass scaffolds with controllable cobalt ion release for bone tissue engineering," *Biomaterials*, vol. 33, no. 7, pp. 2076–2085, 2012.

[25] C. Wu, Y. Ramaswamy, and H. Zreiqat, "Porous diopside (CaMgSi2O6) scaffold: a promising bioactive material for bone tissue engineering," *Acta Biomaterialia*, vol. 6, no. 6, pp. 2237–2245, 2010.

[26] X. Li, L. Zhang, X. Dong, J. Liang, and J. Shi, "Preparation of mesoporous calcium doped silica spheres with narrow size dispersion and their drug loading and degradation behavior," *Microporous and Mesoporous Materials*, vol. 102, no. 1–3, pp. 151–158, 2007.

[27] S. Ni, J. Chang, L. Chou, and W. Zhai, "Comparison of osteoblast-like cell responses to calcium silicate and tricalcium phosphate creamics *in vitro*," *Journal of Biomedical Materials Research Part B*, vol. 80, no. 1, pp. 174–183, 2007.

[28] S. Ni, K. Lin, J. Chang, and L. Chou, "β-$CaSiO_3$/β-$Ca_3(PO_4)_2$ composite materials for hard tissue repair: *in vitro* studies," *Journal of Biomedical Materials Research Part A*, vol. 85, no. 1, pp. 72–82, 2008.

[29] J.-M. Raquez, D. T.-J. Barone, Z. Luklinska et al., "Osteoconductive and bioresorbable composites based on poly-(L,L-lactide) and pseudowollastonite: from synthesis and interfacial compatibilization to *in vitro* bioactivity and *in vivo* osseointegration studies," *Biomacromolecules*, vol. 12, no. 3, pp. 692–700, 2011.

[30] Y.-F. Chou, W. Huang, J. C. Y. Dunn, T. A. Miller, and B. M. Wu, "The effect of biomimetic apatite structure on osteoblast viability, proliferation, and gene expression," *Biomaterials*, vol. 26, no. 3, pp. 285–295, 2005.

[31] D. Dufrane, C. Delloye, I. J. Mckay et al., "Indirect cytotoxicity evaluation of pseudowollastonite," *Journal of Materials Science: Materials in Medicine*, vol. 14, no. 1, pp. 33–38, 2003.

[32] N. Zhang, J. A. Molenda, J. H. Fournelle, W. L. Murphy, and N. Sahai, "Effects of pseudowollastonite ($CaSiO_3$) bioceramic on *in vitro* activity of human mesenchymal stem cells," *Biomaterials*, vol. 31, no. 30, pp. 7653–7665, 2010.

[33] N. Sahai and M. Anseau, "Cyclic silicate active site and stereochemical match for apatite nucleation on pseudowollastonite bioceramic-bone interfaces," *Biomaterials*, vol. 26, no. 29, pp. 5763–5770, 2005.

[34] X. Li, J. Shi, Y. Zhu et al., "A template route to the preparation of mesoporous amorphous calcium silicate with high *in vitro* bone-forming bioactivity," *Journal of Biomedical Materials Research Part B*, vol. 83, no. 2, pp. 431–439, 2007.

[35] K. Xiong, H. Shi, J. Liu, Z. Shen, H. Li, and J. Ye, "Control of the dissolution of Ca and Si ions from $CaSiO_3$ bioceramic via tailoring its surface structure and chemical composition," *Journal of the American Ceramic Society*, vol. 96, no. 3, pp. 691–696, 2013.

[36] D. D. Deligianni, N. D. Katsala, P. G. Koutsoukos, and Y. F. Missirlis, "Effect of surface roughness of hydroxyapatite on human bone marrow cell adhesion, proliferation, differentiation and detachment strength," *Biomaterials*, vol. 22, no. 1, pp. 87–96, 2001.

[37] C. Wu, Y. Zhang, X. Ke et al., "Bioactive mesopore-glass microspheres with controllable protein-delivery properties by biomimetic surface modification," *Journal of Biomedical Materials Research Part A*, vol. 95, no. 2, pp. 476–485, 2010.

Hindawi Publishing Corporation
BioMed Research International
Volume 2014, Article ID 731039, 7 pages
http://dx.doi.org/10.1155/2014/731039

Review Article

RANKL Expression in Periodontal Disease: Where Does RANKL Come from?

Bin Chen,[1] Wenlei Wu,[1] Weibin Sun,[1] Qian Zhang,[1] Fuhua Yan,[1] and Yin Xiao[2]

[1] *Institute and Hospital of Stomatology, Nanjing University Medical School, 30 Zhongyang Road, Nanjing, Jiangsu 210008, China*
[2] *Bone Research Laboratory, Institute of Health and Biomedical Innovation, Queensland University of Technology, Kelvin Grove Campus, Brisbane, Qld 4059, Australia*

Correspondence should be addressed to Fuhua Yan; fhyan2005@126.com and Yin Xiao; yin.xiao@qut.edu.au

Received 13 November 2013; Accepted 22 January 2014; Published 27 February 2014

Academic Editor: Mei Wei

Periodontitis is an inflammatory disease characterized by periodontal pocket formation and alveolar bone resorption. Periodontal bone resorption is induced by osteoclasts and receptor activator of nuclear factor-κB ligand (RANKL) which is an essential and central regulator of osteoclast development and osteoclast function. Therefore, RANKL plays a critical role in periodontal bone resorption. In this review, we have summarized the sources of RANKL in periodontal disease and explored which factors may regulate RANKL expression in this disease.

1. Introduction

Periodontitis is an inflammatory disease characterized by periodontal pocket formation and alveolar bone resorption, and it is one of the most common chronic inflammatory diseases in aged populations. *Porphyromonas gingivalis* (*P. gingivalis*), *Actinobacillus actinomycetemcomitans* (*A. actinomycetemcomitans*), and *Treponema denticola* (*T. denticola*) are major periodontal pathogens involved in various forms of periodontitis; however, simply the variety and count cannot determine the type or severity of periodontitis, which indicated that immune responses against periodontal pathogens may greatly affect the course of periodontal diseases, but the mechanisms of periodontal bone resorption remain to be established [1].

Periodontal bone resorption is induced by osteoclasts. A balance between bone resorption by osteoclasts and bone formation by osteoblasts determines the level of bone mass. Receptor activator of nuclear factor-κB ligand (RANKL), its receptor RANK, and a decoy receptor osteoprotegerin (OPG) are key molecules in regulating osteoclast differentiation, recruitment, and function [2, 3]. RANKL is essential for the complete differentiation of osteoclast precursor cells [4] and plays a critical role in periodontal bone resorption [1]. In this review, we have summarized the sources of RANKL in periodontal disease and explored which factor may regulate RANKL expression in this disease.

2. RANKL Expression in Periodontal Disease

RANKL, a polypeptide of 314 amino acids, encoded by the gene TNFSF11 and expressed in a membrane-bound protein or in secreted forms [5], is a member of the TNF cytokine family and plays a very important role in periodontal bone resorption. The level of RANKL mRNA has been reported to be highest in advanced periodontitis compared with moderate periodontitis or healthy groups. In addition, upregulated RANKL levels are related to the number of *P. gingavalis*, a major periodontal bacterium, in clinically obtained periodontal tissue [6]. Later studies have demonstrated that bone resorption can be decreased by inhibiting the RANK/RANKL signal way during experimental periodontitis in rats [7, 8]. These results suggest that RANKL plays an important role in periodontal resorption and RANKL inhibition can inhibit periodontal bone resorption.

RANKL is identified in lymphocytes, stromal cells, and other types of cells [4, 9–11]. Liu et al. examined RANKL mRNA expression at the cellular level using in situ hybridization and found that RANKL mRNA was expressed in inflammatory cells, mainly lymphocytes and macrophages [11]. In addition, proliferating epithelium at the vicinity of inflammatory cells expressed high levels of RANKL mRNA [11]. Confocal microscopic analyses showed that both B cells and T cells, but not monocytes or fibroblasts, are the major cellular sources of RANKL in the bone resorptive lesion of periodontal disease [10]. However, other cells may also be an important source in this process because they can regulate RANKL expression indirectly by excreting proinflammatory cytokines, which can subsequently regulate the function of lymphocytes.

2.1. B and T Lymphocytes Are the Primary Sources of RANKL in the Bone Resorptive Lesion of Periodontal Disease. To determine the cellular source of RANKL in bone resorptive periodontitis, enzyme-linked immunosorbent assay (ELISA) and double-color confocal microscopic analyses have been used. Results of ELISA demonstrated that soluble RANKL (sRANKL) production was significantly elevated in gingival tissues with periodontal disease compared to healthy gingival tissues. Confocal microscopic analyses showed that both B and T cells, but not monocytes or fibroblasts, were the cellular source of RANKL in the bone resorptive lesions of periodontal disease. Despite the potential involvement of other factors in the bone destruction process, prominent expression of RANKL by B and T cells in the periodontal disease lesions seems to play a primary role in the augmentation of bone resorption processes in this disease [10]. Further study indicated that it is the activated but not naïve B and T lymphocytes that are the major sources of RANKL [10]. We will introduce the RANKL expression of lymphocytes in the following paragraph.

2.2. T Cells Stimulated by Periodontopathic Microorganisms Can Modulate Periodontal Bone Resorption through Upregulation of RANKL Production by an Adaptive Immune Response. Kawai et al. reported that regulation of T-lymphocyte function can affect periodontal bone resorption in periodontal disease [12–14]. Further studies indicate that T lymphocytes specific to *A. actinomycetemcomitans* are associated with periodontal disease and periodontal bone resorption in *A. actinomycetemcomitans*-infected rats occurred because RANKL production was upregulated [14–16].

T cells isolated from the gingival tissue of *A. actinomycetemcomitans*-immunized *P. pneumotropica*$^+$ mice proliferated *in vitro* and produced sRANKL in response to both *antigens* presentation. However, gingival T cells isolated from nonimmunized *P. pneumotropica*$^+$ mice did not show such a proliferative response to either *A. actinomycetemcomitans*-antigen or *P. pneumotropica*-antigen presentation by antigen-presenting cells, nor did they produce sRANKL [17]. These results may also indicate that periodontopathic microorganisms, such as *A. actinomycetemcomitans*, may induce bone resorption by stimulating T cells and then upregulating RANKL expression.

2.3. Different Types of CD4$^+$ T Cells and RANKL Expressions in Periodontal Tissues. Since the bacteria involved in periodontal disease are extracellular pathogens, CD4$^+$ T cells appear to play a major role in the antigen recognition of these bacteria components. Many studies indicated this opinion: Baker et al. have reported that bone loss decreased in CD4$^+$ T cells deficient mice after oral infection by *P. gingivalis*, but no change in mice deficient in CD8$^+$ T cells or NK1$^+$ T cells [18]. Baker et al. demonstrated the importance of the adaptive immune response, especially CD4$^+$ T cells, in the bone loss consequent to oral infection [18]. Another research also indicated that CD4$^+$ T cells were the predominant cell type present in periodontitis gingival tissues, and they expressed RANKL more than dendritic cells or monocytes [19]. Uncommitted (naive) murine CD4$^+$ T helper cells can be induced to differentiate into T helper 1 (Th1), Th2, and Th17 and regulatory T (Treg) phenotypes depending on the local cytokine milieu. IL-27, a member of the IL-6/IL-12 family cytokines, was found to greatly inhibit both mRANKL expression and sRANKL secretion in CD4$^+$ T cells activated by T cell receptor ligation [20]. In contrast, in differentiated Th17 cells, IL-27 much less efficiently inhibited RANKL expression after restimulation [20]. Therefore, different types of T cells may play different roles in RANKL expression regulation.

2.3.1. Th1, Th2 Cells, and RANKL Expression in Periodontal Tissues. In general, Th1-type cloned T-cells produce consistently higher levels of RANKL than Th2-type T-cells, and RANKL expression induced by TCR/CD28 costimulation is suppressed in the presence of IL-4, suggesting that RANKL is predominantly expressed on Th1-type T-cells [14]. In experiments carried out with rat, T-cells, CD28, and TCR stimulation could upregulate more RANKL expression than TCR or CD28 stimulation alone, indicating that costimulatory signals are necessary to maximize RANKL expression. Furthermore, Th1 polarization by IL-12, in addition to TCR/CD28 stimulation, enhanced the expression of RANKL on the T cells, whereas Th2 polarization by IL-4 reduced the RANKL expression on the same T-cells activated with TCR/CD28 stimulation. Thus, Th1-type T-cells seem to be potentiated to express RANKL as compared to Th2-type T-cells. Costimulatory double signals from TCR and CD28 are also required for the optimal expression of RANKL [14].

There is supportive, though not conclusive, evidence that Th1 cells and their cytokines characterize early/stable periodontal lesions [21]. Th1 cell cytokines, IFN-γ and TNF-α, are related to RANKL expression. IFN-γ is a major product of activated T helper cells that can function as a pro- or antiresorptive cytokine. IFN-γ blunts osteoclast formation through direct targeting of osteoclast precursors but indirectly stimulates osteoclast formation and promotes bone resorption by stimulating antigen-dependent T cell activation and T cell secretion of the osteoclastogenic factors RANKL and TNF-α. Analysis of the *in vivo* effects of IFN-γ has been tested in 3 mouse models of bone loss including ovariectomy, LPS injection, and inflammation via silencing of TGF-β signaling in T cells models. The results revealed that IFN-γ has both direct antiosteoclastogenic and indirect

proosteoclastogenic properties *in vivo*. Under the conditions of estrogen deficiency, infection, and inflammation, the net balance of these two opposing forces is biased toward bone resorption. Inhibition of IFN-γ signaling may thus represent a novel strategy to simultaneously reduce inflammation and bone loss in common forms of osteoporosis [22].

2.3.2. Th17 Cells and RANKL Expression in Periodontal Tissues. In recent years, a new subset of $CD4^+$ T-cells has been discovered that helped to explain many of the discrepancies in the classic Th1/Th2 model, and it has been termed "Th17" based on its secretion of the novel proinflammatory cytokine IL-17 [23]. Cardoso et al. have demonstrated the presence of Th17 cells in the sites of chronic inflammation in human periodontal disease. They collected gingival and alveolar bone samples from healthy patients and patients with chronic periodontitis and demonstrated elevated levels of IL-17, TGF-β, IL-1β, IL-6, and IL-23 messenger RNA and protein in diseased tissues as well as the presence of Th17 cells in the gingiva from patients with periodontitis. Moreover, IL-17 and the bone resorption factor RANKL were abundantly expressed in the alveolar bones of diseased patients, in contrast to low expression level in controls [24]. Ohyama et al. have also reported that IL-17 is involved in periodontitis and the IL-23/IL-17 pathway is frequently induced in periodontitis lesions and that this pathway may therefore play an essential role in periodontal biology [25].

The role of IL-17 in periodontal disease is controversial. Whereas elevated IL-17 levels have been found in humans with severe periodontal disease [26], Yu et al. have recently reported that female C57BL/6J mice lacking the IL-17 receptor (IL-17RAKO) are significantly more susceptible to periodontal disease bone loss as a result of defects in the chemokine-neutrophil axis [27]. Further study demonstrates a gender-dependent effect of IL-17 signaling and indicates that gender differences should be taken into account in the preclinical and clinical study [28].

It is worth noticing that Th17 cells do not induce osteoclastogenesis in the absence of osteoblasts, which strongly suggests that RANKL expressed on Th17 cells alone is not sufficient to induce osteoclastogenesis: this is partly because Th17 cells produce a small amount of IFN-γ, which counterbalances the RANKL action [29].

2.3.3. Treg Cells and RANKL Expression in Periodontal Tissues. The percentage of $Foxp3^+$ cells is as low as 5% within the otherwise massive infiltration of $RANKL^+$ lymphocytes found in the diseased gingival tissues. In the peripheral blood lymphocytes can be stimulated with bacteria (*A. actinomycetemcomitans*) in an antigen-dependent fashion; however, mRANKL expression is expressed prominently in Foxp3 negative cells and in $Foxp3^{dim}$ cells, not in $Foxp3^{bright}$ cells, which most probably represent the presence of CD25/Foxp3 double-positive cells. IL-10 suppressed both sRANKL and membrane RANKL (mRANKL) expression by peripheral blood mononuclear cells (PBMC) activated *in vitro* in a bacterial antigen-specific manner. Taken together, these results suggest that Foxp3/CD25 double-positive Treg cells may play a role in the downregulation of RANKL expression by activated lymphocytes in periodontal disease tissues. These results lead to the conclusion that the phenomenon of diminished $CD25^+Foxp3^+$ Treg cells appears to be associated with the increased $RANKL^+$ T cells in the bone resorption lesions of periodontal disease [30].

2.4. B-Cells and RANKL Expression in Periodontal Tissues. More than 90% of B cells recovered from human periodontal diseased tissues express RANKL, as opposed to about 54% of T cells [10]. B cells do not seem to require the presence of T cells to drive bone resorption. In a congenitally athymic rat model of experimental periodontitis injected with donor B cells, RANKL expression and the corresponding induction of osteoclast differentiation increased in rats receiving B cells from *A. actinomycetemcomitans*-immunized animals compared to nonimmune B cells [31]. In a recent study, it is suggested that RANKL expression is upregulated in B cells in the adaptive immune response rather than in the innate immune response to *A. actinomycetemcomitans*, and preimmunization of animals with *A. actinomycetemcomitans* leads to an enhanced B-cell response including increased RANKL expression [32]. A recent *in vitro* study indicated that toll-like receptors (TLRs) may play a role in B cell-mediated RANKL-dependent periodontal bone resorption, and TLR4 and TLR9 diminish RANKL production, probably through the induction of RANKL-expressing immune B cell apoptosis [33].

2.5. Osteoblasts, Osteocytes, and RANKL Expression in Periodontal Tissues. Mice with RANKL deficiency in osteoblast lineage have showed some protection from bone loss induced by ovariectomy as well as from joint destruction associated with arthritis, whereas loss of RANKL in T cells did not confer such protection, which indicated that RANKL expression by osteoblast lineage plays an important role in bone resorption [34]. Atkins et al. reported that RANKL expression was related to the differentiation state of human osteoblasts [35] and RANKL was expressed preferentially by immature osteoblasts and the expression level decreased during their maturation.

The idea that osteoblasts, or their progenitors, support osteoclast formation by expressing the cytokine RANKL is a widely held tenet of skeletal biology. But more recently studies provide evidence that osteocytes, and not osteoblasts or their progenitors, are the major source of RANKL driving osteoclast formation in trabecular bone. Nakashima et al. have reported that purified osteocytes express a much higher amount of RANKL and have a greater capacity to support osteoclastogenesis *in vitro* than both osteoblasts and bone marrow stromal cells. Furthermore, the severe osteopetrotic phenotype that they observed in mice lacking RANKL—specifically, in osteocytes—indicates that osteocytes are the major source of RANKL in bone remodeling *in vivo* [36]. However, femurs in mice lacking RANKL in osteocytes have normal shapes, indicating that modeling of the metaphyseal cortex of long bones is controlled by cells other than osteocytes. Thus, the role of osteocyte-derived RANKL may be limited to bone remodeling [37].

Given the special anatomy of periodontal tissue, the role of osteoblasts and osteocytes in periodontal diseases may be different from other bone resorption diseases, because osteoclasts are formed at different skeletal sites for different purposes. The results of the conditional RANKL deletion studies show that the osteoclasts that form at these different sites require different support cells in each case [37]. Specifically, the finding that osteocyte-derived RANKL is not required for tooth eruption or resorption of calcified cartilage during endochondral bone formation shows that other cell types must supply the RANKL required for osteoclast formation in these processes [38].

2.6. Macrophage and RANKL Expression in Periodontal Tissues. Although macrophage may be not the main source of RANKL expression in periodontal disease [10], it can influence RANKL expression through its pattern recognition receptors (PRRs) and cytokines [39].

2.6.1. Macrophage PRRs and RANKL Expression in Periodontal Tissues. Macrophages express a lot of PPRs, such as TLRs, to recognize periodontal pathogens, and then induce a series of intracellular signaling events, NF-κB activation, and culminating in expression of inflammatory mediators [39, 40]. Interestingly, the number of TLR2-expressing cells, but not of TLR4-expressing cells, tends to increase linearly with gingival inflammation. This may have to do with the fact that most suspected periodontal pathogens preferentially activate TLR2 rather than TLR4. Indeed, *P. gingivalis*, *T. forsythia*, *T. denticola*, *Prevotella intermedia*, *Prevotella nigrescens*, *Capnocytophaga ochracea, A. actinomycetemcomitans*, *Fusobacterium nucleatum,* and *Veillonella parvula* can all activate TLR2, but only the last three can efficiently activate TLR4. The regulated expressions of TLRs in the periodontium and their activation by periodontal bacteria suggest that TLRs are potentially major players in periodontitis. Whether TLRs are involved in protective immunity or destructive inflammation (or both) has yet to be elucidated. Their potentially ambivalent role may be reflected in the studies that aim to correlate single nucleotide polymorphisms of TLR genes with susceptibility to periodontitis, which have been inconclusive when taken together [41]. Clinical and experimental studies have identified that PRR-dependent recognition of *P. gingivalis* is an initial step in host response to this organism, and TLRs have emerged as a major group of PRRs involved in recognition and signaling in the context of *P. gingivalis* exposure. Indeed, experimental studies have identified that signaling through TLR2 leads to oral bone loss in mice [42].

It has been reported that the innate immune response promoted osteoclastogenic activity by activating RANKL via TLR pathways [43]. Others reported that innate immune recognition through TLR signaling is crucial for inflammatory bone loss in response to infection by microorganisms associated with chronic periodontal disease [44]. In a previous study, Rosen et al. showed that *T. denticola* lipooligosaccharide (LOS) produced a concentration-dependent activation of NO and TNF-α in murine macrophages which was inhibited by polymyxin B [45]. In their later study, they showed that this activation is dependent on the TLR4-MyD88 signaling pathway [46].

Despite these reports, clinical studies employing a genetic polymorphism approach are not in agreement regarding major roles for TLRs in periodontal disease. Schröder et al. [47] reported that a TLR4 polymorphism is associated with periodontitis, while Folwaczny et al. [48] failed to observe associations for TLR2 or TLR4. Thus it is likely that in addition to TLRs, other unrecognized PRRs may contribute to periodontal disease and host response to periodontal pathogens. Baer et al. reported that Scavenger receptor A is expressed by macrophages in response to *P. gingivalis* and participates in TNF-α expression [49], which can upregulate RANKL expression [50].

2.6.2. IL-1, TNF-α, and RANKL Expression in Periodontal Tissues. TNF-α potently increased osteoclast proliferation/differentiation in the presence of RANKL. This effect was greatest when RANKL was present before exposure of osteoclast precursor cells to TNF-α. The resorptive activity of osteoclasts generated by TNF-α in the absence of RANKL was critically dependent upon IL-1, which was expressed by lymphocyte-monocyte interaction [51]. Further study indicated that IL-1 and LPS stimulate osteoclastogenesis through two parallel events: direct enhancement of RANKL expression and suppression of OPG expression, which is mediated by PGE2 production [52].

In the process of periodontal disease, a key role for TNF-α and IL-1 has been demonstrated, including regulation of osteoclastogenesis *in vitro* and *in vivo* [10, 50, 53–55]. It is noteworthy that during the progression of experimental periodontitis, high levels of IL-1β and TNF-α have been positively related to RANKL expression [56, 57]. Kawai et al. have also reported that the concentrations of sRANKL and IL-1β examined in the gingival tissue homogenates were significantly elevated in the diseased gingival tissues compared to healthy tissues [10]. Wei et al. reported that IL-1 mediates the osteoclastogenic effect by enhancing stromal cell expression of RANKL and directly stimulating differentiation of osteoclast precursors [50]. Fujihara et al. reported that TNF-α enhances RANKL expression in gingival epithelial cells via protein kinase A signaling [58].

2.7. Periodontal Ligament Fibroblasts, Gingival Fibroblasts, and RANKL Expression. It had been reported that human periodontal ligament cells stimulated with LPS inhibit osteoclastogenesis by producing more effective OPG than RANKL through the induction of IL-1β and TNF-α [59]. Further studies indicated that IL-1α stimulates osteoclast formation by increasing the expression level of RANKL versus OPG via ERK-dependent PGE2 production in PDL cells [9]. But a more recent study reported that OPG was detected at high levels in both fibroblast cultures, whereas RANKL could not be detected [60].

Resorption of bone did not occur by the mononuclear cells (MNCs) formed in the presence of fibroblasts, suggesting that fibroblasts may secrete inhibitors for bone resorption, which leads to the osteoclast-like cells dysfunction. The incapacity of the MNCs to resorb bone under the influence

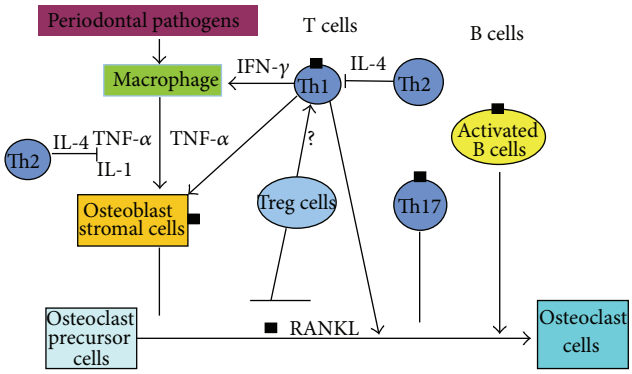

Figure 1: B cells and T cells are primary RANKL expression cells in periodontal bone resorption. Th17 cells can express RANKL; however, RANKL expressed on Th17 cells alone is not sufficient to induce osteoclastogenesis. Treg cells may play a role in the downregulation of RANKL expression by activated lymphocytes in periodontal disease tissues, but the mechanism is unclear. Osteoblast stromal cells may also express RANKL, but they play a role in preventing bone resorption, since additional stimuli are required for the formation of active osteoclasts. Although macrophage may not be the main source of RANKL expression in periodontal disease, it can influence RANKL expression through its cytokines.

of fibroblasts can be reversed by adding macrophage colony-stimulating factor (M-CSF) and RANKL in the culture media. These results suggest that tooth-associated fibroblasts may still be able to trigger the formation of osteoclast-like cells, but more importantly, they play a role in preventing bone resorption, since additional stimuli are required for the formation of active osteoclasts [60].

3. Conclusions

RANKL expression in periodontal tissues is a very complicated process that involves many factors. RANKL is identified in lymphocytes, stromal cells, and many other cell types in periodontal tissues which play an important role in direct or indirect regulatory roles. Cytokines such as IL-1β and TNF-α can upregulate RANKL expression in periodontal cells and increase osteoclast formation. Figure 1 summarizes the major cells and cytokines related to RANKL expression.

Therefore, discovering the pivotal step in RANKL expression may lead to a new insight into periodontal pathogenesis and the development of a new target for periodontal therapy; for example, we can prevent periodontal bone resorption through RANKL expression inhibiting by moderating lymphocytes' function or changing some cytokines' level.

Conflict of Interests

The authors declare that there is no conflict of interests regarding the publication of this paper.

Acknowledgments

This study was supported by the Young Start-up Project for Medical Science Development, Special Funds by Nanjing Health Bureau (no. QYK10166), the Key Project of Science and Technology Bureau of Jiangsu Province (no. BL2013002), and the International Cooperation Research and Develop Project of Nanjing Health Bureau (no. 201303051).

References

[1] T. Nagasawa, M. Kiji, R. Yashiro et al., "Roles of receptor activator of nuclear factor-κB ligand (RANKL) and osteoprotegerin in periodontal health and disease," *Periodontology 2000*, vol. 43, no. 1, pp. 65–84, 2007.

[2] N. Udagawa, N. Takahashi, E. Jimi et al., "Osteoblasts/stromal cells stimulate osteoclast activation through expression of osteoclast differentiation factor/RANKL but not macrophage colony-stimulating factor," *Bone*, vol. 25, no. 5, pp. 517–523, 1999.

[3] T. Suda, N. Takahashi, N. Udagawa, E. Jimi, M. T. Gillespie, and T. J. Martin, "Modulation of osteoclast differentiation and function by the new members of the tumor necrosis factor receptor and ligand families," *Endocrine Reviews*, vol. 20, no. 3, pp. 345–357, 1999.

[4] D. L. Lacey, E. Timms, H.-L. Tan et al., "Osteoprotegerin ligand is a cytokine that regulates osteoclast differentiation and activation," *Cell*, vol. 93, no. 2, pp. 165–176, 1998.

[5] N. C. Walsh, K. A. Alexander, C. A. Manning et al., "Activated human T cells express alternative mRNA transcripts encoding a secreted form of RANKL," *Genes & Immunity*, vol. 14, no. 4, pp. 336–345, 2013.

[6] N. Wara-Aswapati, R. Surarit, A. Chayasadom, J. A. Boch, and W. Pitiphat, "RANKL upregulation associated with periodontitis and porphyromonas gingivalis," *Journal of Periodontology*, vol. 78, no. 6, pp. 1062–1069, 2007.

[7] Q. Jin, J. A. Cirelli, C. H. Park et al., "RANKL inhibition through osteoprotegerin blocks bone loss in experimental periodontitis," *Journal of Periodontology*, vol. 78, no. 7, pp. 1300–1308, 2007.

[8] M. H. Napimoga, B. B. Benatti, F. O. Lima et al., "Cannabidiol decreases bone resorption by inhibiting RANK/RANKL expression and pro-inflammatory cytokines during experimental periodontitis in rats," *International Immunopharmacology*, vol. 9, no. 2, pp. 216–222, 2009.

[9] H. Fukushima, E. Jimi, F. Okamoto, W. Motokawa, and K. Okabe, "IL-1-induced receptor activator of NF-κB ligand in human periodontal ligament cells involves ERK-dependent PGE2 production," *Bone*, vol. 36, no. 2, pp. 267–275, 2005.

[10] T. Kawai, T. Matsuyama, Y. Hosokawa et al., "B and T lymphocytes are the primary sources of RANKL in the bone resorptive lesion of periodontal disease," *American Journal of Pathology*, vol. 169, no. 3, pp. 987–998, 2006.

[11] D. Liu, J. K. Xu, L. Figliomeni et al., "Expression of RANKL and OPG mRNA in periodontal disease: possible involvement in bone destruction," *International Journal of Molecular Medicine*, vol. 11, no. 1, pp. 17–21, 2003.

[12] T. Kawai, H. Shimauchi, J. W. Eastcott, D. J. Smith, and M. A. Taubman, "Antigen direction of specific T-cell clones into gingival tissues," *Immunology*, vol. 93, no. 1, pp. 11–19, 1998.

[13] T. Kawai, R. Eisen-Lev, M. Seki, J. W. Eastcott, M. E. Wilson, and M. A. Taubman, "Requirement of B7 costimulation for Th1-mediated inflammatory bone resorption in experimental periodontal disease," *Journal of Immunology*, vol. 164, no. 4, pp. 2102–2109, 2000.

[14] M. A. Taubman and T. Kawai, "Involvement of T-lymphocytes in periodontal disease and in direct and indirect induction of

bone resorption," *Critical Reviews in Oral Biology and Medicine*, vol. 12, no. 2, pp. 125–135, 2001.

[15] P. Valverde, T. Kawai, and M. A. Taubman, "Selective blockade of voltage-gated potassium channels reduces inflammatory bone resorption in experimental periodontal disease," *Journal of Bone and Mineral Research*, vol. 19, no. 1, pp. 155–164, 2004.

[16] Y. A. Teng, H. Nguyen, X. Gao et al., "Functional human T-cell immunity and osteoprotegerin ligand control alveolar bone destruction in periodontal infection," *The Journal of Clinical Investigation*, vol. 106, no. 6, pp. R59–R67, 2000.

[17] T. Kawai, B. J. Paster, H. Komatsuzawa et al., "Cross-reactive adaptive immune response to oral commensal bacteria results in an induction of receptor activator of nuclear factor-κB ligand (RANKL)-dependent periodontal bone resorption in a mouse model," *Oral Microbiology and Immunology*, vol. 22, no. 3, pp. 208–215, 2007.

[18] P. J. Baker, M. Dixon, R. T. Evans, L. Dufour, E. Johnson, and D. C. Roopenian, "CD4(+) T cells and the proinflammatory cytokines gamma interferon and interleukin-6 contribute to alveolar bone loss in mice," *Infection and Immunity*, vol. 67, no. 6, pp. 2804–2809, 1999.

[19] R. Vernal, N. Dutzan, M. Hernández et al., "High expression levels of receptor activator of nuclear factor-kappa B ligand associated with human chronic periodontitis are mainly secreted by CD4(+) T lymphocytes," *Journal of Periodontology*, vol. 77, no. 10, pp. 1772–1780, 2006.

[20] S. Kamiya, M. Okumura, Y. Chiba et al., "IL-27 suppresses RANKL expression in CD4(+) T cells in part through STAT3," *Immunology Letters*, vol. 138, no. 1, pp. 47–53, 2011.

[21] E. Gemmell, K. Yamazaki, and G. J. Seymour, "The role of T cells in periodontal disease: homeostasis and autoimmunity," *Periodontology 2000*, vol. 43, no. 1, pp. 14–40, 2007.

[22] Y. Gao, F. Grassi, M. R. Ryan et al., "IFN-γ stimulates osteoclast formation and bone loss in vivo via antigen-driven T cell activation," *The Journal of Clinical Investigation*, vol. 117, no. 1, pp. 122–132, 2007.

[23] S. L. Gaffen and G. Hajishengallis, "A new inflammatory cytokine on the block: re-thinking periodontal disease and the Th1/Th2 paradigm in the context of Th17 cells and IL-17," *Journal of Dental Research*, vol. 87, no. 9, pp. 817–828, 2008.

[24] C. R. Cardoso, G. P. Garlet, G. E. Crippa et al., "Evidence of the presence of T helper type 17 cells in chronic lesions of human periodontal disease," *Oral Microbiology and Immunology*, vol. 24, no. 1, pp. 1–6, 2009.

[25] H. Ohyama, N. Kato-Kogoe, A. Kuhara et al., "The involvement of IL-23 and the Th 17 pathway in periodontitis," *Journal of Dental Research*, vol. 88, no. 7, pp. 633–638, 2009.

[26] J. M. Kramer and S. L. Gaffen, "Interleukin-17: a new paradigm in inflammation, autoimmunity, and therapy," *Journal of Periodontology*, vol. 78, no. 6, pp. 1083–1093, 2007.

[27] J. J. Yu, M. J. Ruddy, G. C. Wong et al., "An essential role for IL-17 in preventing pathogen-initiated bone destruction: recruitment of neutrophils to inflamed bone requires IL-17 receptor-dependent signals," *Blood*, vol. 109, no. 9, pp. 3794–3802, 2007.

[28] J. J. Yu, M. J. Ruddy, H. R. Conti, K. Boonanantanasarn, and S. L. Gaffen, "The interleukin-17 receptor plays a gender-dependent role in host protection against Porphyromonas gingivalis-induced periodontal bone loss," *Infection and Immunity*, vol. 76, no. 9, pp. 4206–4213, 2008.

[29] K. Sato, A. Suematsu, K. Okamoto et al., "Th17 functions as an osteoclastogenic helper T cell subset that links T cell activation and bone destruction," *Journal of Experimental Medicine*, vol. 203, no. 12, pp. 2673–2682, 2006.

[30] C. W. O. Ernst, J. E. Lee, T. Nakanishi et al., "Diminished forkhead box P3/CD25 double-positive T regulatory cells are associated with the increased nuclear factor-κB ligand (RANKL+) T cells in bone resorption lesion of periodontal disease," *Clinical and Experimental Immunology*, vol. 148, no. 2, pp. 271–280, 2007.

[31] X. Han, T. Kawai, J. W. Eastcott, and M. A. Taubman, "Bacterial-responsive B lymphocytes induce periodontal bone resorption," *Journal of Immunology*, vol. 176, no. 1, pp. 625–631, 2006.

[32] X. Han, X. Lin, A. R. Seliger, J. Eastcott, T. Kawai, and M. A. Taubman, "Expression of receptor activator of nuclear factor-κB ligand by B cells in response to oral bacteria," *Oral Microbiology and Immunology*, vol. 24, no. 3, pp. 190–196, 2009.

[33] X. Han, T. Kawai, and M. A. Taubman, "Toll-like receptor signaling in B cell-mediated RANKL-dependent periodontitis bone resorption," in *Interface Oral Health Science 2011*, pp. 373–375, Springer Japan.

[34] T. Fumoto, S. Takeshita, M. Ito, and K. Ikeda, "Physiological functions of osteoblast lineage and T cell-derived RANKL in bone homeostasis," *Journal of Bone and Mineral Research*, 2013.

[35] G. J. Atkins, P. Kostakis, B. Pan et al., "RANKL expression is related to the differentiation state of human osteoblasts," *Journal of Bone and Mineral Research*, vol. 18, no. 6, pp. 1088–1098, 2003.

[36] T. Nakashima, M. Hayashi, T. Fukunaga et al., "Evidence for osteocyte regulation of bone homeostasis through RANKL expression," *Nature Medicine*, vol. 17, no. 10, pp. 1231–1234, 2011.

[37] J. Xiong and C. A. O'Brien, "Osteocyte RANKL: new insights into the control of bone remodeling," *Journal of Bone and Mineral Research*, vol. 27, no. 3, pp. 499–505, 2012.

[38] J. Xiong, M. Onal, R. L. Jilka, R. S. Weinstein, S. C. Manolagas, and C. A. O'Brien, "Matrix-embedded cells control osteoclast formation," *Nature Medicine*, vol. 17, no. 10, pp. 1235–1241, 2011.

[39] S. Gordon, "Pattern recognition receptors: doubling up for the innate immune response," *Cell*, vol. 111, no. 7, pp. 927–930, 2002.

[40] H. Heine and E. Lien, "Toll-like receptors and their function in innate and adaptive immunity," *International Archives of Allergy and Immunology*, vol. 130, no. 3, pp. 180–192, 2003.

[41] G. Hajishengallis, "Toll gates to periodontal host modulation and vaccine therapy," *Periodontology 2000*, vol. 51, no. 1, pp. 181–207, 2009.

[42] E. Burns, G. Bachrach, L. Shapira, and G. Nussbaum, "Cutting edge: TLR2 is required for the innate response to Porphyromonas gingivalis: activation leads to bacterial persistence and TLR2 deficiency attenuates induced alveolar bone resorption," *Journal of Immunology*, vol. 177, no. 12, pp. 8296–8300, 2006.

[43] K. Kim, M. Cho, S. Lee et al., "Human rheumatoid synovial fibroblasts promote osteoclastogenic activity by activating RANKL via TLR-2 and TLR-4 activation," *Immunology Letters*, vol. 110, no. 1, pp. 54–64, 2007.

[44] T. Ukai, H. Yumoto, F. C. Gibson III, and C. A. Genco, "Macrophage-elicited osteoclastogenesis in response to bacterial stimulation requires toll-like receptor 2-dependent tumor necrosis factor-alpha production," *Infection and Immunity*, vol. 76, no. 2, pp. 812–819, 2008.

[45] G. Rosen, M. N. Sela, R. Naor, A. Halabi, V. Barak, and L. Shapira, "Activation of murine macrophages by lipoprotein and lipooligosaccharide of Treponema denticola," *Infection and Immunity*, vol. 67, no. 3, pp. 1180–1186, 1999.

[46] G. Nussbaum, S. Ben-Adi, T. Genzler, M. Sela, and G. Rosen, "Involvement of toll-like receptors 2 and 4 in the innate immune response to Treponema denticola and its outer sheath components," *Infection and Immunity*, vol. 77, no. 9, pp. 3939–3947, 2009.

[47] N. W. J. Schröder, D. Meister, V. Wolff et al., "Chronic periodontal disease is associated with single-nucleotide polymorphisms of the human TLR-4 gene," *Genes and Immunity*, vol. 6, no. 5, pp. 448–451, 2005.

[48] M. Folwaczny, J. Glas, H.-P. Török, O. Limbersky, and C. Folwaczny, "Toll-like receptor (TLR) 2 and 4 mutations in periodontal disease," *Clinical and Experimental Immunology*, vol. 135, no. 2, pp. 330–335, 2004.

[49] M. T. Baer, N. Huang, and F. C. Gibson III, "Scavenger receptor A is expressed by macrophages in response to Porphyromonas gingivalis, and participates in TNF-α expression," *Oral Microbiology and Immunology*, vol. 24, no. 6, pp. 456–463, 2009.

[50] S. Wei, H. Kitaura, P. Zhou, F. P. Ross, and S. L. Teitelbaum, "IL-1 mediates TNF-induced osteoclastogenesis," *The Journal of Clinical Investigation*, vol. 115, no. 2, pp. 282–290, 2005.

[51] D. O' Gradaigh, D. Ireland, S. Bord, and J. E. Compston, "Joint erosion in rheumatoid arthritis: interactions between tumour necrosis factor α, interleukin 1, and receptor activator of nuclear factor κB ligand (RANKL) regulate osteoclasts," *Annals of the Rheumatic Diseases*, vol. 63, no. 4, pp. 354–359, 2004.

[52] K. Suda, N. Udagawa, N. Sato et al., "Suppression of osteoprotegerin expression by prostaglandin E2 is crucially involved in lipopolysaccharide-induced osteoclast formation," *Journal of Immunology*, vol. 172, no. 4, pp. 2504–2510, 2004.

[53] R. Assuma, T. Oates, D. Cochran, S. Amar, and D. T. Graves, "IL-1 and TNF antagonists inhibit the inflammatory response and bone loss in experimental periodontitis," *Journal of Immunology*, vol. 160, no. 1, pp. 403–409, 1998.

[54] D. T. Graves, M. Oskoui, S. Volejnikova et al., "Tumor necrosis factor modulates fibroblast apoptosis, PMN recruitment, and osteoclast formation in response to P. gingivalis infection," *Journal of Dental Research*, vol. 80, no. 10, pp. 1875–1879, 2001.

[55] Y. Xiao, C. L. Bunn, and P. M. Bartold, "Effect of lipopolysaccharide from periodontal pathogens on the production of tissue plasminogen activator and plasminogen activator inhibitor 2 by human gingival fibroblasts," *Journal of Periodontal Research*, vol. 36, no. 1, pp. 25–31, 2001.

[56] K. T. Steeve, P. Marc, T. Sandrine, H. Dominique, and F. Yannick, "IL-6, RANKL, TNF-alpha/IL-1: interrelations in bone resorption pathophysiology," *Cytokine and Growth Factor Reviews*, vol. 15, no. 1, pp. 49–60, 2004.

[57] G. P. Garlet, W. Martins Jr., B. A. L. Fonseca, B. R. Ferreira, and J. S. Silva, "Matrix metalloproteinases, their physiological inhibitors and osteoclast factors are differentially regulated by the cytokine profile in human periodontal disease," *Journal of Clinical Periodontology*, vol. 31, no. 8, pp. 671–679, 2004.

[58] R. Fujihara, M. Usui, G. Yamamoto et al., "Tumor necrosis factor-α enhances RANKL expression in gingival epithelial cells via protein kinase A signaling," *Journal of Periodontal Research*, 2013.

[59] N. Wada, H. Maeda, Y. Yoshimine, and A. Akamine, "Lipopolysaccharide stimulates expression of osteoprotegerin and receptor activator of NF-kappa B ligand in periodontal ligament fibroblasts through the induction of interleukin-1 beta and tumor necrosis factor-alpha," *Bone*, vol. 35, no. 3, pp. 629–635, 2004.

[60] T. J. Vries, T. Schoenmaker, N. Wattanaroonwong et al., "Gingival fibroblasts are better at inhibiting osteoclast formation than periodontal ligament fibroblasts," *Journal of Cellular Biochemistry*, vol. 98, no. 2, pp. 370–382, 2006.

Hindawi Publishing Corporation
BioMed Research International
Volume 2014, Article ID 297808, 8 pages
http://dx.doi.org/10.1155/2014/297808

Research Article

Comparing Microspheres with Different Internal Phase of Polyelectrolyte as Local Drug Delivery System for Bone Tuberculosis Therapy

Gang Wu,[1,2] Long Chen,[1,2] Hong Li,[3] Chun-Ling Deng,[1,2] and Xiao-Feng Chen[1,2]

[1] *School of Materials Science and Engineering, South China University of Technology, Guangzhou 510640, China*
[2] *National Engineering Center for Tissue Restoration and Reconstruction, Guangzhou 510006, China*
[3] *Department of Materials Science and Engineering, Jinan University, Guangzhou 510632, China*

Correspondence should be addressed to Gang Wu; imwugang@scut.edu.cn

Received 7 November 2013; Revised 31 December 2013; Accepted 12 January 2014; Published 23 February 2014

Academic Editor: Jiang Chang

We use hydrophobic poly(lactic-co-glycolic) acid (PLGA) to encapsulate hydrophilic ofloxacin to form drug loading microspheres. Hyaluronic acid (HA) and polylysine (Pls) were used as internal phase additives to see their influences on the drug loading and releasing. Double emulsion (water-in-oil-in-water) solvent extraction/evaporation method was used for the purpose. Particle size analysis display that the polyelectrolytes have low impact on the microsphere average size and distribution. Scanning electron microscope (SEM) pictures show the wrinkled surface resulted by the internal microcavity of the microspheres. Microspheres with HA inside have higher drug loading amounts than microspheres with Pls inside. The loading drug amounts of the microspheres increase with the HA amounts inside, while decreasing with the Pls amounts inside. All the polyelectrolytes adding groups have burst release observed in experiments. The microspheres with Pls internal phase have faster release rate than the HA groups. Among the same polyelectrolyte internal phase groups, the release rate increases with the amounts increasing when Pls is inside, while it decreases with the amounts increasing when HA is inside.

1. Introduction

Tuberculosis (TB) is a potentially fatal contagious disease which mainly affects pulmonary system. General method for the disease treating is 9 to 12 months of multidrug chemotherapy. In all diagnosed with this disease, 10 to 20 percent bone infection is reported [1, 2]. In complicated bone infection cases, infection foci debridement and internal fixation were chosen by doctors [3]. Apart from the surgery, antitubercular drug therapy was still indispensable for a time period [4, 5].

Filling the cavity after the debridement using autograft/allograft and implanted materials would remodel the defected bone and restore the function. The material implanted in the cavity after debridement serves as an "in vivo bioreactor" wherein the engineering of the neotissue is achieved by invocation of a healing response within the bioreactor space. Providing the implanted scaffold with the *in situ* drug release function is a promising drug administration mode to therapy the patients infected by bone tuberculosis. It offers a more effective method for specific site delivery, drug dosage optimizer, and release duration simultaneously with new bone regeneration [6, 7]. Furthermore, when combining the growth factors in scaffold, better recovering results are expected [8–13]. That will be very attractive for bone TB therapy in the future.

Ofloxacin has antitubercular activity and has lower hepatotoxicity than the traditional first-line antitubercular drugs (ATD). Moreover, comparing more and more TB involving strains resistant cases to the first-line ATD [14, 15], only a few cases reported the strain resistant to ofloxacin. That makes it currently the most commonly used agents against TB [16], especially for treating patients with underlying chronic liver diseases [17]. To encapsulate this drug effectively is important for the bone TB local drug release systems [18–20].

Table 1: Concentration of internal phase additives.

Internal phase	None (Wt/V%)	Group 1 (Wt/V%)	Group 2 (Wt/V%)	Group 3 (Wt/V%)
Hyaluronic acid	0	0.1	0.3	0.7
Polylysine	0	0.25	0.75	1.0

Table 2: Diameters at the particle cumulated volume ratio of 90%, 50%, and 10%.

	$D[v, 10]$ (μm)	$D[v, 50]$ (μm)	$D[v, 90]$ (μm)
None	5.24 ± 0.43	16.17 ± 1.21	45.18 ± 1.08
HA-1	6.82 ± 0.67	17.28 ± 0.68	35.13 ± 3.16
HA-2	6.75 ± 0.35	18.09 ± 0.59	39.57 ± 0.65
HA-3	7.75 ± 0.43	19.47 ± 0.27	40.06 ± 0.09
Pls-1	8.29 ± 0.81	17.74 ± 0.33	47.29 ± 1.01
Pls-2	6.90 ± 0.57	16.78 ± 1.44	50.55 ± 0.38
Pls-3	8.55 ± 0.82	18.02 ± 2.42	49.46 ± 0.67

Until now, emulsification is still the most common method for drug encapsulation [21, 22]. However, the hydrophilic ofloxacin always results in the low drug loading efficiency in hydrophobic polymeric drug carriers such as polylactide-glycoside and also faces high burst release [18, 19]. Approaches used to prevent the hydrophilic drugs partitioning to the external aqueous phase during emulsification and hardening procedure include presaturation of external phase with drug, altering the aqueous phase pH and using more water-miscible solvents [23–27]. But the efficiency of all these endeavors is still needed to be improved.

Ofloxacin is positively charged drug at the pH value of body fluid. The negatively charged polyelectrolyte would embed ofloxacin in it. Migration of the macromolecular would be more difficult than the small drug molecular during the emulsification procedure. That is hypothesized to retain more ofloxacin in the final microsphere. This would be another alternative method to improve hydrophilic drug loading efficiency.

In this paper, ofloxacin was loaded in PLGA microparticles through water-in-oil-in-water emulsification solvent evaporation technique. We were going to add the HA internal phase additives to increase the drug retaining in the microparticles. Positively charged Pls was added and none additive microspheres were also fabricated to compare the loading efficiency and to testify the hypothesis. The effects of physical adsorption and electrostatic interaction of the polyelectrolytes with the drug on final loading efficiency and release behavior would be discussed.

2. Materials and Methods

2.1. Materials. PLGA (50/50, Mn = 60000) with an intrinsic viscosity of 0.78 dL g^{-1} was purchased from Jinan Daigang Biomaterial Co. Ltd. Hyaluronic acid (HA) was purchased from Shanghai Qisheng Biological Preparation Co. Ltd. Poly-l-lysine (Pls) was purchased from Sigma. Methyl cellulose (MC) was purchased from Sinopharm Chemical Reagent Co. Ltd. Dichloromethane (DCM) was purchased from Guangzhou Chemical Reagent Factory.

2.2. Preparation of Ofloxacin Loaded Microspheres. PLGA microspheres were prepared by a water-in-oil-in-water double emulsification solvent evaporation technique as the following steps. 500 μL ofloxacin/PBS solution (10% w/v) was added into 5 mL PLGA/DCM (10%, w/v) solution and emulsified with the speed of 7200 rpm for 10 minutes using a high-speed stirrer (T10, IKA, German). Then, the primary emulsion was added into 20 mL MC solution (0.5%, w/v) and emulsified for another 10 minutes with the same speed. The emulsions were then transferred into 400 mL 35°C deionized water stirred for 4 h with the speed of 800 rpm and filtered to get the PLGA particles. Finally, The drug loading PLGA spheres were dried at 30°C for 24 hours. Table 1 displays the formulation of the control group and the HA and poly-l-lysine microspheres with different internal phase amounts added in the ofloxacin/PBS solution.

2.3. Material Characterization. The sphere size distribution was measured using a laser diffraction particle size analyzer (Mastersizer 2000, Malvern, UK). The sample was dispersed ultrasonically in deionized water with stirring speed of 2000 rpm, adding samples until an obscuration rate of 5–18% was obtained. Background and sample were measured for 12 s. Optical properties of the sample were defined as follows: refractive index 1.460 and absorption 0.00. Each sample was measured in triplicate. Span index was calculated according to

$$\text{span index} = \frac{D[v, 90] - D[v, 10]}{D[v, 50]}. \quad (1)$$

$D[v, 90]$, $D[v, 10]$, and $D[v, 50]$ are the diameters at the particle accumulated volume ratio of 90%, 50%, and 10%, respectively (Table 2).

The microsphere surface morphology was examined by an environmental SEM (quanta 200, FEI, American). The samples were observed by simply being mounted onto double-sided adhesive tape on the sample stage and with gold presputtering. The test was performed in the low vacuum model (60 Pa) at the acceleration voltage of 10 Kv.

0.5% (Wt/V) sample solution was filled in the testing cell and measured by a potential meter (Malvern Nano ZS) at the temperature of 25°C under the applied voltage of 80 V. Each sample was measured for three times to get the mean value of zeta potential.

2.4. Loading Efficiency Determination. The calibration curve was prepared at the maximum ofloxacin absorption peak of 293.8 nm before the experiment by using an ultraviolet-visible spectrophotometer (Lambda950, Perkinelmer, USA). The equation regarding the calibration curve was $y = 13.21847 * x - 0.55224$ with the $R^2 = 0.9997$. In the equation, y refers to the absorbance data read from the spectrophotometer and x is the concentration of the prepared ofloxacin solution.

Ofloxacin loading efficiency of PLGA microsphere was measured as the following steps. 0.05 g sphere samples were dissolved into 5 mL DCM. 10 mL deionized water was added into the solution to extract the ofloxacin. Then the aqueous solution with the extracted drug was measured at the 293.8 nm to determine the loading amount according to the calibration curve. Drug incorporation efficiency was expressed as in (2). The individual values for three replicate determinations and their mean values were reported:

$$\text{Loading Efficiency (\%)} = \frac{\text{mass of drug in particles}}{\text{mass of drug used in formulation}} \times 100. \quad (2)$$

2.5. Drug Release Study. 50 mg PLGA microsphere was suspended in 6 mL PBS solution. The microsphere suspensions were generally bathed in water at 37°C. At predetermined time intervals, samples were centrifuged at 2000 rpm for 5 min. 5 mL supernatant was taken for analyzing ofloxacin concentration. After this, 5 mL PBS was added in microsphere suspensions. All samples were taken in triplicate.

2.6. Particle Size and Distribution of PLGA Microsphere. Figure 1 displays the average particle size of the drug loaded PLGA microspheres without and with different varying amounts of internal polyelectrolytes. The mean particle sizes of different groups are in the range of 17 μm~20 μm. No big difference is noted among all of them, except the HA groups. The polyelectrolytes added in the internal aqueous phase would increase the aqueous phase osmatic pressure/viscosity and result in difficult aqueous dispersion and larger partial size. As that reported in the paper, the particle size depends largely on processing condition, including mixing shear force, solution mixing ratio, temperature, surfactant amount, and osmatic pressure [20]. In this paper, aqueous solution osmatic pressure of HA groups has increased, since the HA concentration in the aqueous solution resulted in relatively high osmatic pressure. It was also noticed that the solution viscosity of HA groups increased during the experiment.

Figure 2 displays the particles span index. It reflects the particle size polydispersion according to (1). The particle distribution is affected by the internal phase additives. The span index of HA internal phase group is smaller than the control

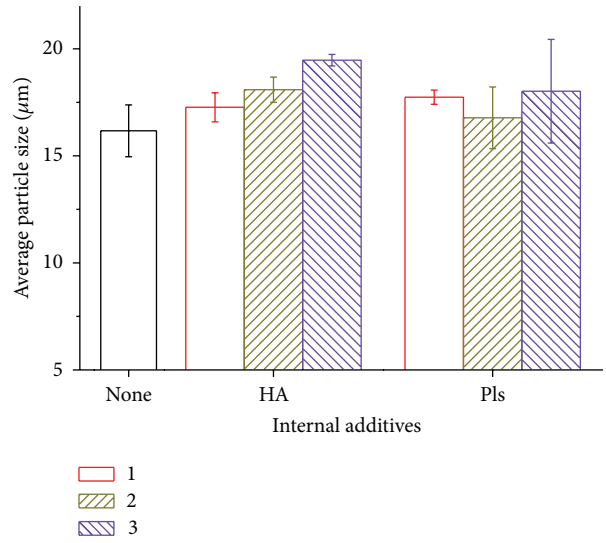

Figure 1: Average particle sizes of ofloxacin-loaded PLGA microspheres with varying amounts of internal additives.

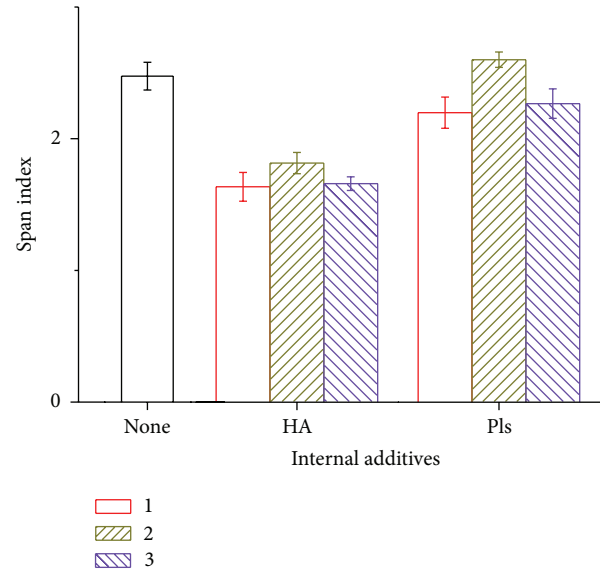

Figure 2: Span index of ofloxacin-loaded PLGA microsphere with varying amount of internal additives.

group since the HA solved inside the aqueous solution increased the viscosity and osmatic pressure. It suggested that the higher the internal phase viscosity, the more difficult for the emulsification procedure to get a wide-range microparticles. Since the viscosity of polylysine aqueous solution is not as high as HA aqueous solution, so the impact of polylysine on the particle span index is not as high as that of HA.

2.7. Morphological Examination. Figure 3 displays the surface morphology of the microparticles produced by this double emulsion and evaporation method. The surface of PLGA microsphere is smooth and without visible pores when

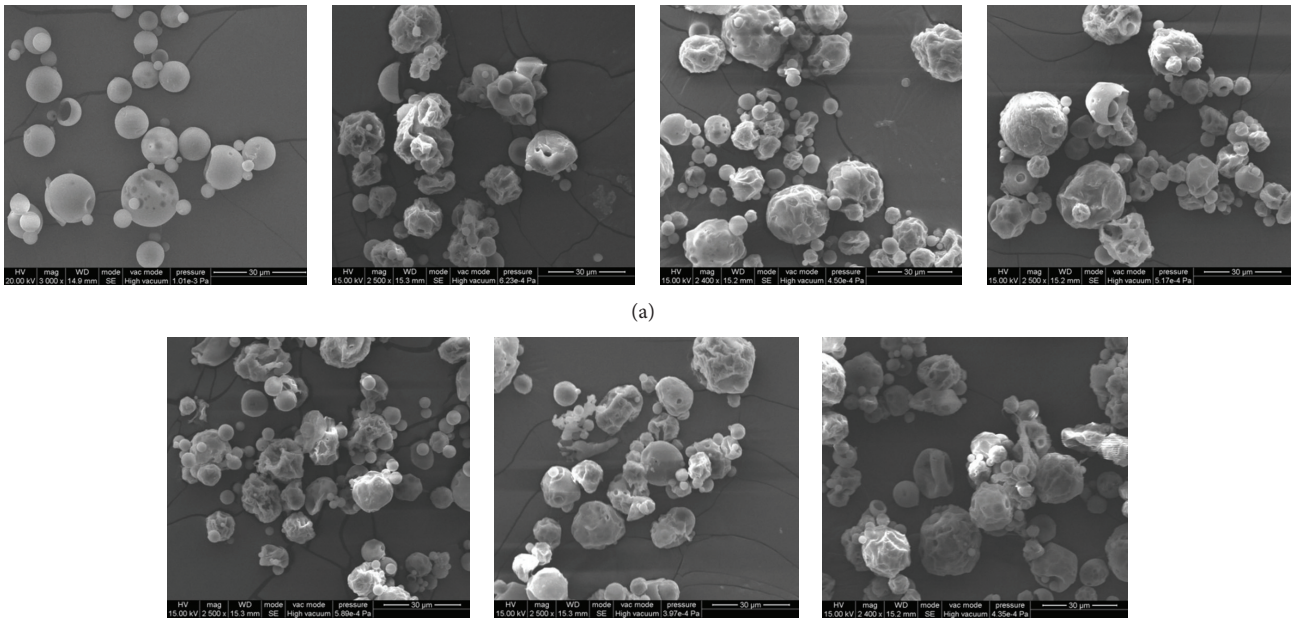

(a)

(b)

Figure 3: Surface morphology of ofloxacin-loaded microsphere ((a): none, HA-1, HA-2, and HA-3, (b): Pls-1, Pls-2, and Pls-3).

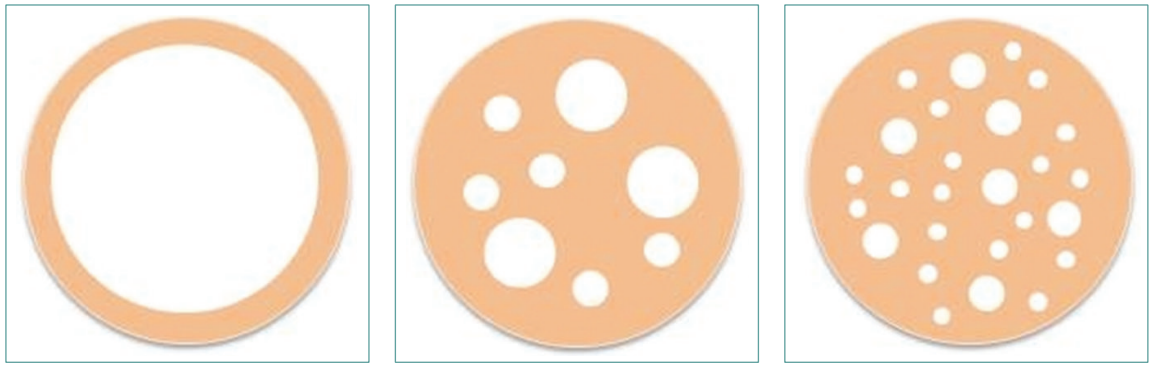

(a) (b) (c)

Figure 4: Sketch of the main type of internal morphology for microparticles.

observed by the environment SEM without gold pre-sputtering (Figure 3(a): none). But after vacuum gold sputter coating, collapsed and wrinkled surface morphology could be observed as those displayed in Figure 3. This could be resulted by the microsphere internal cavities. The internal structure varied from dense solid to empty cavity, multivesicular structure, and matrix like structure depending on the primary emulsion stability [28, 29], as that displayed in Figure 4. With those internal cavities, when the vacuum chamber ventilated after gold coating, the interior and exterior pressure imbalance of the microparticles would cause the surface collapsing. The microcavities would provide more spaces for hydrophilic drug loading. But the uncontrollable internal structure would also result in uneven loading efficiency in different batches.

2.8. Loading Efficiency. Figure 5 displays the encapsulation efficiency when HA and polylysine are added in the inner aqueous phase. Ofloxacin loading efficiency in HA internal phase group is higher than the control group and increased with its amounts inside, from 33% to 51%. This could be the reason of the interaction between the HA macromolecular and the drug. The zeta potential of the HA, polylysine, and the drug is 24 mV, 2.5 mV, and −14 mV, respectively, measured by a Malvern Nano sizer-potential meter.

HA is an acidic mucopolysaccharide. Negatively charged carboxyl groups on the HA would facilitate it to combine positively charged drugs on it through the electrostatic attraction. The entanglement of the HA molecular increases the internal phase viscosity and prevents the emigration of HA to the external aqueous solution during emulsification procedure. This helps to retain more drugs inside the internal phase.

When polylysine was added into the internal aqueous phase, the loading efficiency decreased dramatically as that in Figure 5. When the polylysine amount increased to 1%,

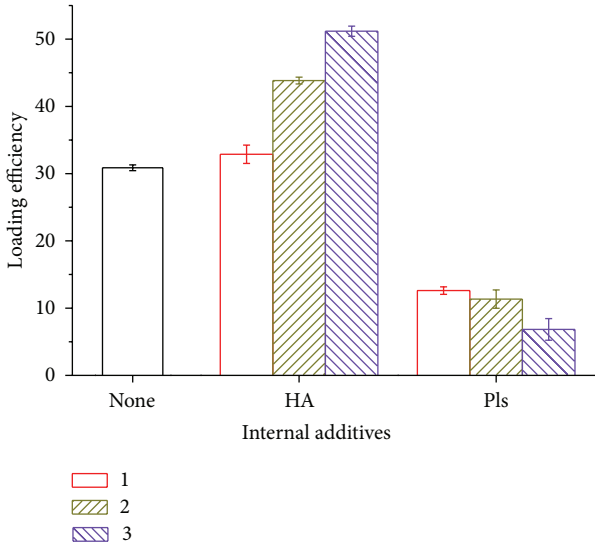

Figure 5: Loading efficiency of PLGA microsphere with varying amount of internal additives.

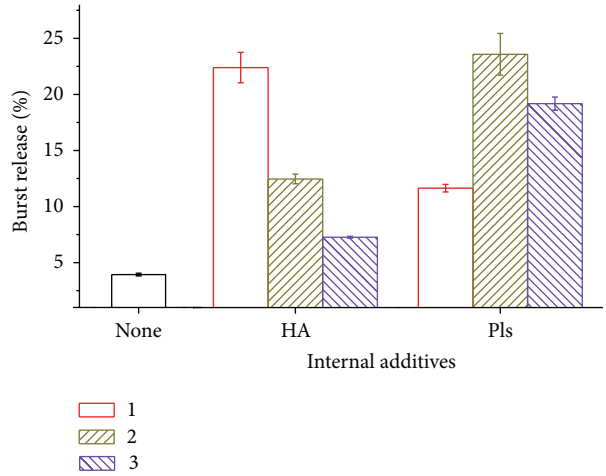

Figure 6: Burst release of PLGA microsphere with varying amount of internal additives at the first day.

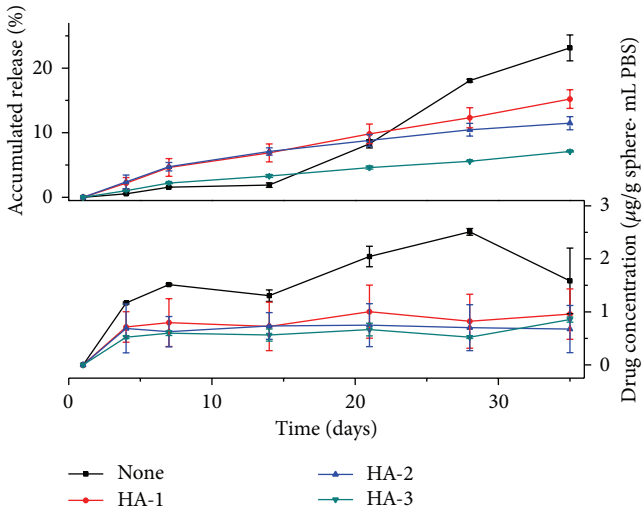

Figure 7: Release profile of ofloxacin/HA/PLGA microparticles.

ofloxacin encapsulation was decreased to 6.84% in PLGA microsphere. Besides the repulsion between the positively charged drug and the positively charged polylysine, the emulsification efficiency decreasing of the anionic surfactant MC in Pls groups could be another reason for this.

The emulsification efficiency is directly related to the macroscopical phase separation time. The macroscopical phase separation time is the time of an emulsion which becomes two phases when this could be observed by naked eye. This describes the stability of the primary emulsion. The average times of the initial macroscopic phase separation for none, HA, and Pls internal phase microsphere were 32 minutes, 67 minutes, and 12 minutes, respectively. The unstable primary emulsion of Pls group results in easier demulsification in the final microparticle formation procedure and lower drug loading efficiency. Furthermore, the electrostatic repulsion between polylysine and ofloxacin will speed the drug migration into the external aqueous solution following the demulsification.

2.9. In Vitro Release Study. Figure 6 presents the burst release of day 1. All groups with polyelectrolytes additives have the higher burst release than the control group. The burst release is mainly caused by the drug adhesive on the surface. During the microsphere fabrication procedure, the drug distributed in the external aqueous solution would be adsorbed onto the formed microspheres' surface. Furthermore, since the HA and polylysine were added in the formulation, the embedded polyelectrolytes in the microspheres would increase the surface hydrophilicity. This would result in more drug surface adsorbed on the particle.

Surface drug adsorption depends on the drug concentration in exterior aqueous solution. As we know from Figure 5, the lowest loading efficiency, the highest drug concentration in exterior aqueous solution. More drugs would be probably adsorbed on the microsphere surface. The drug adsorption and desorption are also influenced by the charged polyelectrolytes embedded in the microspheres.

Negatively charged HA would facilitate the adsorption and hindering the desorption. So, the higher HA inside the microsphere, the lower exterior drug concentration and the least burst release observed. In contrast, positively charged Pls would speed the desorption of the adsorbed drug. High burst release of the Pls groups was observed in the experiment.

Figure 7 displays the released profiles of the microparticle with different HA amounts in the internal phase for 35 days. With deduction of the burst release, the ofloxacin cumulated releases for 34 days were 15.2% of HA-1, 11.4% of HA-2, and 7.1% of HA-3, respectively. The cumulated release of the none additive microsphere was 23.1% at that time. The release speed of all the HA internal phase microspheres was slower than none additive microsphere. It was also noticed that the release speed decreased with the increase of HA amounts added into the internal phase.

Though the HA entrapped in the PLGA membrane material would improve particles' hydrophilicity and speed up PLGA degradation, a slower releasing is observed from Figure 7. That could be caused by the electrostatic attraction between the negative HA and the positive drugs. Furthermore, the slow migration of the HA from the PLGA entrapment is also retarding drug's diffusion from the capsules. The releasing speed could be controlled to be very slow as the HA contents increased to 0.7% in the internal phase by this method.

The minimum inhibitory concentration (MIC) of ofloxacin against the typical tuberculosis bacterium of mycobacterium is 1.0-2.0 μg/mL [30]. Figure 7 displays that the drug concentration in the solution is about 1.0 μg/g microsphere·mL. The drug concentration in the solution depends on two factors, the release rate and drug loading amounts in the microspheres. Though the release rate of the HA-3 internal phase group is slow, the loading amount is high; this group can still maintain the proper drug concentration in the solution.

When the microsphere is added in the tissue engineering scaffold or used directly as a microsphere scaffold, the total weight of the microsphere should be properly adjusted regarding the size of the implanting cavity.

Figure 8 presents the release pattern of the microparticles with different polylysine amounts in inner phase for 35 days. With deduction of the first-day burst release, the ofloxacin cumulated releases for 34 days are 30.1% of polylysine-1, 39.6% of polylysine-2, and 58.1% of polylysine-3, respectively. The release pattern is different as that of HA internal phase microsphere. The release speed of all polylysine internal phase microsphere is faster than none additive microsphere and the release speed increased with the increase of HA amounts added into the internal phase. The polylysine entrapped in the PLGA membrane material would improve particles' hydrophilicity and speed up PLGA degradation. In addition to that, the electrostatic repulsion between the positively charged polylysine and the positive drugs would benefit the drug diffusion to the external solution. Figure 8 displays that the drug concentration in the solution is about 1.0 μg/g microsphere·mL. The concentration falls in the MIC range. The cumulated releasing is high in this group. The total sustain releasing time is shorter than the HA internal phase microspheres.

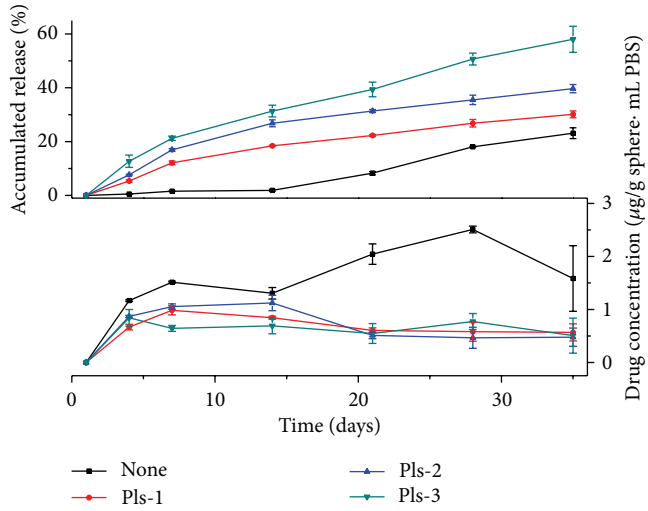

Figure 8: Release profile of ofloxacin/polylysine/PLGA microparticles.

3. Discussion

Biodegradable polylactide and polylactide-co-glycolide polymers have been widely and intensively investigated for the control release of many drugs. However, the low entrapment efficiency of hydrophilic drug by these hydrophobic polymers is still a big problem since those drugs in general have very low affinity to them. Those would result in the drugs moving from the particles to the outer aqueous phase when they were produced by emulsion methods.

Several works had been done in improving this hydrophilic drug's loading efficiency in PLGA microsphere, such as altering the emulsion stabilizer, and changing emulsification time, changing the dilution volume between aqueous and organic phase [29, 31, 32]. The most efficient method to solve this problem is to increase PLGA concentration in DCM solution. But the preparation process was hard to control since that the higher PLGA concentration in the solution would result the higher solution viscosity. And at the same time, many visible pores in the microsphere surface result in as high as 45% burst release [29].

In the future, multipurpose sustained release scaffold implanted into the cavity after surgical bone infection foci debridement should be a promising expectation for bone tuberculosis therapy. This complicated multipurpose carrier system might probably involve hydrophilic, hydrophobic, positively and negatively charged drugs, and bioactive factors. Their sustained and/or procedure releasing would be a big challenge.

In this paper, we presented the possibility that the loading efficiency and release profile could be adjusted by changing the internal phase. This provides alternatives for future sustained hydrophilic drug and protein control release besides previous methods. The method described in the paper also makes it easier for us to tailor the drug releasing profile together with the other methods to gain the best therapy effect.

4. Conclusions

We have demonstrated effects of internal phase polyelectrolytes on the encapsulation efficiency, initial burst, and release profile of the hydrophilic drug ofloxacin. Promoting hydrophilic drug loading efficiency was dominated by adsorption and electrostatic attraction between the internal phase additives and the drug. Release profile and initial burst release were a balance between the wall materials' degradation and the interactions between the internal phase additives and the drug. As for the bone tuberculosis therapy, the 0.7% HA internal phase presented the lowest initial releasing,

longest releasing time, and relatively high loading efficiency. That could be a promising regiment for that disease therapy.

The results of this research also revealed the importance of the internal phase controlling of the microparticles. When combining the controlling wall material's degradation with this method, that will be easier to fabricate a multipurpose in situ drug releasing scaffold for clinic application in the future.

Conflict of Interests

The authors declare that there is no conflict of interests regarding the publication of this paper.

Acknowledgments

The authors acknowledge the financial support by Basic Research Project of China (2012CB619105, 2011CB606204), NSFC project (51173053), National High Technology Research and Development Program of China (2011AA030105), and Guangzhou science and technology program (2012J4100124).

References

[1] I. Grosskopf, A. B. David, G. Charach, I. Hochman, and S. Pitlik, "Bone and joint tuberculosis—a 10-year review," *Israel Journal of Medical Sciences*, vol. 30, no. 4, pp. 278–283, 1994.

[2] M. Martini and M. Ouahes, "Bone and joint tuberculosis: a review of 652 cases," *Orthopedics*, vol. 11, no. 6, pp. 861–866, 1988.

[3] P. C. Jutte and J. H. Van Loenhout-Rooyackers, "Routine surgery in addition to chemotherapy for treating spinal tuberculosis," *Cochrane Database of Systematic Reviews*, no. 1, Article ID CD004532, 2006.

[4] E. E. Vogelpoel, J. J. Been, and A. A. de Gast, "Two-stage treatment of acetabular bone defect in tuberculosis of the hip by intended ankylosis followed by total hip arthroplasty: a case report," *Cases Journal*, vol. 2, article 6532, 2009.

[5] S. Ramachandran, I. J. Clifton, T. A. Collyns, J. P. Watson, and S. B. Pearson, "The treatment of spinal tuberculosis: a retrospective study," *International Journal of Tuberculosis and Lung Disease*, vol. 9, no. 5, pp. 541–544, 2005.

[6] W. Wu, Q. Zheng, X. Guo, and W. Huang, "The controlled-releasing drug implant based on the three dimensional printing technology: fabrication and properties of," *Journal Wuhan University of Technology, Materials Science Edition*, vol. 24, no. 6, pp. 977–981, 2009.

[7] W. Wu, Q. Zheng, X. Guo, J. Sun, and Y. Liu, "A programmed release multi-drug implant fabricated by three-dimensional printing technology for bone tuberculosis therapy," *Biomedical Materials*, vol. 4, no. 6, Article ID 065005, 2009.

[8] D. H. R. Kempen, L. Lu, A. Heijink et al., "Effect of local sequential VEGF and BMP-2 delivery on ectopic and orthotopic bone regeneration," *Biomaterials*, vol. 30, no. 14, pp. 2816–2825, 2009.

[9] T. N. Vo, F. K. Kasper, and A. G. Mikos, "Strategies for controlled delivery of growth factors and cells for bone regeneration," *Advanced Drug Delivery Reviews*, vol. 64, no. 12, pp. 1292–1309, 2012.

[10] X. Wang, E. Wenk, X. Zhang, L. Meinel, G. Vunjak-Novakovic, and D. L. Kaplan, "Growth factor gradients via microsphere delivery in biopolymer scaffolds for osteochondral tissue engineering," *Journal of Controlled Release*, vol. 134, no. 2, pp. 81–90, 2009.

[11] M. Lee, W. Li, R. K. Siu et al., "Biomimetic apatite-coated alginate/chitosan microparticles as osteogenic protein carriers," *Biomaterials*, vol. 30, no. 30, pp. 6094–6101, 2009.

[12] J. Zhao, M. Shinkai, T. Takezawa, S. Ohba, U. I. Chung, and T. Nagamune, "Bone regeneration using collagen type I vitrigel with bone morphogenetic protein-2," *Journal of Bioscience and Bioengineering*, vol. 107, no. 3, pp. 318–323, 2009.

[13] S. S. Kim, S. J. Gwak, and B. S. Kim, "Orthotopic bone formation by implantation of apatite-coated poly(lactide-co-glycolide)/hydroxyapatite composite particulates and bone morphogenetic protein-2," *Journal of Biomedical Materials Research A*, vol. 87, no. 1, pp. 245–253, 2008.

[14] G. B. Migliori, R. Centis, C. Lange, M. D. Richardson, and G. Sotgiu, "Emerging epidemic of drug-resistant tuberculosis in Europe, Russia, China, South America and Asia: current status and global perspectives," *Current Opinion in Pulmonary Medicine*, vol. 16, no. 3, pp. 171–179, 2010.

[15] C. Ködmön, V. Hollo, E. Huitric, A. Amato-Gauci, and D. Manissero, "Multidrug- and extensively drug-resistant tuberculosis: a persistent problem in the European union European union and European economic area," *Euro Surveillance*, vol. 15, no. 11, article 2, 2010.

[16] S. E. Berning, "The role of fluoroquinolones in tuberculosis today," *Drugs*, vol. 61, no. 1, pp. 9–18, 2001.

[17] S. Saigal, S. R. Agarwal, H. P. Nandeesh, and S. K. Sarin, "Safety of an ofloxacin-based antitubercular regimen for the treatment of tuberculosis in patients with underlying chronic liver disease: a preliminary report," *Journal of Gastroenterology and Hepatology*, vol. 16, no. 9, pp. 1028–1032, 2001.

[18] S. M. Hwang, D. D. Kim, S. J. Chung, and C. K. Shim, "Delivery of ofloxacin to the lung and alveolar macrophages via hyaluronan microspheres for the treatment of tuberculosis," *Journal of Controlled Release*, vol. 129, no. 2, pp. 100–106, 2008.

[19] S. Harsha, R. Chandramouli, and S. Rani, "Ofloxacin targeting to lungs by way of microspheres," *International Journal of Pharmaceutics*, vol. 380, no. 1-2, pp. 127–132, 2009.

[20] M. Nasr, G. A. S. Awad, S. Mansour, I. Taha, A. A. Shamy, and N. D. Mortada, "Different modalities of NaCl osmogen in biodegradable microspheres for bone deposition of risedronate sodium by alveolar targeting," *European Journal of Pharmaceutics and Biopharmaceutics*, vol. 79, no. 3, pp. 601–611, 2011.

[21] M. J. Heslinga, E. M. Mastria, and O. Eniola-Adefeso, "Fabrication of biodegradable spheroidal microparticles for drug delivery applications," *Journal of Controlled Release*, vol. 138, no. 3, pp. 235–242, 2009.

[22] V. Tran, J. Benoît, and M. Venier-Julienne, "Why and how to prepare biodegradable, monodispersed, polymeric microparticles in the field of pharmacy?" *International Journal of Pharmaceutics*, vol. 407, no. 1-2, pp. 1–11, 2011.

[23] M. Barzegar-Jalali, M. Alaei-Beirami, Y. Javadzadeh et al., "Comparison of physicochemical characteristics and drug release of diclofenac sodium-eudragit RS100 nanoparticles and solid dispersions," *Powder Technology*, vol. 219, pp. 211–216, 2012.

[24] X. Song, Y. Zhao, W. Wu et al., "PLGA nanoparticles simultaneously loaded with vincristine sulfate and verapamil hydrochloride: systematic study of particle size and drug entrapment efficiency," *International Journal of Pharmaceutics*, vol. 350, no. 1-2, pp. 320–329, 2008.

[25] L. Peltonen, J. Aitta, S. Hyvönen, M. Karjalainen, and J. Hirvonen, "Improved entrapment efficiency of hydrophilic drug substance during nanoprecipitation of poly(l)lactide nanoparticles," *AAPS PharmSciTech*, vol. 5, no. 1, article E16, 2004.

[26] W. S. Cheow and K. Hadinoto, "Enhancing encapsulation efficiency of highly water-soluble antibiotic in poly(lactic-co-glycolic acid) nanoparticles: modifications of standard nanoparticle preparation methods," *Colloids and Surfaces A*, vol. 370, no. 1-3, pp. 79–86, 2010.

[27] M. Ayoub, N. Ahmed, N. Kalaji et al., "Study of the effect of formulation parameters/variables to control the nanoencapsulation of hydrophilic drug via double emulsion technique," *Journal of Biomedical Nanotechnology*, vol. 7, no. 2, pp. 255–262, 2011.

[28] S. Mao, Y. Shi, L. Li, J. Xu, A. Schaper, and T. Kissel, "Effects of process and formulation parameters on characteristics and internal morphology of poly(d,l-lactide-co-glycolide) microspheres formed by the solvent evaporation method," *European Journal of Pharmaceutics and Biopharmaceutics*, vol. 68, no. 2, pp. 214–223, 2008.

[29] Z. Wang, "Effects of the process parameters on the initial burst release of poly(lactide-co-glycolide) microspheres containing bovine serum albumin by the double-emulsion solvent evaporation/extraction method," *Journal of Applied Polymer Science*, vol. 115, no. 5, pp. 2599–2608, 2010.

[30] A. S. Ginsburg, J. H. Grosset, and W. R. Bishai, "Fluoroquinolones, tuberculosis, and resistance," *The Lancet Infectious Diseases*, vol. 3, no. 7, pp. 432–442, 2003.

[31] Y. Y. Yang, T. S. Chung, X. L. Bai, and W. K. Chan, "Effect of preparation conditions on morphology and release profiles of biodegradable polymeric microspheres containing protein fabricated by double-emulsion method," *Chemical Engineering Science*, vol. 55, no. 12, pp. 2223–2236, 2000.

[32] N. Nihant, C. Schugens, C. Grandfils, R. Jerome, and P. Teyssie, "Polylactide microparticles prepared by double emulsion/evaporation technique. I. Effect of primary emulsion stability," *Pharmaceutical Research*, vol. 11, no. 10, pp. 1479–1484, 1994.

Hindawi Publishing Corporation
BioMed Research International
Volume 2014, Article ID 890675, 7 pages
http://dx.doi.org/10.1155/2014/890675

Research Article

The Effect of Hypoxia on the Stemness and Differentiation Capacity of PDLC and DPC

Yinghong Zhou,[1,2] Wei Fan,[3] and Yin Xiao[1,2,3]

[1] *Institute of Health and Biomedical Innovation, Queensland University of Technology, Brisbane, QLD 4059, Australia*
[2] *Australia-China Centre for Tissue Engineering and Regenerative Medicine (ACCTERM), Brisbane, QLD 4059, Australia*
[3] *The State Key Laboratory Breeding Base of Basic Science of Stomatology (Hubei-MOST) and Key Laboratory of Oral Biomedicine Ministry of Education, School and Hospital of Stomatology, Wuhan University, Wuhan 430079, China*

Correspondence should be addressed to Yin Xiao; yin.xiao@qut.edu.au

Received 14 November 2013; Accepted 8 January 2014; Published 20 February 2014

Academic Editor: Jiang Chang

Introduction. Stem cells are regularly cultured under normoxic conditions. However, the physiological oxygen tension in the stem cell niche is known to be as low as 1-2% oxygen, suggesting that hypoxia has a distinct impact on stem cell maintenance. Periodontal ligament cells (PDLCs) and dental pulp cells (DPCs) are attractive candidates in dental tissue regeneration. It is of great interest to know whether hypoxia plays a role in maintaining the stemness and differentiation capacity of PDLCs and DPCs. *Methods*. PDLCs and DPCs were cultured either in normoxia (20% O_2) or hypoxia (2% O_2). Cell viability assays were performed and the expressions of pluripotency markers (Oct-4, Sox2, and c-Myc) were detected by qRT-PCR and western blotting. Mineralization, glycosaminoglycan (GAG) deposition, and lipid droplets formation were assessed by Alizarin red S, Safranin O, and Oil red O staining, respectively. *Results*. Hypoxia did not show negative effects on the proliferation of PDLCs and DPCs. The pluripotency markers and differentiation potentials of PDLCs and DPCs significantly increased in response to hypoxic environment. *Conclusions*. Our findings suggest that hypoxia plays an important role in maintaining the stemness and differentiation capacity of PDLCs and DPCs.

1. Introduction

The regeneration of hard tissue has always been a challenging issue. Although there is a broad range of treatment options available, such as tissue transplantation [1], growth factor delivery [2], and the application of biomaterials [3, 4], the reconstitution of lost structures is still far from satisfaction. During the past decade, advances in the research of cell-based therapy have offered new insights into dental tissue regeneration [5]. Currently, PDLCs and DPCs have received intensive attention because they both possess the ability to differentiate into multiple cell types, which promote structural and functional repairs for dental tissue engineering [6]. However, despite being promising stem cell reservoir for dental tissue regeneration, PDLCs and DPCs inevitably undergo replicative senescence under current culture conditions, resulting in cellular phenotypic changes [7–9]. Therefore, maintaining the stemness of PDLCs and DPCs becomes very important for clinical application.

Recent studies suggest that stem cells are localized in the microenvironment of low oxygen [10, 11], indicating that hypoxia may be critical for stem cell maintenance. Hypoxia has been shown to regulate several cellular processes and signal transductions via hypoxia inducible factor-1 (HIF-1) [12, 13], which consists of two subunits, HIF-1α and HIF-1β. Being a hypoxia response factor, HIF-1α is regulated by the cellular oxygen (O_2) concentration and determines the transcriptional activity of HIF-1 [14]. Research on neural and hematopoietic precursors [15, 16] indicates that low O_2 tension in cell culture has positive effects on the *in vitro* survival and self-renewal of stem cells. Hypoxic microenvironment assists in maintaining the multipotent property

of embryonic stem cell (ESC) [17, 18]. On the other hand, recent reports show that differentiated cells can be reprogrammed to a more primitive state by the introduction of Oct-4, Sox2, and c-Myc and the expression of these markers is essential in maintaining the stem cell properties [19, 20]. However, the effects of hypoxia on the expression of these reprogramming markers and stemness maintenance of PDLCs and DPCs are not well illustrated. In this study, we examined the cell vitality, evaluated the expression of pluripotency markers, and assessed the differentiation potential of PDLCs and DPCs under both normoxic and hypoxic culture conditions.

2. Materials and Methods

2.1. Sample Collection and Cell Culture. Impacted third molars ($n = 6$) were collected from healthy adults (18–30 years old) after obtaining informed consent from each donor and ethics approval from the Ethics Committee of Queensland University of Technology. Periodontal ligament was gently separated from the middle third of the root surface, minced with scalpels, and rinsed with phosphate buffered saline (PBS) [21]. Dental pulp was removed from the root canal, dissected to small pieces, and rinsed with PBS [7]. The tissue explants were transferred to a primary culture dish and supplemented with low glucose Dulbecco's Modified Eagle Medium (DMEM; Life Technologies Pty Ltd., Australia) containing 10% fetal bovine serum (FBS; *In Vitro* Technologies, Australia) and 1% penicillin/streptomycin (P/S; Life Technologies Pty Ltd., Australia) at 37°C in 5% CO_2. After reaching 80% confluence, cells were passaged and replated in cell culture flasks. Cell characterization for PDLCs and DPCs has been carried out in our previous study [21]. For hypoxic exposure, cells were cultured in a hypoxic chamber flushed with 2% O_2 and 5% CO_2, with balance of 93% N_2 at 37°C [22].

2.2. Evaluation of Cell Proliferation. PDLCs and DPCs were cultured in 96-well plates either in normoxia (20% O_2) or hypoxia (2% O_2) at an initial density of 4×10^3 cells per well. On days 1, 3, and 7, 20 μL of 3-(4,5-dimethylthiazol-2-yl)-2,5-diphenyltetrazolium bromide (MTT) solution (0.5 mg/mL; Sigma-Aldrich, Australia) was added to each well and incubated at 37°C. The supernatants were removed after 4 h and replaced with 100 μL dimethyl sulfoxide (DMSO) to solubilize the MTT-formazan product. The absorbance was measured at a wavelength of 495 nm with a microplate reader (SpectraMax, Plus 384, Molecular Devices, Inc., USA).

2.3. Osteogenic Differentiation. Osteogenic induction was stimulated using growth medium (low glucose DMEM with 10% FBS and 1% P/S) containing 10 mM β-glycerophosphate (Sigma-Aldrich, Australia), 50 μM ascorbic acid (Sigma-Aldrich, Australia), and 100 nM dexamethasone (Sigma-Aldrich, Australia). After two weeks of culture in normoxia (20% O_2) or hypoxia (2% O_2), the osteogenically inducted cells were fixed with methanal and the presence of calcium nodules was assessed by Alizarin red S staining.

2.4. Chondrogenic Differentiation. PDLCs and DPCs were chondrogenically differentiated by culturing in high cell density through pellet culture (2×10^5 cells per pellet) in 500 μL chondrogenic differentiation medium. Serum-free chondrogenic differentiation medium consisted of high glucose DMEM supplemented with 10 ng/mL of transforming growth factor-β3 (TGF-β3; R&D Systems, Australia), 10 nM dexamethasone, 50 mg/mL of ascorbic acid, 10 mg/mL of sodium pyruvate (Sigma-Aldrich, Australia), 10 mg/mL of proline (Sigma-Aldrich, Australia), and an insulin-transferrin-selenium supplement. Pellets were allowed to differentiate under 3-dimensional conditions in 15 mL centrifuge tubes at 2% or 20% O_2 tension. After 3 weeks of chondrogenic differentiation, the pellets were fixed with 4% paraformaldehyde (PFA) and embedded in paraffin. Blocks were cut into 5 μm sections and GAG was detected using Safranin O staining.

2.5. Adipogenic Differentiation. Adipogenic differentiation was induced by replacing medium with high glucose DMEM containing 10% FBS, 1% P/S, 0.5 mM isobutylmethylxanthine (Sigma-Aldrich, Australia), 200 μM indomethacin (Sigma-Aldrich, Australia), 1 μM dexamethasone, and 10 μg/mL insulin (Sigma-Aldrich, Australia). After completion of 3 cycles of adipogenic induction [23], cells were kept in adipogenic maintenance medium (10 μg/mL insulin in high glucose DMEM with 10% FBS and 1% P/S) for three weeks, with change of medium every 3 days. After this, cells were washed with PBS, fixed with 4% PFA, and stained with Oil red O to detect the lipid droplets within the differentiated cells cultured in normoxia and hypoxia.

2.6. qRT-PCR. Total RNA was extracted from PDLCs and DPCs after culturing in normoxia and hypoxia for 1 day and 1 week with TRIzol Reagent (Ambion, Life Technologies Pty Ltd., Australia). Complementary DNA was synthesized using Superscript III reverse transcriptase (Invitrogen Pty Ltd., Australia) from 1 μg total RNA following the manufacturer's instructions. qRT-PCR was performed on an ABI Prism 7300 Real-Time PCR system (Applied Biosystems, Australia) with SYBR Green detection reagent. The mRNA expression of Oct-4, Sox2, c-Myc, runt-related transcription factor 2 (Runx2), SRY-box 9 (Sox9), and peroxisome proliferator-activated receptor γ2 (PPARγ2) was assayed and normalized against glyceraldehyde 3-phosphate dehydrogenase (GAPDH) housekeeping gene. All experiments were repeated at least three times for each sample. For the calculation of fold change, $\Delta\Delta$Ct method was applied to compare mRNA expression between cells cultured in normoxia and hypoxia.

2.7. Western Blotting. Total protein was harvested by lysing the cells in a lysis buffer containing a protease inhibitor cocktail (Roche Products Pty. Ltd., Australia). The protein concentration was determined by a bicinchoninic acid (BCA) protein assay kit (Sigma-Aldrich, Australia). 10 μg of protein from each sample was separated on SDS-PAGE gels and transferred onto a nitrocellulose membrane

(Pall Corporation, USA). The membranes were incubated with primary antibodies against HIF-1α (1 : 1000, mouse anti-human, Novus Biologicals, Australia), Oct-4 (1 : 1000, mouse anti-human, Santa Cruz, Australia), Sox2 (1 : 1000, goat anti-human, Santa Cruz, Australia), c-Myc (1 : 1000, mouse anti-human, Santa Cruz, Australia), and α-Tubulin (1 : 5000, rabbit anti-human, Abcam, Australia) overnight at 4°C. The membranes were washed three times in TBST buffer and then incubated with a corresponding secondary antibody at 1 : 2000 dilutions for 1 h. The protein bands were visualized using the ECL Plus Western Blotting Detection Reagents (Thermo Fisher Scientific, Australia) and exposed on X-ray film (Fujifilm, Australia). Band intensities of HIF-1α were quantified by scanning densitometry and analysed using ImageJ software.

2.8. Statistical Analysis. Analysis was performed using SPSS software (SPSS Inc., Chicago, IL, USA). All the data were presented as means ± standard deviation (SD) and analysed using the nonparametric Wilcoxon test to distinguish the differences between the two groups (normoxic culture and hypoxic culture). A P value < 0.05 was considered statistically significant.

3. Results

3.1. Confirmation of Cellular Hypoxia. To confirm that PDLCs and DPCs metabolically respond to hypoxic culture conditions, we assessed whether HIF-1α was activated in the cells exposed to 2% O_2. As demonstrated in Figure 1(a), HIF-1α was detected in both PDLCs and DPCs after exposure to hypoxia. Quantification of the western blots showed a remarkable degradation of HIF-1α when PDLCs and DPCs were cultured in normoxia (Figure 1(b)).

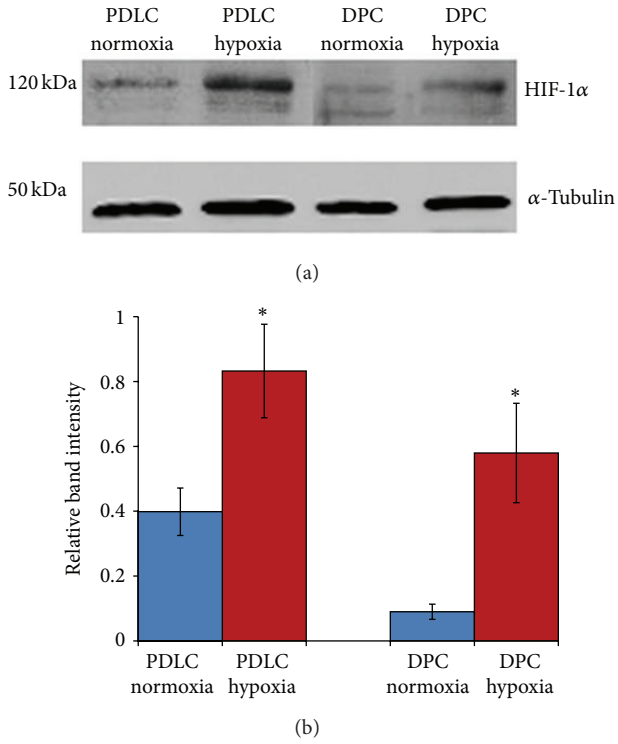

Figure 1: Confirmation of cellular hypoxia. (a) Western blotting analysis revealed degradation of HIF-1α protein in PDLCs and DPCs cultured in normoxia and stable HIF-1α protein expression in the hypoxic samples. (b) Quantification of the western blots ($^*P < 0.05$).

3.2. Effects of Hypoxia on Cell Viability. There was no significant difference in the proliferation rate of PDLCs and DPCs cultured under the normoxic and hypoxic conditions (Figures 2(a) and 2(b)). However, there was a slight upward trend of cell growth in a time-dependent manner in PDLCs and DPCs cultured in hypoxia.

3.3. Effect of Hypoxia on Stemness Maintenance. Hypoxia led to an increased level of mRNA expression of Oct-4, Sox2, and c-Myc in PDLCs and DPCs. The expression of these pluripotency markers was elevated after the cells were cultured under hypoxic conditions for 24 h (Figures 3(a) and 3(d)) and maintained a statistically significant increase on day 7 (Figures 3(b) and 3(e)). The protein expression of these markers (Oct-4, Sox2, and c-Myc) showed a similar trend of upregulation in hypoxic environment (Figures 3(c) and 3(f)).

3.4. Hypoxia Enhanced Differentiation Potential of PDLCs and DPCs. Assay of the differentiation potential of PDLCs and DPCs towards osteo-, chondro-, and adipogenic cell lineages showed considerable variation in different culture microenvironments. More calcium deposits were observed in PDLCs and DPCs after 2 weeks of osteogenic induction in hypoxia (Figures 4(b) and 4(d)) than in normoxia (Figures 4(a) and 4(c)) as revealed by Alizarin red S staining. Under chondrogenic induction, PDLCs and DPCs cultured in hypoxia showed higher staining intensity of proteoglycan-rich extracellular matrix deposition (Figures 4(f) and 4(h)). With regard to adipogenic differentiation, PDLCs and DPCs showed a larger number of clusters of lipid droplets after exposure to hypoxia (Figures 4(j) and 4(l)) than those cultured in normoxia (Figures 4(i) and 4(k)). Our qRT-PCR results showed a significant increase in the mRNA expression of Runx2 after PDLCs and DPCs were inducted towards osteogenic lineage in hypoxia (Figure 4(m)). The hypoxic treatment also led to the enhanced mRNA expression of Sox9 in PDLCs (Figure 4(n)) and PPARγ2 in DPCs (Figure 4(o)).

4. Discussion

To prevent immunological rejection and unexpected infectious diseases in regenerative therapy, one of the solutions is to use the patient's own cells. It is necessary to maximize the pluripotency of the donor cells when they are maintained in culture prior to their differentiation into a specific target lineage [24]. However, the therapeutic potential of PDLCs and

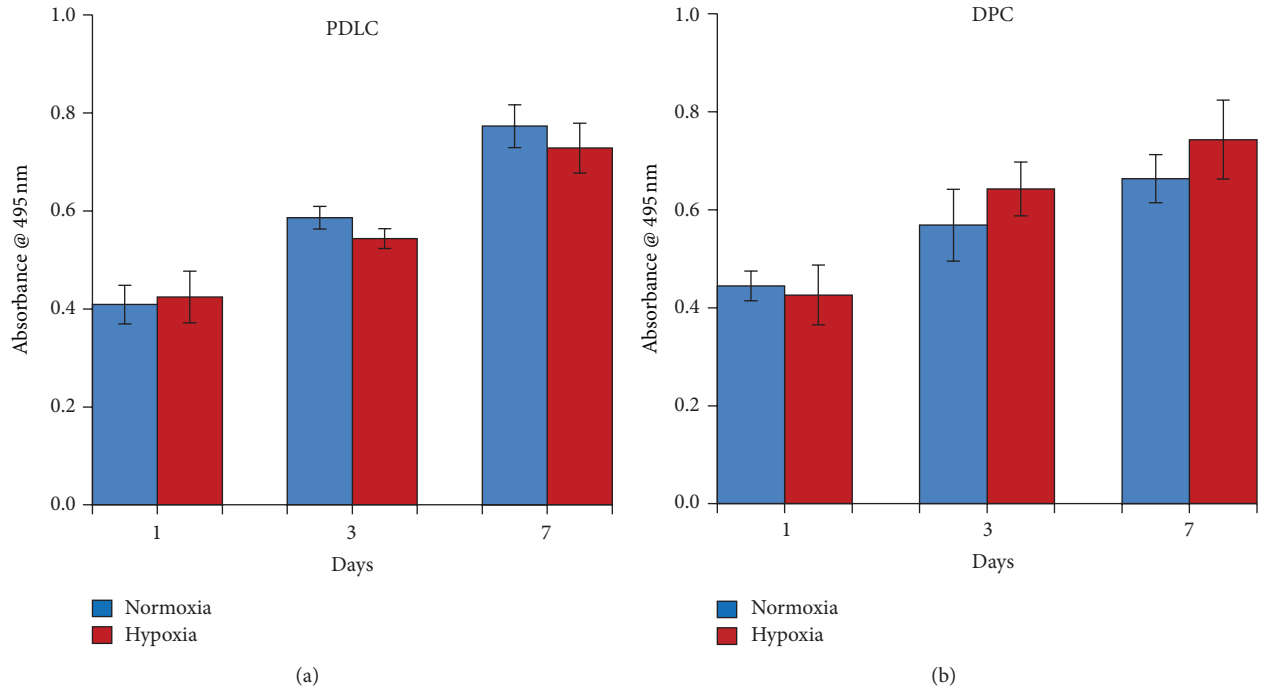

Figure 2: Cell proliferation of PDLCs and DPCs. No significant difference was observed in PDLCs (a) and DPCs (b) cultured in normoxia and hypoxia ($P > 0.05$).

DPCs is hindered by an incomplete understanding of *in vitro* culture conditions that can maintain their stemness and multipotent potential during expansion. Most of the currently identified regulators of stem cell fate are transcription factors and cell cycle regulators such as Oct-4, Sox2, and c-Myc as well as the downstream signalling pathways [25]. A recent study confirms that low oxygen level can activate Oct-4 and may act as a key inducer of a dynamic state of stemness in cancer cells [26]. Oxygen is critical for cellular energy production and metabolism. Previous studies have shown that hypoxia may induce the expression of HIF-1α, which regulates the expression of different target genes affecting the embryonic development [27], cell proliferation [28], differentiation [29], and apoptosis [30]. Recent studies have also revealed that hypoxia is related to the maintenance of undifferentiated state of stem cells in the neural crest and central nervous system [31].

In this study, PDLCs and DPCs were cultured under hypoxic conditions in 2% O_2, compared to the normal culture conditions in 20% O_2. Our results indicated that hypoxia did not negatively affect the proliferation of PDLCs and DPCs. Enhanced expression of Oct-4, Sox2, and c-Myc in PDLCs and DPCs cultured in hypoxia was observed, suggesting that low O_2 microenvironment may be necessary for triggering the expression of these stem cell markers to maintain the stem cell properties of adult PDLCs and DPCs, although the molecular signalling pathways connecting hypoxia and stemness are yet to be elucidated.

It was also shown in our study that *in vitro* hypoxic culture enhanced differentiation potential of PDLCs and DPCs as evidenced by the significantly greater amount of calcified nodules, GAG deposition, and lipid droplets formation. Furthermore, the mRNA levels of Runx2, Sox9, and PPARγ2 increased after the differentiation of PDLCs and DPCs towards different lineages. These findings suggest that 2% O_2 hypoxic treatment may promote differentiation potential of PDLCs and DPCs. Even though the mechanism by which hypoxia influences the differentiation capacity of PDLCs and DPCs is not clearly understood, it could be speculated that HIF-1α is activated in PDLCs and DPCs after exposure to hypoxia and then induces cell signalling pathways such as Wnt, Notch, and Sonic hedgehog (Shh), which help maintain the cell stemness and enhance the differentiation capacity [32, 33]. Further studies need to be conducted to clarify the molecular mechanisms behind these hypoxia-related phenomena.

5. Conclusion

The present study demonstrates that hypoxic microenvironment can maintain proliferation capacity, enhance pluripotency marker expression, and promote differentiation potential of PDLCs and DPCs. Our results indicate that effective isolation and expansion of PDLCs and DPCs under the hypoxic conditions may be a very important technique

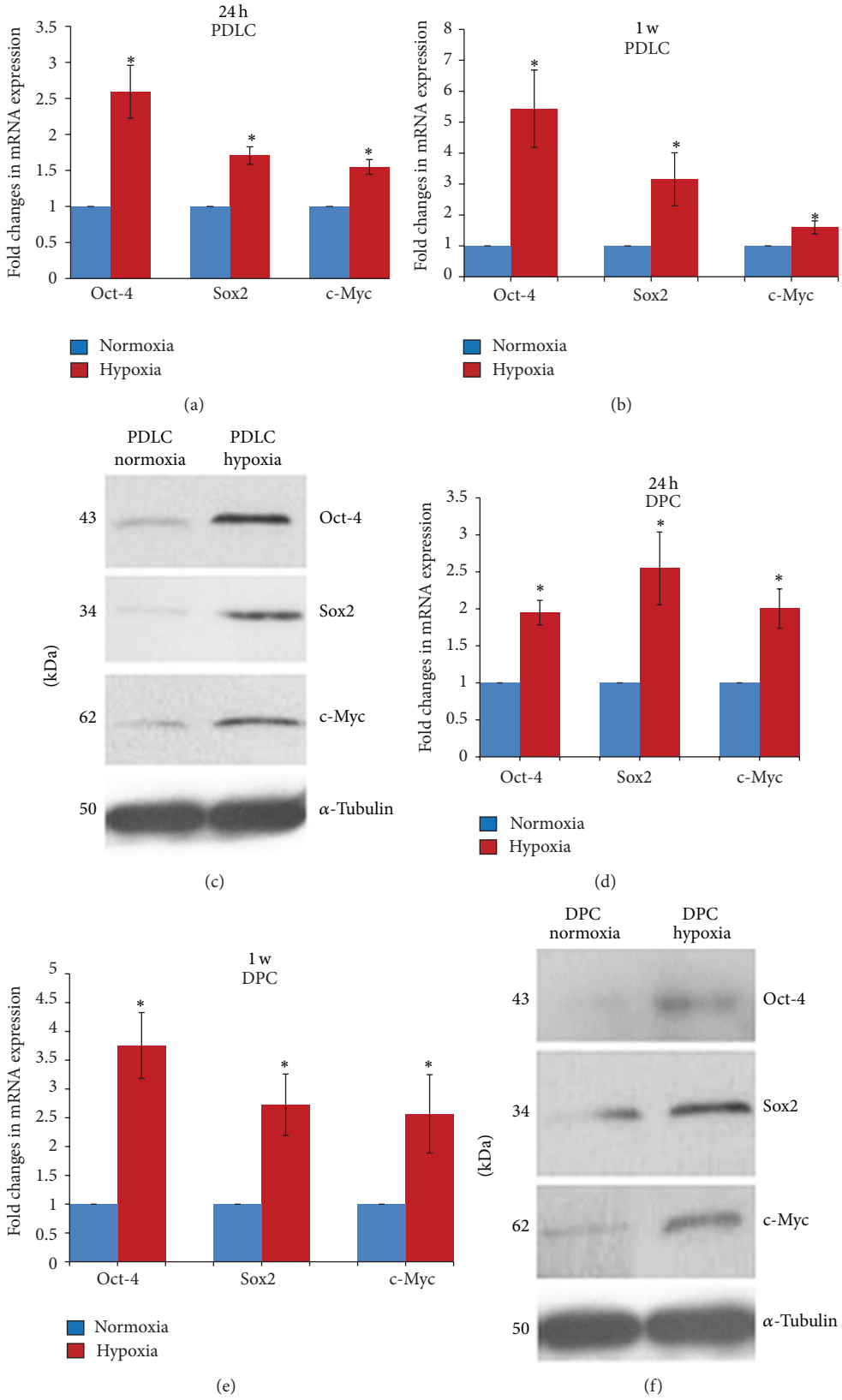

FIGURE 3: Effect of hypoxia on the mRNA expression levels of Oct-4, Sox2, and c-Myc in PDLCs and DPCs. The mRNA expressions of Oct-4, Sox2, and c-Myc in PDLCs significantly increased after exposure to 2% O_2 for 24 h (a) till 7 days (b) ($^*P < 0.05$). Western blotting analysis further confirmed the result in protein level (c). The expressions of Oct-4, Sox2, and c-Myc in DPCs cultured in hypoxia showed a similar pattern ((d)–(f)) ($^*P < 0.05$).

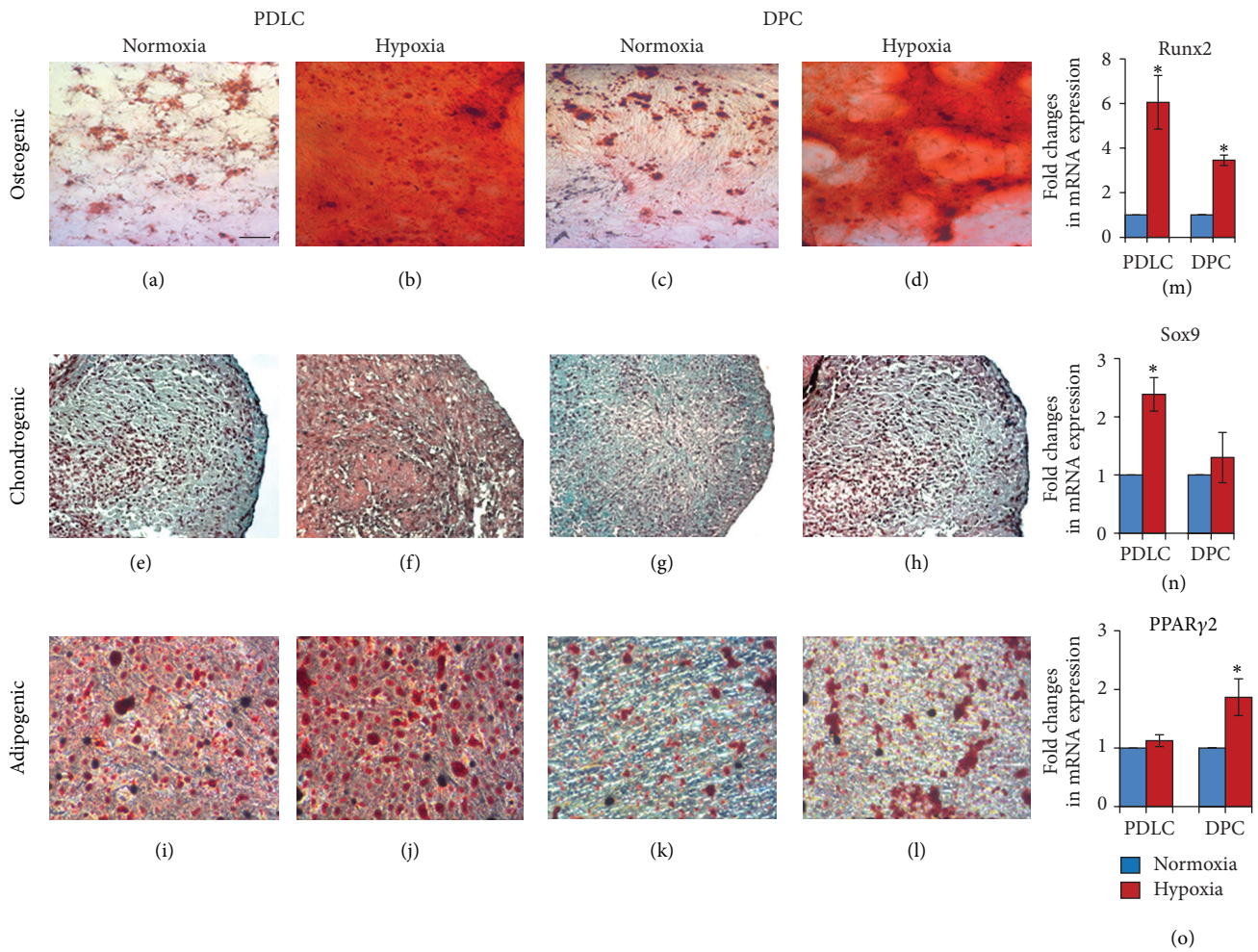

Figure 4: Effect of hypoxia on the osteogenic, chondrogenic, and adipogenic differentiation of PDLCs and DPCs. PDLCs and DPCs that have been osteogenically induced under hypoxic conditions ((b) and (d)) display strong Alizarin red S staining compared to those cultured in normoxia ((a) and (c)). Chondrogenically differentiated PDLCs and DPCs ((f) and (h)) showed higher Safranin O staining intensity when cultured in hypoxia. A larger number of lipid droplets were observed in PDLCs and DPCs after exposure to hypoxia ((j) and (l)) than those cultured in normoxia ((i) and (k)). Bar = 50 μm. The mRNA expression of Runx2, Sox9, and PPARγ2 in PDLCs and DPCs increased after differentiation towards different lineages under hypoxic conditions ((m), (n), and (o)).

for autologous cell-based therapy. Further investigation will be performed to reveal the mechanism of hypoxia in maintaining stemness and promoting differentiation potential of PDLCs and DPCs.

Conflict of Interests

The authors declare that there is no conflict of interests regarding the authorship and/or publication of this paper.

Authors' Contribution

Yinghong Zhou and Wei Fan are cofirst authors and have equal contribution to this work.

Acknowledgment

The authors wish to thank Dr. Michael Doran for his contribution to the cell culture experiment.

References

[1] M. A. Reynolds, M. E. Aichelmann-Reidy, and G. L. Branch-Mays, "Regeneration of periodontal tissue: bone replacement grafts," *Dental Clinics of North America*, vol. 54, no. 1, pp. 55–71, 2010.

[2] J. Lee, A. Stavropoulos, C. Susin, and U. M. E. Wikesjö, "Periodontal regeneration: focus on growth and differentiation factors," *Dental Clinics of North America*, vol. 54, no. 1, pp. 93–111, 2010.

[3] D. Skrtic and J. M. Antonucci, "Bioactive polymeric composites for tooth mineral regeneration: physicochemical and cellular aspects," *Journal of Functional Biomaterials*, vol. 2, no. 3, pp. 271–307, 2011.

[4] H. Zhang, S. Liu, Y. Zhou et al., "Natural mineralized scaffolds promote the dentinogenic potential of dental pulp stem cells via the mitogen-activated protein kinase signaling pathway," *Tissue Engineering A*, vol. 18, no. 7-8, pp. 677–691, 2012.

[5] T. Nakahara, "Potential feasibility of dental stem cells for regenerative therapies: stem cell transplantation and whole-tooth engineering," *Odontology*, vol. 99, no. 2, pp. 105–111, 2011.

[6] H. Ikeda, Y. Sumita, M. Ikeda et al., "Engineering bone formation from human dental pulp- and periodontal ligament-derived cells," *Annals of Biomedical Engineering*, vol. 39, no. 1, pp. 26–34, 2011.

[7] L. Liu, X. Wei, J. Ling, L. Wu, and Y. Xiao, "Expression pattern of Oct-4, sox2, and c-Myc in the primary culture of human dental pulp derived cells," *Journal of Endodontics*, vol. 37, no. 4, pp. 466–472, 2011.

[8] Y. Sawa, A. Phillips, J. Hollard, S. Yoshida, and M. W. Braithwaite, "The *in vitro* life-span of human periodontal ligament fibroblasts," *Tissue and Cell*, vol. 32, no. 2, pp. 163–170, 2000.

[9] B. J. Moxham, P. P. Webb, M. Benjamin, and J. R. Ralphs, "Changes in the cytoskeleton of cells within the periodontal ligament and dental pulp of the rat first molar tooth during ageing," *European Journal of Oral Sciences*, vol. 106, supplement 1, pp. 376–383, 1998.

[10] D. Jing, M. Wobus, D. M. Poitz, M. Bornhäuser, G. Ehninger, and R. Ordemann, "Oxygen tension plays a critical role in the hematopoietic microenvironment *in vitro*," *Haematologica*, vol. 97, no. 3, pp. 331–339, 2012.

[11] A. Mohyeldin, T. Garzón-Muvdi, and A. Quiñones-Hinojosa, "Oxygen in stem cell biology: a critical component of the stem cell niche," *Cell Stem Cell*, vol. 7, no. 2, pp. 150–161, 2010.

[12] J. Mazumdar, V. Dondeti, and M. C. Simon, "Hypoxia-inducible factors in stem cells and cancer," *Journal of Cellular and Molecular Medicine*, vol. 13, no. 11-12, pp. 4319–4328, 2009.

[13] J. D. Webb, M. L. Coleman, and C. W. Pugh, "Hypoxia, hypoxia-inducible factors (HIF), HIF hydroxylases and oxygen sensing," *Cellular and Molecular Life Sciences*, vol. 66, no. 22, pp. 3539–3554, 2009.

[14] G. L. Semenza, "Regulation of metabolism by hypoxia-inducible factor 1," *Cold Spring Harbor Symposia on Quantitative Biology*, vol. 76, pp. 347–353, 2011.

[15] J. Milosevic, S. C. Schwarz, K. Krohn, M. Poppe, A. Storch, and J. Schwarz, "Low atmospheric oxygen avoids maturation, senescence and cell death of murine mesencephalic neural precursors," *Journal of Neurochemistry*, vol. 92, no. 4, pp. 718–729, 2005.

[16] M. Vlaski, X. Lafarge, J. Chevaleyre, P. Duchez, J. Boiron, and Z. Ivanovic, "Low oxygen concentration as a general physiologic regulator of erythropoiesis beyond the EPO-related downstream tuning and a tool for the optimization of red blood cell production *ex vivo*," *Experimental Hematology*, vol. 37, no. 5, pp. 573–584, 2009.

[17] I. Szablowska-Gadomska, V. Zayat, and L. Buzanska, "Influence of low oxygen tensions on expression of pluripotency genes in stem cells," *Acta Neurobiologiae Experimentalis*, vol. 71, no. 1, pp. 86–93, 2011.

[18] S. D. Westfall, S. Sachdev, P. Das et al., "Identification of oxygen-sensitive transcriptional programs in human embryonic stem cells," *Stem Cells and Development*, vol. 17, no. 5, pp. 869–881, 2008.

[19] K. Takahashi and S. Yamanaka, "Induction of pluripotent stem cells from mouse embryonic and adult fibroblast cultures by defined factors," *Cell*, vol. 126, no. 4, pp. 663–676, 2006.

[20] J. Yu, M. A. Vodyanik, K. Smuga-Otto et al., "Induced pluripotent stem cell lines derived from human somatic cells," *Science*, vol. 318, no. 5858, pp. 1917–1920, 2007.

[21] L. Liu, J. Ling, X. Wei, L. Wu, and Y. Xiao, "Stem cell regulatory gene expression in human adult dental pulp and periodontal ligament cells undergoing odontogenic/osteogenic differentiation," *Journal of Endodontics*, vol. 35, no. 10, pp. 1368–1376, 2009.

[22] K. A. Webster, "Regulation of glycolytic enzyme RNA transcriptional rates by oxygen availability in skeletal muscle cells," *Molecular and Cellular Biochemistry*, vol. 77, no. 1, pp. 19–28, 1987.

[23] Y. Zhou, N. Chakravorty, Y. Xiao, and W. Gu, "Mesenchymal stem cells and nano-structured surfaces," *Methods in Molecular Biology*, vol. 1058, pp. 133–148, 2013.

[24] J. Rehman, "Empowering self-renewal and differentiation: the role of mitochondria in stem cells," *Journal of Molecular Medicine*, vol. 88, no. 10, pp. 981–986, 2010.

[25] A. M. Singh and S. Dalton, "The cell cycle and Myc intersect with mechanisms that regulate pluripotency and reprogramming," *Cell Stem Cell*, vol. 5, no. 2, pp. 141–149, 2009.

[26] J. Mathieu, Z. Zhang, W. Zhou et al., "HIF induces human embryonic stem cell markers in cancer cells," *Cancer Research*, vol. 71, no. 13, pp. 4640–4652, 2011.

[27] L. Bentovim, R. Amarilio, and E. Zelzer, "HIF1α is a central regulator of collagen hydroxylation and secretion under hypoxia during bone development," *Development*, vol. 139, no. 23, pp. 4473–4483, 2012.

[28] W. L. Grayson, F. Zhao, B. Bunnell, and T. Ma, "Hypoxia enhances proliferation and tissue formation of human mesenchymal stem cells," *Biochemical and Biophysical Research Communications*, vol. 358, no. 3, pp. 948–953, 2007.

[29] H. H. Lee, C. C. Chang, M. J. Shieh et al., "Hypoxia enhances chondrogenesis and prevents terminal differentiation through PI3K/Akt/FoxO dependent anti-apoptotic effect," *Scientific Reports*, vol. 3, article 2683, 2013.

[30] S. He, P. Liu, Z. Jian et al., "miR-138 protects cardiomyocytes from hypoxia-induced apoptosis via MLK3/JNK/c-jun pathway," *Biochemical and Biophysical Research Communications*, vol. 441, no. 4, pp. 763–769, 2013.

[31] V. K. Bhaskara, I. Mohanam, J. S. Rao, and S. Mohanam, "Intermittent hypoxia regulates stem-like characteristics and differentiation of neuroblastoma cells," *PLoS ONE*, vol. 7, no. 2, Article ID e30905, 2012.

[32] D. C. Genetos, C. M. Lee, A. Wong, and C. E. Yellowley, "HIF-1α regulates hypoxia-induced EP1 expression in osteoblastic cells," *Journal of Cellular Biochemistry*, vol. 107, no. 2, pp. 233–239, 2009.

[33] L. Li, Y. Zhu, L. Jiang, W. Peng, and H. H. Ritchie, "Hypoxia promotes mineralization of human dental pulp cells," *Journal of Endodontics*, vol. 37, no. 6, pp. 799–802, 2011.

Hindawi Publishing Corporation
BioMed Research International
Volume 2014, Article ID 284836, 5 pages
http://dx.doi.org/10.1155/2014/284836

Review Article

Interleukin-10 Inhibits Bone Resorption: A Potential Therapeutic Strategy in Periodontitis and Other Bone Loss Diseases

Qian Zhang,[1] Bin Chen,[1] Fuhua Yan,[1] Jianbin Guo,[2] Xiaofeng Zhu,[2] Shouzhi Ma,[2] and Wenrong Yang[3]

[1] *Institute and Hospital of Stomatology, Nanjing University Medical School, 30 Zhongyang Road, Nanjing, Jiangsu 210008, China*
[2] *School and Hospital of Stomatology, Fujian Medical University, 246 Yangqiaozhong Road, Fuzhou, Fujian 350002, China*
[3] *School of Life and Environmental Science, Waurn Ponds Campus, Deakin University, 75 Pigdons Road, Geelong, VIC 3216, Australia*

Correspondence should be addressed to Fuhua Yan; fhyan2005@126.com and Wenrong Yang; wenrong.yang@deakin.edu.au

Received 13 November 2013; Revised 5 January 2014; Accepted 5 January 2014; Published 16 February 2014

Academic Editor: Yin Xiao

Periodontitis and other bone loss diseases, decreasing bone volume and strength, have a significant impact on millions of people with the risk of tooth loss and bone fracture. The integrity and strength of bone are maintained through the balance between bone resorption and bone formation by osteoclasts and osteoblasts, respectively, so the loss of bone results from the disruption of such balance due to increased resorption or/and decreased formation of bone. The goal of therapies for diseases of bone loss is to reduce bone loss, improve bone formation, and then keep healthy bone density. Current therapies have mostly relied on long-term medication, exercise, anti-inflammatory therapies, and changing of the life style. However there are some limitations for some patients in the effective treatments for bone loss diseases because of the complexity of bone loss. Interleukin-10 (IL-10) is a potent anti-inflammatory cytokine, and recent studies have indicated that IL-10 can contribute to the maintenance of bone mass through inhibition of osteoclastic bone resorption and regulation of osteoblastic bone formation. This paper will provide a brief overview of the role of IL-10 in bone loss diseases and discuss the possibility of IL-10 adoption in therapy of bone loss diseases therapy.

1. Introduction

Bone remodeling is a dynamic lifetime process through the resorption of old bone by osteoclasts and the subsequent synthesis of new bone by osteoblasts. These two closely coupled events are responsible for renewing the skeleton while maintaining its anatomical and structural integrity. Under normal conditions, the amount of absorbed bone equals the regenerated bone; bone remodeling proceeds in recycles in which osteoclasts adhere to bone and subsequently remove it by acidification and proteolytic digestion. Once the osteoclasts leave the resorption sites, osteoblasts will migrate to the resorption sites and start forming new bone by secreting osteoid, which is eventually mineralized [1, 2].

Osteoclasts are specialized cells derived from haematopoietic lineage such as monocytes/macrophage. They develop and adhere to bone matrix and then secrete acid and lytic enzymes to degrade bone [3, 4]. The increase in number and/or activity of bone-resorbing osteoclasts could contribute to excessive bone resorption, disrupts the balance between bone resorption and bone formation, and results in the loss of bone. This may consequently lead to the following bone loss diseases: osteoporosis, rheumatoid arthritis, periodontal bone absorption, malignancy-related skeletal diseases, and so on [5–8].

Periodontitis, a bone loss disease, is a chronic inflammatory disease. As for periodontitis, destruction of connective tissue and alveolar bone can occur and finally results in the loss of teeth. Therefore, it is very critical for periodontists if we can develop a method to inhibit bone resorption and promote alveolar bone regeneration. Given the role of IL-10 in bone remodeling, the use of IL-10 for inhibiting bone

resorption and reducing inflammation may be beneficial for the treatments of periodontitis.

2. Cytokines in Bone Metabolism

It is well known that bone loss diseases are affected by inflammation, hereditary factors, hormones, aging, life style, and so on. Hence, it is imperative for us to develop other therapeutic methods to improve clinical outcome. For decades, a number of attempts have been made to achieve good prognosis for these diseases [9–11]. In particular, much attention has been paid to the importance of cytokines in the pathogenesis of bone resorption. The existing evidences suggested that various cytokines play an important role in both physiologic and pathologic bone resorption [12–14]. Numerous of cytokines exists in the bone tissue, and their functions in bone formation and resorption are still not well understood. It has been demonstrated that receptors in the proinflammatory cytokines IL-1, IL-6, and TNF-α are present on osteoclast precursor cells and mature osteoclasts [13, 15]. A breakthrough in understanding the mechanism is that cytokines regulate proliferation and differentiation of mononuclear preosteoclasts into osteoclast progenitors and fusion of the preosteoclasts into multinucleated osteoclasts [16, 17]. Zhao and coworkers showed that the receptor activator of nuclear factor κB ligand (RANKL), which was secreted by live osteocytes, promotes osteoclastogenesis [18]. Moreover, osteoprotegerin (OPG), as a soluble decoy receptor for RANKL, is also a crucial regulator of osteoclastogenesis [14, 19–22]. OPG can block osteoclastogenesis and maintain normal bone mass by binding RANKL and blocking interaction with RANK. Furthermore, *in vitro* and *in vivo* studies have shown that many cytokines elaborated by inflammation, tumor necrosis factor α (TNF-α), and IL-1 may be attributed to osteoclast differentiation and activation by regulating the production of RANKL and/or OPG [4, 7, 23].

In addition, TNF-α and IL-1 promote resorption activity of osteoclasts by increasing macrophage colony stimulating factors (M-CSF). M-CSF can bind to its receptor, c-fms, on precursor cell for differentiation via the actions of RANKL [24].

3. IL-10 and Bone Metabolism

IL-10 is a potent anti-inflammatory cytokine that suppresses both immunoproliferative and inflammatory responses. So understanding of the role of IL-10 in the bone loss diseases is essential. IL-10 was first identified at molecular level by the DNAX Research Institute [25]. As a factor produced by T helper 2 (Th2) cells, IL-10 inhibits the production of cytokines by Th1 cells [26]. IL-10 has been subsequently shown additional stimulative effects on thymocytes, B cells, and mast cells. It is well known that IL-10 is actually produced by many other cell types, including B cells, mast cells, eosinophils, macrophages, and dendritic cells (DCs), and a large number of subsets of T cells such as $CD8^+$ T cells and antigen-driven regulatory $CD4^+$ T cells [27] in mouse and human systems.

IL-10 can downregulate the synthesis of proinflammatory cytokines and chemokines, such as IL-1, IL-6, and TNF-α [28, 29]. It can also downregulate the synthesis of nitric oxide, gelatinase, and collagenase. Specific neutralization of IL-10 results in upregulating the synthesis of IL-1 and TNF-α [30, 31]. Therefore, IL-10 has been also regarded as an important regulator of bone homeostasis, in homeostatic and inflammatory conditions [32–34].

Recent studies have indicated that the polymorphisms of IL-10 gene, which may affect IL-10 production, are associated with reduced bone mineral density (BMD) in postmenopausal women who were prone to suffered from osteoporosis [35, 36]. However, serum levels of IL-10 are significantly lower in the postmenopausal osteoporotic patient than in postmenopausal healthy women [37]. The low level of IL-10 results in the insufficient inhibition of the proinflammatory cytokines and collagenase, which may have an impact on osteoporosis development [38]. Animal studies have confirmed that lack of IL-10 leads to femur bone loss [39, 40] and alveolar bone loss [33, 40, 41], providing further evidence of bone metabolism by IL-10 [39]. In the oral bone lytic diseases, such as periodontitis and periapical lesions, IL-10 has been shown as an important regulator of alveolar bone homeostasis [40, 42–44]. Herein, we speculate that IL-10 acts on the bone loss diseases based on the following criteria.

(1) IL-10 Inhibits Osteoclasts Formation. Xu and coworkers showed that IL-10 had potent inhibitory effects on osteoclastogenesis in the 1990s [45]. Others suggested IL-10 could directly inhibit osteoclast formation [46, 47]. The inhibitory effect of IL-10 on osteoclast formation through a direct action on osteoclast precursors was reported [47, 48]. Moreover, enhanced osteoclastogenesis has been observed in cultures of bone marrow macrophages deficient in IL-10 production [49]. The molecular mechanism of this inhibition indicated that IL-10 upregulated osteoprotegerin (OPG) expression but downregulated expression of the receptor activator of NF-κB ligand (RANKL) and colony-stimulating factor-1 (CSF-1) [50]. *In vitro* test showed that IL-10 may inhibit osteoclastogenesis by reducing nuclear factor of activated T cells (NFAT) c1 expression [46, 51].

Bone resorption was mediated largely by local production of proinflammatory cytokines, such as TNF-α and IL-1 [4, 17, 23, 25, 26]. These cytokines may act by directly enhancing proliferation and activity of cells in the osteoclast lineage or by indirectly affecting the production of osteoclast differentiation factors such as RANKL and OPG via osteoblast/stromal cells [4]. IL-10 has been recognized to have potent anti-inflammatory activity for a long time, and it is demonstrated to be an important endogenous suppressor of infection-stimulated bone resorption *in vivo* [52]. In conclusion, IL-10 suppresses osteoclastic differentiation via the above several aspects.

(2) IL-10 Promotes Osteoblastic Differentiation Overall. van Vlasselaer and coworkers suggested that IL-10 downregulated early steps of osteogenic differentiation in murine bone marrow cells through the inhibition of transforming growth factor-beta 1 (TGF-β1) production [53, 54]. However, Dresner-Pollak and coworkers indicated that reduced

generation of osteoblasts has been found in bone marrow cell cultures obtained from IL-10(−/−) mice, and IL-10(−/−) mice develop the hallmarks of osteoporosis, that is, decreased bone mass, increased mechanical fragility, and suppressed bone formation [39]. They also suggested that cytokines and inflammatory mediators, including TNF-α, IFN-γ, and NO, which are known to be upregulated in the IL-10(−/−) mice, had deleterious effects on the differentiation, proliferation, and function of osteoblasts [39]. The inhibitory effects in early stages of osteogenic differentiation might be neutralized eventually by the downregulation of inflammatory cytokines of infection, such as TNF-α. In other words, IL-10 enhances the osteoblastic differentiation eventually.

4. IL-10 in Periodontal Diseases and Periodontal Treatment

As an important anti-inflammatory cytokine, IL-10 plays a vital role in periodontal diseases. The lockout of IL-10 may result in accelerating alveolar bone absorption and decreasing bone formation [38–42]. Meanwhile, animal models by the IL-10 knockout mice demonstrated that the IL-10 had the anti-inflammation effect in periodontitis [43]. Currently some studies revealed that polymorphisms of IL-10 gene promoter were involved in the development of periodontal diseases. The specific genotypes (−819TT/−592AA) with low IL-10 expression may aggravate the inflammation response and cause the overgrowth of gingival [55]. The haplotype ATA of IL-10, as a "low interleukin-10 producer," was proved as a risk indicator for generalized aggressive periodontitis [56]. Moreover, others observed that these single-nucleotide polymorphisms (SNPs) of IL-10, including −1082(−1087)A/G, −819(−824)C/T and −592(−597)C/A, were associated with the generalized chronic periodontitis and/or aggressive periodontitis [57–60], which elucidates the role of IL-10 in periodontal diseases.

Smoking is well recognized as a risk factor of periodontitis, and it has been reported that smokers are several times more likely to suffer from periodontitis than nonsmokers [61]. Ebersole and coworkers indicated that smoking may cause the remarkable Th2 response and the elevating of IL-10 [62, 63], suggesting that the periodontitis could be worse by smoking.

Applications of IL-10 have been explored by several animal models [38–41, 64–66]; further evidences are still needed in the future study.

5. Future Perspective

Diseases of the bone loss are severely influencing quality of people's health and life. As IL-10 can contribute to the maintenance of bone mass by inhibition of osteoclastic bone resorption and stimulation of osteoblastic bone formation, we hypothesize that utility of IL-10 will be a novel therapeutic strategy in bone loss diseases. It might especially be an attractive treatment option for inflammation-related bone loss, such as periodontal diseases, periapical lesions, and inflammatory bowel disease. The use of IL-10 will be helpful to accelerate the healing process of fracture and enhance osseointegration with dental implantation in osteoporotic subjects.

6. Conclusions

The strategy of inhibiting osteoclastogenesis and enhancing osteoblastic differentiation can be beneficial for the treatment of bone loss diseases. Given the fact that IL-10 can inhibit bone loss, the use of IL-10 will be an effective therapeutic method for periodontitis and other bone loss diseases. We expect that IL-10 protein therapy could be tested by examining bone loss in ligature-induced periodontitis and bone turnover in ovariectomized rats. The strategies presented in this review can facilitate the future research on IL-10 in bone loss diseases.

Conflict of Interests

The authors declare that there is no conflict of interests regarding the publication of this paper.

Authors' Contribution

Qian Zhang and Bin Chen contributed equally to this work.

Acknowledgments

This study was supported by the Key Project of Science and Technology Bureau of Jiangsu Province (no. BL2013002) and the International Cooperation Research and Develop Project of Nanjing Health Bureau (no. 201303051).

References

[1] N. A. Sims and J. H. Gooi, "Bone remodeling: multiple cellular interactions required for coupling of bone formation and resorption," *Seminars in Cell and Developmental Biology*, vol. 19, no. 5, pp. 444–451, 2008.

[2] K. Henriksen, A. V. Neutzsky-Wulff, L. F. Bonewald, and M. A. Karsdal, "Local communication on and within bone controls bone remodeling," *Bone*, vol. 44, no. 6, pp. 1026–1033, 2009.

[3] K. Redlich and J. S. Smolen, "Inflammatory bone loss: pathogenesis and therapeutic intervention," *Nature Reviews Drug Discovery*, vol. 11, no. 3, pp. 234–250, 2012.

[4] W. J. Boyle, W. S. Simonet, and D. L. Lacey, "Osteoclast differentiation and activation," *Nature*, vol. 423, no. 6937, pp. 337–342, 2003.

[5] D. L. Cochran, "Inflammation and bone loss in periodontal disease," *Journal of Periodontology*, vol. 79, no. 8, pp. 1569–1576, 2008.

[6] R. E. Coleman, A. Lipton, G. D. Roodman et al., "Metastasis and bone loss: advancing treatment and prevention," *Cancer Treatment Reviews*, vol. 36, no. 8, pp. 615–620, 2010.

[7] S. Karmakar, J. Kay, and E. M. Gravallese, "Bone Damage in rheumatoid arthritis: mechanistic insights and approaches to prevention," *Rheumatic Disease Clinics of North America*, vol. 36, no. 2, pp. 385–404, 2010.

[8] T. M. Post, S. C. L. M. Cremers, T. Kerbusch, and M. Danhof, "Bone physiology, disease and treatment: towards disease system analysis in osteoporosis," *Clinical Pharmacokinetics*, vol. 49, no. 2, pp. 89–118, 2010.

[9] J. C. Gallagher and A. J. Sai, "Molecular biology of bone remodeling: implications for new therapeutic targets for osteoporosis," *Maturitas*, vol. 65, no. 4, pp. 301–307, 2010.

[10] R. Hardy and M. S. Cooper, "Bone loss in inflammatory disorders," *Journal of Endocrinology*, vol. 201, no. 3, pp. 309–320, 2009.

[11] S. Roux, "New treatment targets in osteoporosis," *Joint Bone Spine*, vol. 77, no. 3, pp. 222–228, 2010.

[12] S. Ehnert, J. Baur, A. Schmitt et al., "TGF-β1 as possible link between loss of bone mineral density and chronic inflammation," *PLoS ONE*, vol. 5, no. 11, Article ID e14073, 2010.

[13] G. Girasole, G. Passeri, R. L. Jilka, and S. C. Manolagas, "Interleukin-11: a new cytokine critical for osteoclast development," *Journal of Clinical Investigation*, vol. 93, no. 4, pp. 1516–1524, 1994.

[14] E. M. McCoy, H. X. Hong, H. C. Pruitt et al., "IL-11 produced by breast cancer cells augments osteoclastogenesis by sustaining the pool of osteoclast progenitor cells," *BMC Cancer*, vol. 13, no. 16, pp. 1–11, 2013.

[15] R. K. McCormick, "Osteoporosis: integrating biomarkers and other diagnostic correlates into the management of bone fragility," *Alternative Medicine Review*, vol. 12, no. 2, pp. 113–145, 2007.

[16] T. Braun and J. Zwerina, "Positive regulators of osteoclastogenesis and bone resorption in rheumatoid arthritis," *Arthritis Research and Therapy*, vol. 13, no. 4, article 235, 2011.

[17] B. Zhao and L. B. Ivashkiv, "Negative regulation of osteoclastogenesis and bone resorption by cytokines and transcriptional repressors," *Arthritis Research and Therapy*, vol. 13, no. 4, article 234, 2011.

[18] S. Zhao, Y. Kato, Y. Zhang, S. Harris, S. S. Ahuja, and L. F. Bonewald, "MLO-Y4 osteocyte-like cells support osteoclast formation and activation," *Journal of Bone and Mineral Research*, vol. 17, no. 11, pp. 2068–2079, 2002.

[19] T. L. Burgess, Y.-X. Qian, S. Kaufman et al., "The ligand for osteoprotegerin (OPGL) directly activates mature osteoclasts," *Journal of Cell Biology*, vol. 145, no. 3, pp. 527–538, 1999.

[20] N. Nakagawa, M. Kinosaki, K. Yamaguchi et al., "RANK is the essential signaling receptor for osteoclast differentiation factor in osteoclastogenesis," *Biochemical and Biophysical Research Communications*, vol. 253, no. 2, pp. 395–400, 1998.

[21] H. Yasuda, N. Shima, N. Nakagawa et al., "Osteoclast differentiation factor is a ligand for osteoprotegerin/ osteoclastogenesis-inhibitory factor and is identical to TRANCE/RANKL," *Proceedings of the National Academy of Sciences of the United States of America*, vol. 95, no. 7, pp. 3597–3602, 1998.

[22] H. Yasuda, N. Shima, N. Nakagawa et al., "Identity of osteoclastogenesis inhibitory factor (OCIF) and osteoprotegerin (OPG): a mechanism by which OPG/OCIF inhibits osteoclastogenesis in vitro," *Endocrinology*, vol. 139, no. 3, pp. 1329–1337, 1998.

[23] K. Kobayashi, N. Takahashi, E. Jimi et al., "Tumor necrosis factor α stimulates osteoclast differentiation by a mechanism independent of the ODF/RANKL-RANK interaction," *Journal of Experimental Medicine*, vol. 191, no. 2, pp. 275–285, 2000.

[24] N. Udagawa, N. Takahashi, T. Akatsu et al., "Origin of osteoclasts: mature monocytes and macrophages are capable of differentiating into osteoclasts under a suitable microenvironment prepared by bone marrow-derived stromal cells," *Proceedings of the National Academy of Sciences of the United States of America*, vol. 87, no. 18, pp. 7260–7264, 1990.

[25] D. F. Fiorentino, M. W. Bond, and T. R. Mosmann, "Two types of mouse T helper cell—IV. Th2 clones secrete a factor that inhibits cytokine production by Th1 clones," *Journal of Experimental Medicine*, vol. 170, no. 6, pp. 2081–2095, 1989.

[26] S. Pestka, C. D. Krause, and D. Sarkar, "Interleukin-10 and related cytokines and receptors," *Annual Review of Immunology*, vol. 22, pp. 929–979, 2004.

[27] A. O'Garra, F. J. Barrat, A. G. Castro, A. Vicari, and C. Hawrylowicz, "Strategies for use of IL-10 or its antagonists in human disease," *Immunological Reviews*, vol. 223, no. 1, pp. 114–131, 2008.

[28] Y. Houri-Hoddod, W. A. Soskolne, A. Halabi, and L. Shapira, "IL-10 gene transfer attenuates *P. gingivalis*-induced inflammation," *Journal of Dental Research*, vol. 86, no. 6, pp. 560–564, 2007.

[29] D. M. Mosser and X. Zhang, "Interleukin-10: new perspectives on an old cytokine," *Immunological Reviews*, vol. 226, no. 1, pp. 205–218, 2008.

[30] L. Wieten, S. E. Berlo, C. B. ten Brink et al., "IL-10 is critically involved in mycobacterial HSP70 induced suppression of proteoglycan-induced arthritis," *PLoS ONE*, vol. 4, no. 1, Article ID e4186, 2009.

[31] I. Marinou, J. Healy, D. Mewar et al., "Association of interleukin-6 and interleukin-10 genotypes with radiographic damage in rheumatoid arthritis is dependent on autoantibody status," *Arthritis and Rheumatism*, vol. 56, no. 8, pp. 2549–2556, 2007.

[32] S. F. Lee, E. Andrian, E. Rowland, and I. C. Marquez, "Immune response and alveolar bone resorption in a mouse model of Treponema denticola infection," *Infection and Immunity*, vol. 77, no. 2, pp. 694–698, 2009.

[33] A. Al-Rasheed, H. Scheerens, D. M. Rennick, H. M. Fletcher, and D. N. Tatakis, "Accelerated alveolar bone loss in mice lacking interleukin-10," *Journal of Dental Research*, vol. 82, no. 8, pp. 632–635, 2003.

[34] E. E. Carmody, E. M. Schwarz, J. E. Puzas, R. N. Rosier, and R. J. O'Keefe, "Viral interleukin-10 gene inhibition of inflammation, osteoclastogenesis, and bone resorption in response to titanium particles," *Arthritis and Rheumatism*, vol. 46, no. 5, pp. 1298–1308, 2002.

[35] H.-Y. Chen, W.-C. Chen, C.-M. Hsu, F.-J. Tsai, and C.-H. Tsai, "Tumor necrosis factor α, CYP 17, urokinase, and interleukin 10 gene polymorphisms in postmenopausal women: correlation to bone mineral density and susceptibility to osteoporosis," *European Journal of Obstetrics Gynecology and Reproductive Biology*, vol. 122, no. 1, pp. 73–78, 2005.

[36] L. P. Byung, K. H. In, S. L. Ho et al., "Association of interleukin 10 haplotype with low bone mineral density in Korean postmenopausal women," *Journal of Biochemistry and Molecular Biology*, vol. 37, no. 6, pp. 691–699, 2004.

[37] A. Gür, A. Denli, K. Nas et al., "Possible pathogenetic role of new cytokines in postmenopausal osteoporosis and changes during calcitonin plus calcium therapy," *Rheumatology International*, vol. 22, no. 5, pp. 194–198, 2002.

[38] S. L. Cohen, A. M. Moore, and W. E. Ward, "Interleukin-10 knockout mouse: a model for studying bone metabolism during intestinal inflammation," *Inflammatory Bowel Diseases*, vol. 10, no. 5, pp. 557–563, 2004.

[39] R. Dresner-Pollak, N. Gelb, D. Rachmilewitz, F. Karmeli, and M. Weinreb, "Interleukin 10-deficient mice develop osteopenia,

decreased bone formation, and mechanical fragility of long bones," *Gastroenterology*, vol. 127, no. 3, pp. 792–801, 2004.

[40] M. Claudino, T. P. Garlet, C. R. B. Cardoso et al., "Down-regulation of expression of osteoblast and osteocyte markers in periodontal tissues associated with the spontaneous alveolar bone loss of interleukin-10 knockout mice," *European Journal of Oral Sciences*, vol. 118, no. 1, pp. 19–28, 2010.

[41] A. Al-Rasheed, H. Scheerens, A. K. Srivastava, D. M. Rennick, and D. N. Tatakis, "Accelerated alveolar bone loss in mice lacking interleukin-10: late onset," *Journal of Periodontal Research*, vol. 39, no. 3, pp. 194–198, 2004.

[42] A. de Rossi, L. B. Rocha, and M. A. Rossi, "Interferon-gamma, interleukin-10, Intercellular adhesion molecule-1, and chemokine receptor 5, but not interleukin-4, attenuate the development of periapical lesions," *Journal of Endodontics*, vol. 34, no. 1, pp. 31–38, 2008.

[43] H. Sasaki, Y. Okamatsu, T. Kawai, R. Kent, M. Taubman, and P. Stashenko, "The interleukin-10 knockout mouse is highly susceptible to Porphyromonas gingivalis-induced alveolar bone loss," *Journal of Periodontal Research*, vol. 39, no. 6, pp. 432–441, 2004.

[44] X. Zhang and Y.-T. A. Teng, "Interleukin-10 inhibits gram-negative-microbe-specific human receptor activator of NF-κB ligand-positive $CD4^+$-Th1-cell-associated alveolar bone loss in vivo," *Infection and Immunity*, vol. 74, no. 8, pp. 4927–4931, 2006.

[45] L. X. Xu, T. Kukita, A. Kukita, T. Otsuka, Y. Niho, and T. Iijima, "Interleukin-10 selectively inhibits osteoclastogenesis by inhibiting differentiation of osteoclast progenitors into preosteoclast-like cells in rat bone marrow culture system," *Journal of Cellular Physiology*, vol. 165, no. 3, pp. 624–629, 1995.

[46] K. E. Evans and S. W. Fox, "Interleukin-10 inhibits osteoclastogenesis by reducing NFATc1 expression and preventing its translocation to the nucleus," *BMC Cell Biology*, vol. 8, article 4, 2007.

[47] A. C. Lovibond, S. J. Haque, T. J. Chambers, and S. W. Fox, "TGF-β-induced SOCS3 expression augments TNF-α-induced osteoclast formation," *Biochemical and Biophysical Research Communications*, vol. 309, no. 4, pp. 762–767, 2003.

[48] M. H. Hong, H. Williams, C. H. Jin, and J. W. Pike, "The inhibitory effect of interleukin-10 on mouse osteoclast formation involves novel tyrosine-phosphorylated proteins," *Journal of Bone and Mineral Research*, vol. 15, no. 5, pp. 911–918, 2000.

[49] H.-H. Shin, J.-E. Lee, E. A. Lee, S. K. Byoung, and H.-S. Choi, "Enhanced osteoclastogenesis in 4-1BB-deficient mice caused by reduced interleukin-10," *Journal of Bone and Mineral Research*, vol. 21, no. 12, pp. 1907–1912, 2006.

[50] D. Liu, S. Yao, and G. E. Wise, "Effect of interleukin-10 on gene expression of osteoclastogenic regulatory molecules in the rat dental follicle," *European Journal of Oral Sciences*, vol. 114, no. 1, pp. 42–49, 2006.

[51] S. G.-K. Mohamed, E. Sugiyama, K. Shinoda et al., "Interleukin-10 inhibits RANKL-mediated expression of NFATc1 in part via suppression of c-Fos and c-Jun in RAW264.7 cells and mouse bone marrow cells," *Bone*, vol. 41, no. 4, pp. 592–602, 2007.

[52] H. Sasaki, L. Hou, A. Belani et al., "IL-10, but not IL-4, suppresses infection-stimulated bone resorption in vivo," *Journal of Immunology*, vol. 165, no. 7, pp. 3626–3630, 2000.

[53] P. van Vlasselaer, B. Borremans, R. Van den Heuvel, U. Van Gorp, and R. De Waal Malefyt, "Interleukin-10 inhibits the osteogenic activity of mouse bone marrow," *Blood*, vol. 82, no. 8, pp. 2361–2370, 1993.

[54] P. van Vlasselaer, B. Borremans, U. Van Gorp, J. R. Dasch, and R. De Waal-Malefyt, "Interleukin 10 inhibits transforming growth factor-β (TGF-β) synthesis required for osteogenic commitment of mouse bone marrow cells," *Journal of Cell Biology*, vol. 124, no. 4, pp. 569–577, 1994.

[55] Y. X. Luo, Y. M. Gong, and Y. C. Yu, "Interleukin-10 gene promoter polymorphisms are associated with cyclosporin A-induced gingival overgrowth in renal transplant patients," *Archives of Oral Biology*, vol. 58, no. 9, pp. 1199–1207, 2013.

[56] S. Reichert, H. K. G. MacHulla, J. Klapproth et al., "The interleukin-10 promoter haplotype ATA is a putative risk factor for aggressive periodontitis," *Journal of Periodontal Research*, vol. 43, no. 1, pp. 40–47, 2008.

[57] A. Atanasovska-Stojanovska, D. Trajkov, and M. Popovska, "IL10-1082, IL10-819 and IL10-592 polymorphisms are associated with chronic periodontitis in a Macedonian populationw," *Human Immunology*, vol. 73, no. 7, pp. 753–758, 2012.

[58] S. M. Jaradat, K. T. Ababneh, S. A. Jaradat et al., "Association of interleukin-10 gene promoter polymorphisms with chronic and aggressive periodontitis," *Oral Diseases*, vol. 18, no. 3, pp. 271–279, 2012.

[59] C. M. Albuquerque, A. J. Cortinhas, F. J. Morinha et al., "Association of the IL-10 polymorphisms and periodontitis: a meta-analysis," *Molecular Biology Reports*, vol. 39, no. 10, pp. 9319–9329, 2012.

[60] Q. F. Zhong, C. Ding, M. L. Wang et al., "Interleukin-10 gene polymorphisms and chronic/aggressive periodontitis susceptibility: a meta-analysis based on 14 case-control studies," *Cytokine*, vol. 60, no. 1, pp. 47–54, 2012.

[61] T. Fiorini, M. L. Musskopf, R. V. Oppermann et al., "Is there a positive effect of smoking cessation on periodontal health? A systematic review," *Journal of Periodontology*, vol. 85, no. 1, pp. 83–91, 2014.

[62] J. R. Gonzales, J. Michel, A. Diete et al., "Effects of smoking on the ex vivo cytokine production in periodontitis," *Journal of Periodontal Research*, vol. 44, no. 1, pp. 28–34, 2009.

[63] J. L. Ebersole, M. J. Steffen, M. V. Thomas et al., "Smoking-related cotinine levels and host responses in chronic periodontitis," *Journal of Periodontal Research*, 2013.

[64] N. W. D. Jansen, G. Roosendaal, M. J. J. Hooiveld et al., "Interleukin-10 protects against blood-induced joint damage," *British Journal of Haematology*, vol. 142, no. 6, pp. 953–961, 2008.

[65] M. E. R. Meegeren, G. Roosendaal, K. Coeleveld et al., "A single intra-articular injection with IL-4 plus IL-10 ameliorates blood-induced cartilage degeneration in haemophilic mice," *British Journal of Haematology*, vol. 160, no. 4, pp. 512–520, 2013.

[66] M. E. R. Meegeren, G. Roosendaal, N. W. Jansen et al., "IL-4 alone and in combination with IL-10 protects against blood-induced cartilage damage," *Osteoarthritis Cartilage*, vol. 20, no. 7, pp. 764–772, 2012.

Hindawi Publishing Corporation
BioMed Research International
Volume 2014, Article ID 316134, 7 pages
http://dx.doi.org/10.1155/2014/316134

Research Article

Association between Postmenopausal Osteoporosis and Experimental Periodontitis

Kai Luo,[1] Souzhi Ma,[1] Jianbin Guo,[1] Yongling Huang,[1] Fuhua Yan,[2] and Yin Xiao[3]

[1] *School and Hospital of Stomatology, Fujian Medical University, 246 Yangqiao Zhong Road, Fuzhou, Fujian 350002, China*
[2] *Institute and Hospital of Stomatology, Nanjing University Medical School, 30 Zhongyang Road, Nanjing, Jiangsu 210008, China*
[3] *Institute of Health and Biomedical Innovation, Queensland University of Technology, Brisbane, QLD 4059, Australia*

Correspondence should be addressed to Fuhua Yan; fhyan2005@126.com

Received 12 November 2013; Accepted 24 December 2013; Published 10 February 2014

Academic Editor: Mei Wei

To investigate the correlation between postmenopausal osteoporosis (PMO) and the pathogenesis of periodontitis, ovariectomized rats were generated and the experimental periodontitis was induced using a silk ligature. The inflammatory factors and bone metabolic markers were measured in the serum and periodontal tissues of ovariectomized rats using an automatic chemistry analyzer, enzyme-linked immunosorbent assays, and immunohistochemistry. The bone mineral density of whole body, pelvis, and spine was analyzed using dual-energy X-ray absorptiometry and image analysis. All data were analyzed using SPSS 13.0 statistical software. It was found that ovariectomy could upregulate the expression of interleukin- (IL-)6, the receptor activator of nuclear factor-κB ligand (RANKL), and osteoprotegerin (OPG) and downregulate IL-10 expression in periodontal tissues, which resulted in progressive alveolar bone loss in experimental periodontitis. This study indicates that changes of cytokines and bone turnover markers in the periodontal tissues of ovariectomized rats contribute to the damage of periodontal tissues.

1. Introduction

Periodontitis is a chronic and destructive disease of the periodontium caused by various factors such as periodontal pathogens; it is commonly characterized by inflammation of periodontal tissue and alveolar bone absorption [1].

Osteoporosis is a systematic, bone metabolism-related disease with bone loss and destruction of fine bone structures that increases bone fragility and the risk of fracture. It is extremely common among the elderly, particularly in postmenopausal women. Postmenopausal osteoporosis (PMO) is osteoporosis that occurs after menopause because of the decrease in estrogen. The ovariectomized rat is a useful animal model for the study of osteoporotic bone related diseases caused by estrogen deficiency. This model exhibits a progressive loss of bone matrix through a process similar to what occurs during PMO [2, 3].

Epidemiologic research shows that chronic periodontitis is related to osteoporosis. Several studies have already indicated that insufficient estrogen is closely related to periodontitis and osteoporosis. Recently, an increasing number of researchers suggest that PMO promotes periodontitis [4–6]. It has been demonstrated that periodontal bacteria promote the alveolar bone loss in periodontitis. The invasion of periodontal bacteria may reduce bone density and enhance osteoclastic activity by releasing toxins and/or inflammatory cytokines [1]. These cytokines believed to be involved in alveolar bone remodeling are also highly expressed in PMO [7]. Since estrogen inhibits the expression of the inflammatory cytokines, it might be that larger amounts of these cytokines are presented in an inflammatory alveolar bone with estrogen deficiency. Therefore, estrogen deficiency may contribute to the alveolar bone absorption in periodontal disease, either by reducing the bone mass of alveolar bone or by causing increased expression of inflammatory cytokines. However, the underlying mechanisms are still not clear.

The homeostasis of bone tissues is controlled by the dynamic balance between osteoblastic bone formation and osteoclastic bone resorption. An imbalance between these cell activities contributes to various bone metabolic diseases. Osteoclast activation and maturation are regulated by three recently discovered proteins: the receptor activator of

nuclear factor-κB (RANK), RANK ligand (RANKL), and osteoprotegerin (OPG) [8, 9]. The binding of RANKL to RANK on preosteoclasts initiates the differentiation and proliferation of these cells and promotes osteoclast fusion and activation. Moreover, the activation of the RANKL-RANK pathway suppresses osteoclast apoptosis, thereby increasing the number of activated osteoclasts. On the other hand, OPG inhibits this pathway by binding to RANKL. Thus, the aforementioned proteins play essential roles in the development and maintenance of bone tissues [10, 11].

During the past decade, considerable evidence suggests that estrogen prevents bone loss by blocking the production of proinflammatory cytokines, such as interleukin-1 (IL-1), IL-6, IL-10, tumor necrosis factor- (TNF-) α in bone marrow and bone cells [12, 13]. The main consequence of increased cytokine production in the bone microenvironment is expansion of the osteoclastic pool because of increased osteoclast formation and their extended lifespan. To investigate the potential mechanism of PMO in periodontitis initiation and progression, we investigated the correlation between PMO and the pathogenesis of periodontitis in rats under estrogen deficiency (ovariectomy). The expression of IL-1β, IL-6, IL-10, TNF-α, OPG, RANKL, and MMP-8 in periodontal tissues, with or without osteoporosis, was analyzed using enzyme-linked immunosorbent assays and immunohistochemistry.

2. Materials and Methods

2.1. Animals. All animal care and study protocols were approved by the Animal Care and Use Committee of Fujian Medical University. A total of 24 three-month-old female Sprague-Dawley (SD) rats (220–260 g) were purchased from an animal resource centre (SLAC Laboratory Animal Co. Ltd., Shanghai, China). The rats were maintained in an animal room with 12 h day-night cycles, an ambient temperature of 22 ± 2°C. Food and water were provided *ad libitum*.

2.2. Surgical Protocols. Anesthesia was achieved through intramuscular injection of 4 : 1 ketamine-xylazine solution at 0.15 mL/100 g body weight. Bilateral ovariectomy was performed in 12 rats as previously described [14]. Sham surgeries were performed in other 12 rats when the ovaries were exposed but not removed. The rats were randomly divided into four groups: Group I ($n = 6$), sham-operated (SHAM); Group II ($n = 6$), ovariectomy (OVX); Group III ($n = 6$), SHAM + experimental periodontitis (EP); Group IV ($n = 6$), OVX + EP. At 10 weeks after surgery, EP was induced by placing 4-0 sterile silk ligatures around the cervix of the left upper second molar in Groups III and IV.

2.3. Tissue and Serum Preparation. At 2 weeks after ligation, all rats were euthanized using an overdose of anesthetic. Blood samples were taken after euthanizing the rats. The serum was separated by centrifugation for 5 min at 3,000 rpm. The samples of the three molars including the left maxillary were dissected, fixed for 48 h using 4% paraformaldehyde in phosphate-buffered saline (PBS) at 4°C, decalcified, dehydrated, and then embedded in paraffin blocks.

2.4. Measurement of Bone Mineral Density. At 2 weeks after ligation, all rats were euthanized through an overdose of anesthetic. The dual-energy X-ray absorptiometry (DEXA) was used to measure the bone mineral density (BMD) of the whole body, the pelvis, and the spine.

2.5. Measurement of Alveolar Bone Loss. Alveolar bone loss was evaluated using the following indices: (*A*) the area of the periodontal ligament in the root furcation of the upper second molar, with a vertical distance of 1 mm to the top of the furcation; (*B*) the distance from the cement-enamel junction (CEJ) to the alveolar bone crest (ABC) within the placement zone of the ligature and the contralateral zone. Figure 1 shows the method of these measurement indices and the results were analyzed using Image-pro Plus 6.0 (Image-pro Plus, Media Cybernetics, Inc., USA).

2.6. Enzyme-Linked Immunosorbent Assays. The serum levels of BAP, TRAP 5b, IL-1β, TNF-α, and IL-6 were assayed by enzyme-linked immunosorbent assay techniques using commercial kits (R&D Systems, Minneapolis, MN, USA), according to the manufacturers' recommendations. Each serum cytokine was determined through its optical density, recorded at 450 nm using a microplate spectrophotometer.

2.7. Immunohistochemical Analysis. Tissue sections (5 μm) were prepared for immunohistochemical study. After deparaffinization and rehydration, the sections were heated in citrate buffer using a pressure cooker to unmask the antigenicity of antigens masked by aldehyde fixation. They were then washed with PBS and treated with 3% hydrogen peroxide for 10 min to block endogenous peroxidase activity. The sections were incubated for 60 min at room temperature with primary antibodies: goat polyclonal anti-IL-6 (SC-1265; Santa Cruz Biotechnology, Inc., Santa Cruz, CA, USA), goat polyclonal anti-RANKL (SC-7628; Santa Cruz Biotechnology, Inc., Santa Cruz, CA, USA), goat polyclonal anti-OPG (SC-8468; Santa Cruz Biotechnology, Inc., Santa Cruz, CA, USA), rabbit polyclonal anti-IL-1β (SC-7884, Santa Cruz Biotechnology, Inc., Santa Cruz, CA, USA), rabbit polyclonal anti-TNF-α (SC-8301, Santa Cruz Biotechnology, Inc., Santa Cruz, CA, USA), rabbit polyclonal anti-MMP-8 (2145-1, Epitomics Inc., Epitomics, CA, USA), or rabbit polyclonal anti-IL-10 (bs-0698R, Beijing Biosynthesis Biotechnology, Beijing, China). After washing in PBS, the sections were incubated for 15 min at room temperature with one of the following secondary antibodies: HRP polymer anti-rabbit (KIT-5004, Maixin-Bio, Fuzhou, China) to detect IL-1β, TNF-α, MMP-8, and IL-10 positive cells. Samples used to detect IL-6, RANKL, and OPG were incubated for 10 min with biotinylated rabbit antigoat immunoglobulin (KIT-9709, Maixin-Bio, Fuzhou, China) and then incubated for 15 min with peroxidaseconjugated streptavidin at room temperature. After washing in PBS and visualizing using 3,3-diaminobenzidine for 5 min, all the sections were counterstained with hematoxylin for 20 s and then rinsed in running water. Finally, the sections were dehydrated in ascending concentrations of alcohol, cleared with xylene, and

Table 1: BMD values of whole body, pelvis and spine in four groups.

Groups	Whole body (g/cm^2)	Pelvis (g/cm^2)	Spine (g/cm^2)
SHAM	0.173 ± 0.005	0.170 ± 0.004	0.158 ± 0.005
OVX	0.155 ± 0.008*	0.154 ± 0.008*	0.143 ± 0.008*
SHAM + EP	0.170 ± 0.005	0.168 ± 0.005	0.159 ± 0.006
OVX + EP	0.157 ± 0.010**	0.153 ± 0.011**	0.138 ± 0.008**

Values are expressed as means ± SEM; $n = 6$.
$^*P < 0.05$ versus SHAM rats, $^{**}P < 0.05$ versus SHAM + EP rats.

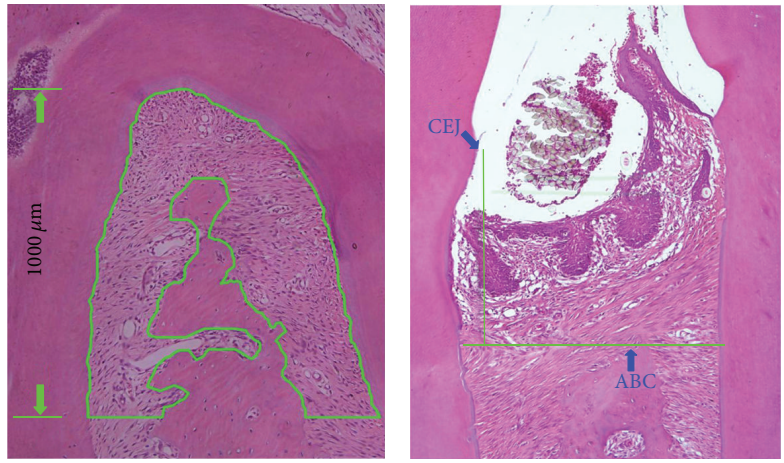

(a) (b)

Figure 1: Quantitative analysis of alveolar bone loss. (a) The area enclosed by the green line represents alveolar bone absorption in upper second molar; (b) the distance from CEJ to ABC represents alveolar bone absorption. CEJ: cemento-enamel junction; ABC: alveolar bone crest.

Table 2: Comparison of alveolar bone loss in different groups.

Groups	Area of the periodontal ligament in the root furcation (mm^2)	Distance from the CEJ to the ABC (mm)
SHAM	0.25 ± 0.05	0.46 ± 0.03
OVX	0.33 ± 0.07*	0.69 ± 0.06*
SHAM + EP	0.35 ± 0.10	0.71 ± 0.06
OVX + EP	0.49 ± 0.12**	0.82 ± 0.07**

Values are expressed as means ± SEM; $n = 6$.
$^*P < 0.05$ versus SHAM rats; $^{**}P < 0.05$ versus SHAM + EP rats.

then mounted. Controls for the immunostaining procedures were obtained by omitting the primary antibodies or substitution with nonspecific antibodies. The sections were evaluated by a single examiner who was blinded to the treatment assignment under a microscope (1X71, Olympus Co., Tokyo, Japan) with a camera mounted on a computer. Three selected areas (50 × 50 μm) in the furcation of each section were used to count positive stained cells.

2.8. Statistical Analysis. The quantitative data include the distance from the CEJ to the ABC, serum cytokine concentrations, the area of the periodontal ligament in the root furcation. All data were subjected to paired t-tests using SPSS 13.0 (SPSS, Chicago, IL, USA) statistical software, and differences were considered significant when $P < 0.05$.

3. Results

3.1. Changes in the Whole Body, the Pelvis, and the Spine BMD Levels. Compared with the SHAM group, the BMD of whole body, pelvis, and spine in the OVX group decreased significantly. Compared with the SHAM + EP group, the BMD values in the OVX + EP group also decreased significantly ($P < 0.05$). Table 1 shows the BMD values in the four groups.

3.2. Histometric Results of Alveolar Bone. At 12 weeks after the EP, the alveolar bone loss in the root furcation and the contralateral zone increased significantly in the ovariectomized rats (Figure 2). As shown in Table 2, the area of the periodontal ligament in the root furcation in the OVX and the OVE + EP groups was significantly bigger than that in the SHAM and SHAM + EP groups, respectively. The same trend was observed in the distance from the CEJ to the ABC.

3.3. Detection of Serum Cytokines. Twelve weeks after the EP, the serum cytokines mentioned previously except BAP were detected by enzyme-linked immunosorbent assay techniques. The activity of BAP was measured by automatic

Table 3: Detection of serum cytokines in four groups of rats.

Groups	BAP (U/L)	TRAP 5b (pg/L)	IL-1β (ng/L)	TNF-α (ng/L)	IL-6 (ng/L)
SHAM	54.8 ± 7.0	1899.2 ± 256.7	22.1 ± 4.4	229.5 ± 52.2	63.8 ± 10.0
OVX	72.5 ± 8.8*	2245.3 ± 350.3*	39.0 ± 6.7*	293.3 ± 37.8*	146.0 ± 17.4*
SHAM + EP	53.8 ± 4.2	1849.0 ± 242.6	27.3 ± 5.0	236.7 ± 55.4	77.4 ± 9.6
OVX + EP	74.7 ± 8.7**	2298.8 ± 299.1**	36.9 ± 5.2**	302.8 ± 36.8**	140.5 ± 13.23**

Values are expressed as means ± SEM; $n = 6$.
$^{*}P < 0.05$ versus SHAM rats; $^{**}P < 0.05$ versus SHAM + EP rats.

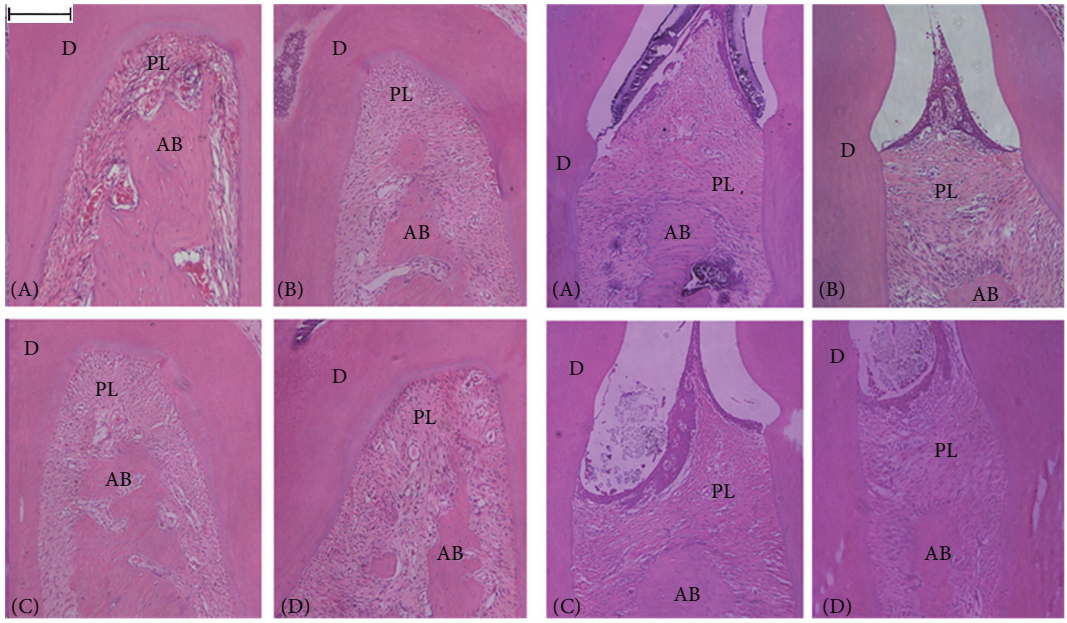

Figure 2: Histological aspect of upper second molar furcation area (a) and the distance from the CEJ to the ABC (b). A: SHAM; B: OVX; C: SHAM + EP; D: OVX + EP. D: dentine; periodontal ligament area; PL: alveolar bone AB: (H&E, Bar = 200 μm.)

Chemistry Analyzer. Increases of BAP, TRAP 5b, IL-1β, TNF-α, and IL-6 were found in the group OVX compared with that in the group SHAM. Similarly, the expression of BAP, TRAP5b, IL-1β, TNF-α and IL-6 were higher in the group OVX + EP compared with that in the group SHAM + EP (Table 3).

3.4. Immunohistochemical Expression of Cytokines. Immunohistochemical staining for IL-6, OPG, RANKL, MMP-8, and IL-10 was carried out in the periodontal tissues and, as shown in Figures 3 and 4, the number of cells positive for IL-6, OPG, RANKL, and MMP-8 in the OVX and OVX + EP groups was significantly higher than that in the SHAM and SHAM + EP groups, respectively ($P < 0.05$), whereas the number of IL-10 positive cells in the OVX and OVX + EP groups was significantly lower ($P < 0.05$) compared to that in the SHAM and SHAM + EP groups, respectively. However, no changes in immunohistochemical staining for IL-1β and TNF-α were noted between these groups.

4. Discussion

Rats are commonly used as experimental animals because the structure of periodontal tissues and the features of PMO in rats are similar to those in humans. In addition, ligation-induced periodontal tissue inflammation is an acute periodontitis model, making it a promising model for investigating the correlation between PMO and experimental periodontitis [15–17]. Tanaka et al. found that estrogen deficiency led to alveolar bone loss, high bone turnover rates, and increased bone formation and resorption [15]. These results imply that ligation-induced periodontitis in ovariectomized rats could be an ideal model for investigating the relationship between PMO and experimental periodontitis. In present study, we demonstrated that the BMD of whole body, pelvis, and spine in ovariectomized rats decreased significantly and serum concentrations of BAP and TRAP increased after ovariectomy. BAP and TRAP are well-established metabolic markers for osteoblastic bone formation and osteoclastic bone resorption, respectively [18]. In this study, elevated serum concentrations of BAP and TRAP in ovariectomized rats implied high levels of bone resorption and formation. These typical osteoporosis profiles indicated that osteoporosis model was established successfully. Moreover, the ligation-induced experimental periodontitis exacerbated alveolar bone loss, which confirms the previous studies that postmenopause is a potential risk factor in the progression of periodontitis [4–6].

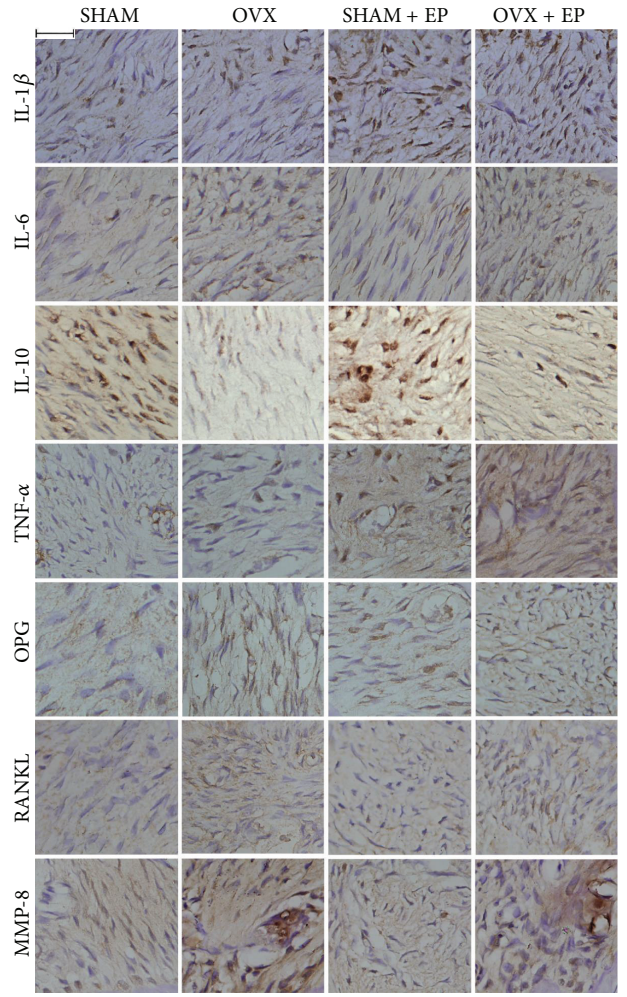

Figure 3: Immunohistochemical staining of the periodontal ligament in the root furcation of upper second molar in the four treatment groups. (Bar = 100 μm.)

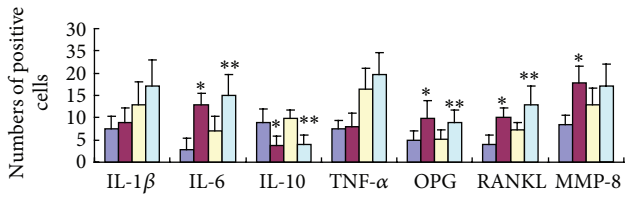

Figure 4: The number of cytokine-positive cells in the periodontal ligament in the root furcation of upper second molar in the four treatment groups under immunohistochemical staining. The blue, red, yellow, and green boxes represent the groups SHAM, OVX, SHAM + EP, and OVX + EP, respectively. $^{*}P < 0.05$ versus SHAM rats; $^{**}P < 0.05$ versus SHAM + EP rats.

Cytokines are soluble proteins which can initiate, mediate, and control immune and inflammatory responses. It has been proposed that pro- and anti-inflammatory cytokines contribute to various bone metabolic diseases including periodontitis and postmenopausal osteoporosis (PMO) [10, 12, 19–21]. Among the proinflammatory, the IL-1, IL-6, and TNF-α have been reported to present fundamental role in periodontal bone destruction [22]. In present study, we found that the serum concentrations of IL-1β, IL-6, and TNF-α increased significantly in ovariectomized rats. Elevated proinflammatory cytokines in the periodontal microenvironment increase the number of osteoclasts by promoting osteoclast precursors to differentiate into osteoclasts and extending the lifespan of osteoclasts [12, 23]. Estrogen blocks bone loss by blocking the production of proinflammatory cytokines in the bone marrow, bone cells, and periodontal ligaments. IL-1β and TNF-α are potent promoters of bone resorption and inhibitors of bone formation, and IL-6 promotes the differentiation of osteoclast precursors into osteoclast and MMP production [16, 24]. The present study showed that the serums IL-6, IL-1β, and TNF-α concentration increased significantly, but IL-1β and TNF-α in periodontal tissue were not significantly changed, which was confirmed by immunohistochemical staining. IL-1β and TNF-α are upstream cytokines that are key factors that induce the production and secretion of downstream cytokines, and their slight upregulation leads to significantly higher expression of downstream cytokines such as IL-6. On the other hand, the lipopolysaccharide (LPS) produced by normal oral flora promotes the production of proinflammatory cytokines in periodontal ligament cells, endothelial cells, monocytes, and macrophages. Therefore, estrogen deficiency upregulates the proinflammatory cytokines produced by host cells after ovariectomy.

Maintaining the balance of proinflammatory and anti-inflammatory cytokines in the body is one of the manifestations of self-regulation [25]. Proinflammatory cytokines and anti-inflammatory cytokines mediate the regulation of periodontal tissues by estrogen. Our data showed that ovariectomy decreased the IL-10 levels in periodontal tissues, which could increase the alveolar bone loss. As far as we know, this is the first study to show IL-10 expression in periodontal tissue in an animal osteoporosis model. IL-10 has been identified as an anti-inflammatory cytokine and a B cell proliferation factor, having protecting effects on periodontal tissues destruction [26]. This interleukin is critical in the initiation and progression of periodontal inflammatory [27, 28]. Clinical researches have shown that IL-10 levels in GCF are lower in periodontitis sites, whereas the expression in healthy sites is higher [29]. Furthermore, alveolar bone loss is reportedly significant in IL-10 knockout mice [30, 31]. IL-10 has been shown to exert an inhibitory on alveolar bone resorption partly through the downregulation of the expression of IL-1β, IL-6, and TNF-α [32–35]. In addition, IL-10 is also able to inhibit MMPs and RANKL expression and concomitantly induces the production of their respective inhibitors TIMPs and OPG, reinforcing its potential protective role in periodontal destruction [35].

Receptor activators of nuclear factor-κB (RANK), RANK ligand (RANKL), and osteoprotegerin (OPG) are the major regulatory proteins in osteoclastogenesis [8–11]. RANK/RANKL interactions have been shown to activate the proliferation, differentiation, multinucleation, and survival of osteoclasts. These stimulatory effects on bone resorption can be prevented by OPG, a soluble neutralizing receptor

for RANKL [11]. It is well known that OPG and RANKL are essential for regulating osteoclast differentiation, maturation, and lifespan, as well as bone resorption. They play an important role in physiologic bone reconstruction and in the pathologic processes of bone loss, such as osteoporosis and periodontal diseases [36]. Studies on RANKL and OPG expression demonstrated higher RANKL and lower OPG expression levels in periodontitis, compared to healthy gingival tissue, in line with the biological mechanisms of these molecules in bone remodelling [37, 38]. Further on, the effects of OPG on periodontal bone resorption were tested in experimental periodontitis model. In this periodontitis model, coadministration of OPG reduced alveolar bone resorption and osteoclast formation on the bone surface [39]. In present study, we observed that the expression of OPG and RANKL increased after ovariectomy, which suggests that bone turnover rate in local bone tissues increased. In addition, RANKL increased more significantly than OPG, indicating that ovariectomy increases alveolar bone resorption in the root furcation area.

IL-1, IL-6, IL-10, and TNF-α regulate the expression of OPG, RANKL, and MMP-8 in periodontal tissues [10]. It has been reported that the regulation of LPS-induced RANKL expression by estrogen probably occurs by inhibiting the upregulation of upstream proinflammatory cytokines such as IL1β, IL-6, and TNF-α, whereas the regulation of OPG by estrogen is unrelated to upstream proinflammatory cytokines [24, 34]. Whether changes in OPG, RANKL, and MMP-8 in periodontal tissues are attributed indirectly to the changes in IL1β, IL-6, and TNF-α or due to the reductions in estrogen is still unclear and further studies are required to better understand the potential mechanisms of estrogen deficiency induced periodontal destruction.

In conclusion, ovariectomy promotes alveolar bone resorption in rats with experimental periodontitis and the possible underlying mechanism may be due to the decreased IL-10 and increased IL-6, OPG, and RANKL in ovariectomized periodontal tissues.

Conflict of Interests

The authors declare no conflict of interests.

Authors' Contribution

Kai Luo and Souzhi Ma contributed equally to this work.

Acknowledgments

This work was supported by the Natural Science Foundation of China (81100761), International Cooperation Key Projects of the Science and Technology Bureau of Fujian Province (2010I0006), the Key Project of Science and Technology Bureau of Jiangsu Province (no. BL2013002), and the Talent Foundation of Institute and Hospital of Stomatology, Nanjing University Medical School (no. 2013-02-250).

References

[1] B. L. Pihlstrom, B. S. Michalowicz, and N. W. Johnson, "Periodontal diseases," *The Lancet*, vol. 366, no. 9499, pp. 1809–1820, 2005.

[2] D. L. French, J. M. Muir, and C. E. Webber, "The ovariectomized, mature rat model of postmenopausal osteoporosis: an assessment of the bone sparing effects of curcumin," *Phytomedicine*, vol. 15, no. 12, pp. 1069–1078, 2008.

[3] S. C. Miller, B. M. Bowman, and W. S. S. Jee, "Available animal models of osteopenia—small and large," *Bone*, vol. 17, no. 4, pp. 117–123, 1995.

[4] R. M. Brennan, R. J. Genco, K. M. Hovey, M. Trevisan, and J. Wactawski-Wende, "Clinical attachment loss, systemic bone density, and subgingival calculus in postmenopausal women," *Journal of Periodontology*, vol. 78, no. 11, pp. 2104–2111, 2007.

[5] A. R. Mohammad, M. Brunsvold, and R. Bauer, "The strength of association between systemic postmenopausal osteoporosis and periodontal disease," *The International Journal of Prosthodontics*, vol. 9, no. 5, pp. 479–483, 1996.

[6] M. Tezal, J. Wactawski-Wende, S. G. Grossi, A. W. Ho, R. Dunford, and R. J. Genco, "The relationship between bone mineral density and periodontitis in postmenopausal women," *Journal of Periodontology*, vol. 71, no. 9, pp. 1492–1498, 2000.

[7] U. H. Lerner, "Bone remodeling in post-menopausal osteoporosis," *Journal of Dental Research*, vol. 85, no. 7, pp. 584–595, 2006.

[8] D. L. Lacey, E. Timms, H.-L. Tan et al., "Osteoprotegerin ligand is a cytokine that regulates osteoclast differentiation and activation," *Cell*, vol. 93, no. 2, pp. 165–176, 1998.

[9] Y.-Y. Kong, H. Yoshida, I. Sarosi et al., "OPGL is a key regulator of osteoclastogenesis, lymphocyte development and lymph-node organogenesis," *Nature*, vol. 397, no. 6717, pp. 315–323, 1999.

[10] T. Miyazaki, T. Matsunaga, S. Miyazaki, S. Hokari, and T. Komoda, "Changes in receptor activator of nuclear factor-kappaB, and its ligand, osteoprotegerin, bone-type alkaline phosphatase, and tartrate-resistant acid phosphatase in ovariectomized rats," *Journal of Cellular Biochemistry*, vol. 93, no. 3, pp. 503–512, 2004.

[11] D. Cappellen, N.-H. Luong-Nguyen, S. Bongiovanni, O. Grenet, C. Wanke, and M. Mira Šuša, "Transcriptional program of mouse osteoclast differentiation governed by the macrophage colony-stimulating factor and the ligand for the receptor activator of NFκB," *The Journal of Biological Chemistry*, vol. 277, no. 24, pp. 21971–21982, 2002.

[12] S. C. Manolagas and R. L. Jilka, "Bone marrow, cytokines, and bone remodeling—emerging insights into the pathophysiology of osteoporosis," *The New England Journal of Medicine*, vol. 332, no. 5, pp. 305–311, 1995.

[13] R. B. Kimble, S. Srivastava, F. P. Ross, A. Matayoshi, and R. Pacifici, "Estrogen deficiency increases the ability of stromal cells to support murine osteoclastogenesis via an interleukin-1- and tumor necrosis factor-mediated stimulation of macrophage colony-stimulating factor production," *The Journal of Biological Chemistry*, vol. 271, no. 46, pp. 28890–28897, 1996.

[14] Z. Du, J. Chen, F. Yan, and Y. Xiao, "Effects of Simvastatin on bone healing around titanium implants in osteoporotic rats," *Clinical Oral Implants Research*, vol. 20, no. 2, pp. 145–150, 2009.

[15] M. Tanaka, S. Ejiri, E. Toyooka, S. Kohno, and H. Ozawa, "Effects of ovariectomy on trabecular structures of rat alveolar bone," *Journal of Periodontal Research*, vol. 37, no. 2, pp. 161–165, 2002.

[16] S. M. Han, T. E. Szarzanowicz, and I. Ziv, "Effect of ovariectomy and calcium deficiency on the ultrasound velocity, mineral density and strength in the rat femur," *Clinical Biomechanics*, vol. 13, no. 7, pp. 480–484, 1998.

[17] A. Kuhr, A. Popa-Wagner, H. Schmoll, C. Schwahn, and T. Kocher, "Observations on experimental marginal periodontitis in rats," *Journal of Periodontal Research*, vol. 39, no. 2, pp. 101–106, 2004.

[18] D. Modrowski and P. J. Marie, "Cells isolated from the endosteal bone surface of adult rats express differentiated osteoblastic characteristics in vitro," *Cell and Tissue Research*, vol. 271, no. 3, pp. 499–505, 1993.

[19] G. P. Garlet, C. R. Cardoso, T. A. Silva et al., "Cytokine pattern determines the progression of experimental periodontal disease induced by *Actinobacillus actinomycetemcomitans* through the modulation of MMPs, RANKL, and their physiological inhibitors," *Oral Microbiology and Immunology*, vol. 21, no. 1, pp. 12–20, 2006.

[20] R. Pacifi, "Editorial: cytokines, estrogen, and postmenopausal osteoporosis—the second decade," *Endocrinology*, vol. 139, no. 6, pp. 2659–2661, 1998.

[21] M. Mogi, J. Otogoto, N. Ota, H. Inagaki, M. Minami, and K. Kojima, "Interleukin 1β, interleukin 6, β2-microglobulin, and transforming growth factor-α in gingival crevicular fluid from human periodontal disease," *Archives of Oral Biology*, vol. 44, no. 6, pp. 535–539, 1999.

[22] D. Graves, "Cytokines that promote periodontal tissue destruction," *Journal of Periodontology*, vol. 79, no. 8, pp. 1585–1591, 2008.

[23] R. Pacifici, "Estrogen, cytokines, and pathogenesis of postmenopausal osteoporosis," *Journal of Bone and Mineral Research*, vol. 11, no. 8, pp. 1043–1051, 1996.

[24] R. R. McLean, "Proinflammatory cytokines and osteoporosis," *Current Osteoporosis Reports*, vol. 7, no. 4, pp. 134–139, 2009.

[25] G. P. Garlet, W. Martins Jr., B. A. L. Fonseca, B. R. Ferreira, and J. S. Silva, "Matrix metalloproteinases, their physiological inhibitors and osteoclast factors are differentially regulated by the cytokine profile in human periodontal disease," *Journal of Clinical Periodontology*, vol. 31, no. 8, pp. 671–679, 2004.

[26] P. M. Preshaw and J. J. Taylor, "How has research into cytokine interactions and their role in driving immune responses impacted our understanding of periodontitis?" *Journal of Clinical Periodontology*, vol. 38, no. 11, pp. 60–84, 2011.

[27] A. J. P. Smith and S. E. Humphries, "Cytokine and cytokine receptor gene polymorphisms and their functionality," *Cytokine & Growth Factor Reviews*, vol. 20, no. 1, pp. 43–59, 2009.

[28] A. P. Sumer, N. Kara, G. C. Keles, S. Gunes, H. Koprulu, and H. Bagci, "Association of interleukin-10 gene polymorphisms with severe generalized chronic periodontitis," *Journal of Periodontology*, vol. 78, no. 3, pp. 493–497, 2007.

[29] L. J. Suárez, A. M. Ocampo, R. E. Dueñas, and A. Rodríguez, "Relative proportions of T-cell subpopulations and cytokines that mediate and regulate the adaptive immune response in patients with aggressive periodontitis," *Journal of Periodontology*, vol. 75, no. 9, pp. 1209–1215, 2004.

[30] A. Al-Rasheed, H. Scheerens, A. K. Srivastava, D. M. Rennick, and D. N. Tatakis, "Accelerated alveolar bone loss in mice lacking interleukin-10: late onset," *Journal of Periodontal Research*, vol. 39, no. 3, pp. 194–198, 2004.

[31] M. Claudino, T. P. Garlet, C. R. B. Cardoso et al., "Down-regulation of expression of osteoblast and osteocyte markers in periodontal tissues associated with the spontaneous alveolar bone loss of interleukin-10 knockout mice," *European Journal of Oral Sciences*, vol. 118, no. 1, pp. 19–28, 2010.

[32] G. Berg, C. Ekerfelt, M. Hammar, R. Lindgren, L. Matthiesen, and J. Ernerudh, "Cytokine changes in postmenopausal women treated with estrogens: a placebo-controlled study," *American Journal of Reproductive Immunology*, vol. 48, no. 2, pp. 63–69, 2002.

[33] D. Liu, S. Yao, and G. E. Wise, "Effect of interleukin-10 on gene expression of osteoclastogenic regulatory molecules in the rat dental follicle," *European Journal of Oral Sciences*, vol. 114, no. 1, pp. 42–49, 2006.

[34] K. W. Moore, R. de Waal Malefyt, R. L. Coffman, and A. O'Garra, "Interleukin-10 and the interleukin-10 receptor," *Annual Review of Immunology*, vol. 19, pp. 683–765, 2001.

[35] G. P. Garlet, "Destructive and protective roles of cytokines in periodontitis: a re-appraisal from host defense and tissue destruction viewpoints," *Journal of Dental Research*, vol. 89, no. 12, pp. 1349–1363, 2010.

[36] L. C. Hofbauer, C. A. Kühne, and V. Viereck, "The OPG/RANKL/RANK system in metabolic bone diseases," *Journal of Musculoskeletal & Neuronal Interactions*, vol. 4, no. 3, pp. 268–275, 2004.

[37] T. Crotti, M. D. Smith, R. Hirsch et al., "Receptor activator NF κB ligand (RANKL) and osteoprotegerin (OPG) protein expression in periodontitis," *Journal of Periodontal Research*, vol. 38, no. 4, pp. 380–387, 2003.

[38] H.-K. Lu, Y.-L. Chen, H.-C. Chang, C.-L. Li, and M. Y.-P. Kuo, "Identification of the osteoprotegerin/receptor activator of nuclear factor-kappa B ligand system in gingival crevicular fluid and tissue of patients with chronic periodontitis," *Journal of Periodontal Research*, vol. 41, no. 4, pp. 354–360, 2006.

[39] Y.-T. Teng, H. Nguyen, X. Gao et al., "Functional human T-cell immunity and osteoprotegerin ligand control alveolar bone destruction in periodontal infection," *The Journal of Clinical Investigation*, vol. 106, no. 6, pp. R59–R67, 2000.

Hindawi Publishing Corporation
BioMed Research International
Volume 2013, Article ID 832790, 9 pages
http://dx.doi.org/10.1155/2013/832790

Research Article

Cellular Performance Comparison of Biomimetic Calcium Phosphate Coating and Alkaline-Treated Titanium Surface

Xiaohua Yu and Mei Wei

Department of Materials Science and Engineering, University of Connecticut, 97 North Eagleville Road, Unit 3136, Storrs, CT 06269, USA

Correspondence should be addressed to Mei Wei; meiwei@engr.uconn.edu

Received 24 July 2013; Accepted 28 November 2013

Academic Editor: Michael Gelinsky

The influence of biomimetic calcium phosphate coating on osteoblasts behavior *in vitro* is not well established yet. In this study, we investigated the behavior of osteoblastic rat osteosarcoma 17/2.8 cells (ROS17/2.8) on two groups of biomaterial surfaces: alkaline-treated titanium surface (ATT) and biomimetic calcium phosphate coated ATT (CaP). The cell attachment, proliferation, differentiation, and morphology on these surfaces were extensively evaluated to reveal the impact of substrate surface on osteoblastic cell responses. It was found that the ROS17/2.8 cells cultured on the ATT surface had higher attachment and proliferation rates compared to those on the CaP surface. Our results also showed that the calcium phosphate coatings generated in this work have an inhibiting effect on osteoblast adhesion and further influenced the proliferation and differentiation of osteoblast compared to the ATT surface *in vitro*. Cells on the ATT surface also exhibited a higher alkaline phosphatase activity than on the CaP surface after two weeks of culture. Immunofluorescence staining and scanning electron microscopy results showed that the cells adhered and spread faster on the ATT surface than on the CaP surface. These results collectively suggested that substrate surface properties directly influence cell adhesion on different biomaterials, which would result in further influence on the cell proliferation and differentiation.

1. Introduction

Titanium and its alloys have been used for orthopedic applications for decades because of their excellent mechanical properties, superior biocompatibility, and good corrosion resistance [1]. However, these titanium-based materials also suffer from drawbacks, such as insufficient bioactivity which leads to poor osseointegration of the implant with host bone [2]. Tremendous efforts have been made to optimize the surface property of titanium such as surface chemistry, composition, and topography in order to improve the bioactivity of Ti implants and accelerate bone healing [3–5]. For instance, calcium phosphate (CaP) has been coated on Ti implant surfaces to provide the implants with superior osteoconductivity due to the physiochemical property of CaP ceramics [6–8]. A variety of CaP coating technologies have been developed, such as plasma splaying, sputtering deposition, sol-gel coating, and ion implantation. They have been used to obtain CaP coatings on Ti implant surfaces [9–11]. Recently, an approach in creating biomimetic coating has attracted substantial interests of researchers due to its simplicity, flexibility, and low cost [12–15]. A bone-mineral-like CaP coating can be achieved on titanium surface by simply incubating the implants in modified simulated body fluid (m-SBF) at ambient conditions [16]. Many studies have demonstrated that the biomimetic CaP coating could actively promote bone ingrowth and improve implant-bone integration [17–21].

Biomimetic CaP coatings have shown their impact on regulating diverse cell behaviors. However, researchers from different groups obtained conflicting results regarding CaP coating-cell interactions. Most of the earlier studies supported that CaP coating improved osteoblast adhesion, proliferation, and differentiation *in vitro*, as well as accelerated bone growth, bone matrix apposition, and biomineralization process *in vivo* [22–25]. However, more recent reports showed some conflicting results that CaP coating suppressed the activity of osteoblasts such as lowering cell proliferation and reducing cell differentiation [26, 27]. Lee and his colleagues demonstrated that osteoblasts had a lower

proliferation rate on apatite surface compared to tissue culture dish [28]. Murphy et al. suggested that bone-like mineral accelerated cell proliferation and growth but inhibited cell differentiation with a lower osteogenic marker expression [29]. The diverse influence of CaP coating on osteoblasts behavior may be attributed to its materials characteristics, such as surface topography, composition, crystallinity, crystal size, and dissolution rate [30, 31]. When biomimetic CaP coating is applied on biomaterial surfaces, it does not only change the topography of the original surface, but also changes the chemical composition which interacts directly with cells [32]. Although the effect of surface topography on cell responses has been extensively investigated, the influence of the combination of chemical surface modification and designed topography on cell responses still remains unexplored.

In this study, two groups of biomaterial surfaces: alkaline-treated titanium surface (ATT) and biomimetic calcium phosphate coated titanium surface (CaP) were employed to represent two types of materials surfaces with distinct surface topography and chemical composition. Osteoblastic cell line ROS17/2.8 was used to systemically investigate the impact of substrate signals on cellular responses. In particular, the cell adhesion behavior on the tested material surfaces was correlated with the long-term cell growth and differentiation to reveal the relationship between biomaterial surface and implant performance.

2. Materials and Methods

2.1. Preparation and Characterization of Biomimetic CaP Coating. Biomimetic CaP coatings were prepared on titanium substrates using a method described in earlier studies [24, 33]. Commercially available pure titanium strips (10 mm × 10 mm × 0.2 mm) were used in the current study. They were roughened using 800 sandpapers, followed by alkaline treatment in 5 M NaOH at 60°C for 24 h. All the samples were then thoroughly washed with deionized water and dried in air at room temperature. Half of the samples were reserved at this point for cell culture study. The treated titanium foils were soaked in modified simulated body fluid (m-SBF) (6.0 mM NaCl, 3.0 mM $K_2HPO_4 \cdot 3H_2O$, 3.0 mM $MgCl_2 \cdot 6H_2O$, 50 mM HEPES, 8.0 mM $CaCl_2$, 18 mM $NaHCO_3$) to achieve a layer of bone-like apatite coating. The plates were immersed in the m-SBF at 42°C for 24 h. After the coating process, all coated titanium plates were rinsed with deionized water and dried at room temperature. Two groups of materials were used for cell culture in the subsequent study: alkaline-treated pure titanium plates (ATT) and alkaline-treated and biomimetic CaP coated titanium plates (CaP). All the plates were sterilized at 121°C for 55 min before cell culture.

2.2. Surface Characterization. The surface morphology of the two tested surfaces was observed using field emission scanning electron microscopy (FESEM, JEOL6335F) at 5 kV (see Figure 1). CaP coating was also examined using X-ray diffractometer (Bruker AXS D5005) with a copper target. The voltage and current setups were 40 kV and 40 mA, respectively. Plus, the CaP coating was also evaluated using Fourier transform infrared spectroscopy (FTIR, Nicolet Avatar 360). The FTIR spectrum was recorded in the range 400–2000 cm^{-1}.

2.3. Cell Culture. Rat osteosarcoma ROS17/2.8 cells were cultured in F12 medium supplemented with 10% FBS (Cellgro, USA) and 1% pen-strep (Cellgro, USA). Cells were grown in a humidified atmosphere of 5% CO_2 at 37°C. Culture media were changed every other day. An osteogenic medium, which consists of F12 plus 10 mM β-glycerol phosphate, 10 nM dexamethasone, and 50 μg/mL L-ascorbic acid (Sigma, St. Louis, MO), was used after the cells were grown on the materials for one week.

2.4. Cell Attachment. ROS17/2.8 cells were seeded on ATT and CaP plates in a 24-well plate at a density of 2×10^4 cells/cm^2 in 1.0 mL medium ($n = 5$). The cells were allowed to attach on the test surfaces for 4 h before all culture medium was aspirated from each well. The samples were then washed by PBS three times to remove the unattached and loosely bound cells from material surfaces. An Alamar Blue assay was chosen to measure the density of cells left on the samples. 0.5 mL fresh medium containing 10% Almar Blue dye (Biosource International, USA) was added to each well and incubated for 2 h. The incubated medium was then transferred into a 96-well plate and read by a microplate reader (Biotek MQX, USA) at absorption wavelengths of 570 and 600 nm. The cell numbers on different substrates were calculated based on a calibration curve with known amount of cells in each well.

2.5. Cell Proliferation. ROS17/2.8 cells were seeded onto ATT and CaP plates in a 24-well plate at a density of 2×10^4 cells/cm^2 in 1.0 mL medium ($n = 5$). The medium was refreshed every two days. After 3, 7, and 14 days of incubation, the cell numbers on different substrates were measured using the Alamar Blue assay as described in Section 2.3. At each time point, 200 uL 10% Alamar Blue in culture medium was added into each well after aspirating the existing medium. After incubating at 37°C for 2 h, 100 uL of the solution was transferred from each well into a 96-well plate and ready at $\lambda_{ex}/\lambda_{em} = 570/600$ nm The results were expressed as relative cell number compared with the control (cell number on ATT) at day 3.

2.6. Cell Differentiation. The activity of alkaline phosphatase (ALP) was measured as described previously [33]. ROS17/2.8 cells were seeded and cultured in the same way as in the proliferation study. Cell differentiation ability was evaluated at days 3, 7, and 14 ($n = 5$). To measure ALP activity, the cells were washed with PBS and lysed with 0.2 mL 0.5% Triton X-100 in PBS. The lysis was sonicated for 60 s and centrifuged at 5×10^3 RPM 4°C for 10 minutes. Aliquots of supernatants were subjected to a total protein assay using a BCA assay

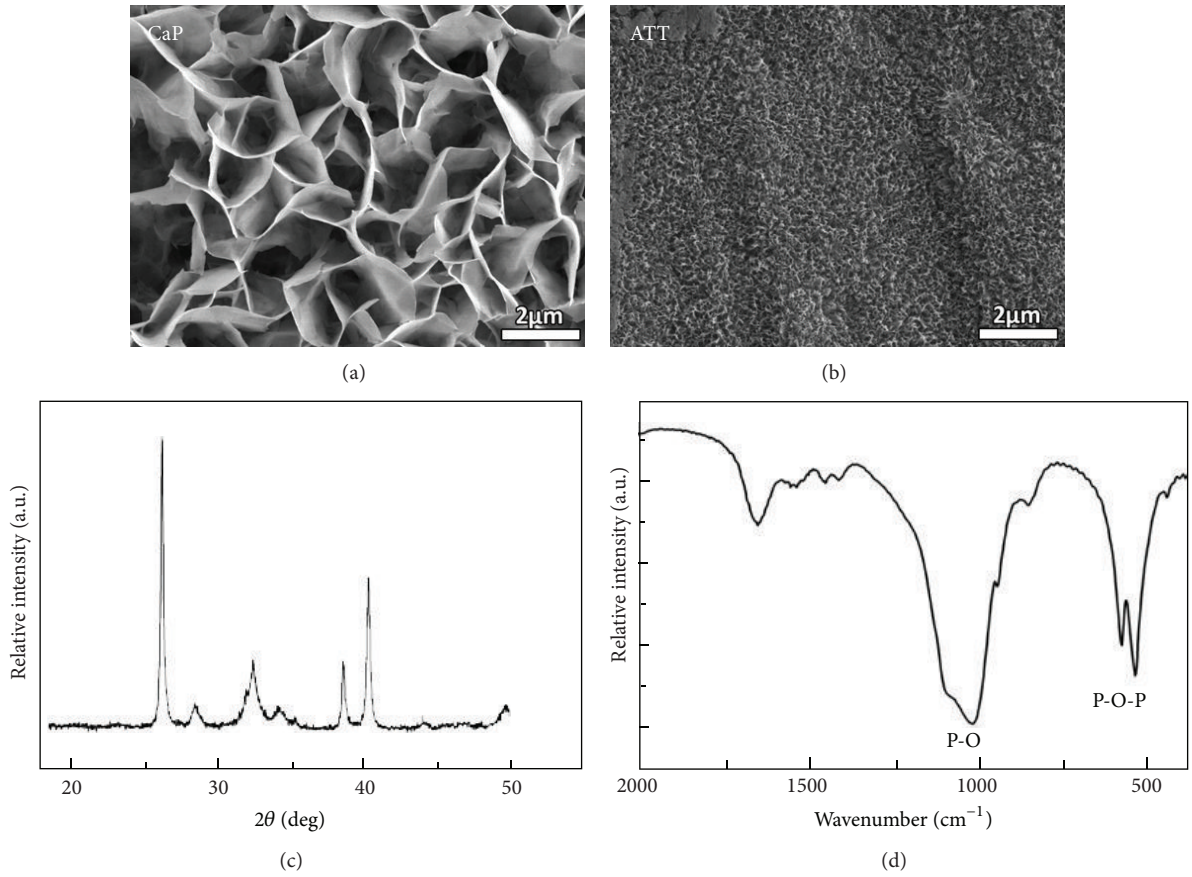

Figure 1: Characterization of different substrates. Upper panel: CaP: FESEM micrograph of biomimetic calcium phosphate surface. ATT: FESEM micrograph of alkaline-treated titanium surface. Lower level: X-ray diffraction pattern of CaP. FTIR spectrum of the CaP.

kit (Pierce, USA). The ALP activity was measured by colorimetry in ALP assay reagent mixture composed of 5 mM *p*-nitrophenol phosphate disodium (*p*-NPP), 1 mM $MgCl_2$, and 0.15 M 2-amino-2-methyl-1-propanol (AMP) (Sigma, USA) with an equal volume amount of nitrophenyl phosphate (10 mM). The absorbance was measured at 405 nm using a μQuant microplate reader (μQuant, Bio-Tek, USA). The ALP activity was expressed as per microgram total protein for each sample.

2.7. Immunofluorescence Staining. ROS 17/2.8 cells were seed on ATT and CaP plates in a 24-well plate at a final density of 1.0×10^4 cells/cm^2 for 12 and 24 h. At each time point, the specimens were rinsed with PBS. They were then fixed with 4% formaldehyde in PBS for 20 min at room temperature, permeabilized in 0.5% Triton X-100 in PBS for 15 min, and finally incubated with 1% BSA in PBS for 1 h at room temperature. Antivinculin antibody (Sigma, USA) was diluted at a ratio of 1 : 128 and incubated with the cells for 1 h at 37°C. After thorough rinses using PBS, the specimens were incubated with a goat-anti-mouse-IgG-FITC-conjugated secondary antibody (1 : 150, Sigma, USA). To detect actin and nucleus simultaneously, tetramethylrhodamine isothiocyanate- (TRITC-) conjugated phalloidin (1 : 400, Invitrogen, USA) and 0.5 μg/mL 4′,6-diamidino-2-phenylindole dihydrochloride (DAPI) were added in the secondary antibody solution. Triple-stained cells were observed using a fluorescent microscope (Zeiss Axiovert 200 M) with filters appropriate for FITC, TRITC, and DAPI.

2.8. Cell Morphology. Cells were seeded on ATT and CaP plates in a 24-well plate at a density of 1.0×10^4 cells/cm^2 for 6, 12, 24, and 48 h, respectively. After culture, the cells were fixed in 2.5% glutaraldehyde buffer for 1 h and incubated in 0.1 M sodium cacodylate buffer for another hour. The fixed cells were then dehydrated in graded ethanol series and followed by a critical point drying. All the samples were sputter-coated with gold palladium. Finally, the cell morphology on different substrates was examined using field emission scanning electron microscopy (FESEM, LEO/Zeiss DSM 982). To assess the cell distribution and extracellular matrix deposition, cells were seeded and cultured on ATT and CaP plates for 2 weeks. After that, all the specimens were prepared as described earlier in this section and then subjected to FESEM observations.

2.9. Statistical Analysis. All the data were illustrated as the mean ± standard deviations. The statistical difference was

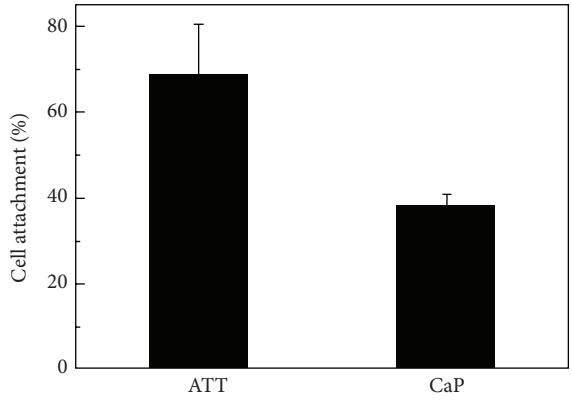

Figure 2: Cell attachment on different substrates measured by the Alamar Blue assay. Incubated for 4 h, significantly more cells ($P < 0.05$) were attached to the surface of ATT than CaP.

analyzed using analysis of variance (ANOVA), and $P < 0.05$ was considered significant.

3. Results

3.1. Surface Characterization. The morphology of the two tested surfaces showed distinct differences. The CaP coating surface demonstrated a plate-like structure uniformly covering the titanium surface. The size of these plate-like structure is around 3-4 μm. In comparison, the ATT surface exhibited a porous network associated with a nanometer sized structure in a scale of approximately 100–200 nm. The XRD spectrum of CaP showed a cluster of peaks around 31–33° which are assigned to (211), (112), and (300) planes of hydroxyapatite. The FTIR spectrum showed characteristic bands at 1040, 602, and 563 cm^{-1} which could be assigned to P-O stretching and O-P-O bending mode. These data collectively suggest that the CaP coating is poorly crystalline apatite.

3.2. Cell Attachment and Proliferation. Cell attachment on tested material surfaces was assessed by performing a short time cell adhesion assay. Figure 2 shows ROS17/2.8 cell attachment expressed as a percentage of total cells seeded on ATT and CaP surfaces. The seeded cells successfully attached to both ATT and CaP surfaces after 4 h incubation, but the number of cells on each type of material appeared to be substantially different. ROS17/2.8 cells seed onto the ATT surface (69%, $P < 0.05$) exhibited significantly higher cell attachment than that of CaP (38%, $P < 0.05$), which indicates that the cells might have attached to the ATT surface faster than that of the CaP.

The cell proliferation was expressed as the number of living cells present on both groups of surfaces at day 3, 7, and 14 of culture (Figure 3). The cell number increased steadily on both materials as the culture time extended. At day 3, the cell number on ATT was significantly higher than that on CaP ($P < 0.05$). At day 7 and 14, the difference of cell numbers between these two groups became more significant. The cell number on ATT at day 14 was almost 4-fold of that on CaP at this time point. Besides, the cell generation time of ROS17/2.8 cells was also calculated based on the following equation:

$$N_t = N_0 2^{tf}, \quad (1)$$

where N_0 is the initial cell number, N_t is the cell number after t days of culture, t is the culture period, and $1/f$ is the generation time (h/generation).

It was found that although the cell number on CaP was much lower than on ATT, there is no significant difference between cell doubling times from day 3 and day 7 (Table 1) for these two surfaces. Surprisingly, the cell doubling time on CaP is 133 h between days 7 and 14, which is significantly shorter than that of ATT (162 h).

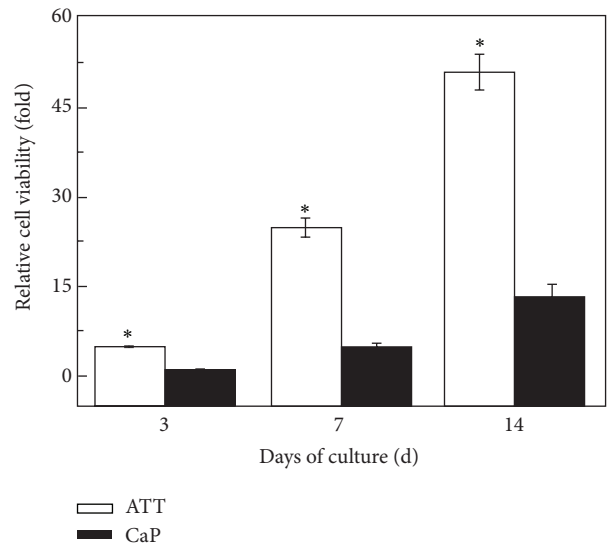

Figure 3: Proliferation of osteoblastic cells cultured on ATT and CaP surfaces for 3, 7, and 14 days. The cell proliferation was significantly higher on ATT than on CaP ($P < 0.05$) at all time points.

Table 1: ROS17/2.8 generation time ($1/f$) on ATT and CaP at different time periods.

Generation time ($1/f$)	Day 7	Day 14
ATT	41.61 ± 1.89	162.23 ± 2.86
CaP	41.79 ± 3.61	133.23 ± 5.93

3.3. Cell Differentiation. Alkaline phosphatase (ALP) activity is one of the most widely used marker for early differentiation of osteoblasts [34]. Although the ALP level on both surfaces started low in the first week, it dramatically increased in the second week of culture. Importantly, it was noticed that the ALP activity of the cells on ATT group was higher than on CaP at all time points. However, the ALP increase rate of the two groups was very similar. While ALP activity of the ATT group at days 3 and 7 was more than two times higher than the CaP group, it dropped to only onefold higher than that of CaP at day 14 (see Figure 4).

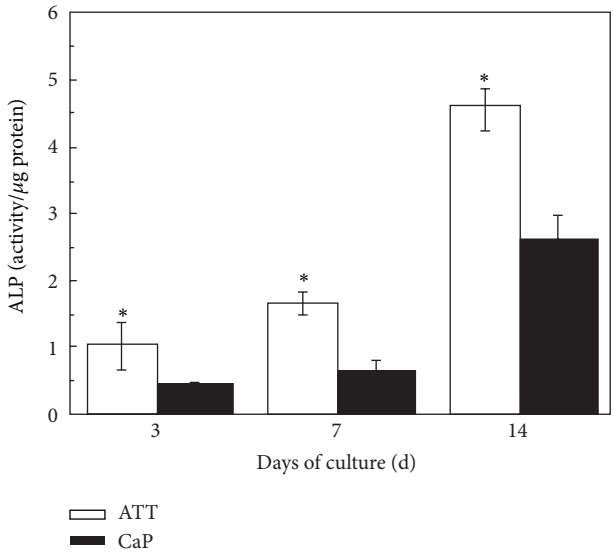

Figure 4: ALP activity normalized to total protein content of osteoblastic cells cultured on ATT and CaP surfaces for 3, 7, and 14 days. ALP activities were significantly higher on ATT than on CaP ($P < 0.05$) at all time points.

3.4. Immunofluorescence Staining. Immunocytochemistry was conducted to evaluate cell adhesion on both groups of materials (Figure 5). Cells plated on ATT surface spread out well and organized actin into stress fibers after 12 h, while the cells on CaP surface showed a more round shape and failed to form stress fibers (Figures 5(a) and 5(c)). After 24 h of incubation, the cells on ATT reached full spreading and developed a distinct focal adhesion (Figure 5(f)). Focal contact clusters were readily found near the periphery of cells. In contrast, the cells on CaP illustrated a more slim and elongated shape which indicates insufficient spreading of the cells (Figures 5(b) and 5(d)). There was no focal contact clusters formed in the cells on CaP (Figure 5(h)).

3.5. Cell Morphology. Figure 6 shows the morphology of ROS17/2.8 cells cultured on ATT and CaP surfaces at different time points. SEM micrographs were taken at 4, 8, 12, and 24 h to record the complete cell adhesion process on different substrates. After cells were seeded on the substrates for 4 h, the cells on CaP demonstrated a round morphology while those on ATT were spread out. At 8 h, the cells on CaP also began to spread with some short filopodia formed around the cellular body. In contrast, the cells on ATT stretched to a great extent and long filopodia were found anchoring to the material surface. The cells on CaP kept expanding and became much flatter in the next four hours while the cells on ATT almost reached a full degree of spreading. After culturing for 24 h, the cells on CaP finally displayed a complete spreading and developed a good adhesion to the underlying surface, while the cells on ATT also attached closely to the surface but with a larger contacting area.

Figure 7 shows the ROS17/2.8 cells growing on the two types of surfaces after 14 days of culture. Both surfaces were covered uniformly with a layer of cells. In particular, cells on ATT grew tightly to each other and tended to form cell colonies (Figure 7(b)). Cells on CaP grew more sparsely instead of forming tight contact with each other (Figure 7(a)). At a high magnification, numerous filopodia were observed on cells grown on ATT, but less filopodia were observed in cells on CaP (Figures 7(c) and 7(d)).

4. Discussion

Biomaterial surfaces play a vital role in tissue engineering and regenerative medicine because most biological reactions during implantation occur between the implant surface and the biological environment [35]. Calcium phosphate coatings on implant surfaces have been employed to improve the performance of implants through enhanced osteoblastic cell activities, such as cell proliferation, differentiation, and mineral deposition on the implants [36, 37]. However, recent studies also reported conflicting results of the impact of CaP coating on osteoblastic cells [28, 29]. In this work, we aimed at correlating the cell adhesion behavior with long-term cellular performance on two types of biomaterial surfaces in order to illustrate the critical role of CaP coating to cellular responses. We found that osteoblastic attachment and adhesion were weakened on the so-prepared CaP coating surface compared to the alkaline-treated ATT surface. As a result, osteoblasts proliferate and differentiate on the CaP surface were significantly delayed and impaired. Our results indicate that osteoblast-biomaterial interactions are significantly affected by substrates surface properties [38].

The adhesion of osteoblast on biomaterials mainly depends on the surface properties of materials such as topography, chemistry, and composition [39–41]. Osteoblasts seeded on ATT demonstrated better organized actin and more focal adhesion compared to those on CaP. SEM observations also exhibited that cell attachment on ATT is faster than on CaP (Figures 5 and 6). It has been reported that nanometric topography of a biomaterial had a significant impact on cell adhesion [42]. Surface characterization of the two tested groups showed distinct topographical features on ATT and CaP: formation of the CaP on titanium substrate resulted in micrometric topography, while alkaline-treated titanium substrate demonstrated nanometric topography. This distinction of surface topography substantially affected the follow-up *in vitro* tests such as protein adhesion, focal plaques formation, and cell spreading [43]. Protein adsorption on a nanometric topographical titanium substrate was found to be much higher and more oriented compared to a micrometric titanium surface [44]. Thus, the ATT might enable more adhesive protein adsorption such as fibronectin and laminin from the serum. Besides, focal plaque mediated cell adhesion was also enhanced by the presence of nanotopography on biomaterials surface [45]. For instance, Okada et al. found that focal adhesion could only be formed on hydroxyapatite surface with nanoscale feature but not on a smooth dense surface [46]. More cell adhesion receptors could have been activated when there were adequate interactions between cells and ATT, a substrate with high surface energy, resulting

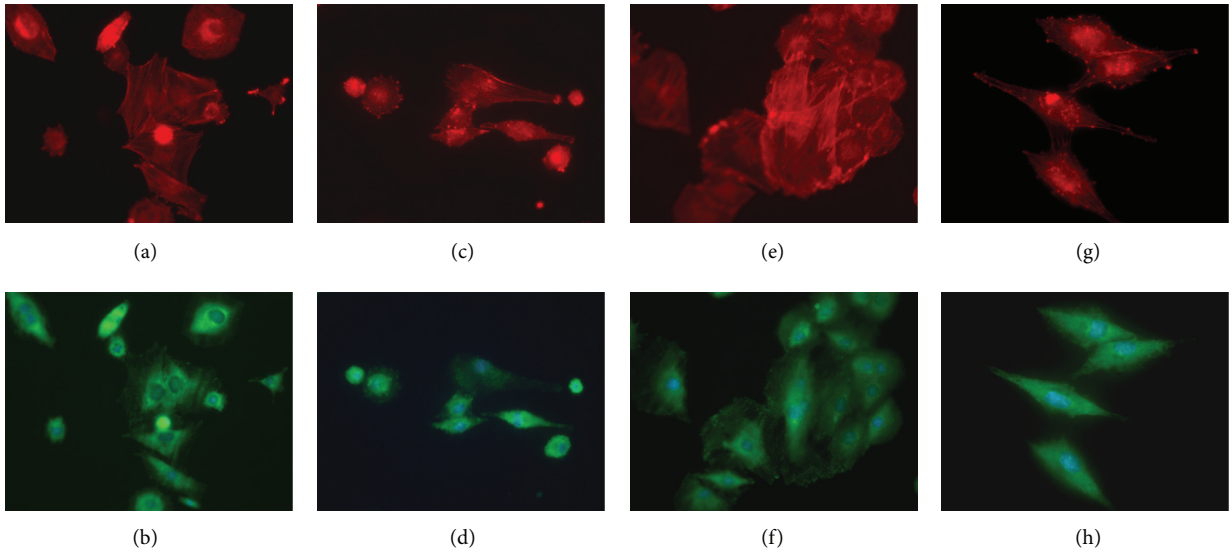

Figure 5: Immunostaining of vinculin, actin, and nuclei showing ROS17/2.8 osteoblastic cells cultured on ATT and CaP surfaces for 24 and 48 h, respectively. (a) and (b) ATT at 24 h, (c) and (d) CaP at 24 h, (e) and (f) ATT at 48 h, and (g) and (h) CaP at 48 h. Green: vinculin; Red: actin; Blue: nuclei.

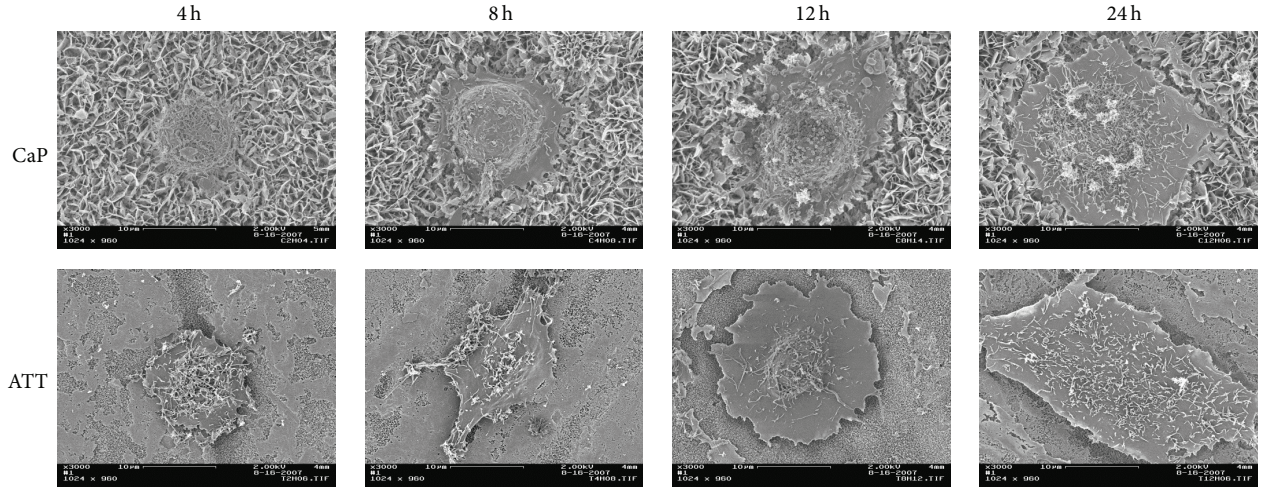

Figure 6: SEM micrographs showing ROS17/2.8 osteoblastic cell morphologies on ATT and CaP surfaces for different time periods. Scale bar = 10 μm.

in earlier cell adhesion [46]. In contrast, the slender cell shape and delayed cell adhesion on the CaP substrate indicated that the cells did not interact well with the substrate (Figures 5 and 6). Therefore, both the literature and our observations suggest the unique nanotopography of the ATT surface might have played a crucial role in cell adhesion in this context.

Cell adhesion influences many aspects of cell behavior, including proliferation, differentiation, morphology, and migration [47]. There are studies showing that cell membrane in contact with the nanostructured topography was subject to tensile and relaxation mechanical forces that trigger cell behavior in certain ways [48]. Recent research has shown that signaling pathways triggered by growth factors require strong cell adhesion for cell cycle progression and proliferation [49]. The high cell proliferation rate of ROS17/2.8 cells on ATT may be due to their better adhesion on the surface (Figures 5 and 6). As a result, cell cycle phase progression and proliferation on ATT are triggered earlier than CaP. Lee and colleagues also reported similar results that CaP coating had negative influence on cell proliferation due to its provision of insufficient adhesion signals [26]. It was unexpected that the cell doubling time of cells on CaP is shorter than on ATT during the second week of culture. A possible explanation is that the negative influence of weak adhesion is only present in the early stage of cell growth. Once the cell adhesion is completed, cell proliferation may not be affected by the adhesion as much as the initial stage. This might also explain the ALP result. Although the ALP activity on CaP is much lower than that of ATT at the initial stage, the ALP activity increased 4-folds on CaP in the second week, while it only

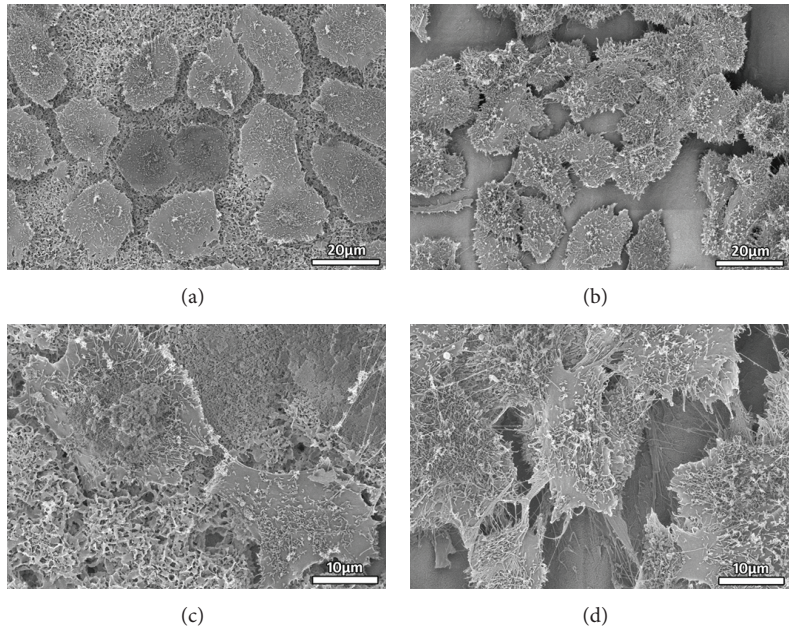

Figure 7: SEM micrographs showing ROS17/2.8 osteoblastic cell morphologies cultured on the ATT and the CaP coating surfaces for 14 days. (a) CaP (at low mag), (b) ATT (at low mag), (c) CaP (at high mag), and (d) ATT (at high mag).

increased 2.78-folds on ATT. It is likely that the negative effect of poor adhesion on CaP gradually faded out in the second week and the other positive aspects of CaP coating such as Ca^{2+} release pushed the CaP coating to catch up on cell differentiation.

Although *in vitro* cell culture results have provided useful information for initial-stage biological screening of biomaterials, the data from cell culture cannot yet be fully correlated with *in vivo* implant performances. Some recent published studies have shown inhibitory effect of calcium phosphate coatings on osteoblasts *in vitro* [50, 51], but their performance *in vivo* cannot be completely predicted by these data. It is noteworthy that most of these studies showing negative influence of calcium phosphate coating were based on cell culture study. Better cell adhesion on titanium *in vitro* does not necessarily suggest ATT demonstrates better biological properties than CaP *in vivo*. Distinct differences have been found between titanium and calcium phosphate when they were implanted into animal bodies. Compared to titanium which is basically inert in the body, calcium phosphate is bioactive during the bone healing. Calcium phosphate provides direct bone contact at the implant-bone interface and guide bone formation along their surfaces by formation of a biological apatite layer [52]. In the case of titanium, macrophages often show up adjacent to the titanium implants which did not have direct bone bonding [53, 54]. Although surface treated titanium showed better cellular interactions than biomimetic CaP coating *in vitro* in this work, when they are applied to the physiological environment, the tissue reaction may vary substantially. Besides, the long-term performance of titanium has raised certain concerns due to corrosion and formation of wear debris [3]. Thus, it is critical to notice that the cell culture model might provide useful information for biomaterials screening; the merit of the biomaterials can only be confirmed in animal models and other clinical trials.

5. Conclusion

In this study, the cellular responses to biomimetic calcium phosphate coating were systematically investigated in comparison with an alkaline-treated titanium surface. It was found that the calcium phosphate coating used in this work had an inhibiting effect osteoblast proliferation and differentiation. The inhibitory impact of the calcium phosphate coating might be caused by the poor adhesion of cells at the initial stage of cell-surface interactions. Thus, the results of this study collectively highlights that cellular performance of biomaterials might be varied by multiple material surface properties such as composition, topography, surface energy and other related factors.

Conflict of Interests

The authors declare that they have no conflict of interests associated with this paper.

Acknowledgments

The authors would like to thank the National Science Foundation (BES 0503315 and CBET-1133883) and the NIH (R21AR059962) for their support of the research. The authors would like to thank Dr. Carol Norris of the Department of Molecular and Cell Biology, University of Connecticut for her help with fluorescence microscopy and Dr. Jim Romanow of

the Department of Physiology and Neurobiology, University of Connecticut for his help with SEM sample preparation.

References

[1] X. Y. Liu, P. K. Chu, and C. K. Ding, "Surface modification of titanium, titanium alloys, and related materials for biomedical applications," *Materials Science and Engineering R*, vol. 47, no. 3-4, pp. 49–121, 2004.

[2] R. Narayanan, S. K. Seshadri, T. Y. Kwon, and K. H. Kim, "Calcium phosphate-based coatings on titanium and its alloys," *Journal of Biomedical Materials Research B*, vol. 85, no. 1, pp. 279–299, 2008.

[3] M. Geetha, A. K. Singh, R. Asokamani, and A. K. Gogia, "Ti based biomaterials, the ultimate choice for orthopaedic implants—a review," *Progress in Materials Science*, vol. 54, no. 3, pp. 397–425, 2009.

[4] L. Le Guéhennec, A. Soueidan, P. Layrolle, and Y. Amouriq, "Surface treatments of titanium dental implants for rapid osseointegration," *Dental Materials*, vol. 23, no. 7, pp. 844–854, 2007.

[5] X. Yu, H. Qu, D. A. Knecht, and M. Wei, "Incorporation of bovine serum albumin into biomimetic coatings on titanium with high loading efficacy and its release behavior," *Journal of Materials Science: Materials in Medicine*, vol. 20, no. 1, pp. 287–294, 2009.

[6] F. Barrère, P. Layrolle, C. A. van Blitterswijk, and K. de Groot, "Biomimetic calcium phosphate coatings on Ti6Al4V: a crystal growth study of octacalcium phosphate and inhibition by Mg^{2+} and HCO_3^-," *Bone*, vol. 25, no. 1, supplement 1, pp. 107S–111S, 1999.

[7] P. Habibovic, F. Barrère, C. A. van Blitterswijk, K. de Groot, and P. Layrolle, "Biomimetic hydroxyapatite coating on metal implants," *Journal of the American Ceramic Society*, vol. 85, no. 3, pp. 517–522, 2002.

[8] X. Yu, Z. Xia, L. Wang et al., "Controlling the structural organization of regenerated bone by tailoring tissue engineering scaffold architecture," *Journal of Materials Chemistry*, vol. 22, no. 19, pp. 9721–9730, 2012.

[9] J. Weng, M. Wang, and J. Chen, "Plasma-sprayed calcium phosphate particles with high bioactivity and their use in bioactive scaffolds," *Biomaterials*, vol. 23, no. 13, pp. 2623–2629, 2002.

[10] J. G. C. Wolke, K. de Groot, and J. A. Jansen, "In vivo dissolution behavior of various RF magnetron sputtered Ca-P coatings," *Journal of Biomedical Materials Research*, vol. 39, pp. 524–530, 1998.

[11] E. Milella, F. Cosentino, A. Licciulli, and C. Massaro, "Preparation and characterisation of titania/hydroxyapatite composite coatings obtained by sol-gel process," *Biomaterials*, vol. 22, no. 11, pp. 1425–1431, 2001.

[12] T. Kokubo, S. Ito, Z. T. Huang et al., "Ca, P-rich layer formed on high-strength bioactive glass-ceramic A-W," *Journal of Biomedical Materials Research*, vol. 24, no. 3, pp. 331–343, 1990.

[13] F. Barrere, C. A. Van Blitterswijk, K. De Groot, and P. Layrolle, "Influence of ionic strength and carbonate on the Ca-P coating formation from SBF×5 solution," *Biomaterials*, vol. 23, no. 9, pp. 1921–1930, 2002.

[14] H. B. Wen, J. R. de Wijn, C. A. van Blitterswijk, and K. de Groot, "Incorporation of bovine serum albumin in calcium phosphate coating on titanium," *Journal of Biomedical Materials Research*, vol. 46, pp. 245–252, 1999.

[15] Z. Xia, X. Yu, and M. Wei, "Biomimetic collagen/apatite coating formation on Ti6Al4V substrates," *Journal of Biomedical Materials Research B*, vol. 100, no. 3, pp. 871–881, 2012.

[16] W.-Q. Yan, T. Nakamura, K. Kawanabe, S. Nishigochi, M. Oka, and T. Kokubo, "Apatite layer-coated titanium for use as bone bonding implants," *Biomaterials*, vol. 18, no. 17, pp. 1185–1190, 1997.

[17] D. R. Jordan, S. Brownstein, S. Gilberg, D. Coupal, S. Kim, and L. Mawn, "Hydroxyapatite and calcium phosphate coatings on aluminium oxide orbital implants," *Canadian Journal of Ophthalmology*, vol. 37, no. 1, pp. 7–13, 2002.

[18] P. Li, "Biomimetic nano-apatite coating capable of promoting bone ingrowth," *Journal of Biomedical Materials Research A*, vol. 66, no. 1, pp. 79–85, 2003.

[19] M. Nagano, T. Kitsugi, T. Nakamura, T. Kokubo, and M. Tanahashi, "Bone bonding ability of an apatite-coated polymer produced using a biomimetic method: a mechanical and histological study in vivo," *Journal of Biomedical Materials Research A*, vol. 31, pp. 487–494, 1996.

[20] X. Yu and M. Wei, "Preparation and evaluation of parathyroid hormone incorporated CaP coating via a biomimetic method," *Journal of Biomedical Materials Research B*, vol. 97, pp. 345–354, 2011.

[21] Z. Xia, X. Yu, X. Jiang, H. D. Brody, D. W. Rowe, and M. Wei, "Fabrication and characterization of biomimetic collagen-apatite scaffolds with tunable structures for bone tissue engineering," *Acta Biomaterialia*, vol. 9, pp. 7308–7319, 2013.

[22] A. Okumura, M. Goto, T. Goto et al., "Substrate affects the initial attachment and subsequent behavior of human osteoblastic cells (Saos-2)," *Biomaterials*, vol. 22, no. 16, pp. 2263–2271, 2001.

[23] R. Shu, R. McMullen, M. J. Baumann, and L. R. McCabe, "Hydroxyapatite accelerates differentiation and suppresses growth of MC3T3-E1 osteoblasts," *Journal of Biomedical Materials Research A*, vol. 67, no. 4, pp. 1196–1204, 2003.

[24] X. Yu, L. Wang, Z. Xia et al., "Modulation of host osseointegration during bone regeneration by controlling exogenous stem cell differentiation using a material approach," *Biomaterials Science*, 2014.

[25] X. Yu, L. Wang, F. Peng et al., "The effect of fresh bone marrow cells on reconstruction of mouse calvarial defect combined with calvarial osteoprogenitor cells and collagen-apatite scaffold," *Journal of Tissue Engineering and Regenerative Medicine*, 2012.

[26] R. O. C. Oreffo, F. C. M. Driessens, J. A. Planell, and J. T. Triffitt, "Effects of novel calcium phosphate cements on human bone marrow fibroblastic cells," *Tissue Engineering*, vol. 4, no. 3, pp. 293–303, 1998.

[27] Y.-F. Chou, W. Huang, J. C. Y. Dunn, T. A. Miller, and B. M. Wu, "The effect of biomimetic apatite structure on osteoblast viability, proliferation, and gene expression," *Biomaterials*, vol. 26, no. 3, pp. 285–295, 2005.

[28] Y.-J. Lee, J. S. Ko, and H.-M. Kim, "The role of cell signaling defects on the proliferation of osteoblasts on the calcium phosphate apatite thin film," *Biomaterials*, vol. 27, no. 20, pp. 3738–3744, 2006.

[29] W. L. Murphy, S. Hsiong, T. P. Richardson, C. A. Simmons, and D. J. Mooney, "Effects of a bone-like mineral film on phenotype of adult human mesenchymal stem cells in vitro," *Biomaterials*, vol. 26, no. 3, pp. 303–310, 2005.

[30] Y.-F. Chou, J. C. Y. Dunn, and B. M. Wu, "In vitro response of MC3T3-E1 preosteoblasts within three-dimensional apatite-coated PLGA scaffolds," *Journal of Biomedical Materials Research B*, vol. 75, no. 1, pp. 81–90, 2005.

[31] Z. Meleti, I. M. Shapiro, and C. S. Adams, "Inorganic phosphate induces apoptosis of osteoblast-like cells in culture," *Bone*, vol. 27, no. 3, pp. 359–366, 2000.

[32] S. Choi and W. L. Murphy, "The effect of mineral coating morphology on mesenchymal stem cell attachment and expansion," *Journal of Materials Chemistry*, vol. 22, Article ID 25288, 2012.

[33] H. B. Qu and M. Wei, "Improvement of bonding strength between biomimetic apatite coating and substrate," *Journal of Biomedical Materials Research B*, vol. 84, no. 2, pp. 436–443, 2008.

[34] A. Sabokbar, P. J. Millett, B. Myer, and N. Rushton, "A rapid, quantitative assay for measuring alkaline phosphatase activity in osteoblastic cells in vitro," *Bone and Mineral*, vol. 27, no. 1, pp. 57–67, 1994.

[35] D. G. Castner and B. D. Ratner, "Biomedical surface science: foundations to frontiers," *Surface Science*, vol. 500, no. 1–3, pp. 28–60, 2002.

[36] P. Habibovic, C. M. van der Valk, C. A. van Blitterswijk, K. De Groot, and G. Meijer, "Influence of octacalcium phosphate coating on osteoinductive properties of biomaterials," *Journal of Materials Science*, vol. 15, no. 4, pp. 373–380, 2004.

[37] J. Wang, J. de Boer, and K. de Groot, "Proliferation and differentiation of osteoblast-like MC3T3-E1 cells on biomimetically and electrolytically deposited calcium phosphate coatings," *Journal of Biomedical Materials Research A*, vol. 90, no. 3, pp. 664–670, 2009.

[38] K. Anselme, "Osteoblast adhesion on biomaterials," *Biomaterials*, vol. 21, no. 7, pp. 667–681, 2000.

[39] X. Liu, J. Y. Lim, H. J. Donahue, R. Dhurjati, A. M. Mastro, and E. A. Vogler, "Influence of substratum surface chemistry/energy and topography on the human fetal osteoblastic cell line hFOB 1.19: phenotypic and genotypic responses observed in vitro," *Biomaterials*, vol. 28, no. 31, pp. 4535–4550, 2007.

[40] E. A. Dos Santos, M. Farina, G. A. Soares, and K. Anselme, "Surface energy of hydroxyapatite and β-tricalcium phosphate ceramics driving serum protein adsorption and osteoblast adhesion," *Journal of Materials Science*, vol. 19, no. 6, pp. 2307–2316, 2008.

[41] X. Zhu, J. Chen, L. Scheideler, T. Altebaeumer, J. Geis-Gerstorfer, and D. Kern, "Cellular reactions of osteoblasts to micron- and submicron-scale porous structures of titanium surfaces," *Cells Tissues Organs*, vol. 178, no. 1, pp. 13–22, 2004.

[42] W. Xue, J. L. Moore, H. L. Hosick et al., "Osteoprecursor cell response to strontium-containing hydorxyapatite ceramics," *Journal of Biomedical Materials Research A*, vol. 79, no. 4, pp. 804–814, 2006.

[43] S. Minagar, J. Wang, C. C. Berndt, E. P. Ivanova, and C. Wen, "Cell response of anodized nanotubes on titanium and titanium alloys," *Journal of Biomedical Materials Research A*, vol. 101, pp. 2726–2739, 2013.

[44] C. Galli, M. Collaud Coen, R. Hauert et al., "Protein adsorption on topographically nanostructured titanium," *Surface Science*, vol. 474, no. 1–3, pp. L180–L184, 2001.

[45] C. Luo, L. Li, J. Li et al., "Modulating cellular behaviors through surface nanoroughness," *Journal of Materials Chemistry*, vol. 22, Article ID 15654, 2012.

[46] S. Okada, H. Ito, A. Nagai, J. Komotori, and H. Imai, "Adhesion of osteoblast-like cells on nanostructured hydroxyapatite," *Acta Biomaterialia*, vol. 6, no. 2, pp. 591–597, 2010.

[47] K. Burridge, K. Fath, T. Kelly, G. Nuckolls, and C. Turner, "Focal adhesions: transmembrane junctions between the extracellular matrix and the cytoskeleton," *Annual Review of Cell Biology*, vol. 4, pp. 487–525, 1988.

[48] E. Martínez, E. Engel, J. A. Planell, and J. Samitier, "Effects of artificial micro- and nano-structured surfaces on cell behaviour," *Annals of Anatomy*, vol. 191, no. 1, pp. 126–135, 2009.

[49] R. K. Assoian and M. A. Schwartz, "Coordinate signaling by integrins and receptor tyrosine kinases in the regulation of G1 phase cell-cycle progression," *Current Opinion in Genetics and Development*, vol. 11, no. 1, pp. 48–53, 2001.

[50] J. B. Nebe, L. Müller, F. Lüthen et al., "Osteoblast response to biomimetically altered titanium surfaces," *Acta Biomaterialia*, vol. 4, pp. 1985–1995, 2008.

[51] R. O. C. Oreffo, F. C. M. Driessens, J. A. Planell, and J. T. Triffitt, "Growth and differentiation of human bone marrow osteoprogenitors on novel calcium phosphate cements," *Biomaterials*, vol. 19, no. 20, pp. 1845–1854, 1998.

[52] X. Yu, L. Wang, X. Jiang, D. Rowe, and M. Wei, "Biomimetic CaP coating incorporated with parathyroid hormone improves the osseointegration of titanium implant," *Journal of Materials Science: Materials in Medicine*, vol. 23, pp. 2177–2186, 2012.

[53] M. Gottlander, C. B. Johansson, and T. Albrektsson, "Short- and long-term animal studies with a plasma-sprayed calcium phosphate-coated implant," *Clinical Oral Implants Research*, vol. 8, no. 5, pp. 345–351, 1997.

[54] S. B. Goodman, J. A. Davidson, and V. L. Fornasier, "Histological reaction to titanium alloy and hydroxyapatite particles in the rabbit tibia," *Biomaterials*, vol. 14, no. 10, pp. 723–728, 1993.